Experimental and numerical study of the structural effects of steel corrosion in continuous RC beams

PhD DISSERTATION

Doctoral Thesis

Ignasi Fernandez Perez

Supervised by:

Prof. Antonio R. Marí Bernat

Prof. Jesús Miguel Bairán García

Barcelona, June 2015

Universitat Politècnica de Catalunya - Barcelona Tech
Departament d´Enginyeria de la Construcció

UNIVERSITAT POLITÈCNICA DE CATALUNYA BARCELONATECH

Departament d'Enginyeria de la Construcció

PhD dissertation

Experimental and numerical study of the structural effects of Steel corrosion in continuous RC beams

Presented by

Ignasi Fernandez Perez
Civil Engineer, Universitat Politècnica de Catalunya

for the degree of Doctor with International Mention

by the Universitat Politècnica de Catalunya

Supervised by

Prof. Antonio R. Marí

Prof. Jesús Miguel Bairán

This research has received the financial support of the *Ministerio de Educación y Ciencia* through the research project ADRESS (*Assessment of deteriorated, repaired and strengthened structures: theoretical model and experimental verification,* ref. num. BIA2009-11764), the European Regional Development Fund (ERDF), the *Col·legi d'Enginyers de Camins, Canals i Ports de Catalunya* and *Infraestructures de Catalunya* (ICAT).

Keywords: statically undetermined structures, two span continuous beams, steel corrosion, bond-slip, mechanical properties, 3D scan, numerical simulation.

Printed in Barcelona, Catalonia, June 2015

A mi familia. A Miriam

"El nacimiento de un conjunto estructural, resultado de un proceso creador, fusión técnica con arte, de ingenio con estudio, de imaginación con sensibilidad, escapa del puro dominio de la lógica para entrar en las secretas fronteras de la inspiración"

Eduardo Torroja

Agradecimientos

Con estas líneas culmina la que ha sido, hasta ahora, la etapa más larga de mi vida. Muchos años han pasado desde aquel 7 de Julio de 2002, cuando decidí embarcarme en el maravilloso mundo de la ingeniería, por aquel entonces de Caminos, Canales y Puertos, en la Universitat Politècnica de Catalunya. Un instante fugaz en el cual elegí como primera opción Caminos. Trece años después puedo ponerle cierre a una inmensidad de momentos, recuerdos y personas que me han acompañado, con total entrega, mediante la finalización de esta tesis.

En primer lugar agradecerle a mi guía y tutor, Toni, por todo su apoyo, energía, conocimiento y perseverancia, elementos sin los cuales no hubiera sido posible finalizar este trabajo. Siempre ha tenido la puerta abierta para todo, personal o laboral, y por ello no puedo ofrecerle nada más que mi más profundo y sentido agradecimiento. Numerosas han sido las veces en las que me he acordado del día que nos conocimos, en el hospital visitando a una amiga común, y sus palabras, que me abrieron un campo de posibilidades para un futuro por aquél entonces, verdaderamente incierto. Mil gracias por haber apostado por mí y hacer posible este trabajo.

A Jesús, al cual debo agradecerle, no menos, que aportar la luz necesaria cuando todo esta oscuro. Su capacidad de ver caminos donde no los hay, de construir y profundizar en temas de esta y otra dimensión me acompañarán para siempre, y espero desde lo más profundo, que parte de los casi 5 años vividos juntos hayan servido para llevarme parte de eso conmigo.

A Miren que entre otras muchas cosas, me ha enseñado lo que es la pasión por nuestro trabajo, algo sin lo que no se debería vivir. Su perseverancia y su buen hacer han sido siempre una motivación, pero lo que realmente más le agradezco han sido esos momentos para desahogos y discusiones profundas.

A Manuel F. Herrador que desde la lejanía siempre ha sabido como estar cerca. Esos km que nos separan nunca han sido un impedimento para estar aquí cuando ha sido necesario y aportar su ilusión y su optimismo, que tan bien lo caracterizan. También mencionar sus pensamientos en las redes sociales que tantas risas me han proporcionado.

Pero más allá del trabajo, las personas que están contigo, y que a su vez, poco a poco, te construyen como individuo. Noemí, Anna, Raúl, gracias, habéis sido muchas veces el motivo por el cual esbozar una sonrisa y encontrar ganas para ir a la Universidad, habéis hecho de éste, un camino mejor. A Ramón, mi eterno compañero, prácticamente de toda mi vida y que

además tuvo a bien de coger el barco de la ingeniera conmigo, gracias. A Jesús, mi artista preferido. A Mireia y Sonia, el día que os conocí mi vida cambió.

It cannot be missed in these lines a special mention to an enigmatic and wonderful country, Sweden, where I could enjoy one of the best part of my PhD degree. I cannot say more than it deeply marked me in the professional field, due to its ways to do things. Thank you Karin and Kamyab. Also in the personal field, I am very glad to have had the opportunity to meet exceptional people with whom I am sure I am going to share new terrific moments. Gracias Carlos, thanks Thomas and Natalie.

A mi familia; mi madre, mi padre, mi hermana y el último recién llegado, mi sobrinito, gracias por vuestra ayuda y perseverancia para hacerme avanzar siempre en la dirección correcta. Ha sido un trabajo duro, de fondo, pero que ha dado buenos resultados. Esto no hubiera sido posible sin vosotros. Gracias, os quiero.

Pero sin duda, lo mejor que me llevo de estos años, es que el tomar esa primera decisión de empezar este camino, me permitió conocer a Miriam, la persona con la que he compartido y comparto plenamente mi vida y con la que espero seguir haciéndolo allá donde nos lleve nuestro camino. Gracias por estar siempre a mi lado, apoyarme en los momentos difíciles, animarme con tu esplendida y contagiosa sonrisa y hacerme ser cada día mejor persona.

∞

Summary

Many reinforced concrete structures suffer damage due to aging and due to the environmental agressivity, thus affecting their serviceability performance and safety. Structural evaluation of a deteriorated structure is necessary to assess the actual structure state, to determine whether the structure should be strengthened or demolished and to optimize the interventions required to guarantee its serviceability and safety. In order to objectively take such decisions, refined analytical models are needed, capable to capture the structural effects of the deterioration, as well as the effects of repair or strengthening interventions, accounting for the structure previous state.

In the case of statically indeterminate structures, as many of the existing bridges and buildings, the damage produced by local or general deterioration processes may affect the whole structure state of forces, stresses and cracks. However, even though the difficulties to adequately assess such type of structures very scarce resarch works have been done, up to now, in this field

The present research aims to contribute to those goals presenting an extensive experimental campaign, at the material and at the structural levels. Furthermore, theoretical and numerical studies based on mechanical non-linear models were performed in order to reproduce the observed experimental behaviour and to contribute to the modelling of the performance of deteriorated structures.

The global effects of the structural damage were addressed by means of an experimental study, which encompassed twelve continuous two span large-scale beams. The cast beams divided in four groups of three beams each were submitted to different corrosion levels, except one group, which was left uncorroded as a benchmark. Each beam was loaded with different dead weights to assess the load effect when corrosion phenomena took place. Thereafter, the beams were unloaded and loaded again up to failure. The defining structural variables, such as reactions, mid-span deflections, steel stress/strain and slips at the bar-end were measured, and thereafter compared with the uncorroded specimens.

On the other hand, the local effects of steel corrosion were analysed by means of two different experimental studies. The first study encompassed more than 192 corroded steel bars covering a wide range of corrosion levels from 7% up to 28%, extracted from the tested concrete beams. The specimens were cleaned, and after, characterized under cyclic and monotonic loads. Hence, the specific σ-ε and fatigue life regarding the corrosion level was obtained. The second study encompassed 48 cubic concrete specimens with embedded steel

reinforcement bars. Different concrete types were used, including recycled aggregate concretes. The steel was submitted to accelerated corrosion and thereafter was pulled out from the cubic specimen assessing the effect of corrosion on the bond behaviour.

Finally, modelling of the mechanical properties of corroded steel bars and bond in concrete was done. A model to evaluate the corroded steel reinforcement mechanical properties, σ-ε and fatigue life, was developed. In addition, the 3D scan novel technique was used to characterise the outer surface of corroded steel reinforcing bars, by which the study of the corrosion pitting distribution and the critical cross-section was possible. Thereafter 3D solid models were performed from this detailed surface. To put an end to this part, different approaches to model bond between concrete and steel were used identifying their benefits and drawbacks.

Corrosion of steel reinforcement produced a substantial increment of the deflections as well as the stresses at the steel, both in the corroded and the uncorroded regions, due to the redistributions that took place in the continuous beams as a consequence of the loss of steel section. Furthermore, the redundancy of the structure provided them an extra load capacity with respect to a statically determinate beam. On the other hand, the ultimate load capacity was severely reduced; mainly a reduction of bond capacity was attributed to that behaviour.

A non-linear reduction of the corroded steel mechanical properties was found. Yielding and ultimate stresses described a good correlation with respect to the corrosion level. However, the results for modulus and ultimate strain presented more dispersion, which made difficult to establish good correlations with respect to the corrosion level.

Bond capacity of recycled concrete aggregates was showed to be similar to natural aggregate concretes. Nevertheless, when corrosion comes to play, recycled aggregate concretes showed better performance describing lower ultimate bond reduction with respect to those of conventional concrete. However, very high corrosion levels showed similar ultimate bond strength for both.

The presented mechanical model defined with an excellent reliability yielding and ultimate stresses for corroded bars up to 60% of corrosion levels. The statistical model presented for the pitting depth calibration allowed to define the upper and lower bounds of the pitting depth regarding to corrosion level. The validation tests fell within these limits.

A validation of some hypothesis performed in the mechanical model was done using the 3D scan results. A comparison between the real critical cross-section extracted from the 3D scan results and the pitted critical cross-section defined with the mechanical model, was

presented. The study of the effects of non-uniform stress distribution throughout the cross-section due to different phenomena such as non-homogeneous material properties distribution or pitting in the cross-section was done using 3D solid models. A significant multi-axial stress state was observed throughout the corroded bar. Thus, uniaxial sectional fibre models cannot represent 3D stress state, which are intended to reproduce the overall corroded bar behaviour, not the critical cross-section only.

Model of anchorage failure was satisfactorily done using different approaches. 1D analysis described good results for the ultimate load estimation. Nevertheless, were not enough to describe the overall behaviour. However, 3D models, which were very useful to assess not the ultimate load but the whole behaviour, were more complex and required much detailed information to be performed.

TABLE OF CONTENT

I. INTRODUCTION

II. ESTADO DEL CONOCIMIENTO

Table of figures

List of tables

Chapter I

INTRODUCTION

I.1 Background and motivation

The repair of structures, as well as the design and execution of more durable new ones, takes a particular relevance in the actual frame of knowledge, becoming a spearhead for councils and governments, in order to rationalize the existing resources and to better invest them. Broad knowledge about the structural behaviour and about the deterioration phenomena in which structures could be involved becomes really important, not only for existing structures but also for new ones, whose projects should account for the appearance of such deterioration phenomena in order to guarantee their durability and their service life. Engineers often must assess and quantify the structural damage (Figure I-1), with the aim to decide, at the end of the structure's service life, what means are needed for its demolition, or whether it is more convenient to have it repaired and strengthened, investing money to extend its service life. All of this, under the safety and cost control criteria.

Figure I-1. Structure deterioration due to steel corrosion

Corrosion of steel reinforcement is one of the main deterioration phenomena in reinforced concrete structures that directly affect their service life. To study the corrosion effects is crucial for a better understanding of the structural behaviour of existing impaired concrete structures. Many researchers have performed studies of corrosion effects for several years. Despite the larger database of experimental studies, they mostly encompass simple specimens, reduced in dimensions and statically determined (Figure I-2). Thus, the structural effects on statically undetermined beams are presented as a challenging investigation to increase the database and to observe the effect of corrosion in this type of structures, widely employed in construction around the world. The impact of corrosion on statically undetermined beams may be different because of their internal forces redistribution capacity; for example, bending moments shift from the stiffer to the weaker zones and vice versa. This capability might result in a better response regarding reinforcement corrosion and its effects if that internal forces redistribution becomes naturally from the corroded zones to the uncorroded ones, for example.

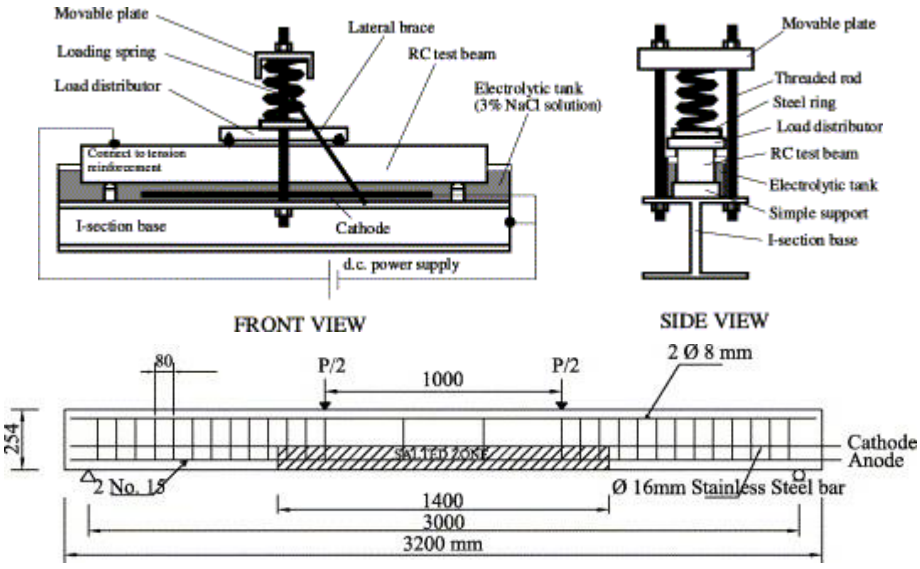

Figure I-2. Test setup of different studies carried out

In addition to understanding the overall structural behaviour of statically-undetermined beams is necessary to go in depth into the local effects that corrosion produces in the structure. The local effects such as cover cracking, loss of steel cross-section or bond reduction between steel and concrete have a significant impact on the overall behaviour. Although most of the investigations are not focused on these local effects, steel reinforcement corrosion yields into material mechanical properties changes too. The study of the local impacts of corrosion such as changes at the material level is critical for defining the new steel bars properties due to corrosion. The change in steel behaviour can become into an unexpected structural response, even producing undesired brittle failures.

Another local effect is the steel reinforcement unconfinement, due to cover cracking or spalling of concrete cover, as well as rust between both materials. These facts quick decrease the bond strength, thus changing the structural behaviour and inducing anchorage failures. Many researchers have studied the effect of the corrosion procedure on bond deterioration. Several studies have investigated parameters that may influence the bond and anchorage capacity of corroded structures. Models studying the interaction between both materials, and numerous experimental studies identifying and studying this phenomenon can be found in the literature. Even though, the literature on works covering bond behaviour on recycled aggregates or other special concrete considering steel corrosion is very scarce.

The implementation of such phenomena in deterioration models is presented as a powerful tool to assess and predict the structural behaviour under the influence of different deterioration scenario, also allowing improve the structural design in the project phase. These models should be capable of predicting reliably and precisely the structural state in a

realistic way. These models should provide enough information to quantify the structural deterioration and to define proper criteria to take the decision whether to demolish or strengthen.

I.2 Scope and objectives

The main objective of the present thesis is to study the global and local structural effects of steel reinforcement corrosion. Focus is made on statically-undetermined structures where the effects due to structural deterioration result in more complex structural behaviours than for isostatic structures. Due to the scarce number of test carried out on corroded statically undetermined beams in the literature, to perform an experimental campaign has been considered as an adequate methodology to contribute to the understanding and modelling of the structural effects of corrosion. In addition, the definition of the more significant local corrosion effects for the structural response and how to model them is done.

The following goals are defined to achieve the main objective of the thesis:

- To study the deterioration causes, the corrosion phenomenon and its developing mechanism
- To study the deterioration effects on statically undetermined beams at the service and ultimate load levels
- To identify the local effects that cause the observed structural behaviour
    - Mechanical properties of the corroded and uncorroded steel bars
    - Bond between concrete and steel
- Modelling of the local effects to be implemented in global structural models
    - Modelling of the corrosion effects in the steel bars to numerically assess the mechanical properties of corroded and uncorroded steel
        - Model calibration by means of experimental test
        - Model validation by means of existing experimental test in the literature
        - 3D models using 3D scanning technique of corroded steel
    - Study of different bond approaches in structures, to define their scope and applicability, as well as to select which methodology to apply to global models
        - Scope of 1D models
        - Scope of 1D bond models in 3D structural models

I.3 Research significance

Due to the lack of experimentation with complex concrete structures subjected to forced corrosion, an experimental study encompassing twelve continuous beams with two equal spans was performed. In addition, the effect of service load during the corrosion phenomena has been studied by means of different levels of applied load during the corrosion procedure.

Local effects of steel reinforcement corrosion such as the variation of mechanical steel properties, the non-homogeneous material distribution or the bond reduction between concrete and reinforcement have been deeply studied. The variation of mechanical properties has been studied by means of test performed on corroded steel bars under high cycle loads (high cycle) and monotonic loads. The non-homogeneous material distribution was assessed using tensile test of steel bars with different reduced diameters. Regarding bond between concrete and steel, the effect of the type of concrete, which included recycled aggregate concretes, in the variation of bond under different corrosion levels has been confirmed.

By implementing either generalised or pitting corrosion by means of an idealised pitted cross-section into a existing non-linear sectional analysis model, it is possible to describe the mechanical properties of both corroded and uncorroded steel under either pitting or generalised corrosion. On the other hand, the performed studies regarding modelling bond in concrete revealed the possibility to describe the phenomenon, according to different degrees of complexity.

In addition the outer geometry of corroded steel bars was obtained by means of 3D scan novel technique. A high-resolution mesh of the corroded steel surface is obtained which permits to observe the pitting distribution, the critical cross-section, etc. A validation of some hypothesis made for the developed model of mechanical properties of corroded steel was done by means of the 3D scan results. 3D models were performed from the surface mesh with the underlying purpose to reproduce the corroded and uncorroded steel behaviour under cyclic and monotonic loads and study the local effects of corrosion in the steel bar.

I.4 Outline and contents of this thesis

Figure I-3 shows the overall outline of the thesis organisation, with the different aspect studied along the presented work.

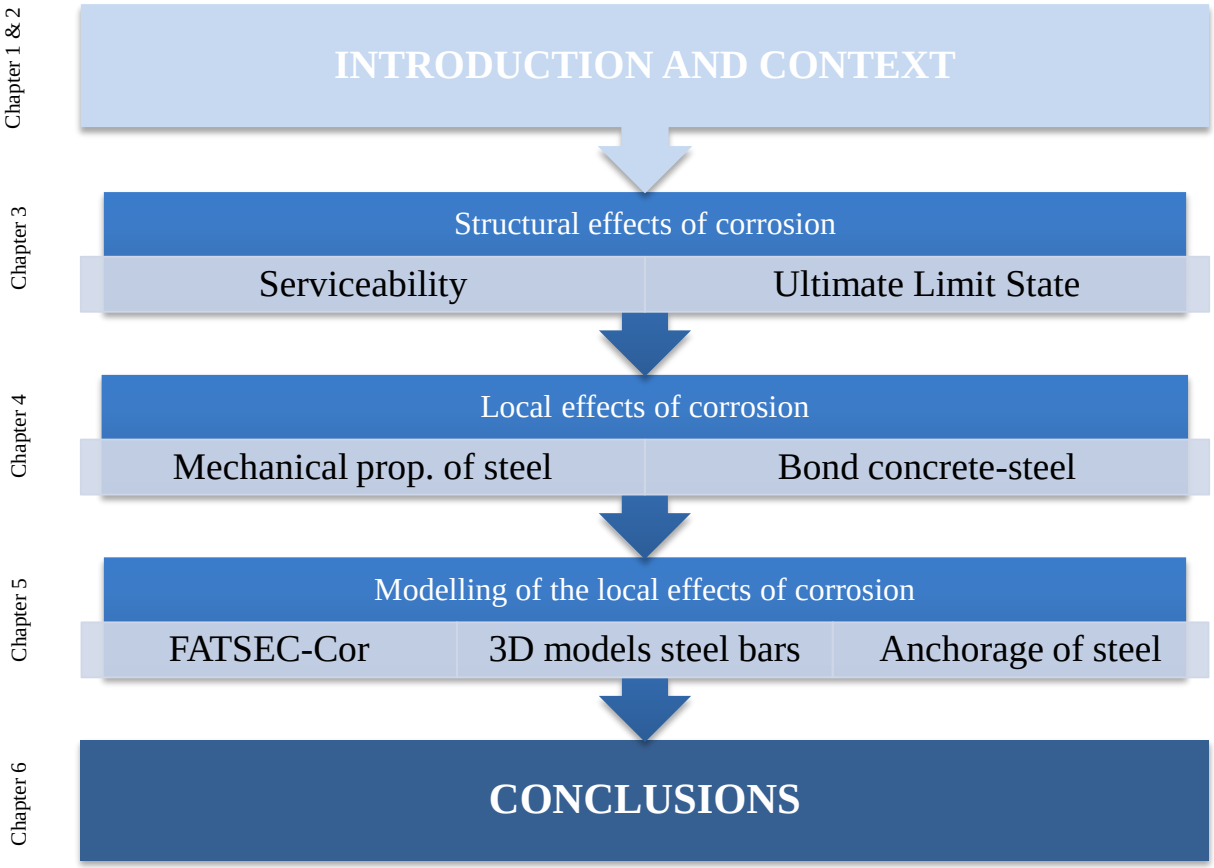

Figure I-3. Outline of the thesis.

The thesis is divided into 6 chapters. Chapter 2 is focused on describing the corrosion problem by means of a general state of the art. First, the primary causes of reinforced concrete structures deterioration and their mechanisms are analysed. Hence, the main structural effects and their local effects are stated.

In Chapter 3, the structural behaviour due to steel reinforcement corrosion was studied. The main experimental programme performed in this thesis to assess the corrosion effects on statically undetermined structures is described. Different structural variables were studied and later compared with uncorroded specimens. The chapter is organised in two separate parts. The first part analyses the structural behaviour under the different applied service loads during the steel corrosion procedure. The second part goes in depth into the response of corroded structures at ultimate state, analysing possible failure modes changes, and reduction of the ultimate load capacity. The main corrosion effects that affected the structural behaviour were identifyed.

Chapter 4 focuses on the study of the local phenomena of steel corrosion identified in Chapter 3. Mainly two phenomena were studied. The first part of the chapter is focused on the change of the mechanical steel behaviour due to corrosion (σ-ε and fatigue). The second part is focused on the study on bond between concrete and corroded steel bars, including the effect of different concrete types. The chapter encompass two experimental studies, one for each part: the first is oriented to define the modification of the corroded steel fatigue and **σ-ε** properties, the second is oriented to assess the effect of corrosion on bond considering different type of concretes, which includes recycled aggregate concretes.

Chapter 5 is focused on modelling of the local deterioration effects presented in Chapter 4. First, a model to determine the corroded and uncorroded mechanical steel properties is shown. Second, 3D models from corroded steel bars are performed by means of the novel 3D scan technique, which made possible to describe the corroded steel outer surface using a coarse mesh. Hence, the last part of the chapter implies the use of different approaches to modelling bond between concrete and steel and between concrete and textile reinforcement.

The major findings of the exposed research work are presented in Chapter 6. In addition, future research lines are proposed to complement the work performed here.

Chapter II

ESTADO DEL CONOCIMIENTO

II.1 Preámbulo

El hormigón como material consiste de una mezcla de elementos heterogéneos, a los cuales mediante un ligante a base de cal es posible darle cierta forma durante el proceso de endurecimiento. Básicamente podemos hablar de tres materiales que constituyen dicho material, el cemento, que es el material ligante, el agua y los áridos, siendo generalmente estos últimos, los encargados de dotar al hormigón de resistencia. Si mezclamos estos tres materiales en diferentes proporciones se obtiene una mezcla trabajable durante un cierto periodo de tiempo. Además de trabajable, esta mezcla es capaz de adoptar la geometría deseada si la disponemos sobre superficies capaces de aguantar el peso de la misma.

La mezcla, una vez endurecida, es la que se conoce como hormigón. El hormigón se caracteriza por tener unas propiedades mecánicas específicas que dependen de la proporción de cada uno de los elementos que lo componen y de la calidad de los mismos. A pesar de

ello, independientemente del tipo de hormigón que se fabrique y de los materiales que se empleen en su confección, el conjunto converge en su poca resistencia a tracción. A groso modo se puede cuantificar su resistencia a tracción en el entorno del 10 % de su resistencia a compresión, por lo que se tiene un material con grandes propiedades trabajando a compresión, pero que necesita de alguna solución para compensar su limitada capacidad de resistir a tracción. Esta limitación coge especial énfasis cuando el material, por ejemplo, debe trabajar a flexión, ya que las fibras superiores pueden aprovechar toda la capacidad del material pero las fibras inferiores no resisten apenas. Sin embargo, en situaciones donde el hormigón se encuentra completamente comprimido como en pilares y soportes, el material tiene un comportamiento excelente y se puede aprovechar toda su capacidad.

Por esta limitación en tracción se introduce un nuevo material en la mezcla, que es el acero. Mediante la disposición de barras de acero en el interior de la mezcla, se puede dotar al hormigón de una capacidad suficiente, para resistir dichos esfuerzos, y así trabajar como se desee. De esta manera, se compensa la falta de capacidad de resistir tracciones del hormigón por acero, que tiene enormes prestaciones tanto a tracción como a compresión. La introducción del acero en el hormigón, lo que se conoce como hormigón armado, es lo que permite el empleo de dicho material en elementos, esencialmente, que trabajan a flexión.

Además de dotar al hormigón de las propiedades mecánicas de las que carece, también se podría decir que el hormigón y el acero son perfectos compañeros de viaje, ya que las propiedades químicas del hormigón constituyen un medio perfectamente seguro para el acero, hablando en términos de durabilidad. Bajo la mayoría de condiciones, un hormigón bien diseñado y ejecutado correctamente, presenta una muy buena durabilidad.

La mezcla del hormigón está constituida por substancias de carácter muy básico. Esta alcalinidad, que proporcionan al hormigón pH superiores a 12-13, propicia un ambiente idóneo de protección para el acero. En estas condiciones una capa muy fina y densa de acero oxidado se forma sobre las barras. Esta capa protectora es la que se conoce como capa pasivadora. Esta capa pasivadora es la encargada de mantener protegido al acero que se encuentra bajo la misma, de los diferentes posibles ataques que el medio puede causarle, reduciendo la movilidad de iones entre el acero y el hormigón que lo envuelve, manteniendo el ratio de corrosión prácticamente negligible [1]. La capa pasivadora, se encuentra en perfecto equilibrio con el medio, y es necesaria la intervención de agentes externos agresivos para desestabilizarla y permitir el deterioro de las armaduras. El medio que la rodea, el líquido de los poros, gracias a esta alcalinidad, constituye un aliado perfecto para equilibrar

las condiciones en el entorno de la barra y consolidar el efecto protector de dicha capa pasivadora.

Cada uno de estos materiales, bajo condiciones normales, se encuentra en equilibrio, tanto a nivel interno como con el medio, por lo que se podría hablar de que una estructura por sí misma, no debería tener una vida útil limitada. A pesar de ello, como es sabido, una estructura tiene que cumplir sus objetivos de diseño durante cierto número de años y durante estos años los materiales que constituyen la misma deben permanecer inertes e inalterados.

El equilibrio en el que se encuentra dicha estructura, frecuentemente se ve roto por diferentes causas. A estas causas son las que se conocen como causas del deterioro, y suponen la ruptura de las condiciones de equilibrio entre los diferentes materiales que constituyen el hormigón. Generalmente el deterioro en el hormigón viene dado por las variaciones de las condiciones ambientales, que introducen nuevos agentes en el hormigón y desestabilizan, de alguna manera, el equilibrio asumido. A pesar de ello, no todas las causas de deterioro son de origen externo, también los propios materiales pueden ser responsables mediante la aportación de alguna substancia o incluso la transformación de los mismos, de la ruptura de este equilibrio iniciando así los procesos de deterioro.

Cuando se habla de procesos o causas de deterioro, nos encontramos ante un amplio abanico de causas que reducen considerablemente las prestaciones del hormigón armado y pretensado. Dependiendo del origen del ataque se puede manifestar mediante unas u otras consecuencias, pero generalmente se puede hablar de un deterioro global de la estructura con unos efectos claros en cuestión de seguridad estructural y vida útil.

II.2 Principales causas del deterioro

Las causas de deterioro se podrían separar en dos grandes grupos. Por un lado se puede hablar de causas asociadas a un deterioro de los componentes del hormigón y por otro lado a un deterioro del acero, mediante la corrosión del mismo, siendo este último el problema que más afecta a las estructuras de hormigón armado [2]. A pesar de esta separación de las causas de deterioro, si es cierto que en muchos casos el deterioro de uno de los materiales lleva asociado el deterioro del otro y viceversa.

Ya que no es principal objeto del presente trabajo se describirán a continuación en grandes rasgos las casusas de deterioro en el hormigón.

II.2.1 Reacciones de expansión endógena

Una de las causas importantes de deterioro del hormigón, por modificación de las propiedades volumétricas de los materiales que lo componen, son las reacciones de expansión endógena. Como se puede deducir del nombre, se trata de expansiones descontroladas de algunos de los materiales que componen la mezcla del hormigón. Generalmente los ataques asociados a una reacción de expansión los podemos englobar en dos grupos:

- Reacción álcalis-árido
- Formación de etringita secundaria

II.2.1.1 Reacción álcalis-árido

Una parte importante en la que se sustenta el buen funcionamiento del hormigón como material de la construcción, es la armonía entre los diferentes materiales que lo conforman. Como se ha explicado con anterioridad, el hormigón se trata de una mezcla heterogenia, la cual por medio del cemento como ligante, queda compacta. Uno de los puntos más relevantes en el buen funcionamiento del conjunto es la adherencia entre los áridos y la pasta de cemento. Es importante pues, que para el buen funcionamiento del hormigón como material estructural, estos áridos se mantengan bien cohesionados y unidos. Por lo tanto, que no se deteriore la unión entre estos y el cemento. Por ello, los áridos empleados en la mezcla del hormigón deberán ser lo que se puede llamar como estables. Éstos no deberían interaccionar químicamente de ninguna manera con la pasta de cemento, debiendo ser completamente inertes.

A pesar de ello, existen ciertas condiciones en las que la naturaleza mineralógica del árido puede tener una influencia decisiva sobre la resistencia y comportamiento del hormigón.

Ciertos tipos de áridos y los componentes de la fase intersticial del hormigón conllevan a la formación de fases nuevas en la interface de contacto árido-cemento que pueden provocar el deterioro del hormigón.

A este tipo de reacciones o formaciones es a lo que llamamos reacción álcalis. La estabilidad del árido que se ha definido como como la capacidad para mantener su integridad y no sufrir cambios físicos, químicos o mecánicos, puede depender del comportamiento preciso del hormigón en unas condiciones ambientales determinadas. Esto quiere decir que dependiendo de las condiciones climáticas de nuestra estructura podría ser necesario emplear áridos de mayor o menor calidad.

Esta reacción, que modifica la interface entre el árido y el hormigón, se produce por una interacción entre el líquido de los poros, que tiene un pH superior a 12, y los iones alcalinos con fases minerales de los áridos. Esta reacción conduce a la formación de nuevos compuestos, que a diferencia de los compuestos originales, pueden ser capaces de absorber agua, con lo que conllevaría un aumento volumétrico importante que podría desencadenar la rotura prematura del hormigón.

El proceso de reacción álcali-sílice necesita de tres elementos simultáneamente para producirse:

- Cantidad crítica de sílice reactiva en el árido
- Solución alcalina de los poros
- Humedad suficiente

Si dichos tres componentes se dan al mismo tiempo en las condiciones adecuadas, se desencadena inevitable la reacción álcali-sílice, iniciándose los procesos de deterioro.

II.2.1.2 Formación de etringita secundaria

En el proceso de hidratación de la pasta de cemento se forman una serie de sustancias que constituyen la mezcla final y dotan de las propiedades mecánicas al hormigón. Durante la fase de fraguado hay determinados compuestos que se transforman y acaban derivando en otros nuevos definitivos. Uno de ellos es el que se llama etringita. Este nace de la hidratación del calcio y constituye una de las sustancias más representativas de la mezcla. La etringita

que se forma durante el proceso inicial de hidratación del cemento es la que se llama y conoce como etringita primaria.

A pesar de ello la pasta de cemento como se ha visto puede presentar modificaciones a lo largo de su vida útil. Una de ellas es la formación de nueva etringita. Se conocen dos tipos más de etringita en el hormigón además de la etringita primaria.

- Etringita secundaria: que se forma con la aportación de sulfatos externos, ya sea mediante la aportación de los mismos por agua contaminada o por áridos con sulfuros o sulfatos en su composición.
  La etringita es uno de los compuestos que ocupa más volumen en la cristalización de la pasta de cemento. La cristalización de nueva etringita con la pasta endurecida puede ser muy perjudicial, ya que la formación de dicho compuesto generará tensiones importantes en la pasta de cemento, llegando a fisurar.

- Etringita diferencial: que aparece por descomposición térmica y presencia de humedad elevada. La etringita primaria al someterse a temperaturas elevadas se convierte en un compuesto soluble en agua. Con la presencia de humedad elevada esta etringita se disuelve. Esta es adsorbida por el CSH que una vez a temperatura ambiente y humedad, recristaliza la etringita. Esta recristalización rompe la estructura CSH, provocando expansión y fisuración de la pasta de cemento.
  La formación de dicha etringita requiere de los siguientes factores determinantes:
  - Temperatura y duración de este aumento de temperatura
  - Composición química del cemento específica que permita las condiciones
  - Dosificación del hormigón
  - Condiciones ambientales circundantes, como la presencia de humedad

II.2.2 Corrosión de armaduras

En el otro bloque, en términos de deterioro, se encuentran los ataques sobre el acero de armar. Hasta aquí se ha visto cómo afectan diferentes ataques sobre el hormigón. Pero si bien es cierto que estos son muy dañinos y se deben tener en cuenta y controlar, también lo es que el principal daño que puede sufrir una estructura de hormigón, y el más habitual, es el deterioro de sus armaduras. La corrosión de armaduras ha sido identificada como la primera causa de deterioro de estructuras de hormigón así como de fallo de las mismas durante las últimas décadas, además representa un alto coste a la sociedad en término de reparaciones, monitorización o reemplazo de estructuras [3].

El acero de las armaduras como material metálico, cuenta dentro de sus propiedades con unas espléndidas características mecánicas, superando ampliamente al hormigón. El acero de armar convencional tiene resistencias del entorno de los 500 MPa, 10 veces más que el hormigón convencional a compresión, y cien veces más que la resistencia a tracción del mismo. Por ello se destina su empleo generalmente a paliar la poca capacidad a tracción del hormigón. Sin embargo, como material metálico también tiene ciertos inconvenientes, que van más allá de su coste.

El principal inconveniente a nivel de deterioro es la facilidad con la que este material se corroe. Y es que el acero, de manera natural, cuenta con un potencial de corrosión muy elevado por lo que es muy susceptible a oxidarse y perder electrones. Esto pone de manifiesto la necesidad importante de controlar y conocer los mecanismos de corrosión de las armaduras de manera exhaustiva, así como sus efectos en la estructura y el material. A continuación se detallan los mecanismos de la corrosión de armaduras dentro del hormigón.

II.3 Mecanismos de la corrosion de armaduras

El fenómeno de corrosión de armaduras se puede resumir como una pila, con un ánodo que pierde electrones por lo que se oxida, y un cátodo que los recibe y por lo tanto se reduce.

Es importante conocer todos los agentes que intervienen e identificar el papel que juegan en el proceso de la corrosión de las armaduras cada uno de ellos. Esto permite entender el proceso, intervenir y actuar para detener el mismo, y si procede reparar. Así mismo una buena comprensión del mismo será útil para mejorar el diseño estructural y así construir estructuras más durables y seguras.

El fenómeno de corrosión de las armaduras en el hormigón se puede dividir de una manera simplificada en dos etapas, tal y como se define en el modelo de vida útil de Tutti (Ilustración II-1).

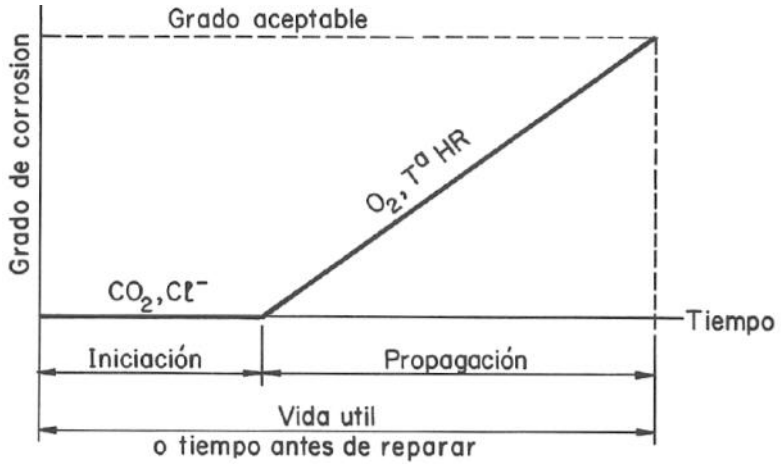

Ilustración II-1. Diagrama de Tutti [1]

Si bien es una manera muy esquemática y simplificada de reproducir el proceso de corrosión en una estructura, es útil para comprender y hacerse una idea cualitativa del proceso del fenómeno.

El diagrama de Tutti, esencialmente establece dos fases que definen la vida útil de una estructura. De manera muy esquemática, en la primera fase se produce propagación de los agentes externos encargados o motivadores del deterioro del acero, que penetran hasta el mismo. La segunda fase, que se inicia cuando éstos han alcanzado el acero, define el tiempo del que se dispone desde que los agentes activos inician la corrosión del acero hasta que es requisito necesario la seguridad estructural se ha visto muy mermada y es necesaria la intervención. Lo interesante del gráfico anterior es la división fenomenológica del proceso en dos etapas claramente diferenciadas, donde en una fase donde el daño no se ha producido todavía y otra donde el daño ya es existente.

Como se ha descrito, la barra sin patologías se encuentra en un medio estable. Éste es un medio acuoso debido al líquido de los poros del hormigón. Durante la hidratación del cemento se forma el CSH y CH, elementos que se encargan de dotar de la resistencia necesaria a la pasta de cemento. Este líquido que tiene un contenido importante de CH disuelto se encarga de dar alcalinidad al hormigón, con un pH superior a 12-13. A esta solución [4], que envuelve las armaduras, es la que se conoce como solución tampón o solución reguladora, que es la encargada de regular constantemente el ambiente fuertemente alcalino, disolviendo o precipitando $Ca(OH)_2$ y estabilizando el hormigón y el acero [1].

Éste líquido supone para el acero una protección importante, ya que permite mantener la capa pasivadora, y evita la corrosión natural de las barras de acero. Además, el recubrimiento de hormigón de las armaduras supone una protección física que recubre las armaduras y cuya eficacia, depende de su permeabilidad y espesor. Este recubrimiento, también es un elemento determinante para mantener dichas condiciones de estabilidad sobre las armaduras.

Los metales en la naturaleza se encuentran combinados con otros materiales. Para obtenerlos y extraerlos es necesaria la aportación de energía que permite la reducción de los mismos de manera artificial y obtener así el material aislado, sin combinar, por ejemplo el Fe^{2+}. Por ello, la tendencia natural de los mismos será la oxidación, combinándose con otras substancias, pasando así a su forma más estable de nuevo. Hay que tener en cuenta que es un proceso natural y espontáneo, he ahí su problemática y la necesidad de controlar el proceso para que esto no ocurra. En un medio acuoso el fenómeno que se produce es electroquímico, formándose lo que se conoce como pila de oxidación. En el medio acuoso se produce una reacción de reducción y otra de oxidación y la circulación de iones a través del electrolito [3].

Por lo tanto el proceso de corrosión supone la generación de una pila, en la cual, si se detiene en algún punto el circuito cerrado que constituye, se detiene el proceso de corrosión.

El proceso se puede definir como se ve en la Ilustración II-2.

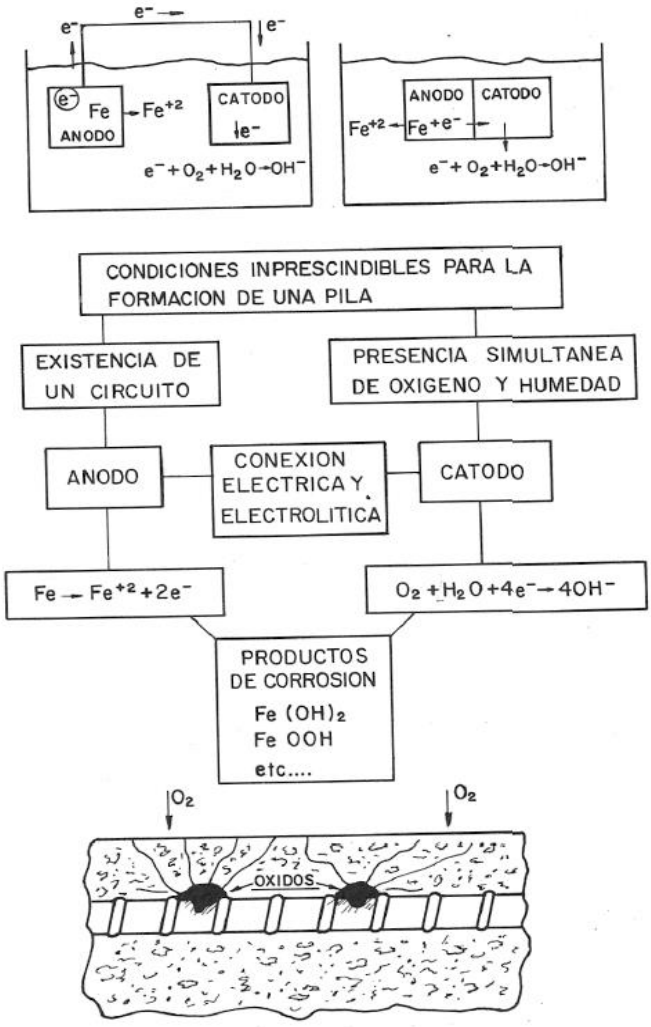

Ilustración II-2. Proceso de deterioro de armaduras – pila de oxidación [5]

Será necesaria pues, la presencia de tres elementos básicos para que el mecanismo de corrosión se inicie y se mantenga a lo largo del tiempo, el ánodo, el cátodo y el electrolito o medio.

Durante la fase de iniciación que se anunciaba en el diagrama de Tutti, es donde se disponen todos los prequisitos necesarios para que el proceso de oxidación, la formación de dicha pila, surja efecto. Es durante esta fase donde se define el ánodo, rompiéndose la capa natural protectora del acero y se inicia el intercambio de electrones con el cátodo.

II.3.1 Protección natural

Cada material metálico tiene un potencial V de oxidación que se mide formando una pila con un electrodo de referencia, generalmente platino sumergido en un ácido, en condiciones

ambientales normales. Este valor es el potencial necesario para que se inicie un proceso de oxidación en el material de manera natural.

El diagrama de Pourbaix (Ilustración II-3) define los diferentes valores de potencial en relación a las variaciones de alcalinidad del medio, del pH del líquido de los poros, para el Fe. Este diagrama arroja datos interesantes respecto al empleo de acero en el hormigón y permite controlar y evaluar su estabilidad dentro de la mezcla. Como se muestra en dicho diagrama, los procesos de corrosión del Fe en medios alcalinos son muy difíciles de suceder, a partir de pH superiores a 9 las condiciones de estabilidad son muy altas y es complejo que se pueda formar la pila de oxidación. Además en el caso de formarse dicha pila, la bajada del potencial detendrá por si solo el proceso de oxidación entrando en fase de inmunidad o pasivación. Este estado de pasivación en pH elevados es muy importante ya que se trata de una protección natural del acero a corroerse y es en el medio donde se encuentra dentro del hormigón. Esta capa de pasivación se produce por la oxidación del Fe, que forma una capa estable sobre el mismo, frenando así el proceso de corrosión y por lo tanto rompiendo la formación de la pila. Siempre que tengamos esta capa se tendrá el acero protegido y su degradación será tan lenta que se podrá considerar nula.

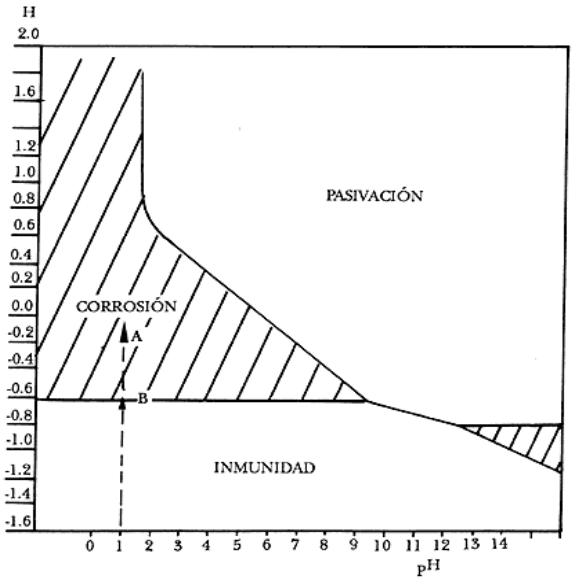

Ilustración II-3. Diagrama de Pourbaix [6]

Generalmente se puede hablar de dos fenómenos que propician dicha ruptura en las condiciones de equilibrio para las barras [7].

II.3.2 Carbonatación del hormigón

Como se ha apuntado anteriormente la alcalinidad del líquido de los poros es la mayor responsable en garantizar dicho equilibrio. Por lo tanto, una pérdida de dicha alcalinidad, sería suficiente para desestabilizar la capa de pasivación e iniciar el proceso de corrosión de las barras. Si se retoma el diagrama de Pourbaix se puede observar como la zona pasivación del acero disminuye rápidamente con la bajada de pH del medio.

El principal responsable de la alcalinidad de la solución de los poros, es la disolución de CH, que son capaces de formar una solución tampón auto equilibrada en forma de precipitación de CH y disolución del mismo, por lo que mantiene de manera estable el pH en la mezcla.

$$Ca^{2+} + 2OH^{-} \text{ ------ } Ca(OH)_2$$

Si entra más OH^- en la mezcla precipita $Ca(OH)_2$, y si al contrario entra H^+, se disuelve $Ca(OH)_2$ según la reacción:

$$Ca(OH)_2 + 2H^{+} \text{ ------ } Ca^{2+} + 2H_2O$$

A pesar de ello, gran parte de estructuras de hormigón se encuentran en medios agresivos que pueden desestabilizar esta solución tampón provocando variaciones en el pH del hormigón, superando la capacidad de regulación de ésta. Un elemento altamente desestabilizador de la reacción es el CO_2.

El hormigón, al tratarse de una estructura porosa, forma una red de poros interconectados que permite la circulación de diferentes substancias por el interior del mismo, con mayor o menor dificultad, según los criterios de dosificación del mismo. El CO_2 que se encuentra en la atmósfera, producto de la combustión, penetra a través de esta red de poros. Una vez en el interior del hormigón, mediante el mecanismo de difusión, consigue penetrar lentamente y uniformemente por la superficie del mismo hasta alcanzar las armaduras. Este CO_2 con la presencia de agua forma ácido carbónico, que a su vez ataca al CH convirtiéndolo en carbonato de calcio ($CaCO_3$) (proceso conocido como carbonatación). El avance del mismo depende de muchos factores, el tamaño de los poros del hormigón, su interconexión, la cantidad de agua presente, la humedad relativa, la temperatura, etc… pero a pesar de ello la penetración del CO_2 se produce de manera natural en ambientes con una concentración importante del mismo.

La pérdida continuada de CH que conlleva la entrada del CO_2 en la mezcla produce rápidamente una bajada del pH, ya que la solución tampón no es capaz de controlar el

proceso y equilibrar el pH. Esta bajada del pH, inmediatamente provoca la despasivación de las armaduras y por ende, elimina la protección natural de las mismas dejándolas expuestas al ataque de cualquier agente agresivo.

Ilustración II-4. Carbonatación del hormigón

La carbonatación en sí misma (Ilustración II-4), no es un proceso de corrosión de las armaduras, sino un ataque sobre el hormigón, que provoca un cambio en las condiciones de equilibrio entre ambos materiales. La importancia de la carbonatación es el fenómeno asociado de desprotección del acero, lo que permite que se inicie el proceso de pila de oxidación con mucha más facilidad. Además de esto, otro gran problema asociado a la carbonatación es que la pérdida de protección sobre las armaduras es uniforme, por lo que las armaduras quedan expuestas en su totalidad induciendo a la corrosión generalizada de las mismas.

II.3.3 Corrosión por cloruros

El segundo fenómeno de corrosión de armaduras, es la corrosión por presencia de cloruros.

En esta situación el ion cloro penetra en el hormigón por la estructura de poros hasta alcanzar las armaduras. Los iones cloro solamente penetran en el hormigón disueltos en agua, por lo que el proceso de penetración de los Cl^- se inicia por succión capilar de este agua. Por ello se requiere para la iniciación del proceso una fuente externa que sea capaz de aportar la cantidad necesaria de cloruros al hormigón. Generalmente este tipo de corrosión se da en

zonas costeras donde la concentración de cloruros aportada por el mar, es constante y muy importante. Las normativas vigentes establecen como zona costera hasta los primeros 5 Km de tierra desde línea de mar, donde se considera que la concentración de cloruros ambiental es suficientemente alta como para tener que aplicar medidas al respecto.

Las zonas más perjudicadas por el proceso de corrosión por cloruros, son las estructuras en zona de salpicadura y mareas. Como es de esperar estas estructuras están sometidas a ciclos constantes de mojado y secado. Este fenómeno es altamente destructivo para el hormigón armado ya que permite una aportación constante y permanente de cloruros a la estructura en cada uno de los ciclos, aportación externa de cloruros durante el mojado y absorción de los mismos por succión capilar durante el secado.

Una vez los cloruros han penetrado, mediante procesos de difusión los iones Cl^- se desplazan por diferencia de concentraciones hacia el interior de la estructura, ya que intentan equilibrar la concentración de cloruros a lo largo de la estructura. Este proceso se produce de manera natural por la tendencia de igualar concentraciones de los iones que contiene dos líquidos en contacto. Así, este proceso no se detendrá hasta que la aportación de cloruros sea nula, por lo que en una zona costera, la tendencia es que la penetración de cloruros sea permanente y creciente a lo largo de la vida útil de la estructura.

Cuando la concentración de cloruros es suficiente en el entorno de la barra, tal y como sucede en el fenómeno de carbonatación, se destruye la capa de pasivación, quedando la armadura desprotegida. Esto sucede solamente cuando la concentración de cloruros alcanza el nivel conocido *contenido crítico de cloruros* [8]. Este proceso de deterioro de la capa pasivadora requiere la desestabilización de la solución tampón, y para ello es necesaria esta concentración crítica de cloruros en la solución que reaccionan con los OH^-, y permiten la bajada del pH en el hormigón, iniciándose así la destrucción de la capa protectora.

A diferencia de la corrosión por carbonatación, generalmente hablamos de un ataque localizado, puntual en las armaduras donde la concentración de cloruros es mayor a este límite mencionado y rompe localmente la capa de pasivación. Normalmente esta concentración crítica de cloruros se produce en zonas puntuales a lo largo de las armaduras, no en toda su longitud. Generalmente las zonas de la estructura más expuestas al cloruro son las que llegan a esta concentración crítica primero, y es en estos puntos localizados donde se produce la ruptura de condiciones de equilibrio y por ende el ataque corrosivo. Por ello se trata de un ataque completamente diferente al producido debido a la carbonatación, ya que este, generalmente, tiene un efecto mucho más local.

II.3.4 Fenómeno de difusión

Como se ha visto hasta ahora el principal mecanismo de deterioro considerado en el hormigón es la penetración de los agentes agresivos por la red de poros del hormigón mediante el mecanismo de difusión.

El mecanismo de difusión en el hormigón está ampliamente estudiado por muchos autores y es conocido su funcionamiento, existiendo numerosos modelos desarrollados capaces de predecir de una manera precisa la penetración de estos agentes a lo largo de la vida útil de una estructura [9].

La penetración de cloruros por difusión generalmente se modela empleando la segunda Ley de Fick Ec. 1 [1].

Ecuación II.1

$$C_x - C_b = (C_s - C_b) \cdot \left\{1 - erf \cdot \frac{x}{2\cdot\sqrt{D\cdot t}}\right\}$$

Donde,

C_x=cloruros a una profundidad x

C_s=contenido de cloruros en la superficie

C_b=cloruros iniciales (de los componentes de hormigón)

D=coeficiente de difusión efectivo de cloruros

t=periodo de exposición

erf=función error

Las ecuaciones de Fick suponen una estructura de poros homogénea y por ello el coeficiente de difusión no depende de las condiciones de humedad, concentración de cloruros y temperatura. Además supone que la isoterma de fijación de cloruros es lineal [10]. En realidad el transporte de iones cloruro en el hormigón es un proceso complejo, en el cual los iones solo pueden moverse por el interior de los poros y no a través de las paredes sólidas de los mismos. A pesar de ello se considera como válida la aplicación de dicha Ley para definir el comportamiento de la difusión.

Además, aun siendo el mecanismo de difusión gobernado por la Ley de Fick el principal mecanismo de transporte, existen otros mecanismos secundarios que participan también en el transporte de los cloruros al interior del hormigón. Por ello el coeficiente D empleado en

la ecuación de Fick no responde a un coeficiente de difusión "puro" sino que incluye la interacción de los diferentes factores que ayudan a la penetración de agentes (absorción, difusión, fijación). A este coeficiente es al que llamamos coeficiente de Difusión "aparente". En las mezclas donde el coeficiente de difusión presenta un valor muy bajo, se considera que el principal mecanismo de transporte es la absorción, sin embargo cuando el valor del coeficiente de difusión es elevado el mecanismo de transporte dominante se puede considerar la difusión [11]. A largo plazo se considera que el mecanismo dominante será la difusión.

II.3.4.1 Recubrimiento, abertura de fisura y tipo de cemento

Si bien es cierto que la Ley de Fick es muy útil para la determinación de la penetración de agentes externos también lo es que los mecanismos de transporte se ven fuertemente influenciados por factores que modifican la perspectiva clásica. Así la influencia del tipo de cemento, la cantidad de adiciones, la relación a/c, el entorno, la humedad, la temperatura, carbonatación, fisuración o el recubrimiento juegan un papel crucial en la velocidad de corrosión.

La concentración critica de cloruros necesaria en el entorno de las armaduras para iniciar la corrosión, ha sido ampliamente estudiada, aunque sin un consenso claro ya que revela un amplio rango, desde el 0,25% hasta el 1,7% de cloruros en peso de cemento para iniciar la corrosión [12,13]. Muchos factores entran en juego en este valor, como por ejemplo la cantidad de cloro ligado y la cantidad de cloro libre.

La presencia de fisuración transversal no está asociada a un incremento de la velocidad de corrosión aunque si se asocia a un inicio de más temprano de la corrosión. Esto es debido principalmente a que la presencia de fisuración transversal modifica los mecanismos de transporte prevaleciendo otros por encima de la difusión.

II.4 Tipos de corrosión y efectos sobre la estructura

Cuando se construyen estructuras de hormigón armado, el principal objetivo para un buen diseño y proyecto de las mismas es que tengan una seguridad estructural suficientemente elevada como para evitar siniestros.

La corrosión de armaduras conlleva una serie de consecuencias desfavorables sobre la estructura. Este fenómeno juega un papel determinante en los procesos de deterioro, tratándose de la tercera causa de fallo estructural después de los fallos de ejecución y proyecto [2]. Es importante conocer y evaluar los efectos que producen la corrosión de armaduras para permitir una actuación e intervención eficaz sobre las estructuras, así como un buen diseño de las mismas.

Los efectos de la corrosión de las armaduras se pueden englobar en dos grupos, los efectos sobre las armaduras y los efectos sobre el hormigón.

El hecho de iniciación del proceso de corrosión supone un deterioro directo de la armadura. Ésta que está compuesta esencialmente por hierro, se disuelve lentamente combinándose con otras sustancias. Esta combinación tiene un efecto directo sobre las armaduras que es la pérdida de material de las mismas, o lo que es lo mismo la pérdida de sección de la barra [1].

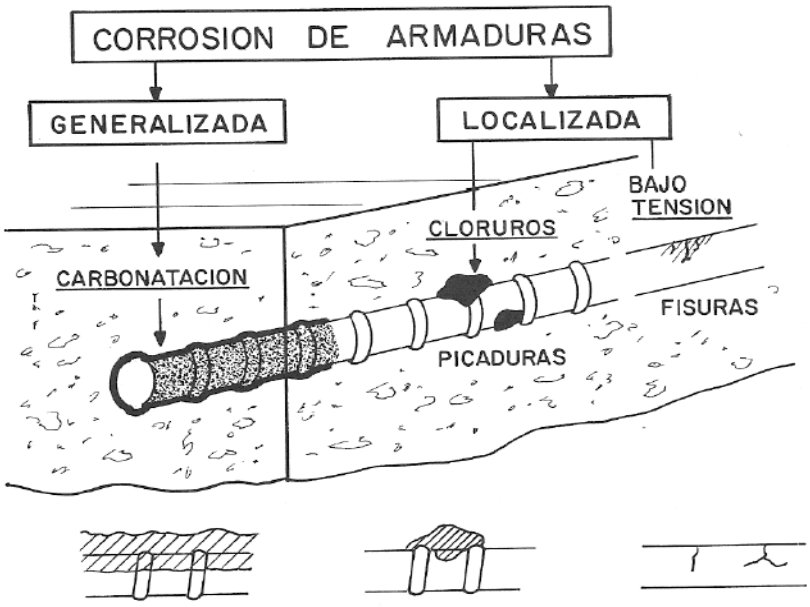

Ilustración II-5. Tipos de corrosión de armaduras [5]

Como se ha visto este fenómeno tendrá un efecto localizado o generalizado dependiendo del origen de la corrosión (Ilustración II-5). A esto es lo que llamamos corrosión generalizada,

cuando el origen de la corrosión es un ataque después de un fenómeno de despasivación de toda la barra, por ejemplo por carbonatación. En cambio, cuando se trata de un ataque únicamente por penetración de cloruros, el efecto es muy puntual y es lo que se conoce como corrosión por picadura [14]. Evidentemente cada tipo de corrosión deriva en unas consecuencias u otras a nivel estructura.

II.4.1 Corrosión generalizada

La corrosión generalizada tiene un efecto más o menos homogéneo a lo largo de la barra. Ésta no es excesivamente agresiva y se produce una pérdida de material más o menos constante en toda la longitud afectada a lo largo del tiempo. Una consecuencia directa de esta pérdida de material de la barra, de acero, es la formación de materiales nuevos. Los productos de oxidación formados durante el proceso de corrosión de las barras, genera hasta 6 compuestos nuevos, combinando las diferentes substancias que intervienen en el proceso. Estos productos a los que se conoce como óxido (*rust*) o productos de la corrosión, tienen una propiedad muy característica y trascendente para la estructura, que es que aumentan de volumen de manera importante respecto al volumen de acero corroído. Este aumento de volumen se puede cuantificar en más de 7 veces el volumen original [15,16] para algunas de las substancias formadas, por lo que es evidente que tiene unas consecuencias importantes. De media se puede considerar como válido que el volumen ocupado por el óxido es hasta 3 veces el volumen de acero corroído [17]. En la Ilustración II-6 se puede observar la relación entre la sección de acero inicial, la sección de acero corroída y el volumen de productos de oxidación formados.

En las fases iniciales de la corrosión, los productos derivados se van dispersando y ocupan los huecos y poros del hormigón en el entorno de la barra. Si el proceso es suficientemente lento, el óxido tiene tiempo a distribuirse y a ocupar el espacio de los poros sin provocar grandes aumentos de tensiones alrededor de la barra [18]. Sin embargo, si el proceso de corrosión es relativamente rápido, el óxido formado no tiene tiempo a distribuirse y rápidamente aparecen tracciones en el hormigón, las cuales no son bien toleradas provocando la fisuración del mismo, abriendo vías de escape por donde el óxido puede escaparse y liberar las tensiones [19].

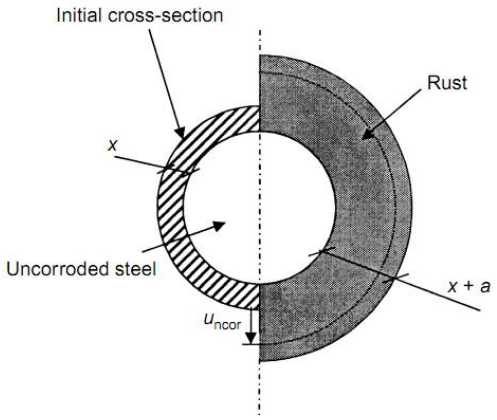

Ilustración II-6. Proceso de corrosión de armadura pasiva [20]

Dependiendo de la velocidad de corrosión, los patrones de fisuración sobre el hormigón serán unos u otros, pero en todos los casos éstas fisuras se desarrollan en la parte del recubrimiento, que es la zona más débil en el entorno de la barra. Si este recubrimiento es suficientemente grueso, las tensiones de tracción provocadas por el óxido, no son capaces de abrir una fisura hacia el exterior, por lo que se forma cierta microfisuración en el entorno de la barra que permite la ubicación de estos productos alrededor de la barra.

Por otro lado, si el espesor de recubrimiento no es suficiente para resistir dichas tensiones, o el ataque es muy agudo y la corrosión del acero es rápida y fuerte, las tensiones de tracción a lo largo de toda la longitud de la barra, generan una fisuración que se caracteriza por ser longitudinal en la dirección de las barras. Este tipo de fisuración es de las menos deseables ya que deja expuesta completamente las barras permitiendo el acceso a los agentes agresivos en toda la longitud, retroalimentando los procesos de corrosión de las armaduras.

Si el proceso de deterioro de las armaduras continúa y no se detiene, la fisuración se hace mayor y acaba provocando la pérdida o salto del recubrimiento, dejando las barras aún más expuestas al medio.

En la Ilustración II-7 se pueden observar los diferentes patrones de fisuración el recubrimiento debido al proceso de corrosión de las barras.

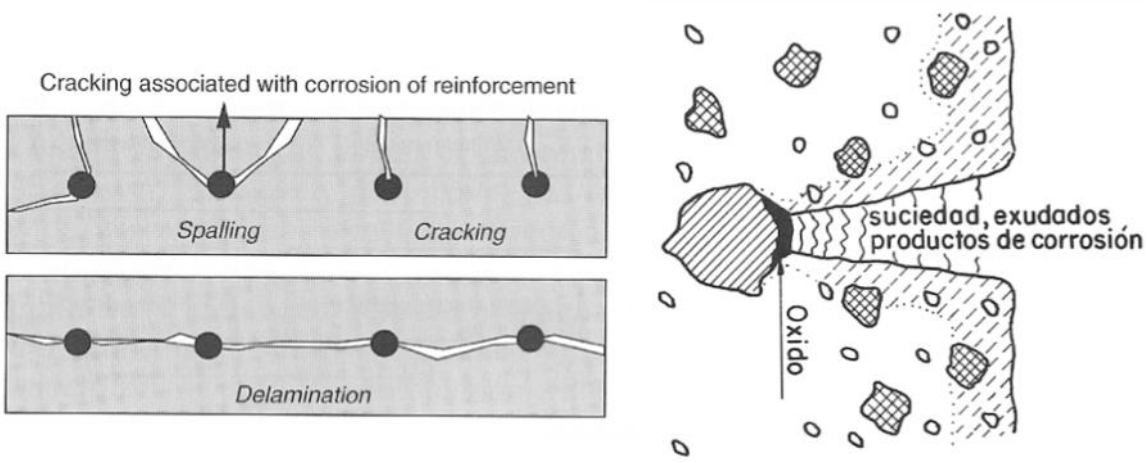

Ilustración II-7. Tipos de fisuración por corrosión de armaduras [21]

A pesar de ser un problema en términos de durabilidad, la fisuración longitudinal una vez finalizado o detenido el proceso de corrosión, debido a la suciedad, exudados i productos de oxidación generalmente queda sellada. Esto implica que esta no presente un problema para la estructura a largo plazo en estas condiciones, siempre y cuando se garantice que el proceso de corrosión se ha detenido por completo.

En cambio si el proceso de corrosión deriva en un ataque muy agresivo, la fisuración longitudinal conlleva ciertas consecuencias graves. La más importante de ellas es la descamación del recubrimiento. La fisuración es tan importante que la parte de hormigón de recubrimiento salta dejando desnudas las barras, acelerando aún más el proceso de corrosión. Estos fenómenos conocidos como “spalling” o “delamination”, se producen usualmente en estados muy avanzados de corrosión. El impacto de estos fenómenos es muy fuerte ya que una vez producidas dichas fisuras las barras de acero quedan completamente expuestas a los diferentes agentes y el proceso de deterioro no se detiene de manera natural. Es necesaria una intervención ajena para restablecer los recubrimientos y la protección sobre las barras de acero, ver Ilustración II-8.

Ilustración II-8. Fuerte corrosión de armaduras

II.4.2 Corrosión por picadura

Los efectos de corrosión localizada o corrosión por picadura son ligeramente diferentes. Si bien el mecanismo de formación de óxidos responde a las mismas causas y reacciones, las consecuencias son algo diferentes. En primer lugar tal y como indica el nombre la corrosión por picadura no afecta globalmente a toda la barra, sino al contrario, afecta tan sólo en el punto donde se produce, donde la concentración de cloruros es suficientemente grande como para romper la capa protectora de pasivación. Así pues, aún y todo teniendo los mismos productos de oxidación que en el caso de la corrosión generalizada, los efectos relacionados con la fisuración del hormigón son mucho menos perjudiciales, ya que los productos altamente expansivos de la oxidación pueden repartirse y distribuirse a lo largo de la zona afectada. A pesar de ello si el proceso de corrosión es muy rápido, si se puede llegar a producir cierta microfisuración por la rápida formación de dichos productos en el entorno de la picadura; difícilmente esta microfisuración se convierta en una fisura hacia el exterior.

De hecho los fenómenos de corrosión por picadura tienen un fuerte impacto en las zonas de fisuración transversal, donde encontramos una "puerta de acceso" a las armaduras debido a la obertura de fisuras por flexión. Si bien es cierto que la normativa vigente regula el ancho de fisura en función de los ambientes debido a estos problemas de durabilidad, también lo es que un fallo en el diseño o en su ejecución o una modificación de las condiciones de contorno de la estructura, puede llevar a un incumplimiento de estas restricciones, dando pie a la iniciación de estos fenómenos.

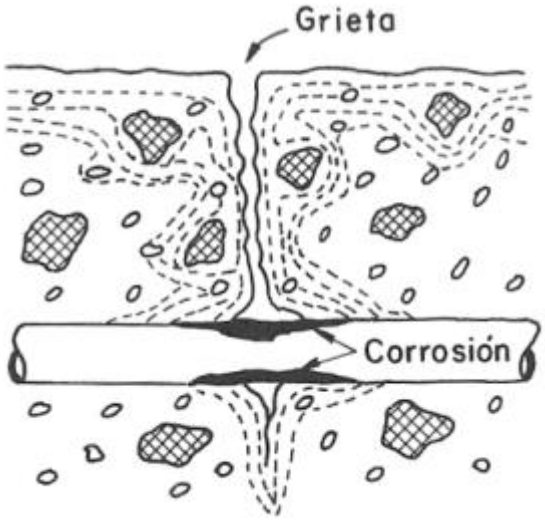

Ilustración II-9.Mecanismos de penetración de agentes agresivos [21]

Del mismo modo que para la fisuración longitudinal, los productos de oxidación suciedad y otras substancias, también resultan un elemento de sellado para las grietas (Ilustración II-9), por lo que si la concentración de cloruros se sitúa por debajo del límite necesario los procesos de deterioro se detienen y se recuperan las condiciones de durabilidad exigidas.

Otra de las consecuencias de la corrosión por picadura, es justamente que todo el proceso de corrosión se centra en un mismo punto por lo que produce pérdidas de sección de las armaduras muchísimo más significativas que la corrosión generalizada. Este efecto es comprensible ya que la pila de corrosión siempre actúa en una misma zona de armadura, la zona que se ha despasivado, por lo que el proceso constantemente se alimenta de la misma porción de acero. Así pues se puede decir que es un efecto mucho más agresivo en términos de pérdida de material respecto a la corrosión generalizada, resultando en zonas muy debilitadas.

II.5 Efectos estructurales de la corrosión

Cuando se habla de corrosión en las armaduras, suceden sobre la estructura ciertos cambios que producen una modificación de las condiciones iniciales y por ello un cambio en el comportamiento global de la estructura.

Generalmente un episodio de corrosión sobre una estructura conlleva una reducción de la seguridad estructural y un empeoramiento del comportamiento en servicio de la misma.

Los diferentes fenómenos locales que envuelve la corrosión de armaduras, como la pérdida de sección de acero, la modificación de la relación de adherencia hormigón-acero, la modificación de las propiedades mecánicas del acero y del hormigón, el salto de recubrimiento, etc… conllevan inexorablemente a un cambio de comportamiento de la estructura.

II.5.1 Ensayos existentes

El estudio de los efectos estructurales tanto en servicio como en estado límite último se ha llevado a cabo por numerosos autores [22–25]. A pesar de ello la experimentación existente en estos términos, se ha centrado básicamente en estructuras "simples", estructuras isostáticas de un solo vano de cortas dimensiones y bajo las mismas condiciones de carga, generalmente peso propio solamente. Así mismo, los procesos de deterioro se reproducen en zonas específicas de la estructura dando una perspectiva limitada del fenómeno. Probablemente dada la dificultad de reproducir un deterioro de este tipo de manera acelerada en condiciones aceptables, ha derivado en una simplificación de la experimentación.

Pocos han sido los ensayos donde se han estudiado los efectos de la carga durante un episodio de corrosión [26–28], por ejemplo. Menos aún los ensayos con estructuras complejas, estructuras hiperestáticas, donde los fenómenos redistributivos juegan un papel determinante.

II.5.2 Estructuras hiperestáticas

Como se ha descrito en puntos anteriores el estudio de la corrosión en estructuras en condiciones de laboratorio, ha sido objeto de investigación durante los últimos años. Los efectos estructurales durante un proceso de corrosión en estructuras simples, son relativamente sencillos de reproducir mediante modelos más o menos complejos que incluyan en mayor o menor medida los efectos locales del deterioro. En cambio en

estructuras hiperestáticas la interacción entre las diferentes partes de la estructura dificulta en gran medida esta tarea y añade otra variable más al fenómeno.

En la actualidad se encuentran muy pocos ensayos que incluyan estructuras hiperestáticas [29]. Teniendo en cuenta que el uso de este tipo de estructuras está ampliamente extendido en la ingeniería el conocimiento del comportamiento de las mismas durante un proceso de deterioro se antoja importante i relevante.

II.5.3 Corrosión natural

En los últimos años, debido a la existencia de un parque de estructuras muy longevo en muchos países el cual ha sido objeto de ataques medio ambientales, se está intentando realizar experimentación mediante estructuras naturalmente corroídas. Si bien, es sabido que los fenómenos de corrosión mediante técnicas aceleradas no reproducen exactamente las condiciones de daño sobre la estructura de episodios de corrosión natural, no es sencillo la obtención de elementos estructurales de cierta envergadura naturalmente corroídos.

Más complejo aún es conocer el daño previo de la estructura antes de ensayar el elemento. El desconocimiento del estado de la estructura, como el nivel de corrosión de las armaduras, el daño interno del hormigón por hielo y deshielo, por ejemplo, entre muchos otros añade un número importante de variables al problema, ya de por sí, complejo.

Así mismo la obtención de estructuras naturalmente corroídas, que a priori presenta bondades por reproducir de manera real un proceso de deterioro, no permite el estudio de la estructura en servicio, importante en muchos casos para cuantificar el impacto de la corrosión de armaduras en las flechas o abertura de fisura. Esto requeriría la monitorización de estructuras existentes durante muchos años para así poder observar la evolución de los diferentes fenómenos. Algunos autores han centrado sus esfuerzos, sobre todo durante los últimos años en este campo [30,31].

II.6 Efectos locales de la corrosion

Los fenómenos locales asociados a la corrosión de armaduras se han mostrado como los causantes de las modificaciones del comportamiento estructural tanto en servicio como en rotura. Los principales efectos locales que afectan a la estructura durante la corrosión de sus armaduras son los que se detallan en los puntos predecesores.

II.6.1 Adherencia hormigón-acero

Las condiciones de adherencia entre acero y hormigón, representan la piedra angular para el correcto funcionamiento de una estructura de hormigón armado. La adherencia entre ambos materiales es la encargada de dotar al conjunto acero-hormigón de un comportamiento homogéneo, permitiendo así explotar las propiedades y bondades de ambos materiales simultáneamente. El fenómeno como tal ha sido ampliamente estudiado y de pueden encontrar numerosos estudios en la literatura donde se estudia dicho comportamiento y sus efectos en la estructura.

II.6.1.1 Mecanismos que intervienen en la adherencia entre el acero y el hormigón

La adherencia entre el hormigón y el acero se puede caracterizar por tres fenómenos:

- Adherencia por contacto: la barra y el hormigón están adheridos entre si debido al proceso de cementación o adhesión química entre ambos materiales de manera natural. Esta adherencia es la primera en desarrollarse.

- Adherencia por rozamiento: el deslizamiento relativo entre dos materiales genera un rozamiento que se opone a dicho movimiento, este rozamiento aparece de manera natural y se caracteriza por el coeficiente de rozamiento, el coeficiente $\mu = 0.3 – 0.6$, dependiendo del tipo de acero. Esta adherencia será mayor cuanto mayor sea el confinamiento de las barras de acero.

- Adherencia por acuñamiento: la presencia de las corrugas en el acero ejerce un efecto de acuñamiento entre estos y el hormigón en cuanto se produce algún tipo de movimiento relativo. Se generan sobre las corrugas una serie de esfuerzos de compresión tracción que resisten el movimiento relativo, ver Ilustración II-10.

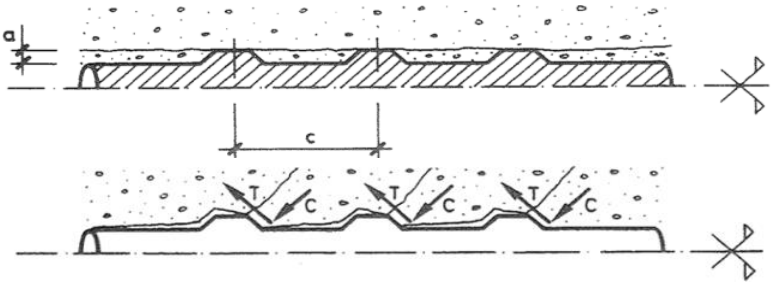

Ilustración II-10. Mecanismo de acuñamiento de armaduras

Asimismo esta adherencia tiene diferentes orígenes:

- Materiales. Por un lado los materiales son responsables de la adherencia tanto que el acero caracterizan el coeficiente de rozamiento entre ambos materiales. Además el hormigón será el encargado de resistir los esfuerzos de acuñamiento por lo que también este determinará la adherencia.

- Condiciones geométricas. Por un lado el recubrimiento de las barras definirá en gran parte el valor de la adherencia por una cuestión de confinamiento de las mismas. Por otro lado la posición de esta barra también tendrá una influencia sobre la adherencia ya que el hormigón es un material anisótropo pudiendo generar diferencia entre la adherencia de las barras longitudinales y transversales, e incluso entre partes de una misma barra, por huecos debajo de las mismas en el hormigonado.

Tipo de solicitación. El tipo de solicitación también tiene una importante influencia sobre la adherencia, ya que por ejemplo las solicitaciones de carácter repetitivo, disminuyen de manera importante la adherencia por desgaste del hormigón entre corrugas. Por otro lado las solicitaciones en dirección perpendicular a las barras aumentan la adherencia ya que favorecen el confinamiento de las mismas.

A nivel de esfuerzos, todo lo anterior se puede traducir a un equilibrio interno de la estructura entre todas las tensiones que se movilizan durante un proceso de carga de la misma. En la Ilustración II-11 se muestra un diferencial de viga sometido a una carga externa y las tensiones movilizadas:

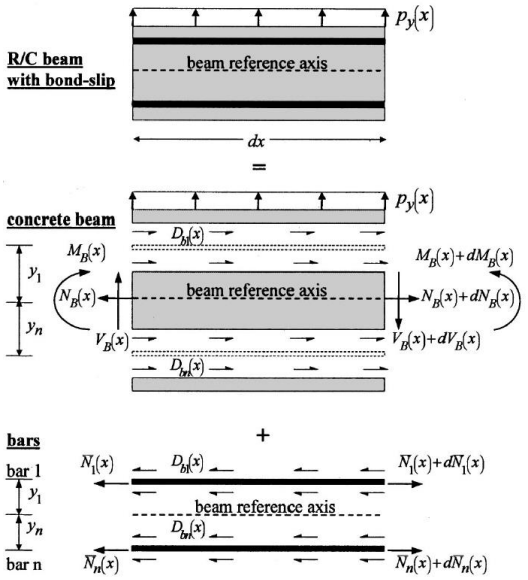

Ilustración II-11. Equilibrio de tensiones de adherencia en el elemento [32]

Como se aprecia, el hecho de someter a una carga externa la estructura, provoca la aparición de un momento flector y un cortante. Estos esfuerzos se traducen en un estado tensional sobre los diferentes elementos que deben estar en equilibrio. Sobre la barra se desarrolla una tensión superficial, que es la que llamamos tensión de adherencia. La movilización de dicha tensión es la responsable de mantener en equilibrio en las deformaciones entre el acero y el hormigón. Si no se movilizaran estas tensiones la barra podría deslizar libremente por dentro del hormigón, y trabajaría como un tirante.

II.6.1.2 Curvas bond-slip

Pero dicho mecanismo de adherencia no es perfecto, y debido al deterioro que sufre, sobretodo el hormigón circundante, a pesar de ser capaz de movilizar gran parte de las tensiones de adherencia, se produce cierto corrimiento relativo entre ambos materiales. Cualquier modificación de los mecanismos que permiten la aparición de dichas tensiones será responsable de la pérdida de adherencia de las barras. Una vez que entra el juego la adherencia por acuñamiento de las corrugas en el hormigón, el deterioro del mismo por tensiones excesivas es el máximo responsable de dicho corrimiento.

A pesar de todo, este deterioro no es aleatorio. Si bien el esquema de microfisuración, el comportamiento químico de los materiales, etc… son complicados de reproducir localmente, el comportamiento resultante, el estudio del corrimiento en función de la tensión aplicada a la armadura, es posible de reproducirse mediante ensayos de arrancamiento.

Este tipo de ensayos, nos permiten estudiar el comportamiento de un trozo de barra embebida en el hormigón, y así evaluar los efectos de la pérdida de adherencia o de corrimiento. Si se instrumenta dicha barra y se tira de ella, mediante una tensión creciente y conocida, se puede perfectamente asignar a cada tensión de adherencia un corrimiento obteniendo así una relación de τ-υ, ver Ilustración II-12.

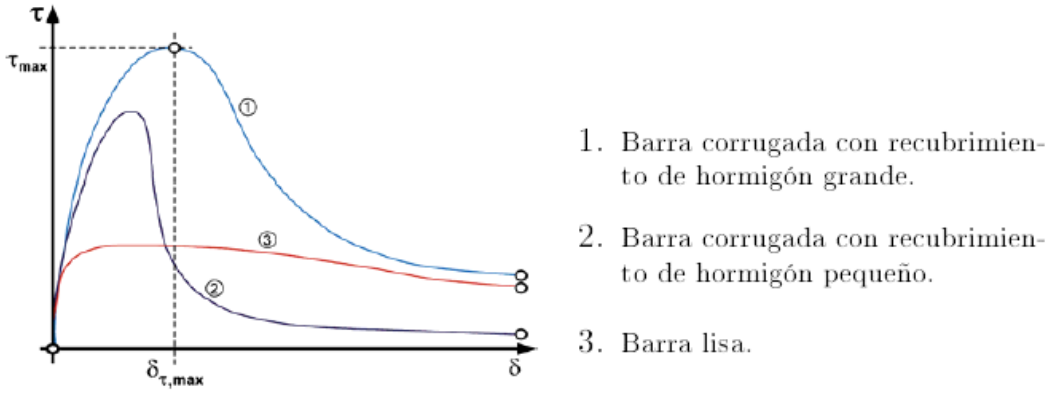

Ilustración II-12. Curvas bond-slip acero hormigón [33]

Numerosos factores determinan el comportamiento adherente entre ambos materiales. La relación geométrica entre diámetro de la barra-recubrimiento de hormigón, el tipo de barra empleado, lisa o corrugada, la separación entre barras, el diámetro de las mismas, las propiedades mecánicas del hormigón y el acero, etc… [34,35] A pesar de ello, hay cierto consenso en la literatura al respecto, en que al margen de los parámetros geométricos la resistencia a compresión del hormigón, es la que domina el fenómeno [36–38].

La obtención de dichas curvas mediante este tipo de ensayos se basa esencialmente en la hipótesis de corta longitud embebida [39,40]. Si la longitud embebida adherida en el hormigón es menor a cinco veces el diámetro de la barra, aproximadamente, es posible asumir en el marco de la hipótesis anterior, distribución de tensiones tangenciales uniformes a lo largo de la barra. La implicación directa que conlleva dicha hipótesis es la posibilidad de asumir que la fuerza aplicada a la barra, es igual a la tensión superficial sobre la barra. Mediante la Eq. [2], es posible conocer las tensiones de adherencia en función de la fuerza aplicada.

Ecuación II.2 $$\tau = P / \pi \Phi L$$

Donde, P es la fuerza aplicada a la barra, Φ es el diámetro nominal de la barra de acero, y L es la longitud embebida adherida.

En la Ilustración II-13. Modificación de la ley bond-slip considerando corrosión del acero se describe paso a paso el comportamiento de la barra, movilizando cada una de las adherencias descritas anteriormente, que definen el comportamiento de arrancamiento.

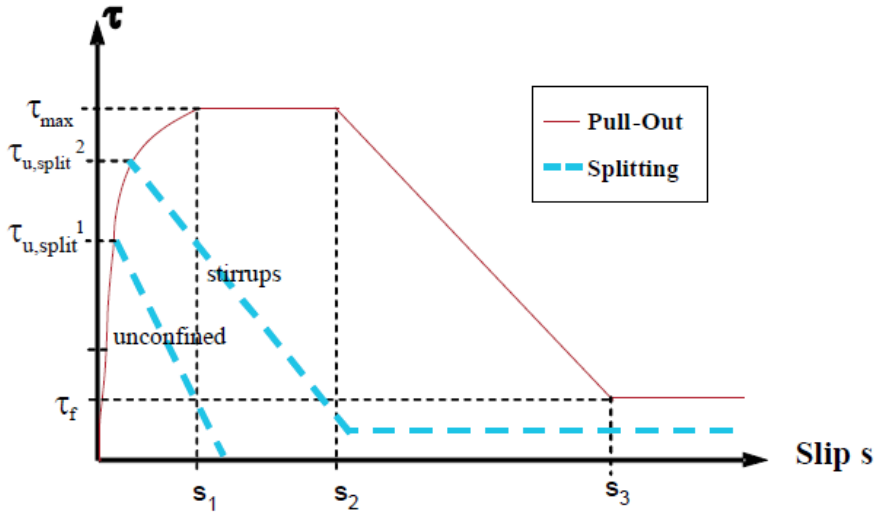

Ilustración II-13. Modificación de la ley bond-slip considerando corrosión del acero [41]

Hay que tener en cuenta que las curvas obtenidas mediante este tipo de ensayos son curvas locales de adherencia. Básicamente describen localmente en un elemento diferencial de barra y hormigón cual es la relación entre ambos materiales. Es necesario la integración de dicho comportamiento a lo largo de una sección específica de estructura para obtener el comportamiento real entre acero-hormigón.

II.6.1.3 Efectos del deterioro de armaduras en el bond-slip

Debido a la formación de la capa de óxido alrededor de las armaduras y de la obertura de la fisuración longitudinal o spalling, inevitablemente se modifican las condiciones de contorno entre el acero y el hormigón que lo envuelve, por lo que hay un fuerte impacto en la adherencia entre ambos materiales [42][43].

Se han realizado numerosos ensayos pull-out, o de arrancamiento, sometiendo a las barras de acero a corrosión acelerada, que pretenden estudiar dicho fenómeno. A pesar de ello, es un estudio complejo que requiere tener en cuenta numerosas variables, por lo que todavía no

hay un consenso claro sobre un modelo específico que permita reproducir exactamente el comportamiento apreciado [44][45]. Sin embargo si existen convenciones sobre ideas generales que envuelven el fenómeno de la adherencia y su deterioro por la corrosión de las armaduras [46].

En general la pérdida de adherencia debida a la corrosión de la barra, motiva modificaciones en cuanto al comportamiento de los parámetros descritos anteriormente. Así pues, estudiar el comportamiento adherente de una barra corroída implica entender como los parámetros anteriores se ven alterados y en qué grado, por los productos de corrosión.

En primer lugar, al margen de lo descrito hasta el momento, también es importante caracterizar el comportamiento mecánico del óxido [15]. Este es un punto importante de discusión entre la comunidad científica, y a pesar de que hay una clara tendencia que establece que el comportamiento del óxido es asimilable al comportamiento de un material granular cohesivo, no hay claro consenso al respecto. Evidentemente los modelos presentan variaciones importantes de tener a no tener en cuenta el óxido y sus características mecánicas.

En lo que sí se puede mostrar consenso es en que la capa de óxido tiene peor comportamiento que el acero original, por lo que en se puede afirmar que hay un deterioro de las propiedades adherentes acero-hormigón.

Hasta ahora se han visto los fenómenos que permiten el desarrollo de las tensiones de adherencia en el hormigón. Es evidente que la modificación de cualquiera de los parámetros que intervienen en la aparición de dichas tensiones, tendrá un efecto directo sobre las mismas.

Las propiedades de cementación entre ambos materiales se ven completamente anuladas en el momento de aparición de dicha capa de óxido, ya que las presiones resultantes de la formación de esta separan ambos materiales. La formación de una capa intermedia entre el acero y el hormigón, el óxido, impide a movilización de dicha adherencia. De todas maneras la adherencia por cementación de ambos materiales, es la primera en entrar en juego, y también la primera en deteriorarse rápidamente, en cuanto aparecen los primeros deslizamientos relativos por las solicitaciones externas.

La adherencia por rozamiento, es la que genera más controversia durante un episodio de corrosión. La formación de la capa de óxido, se interpone entre el acero y el hormigón, por lo que ahora el rozamiento entre ambos materiales depende de las propiedades mecánicas del óxido, y a su vez estas no están todavía perfectamente definidas. Entonces vemos

disminuida la capacidad adherente de nuestra barra por la aparición del óxido debido a una reducción importante del coeficiente de rozamiento, al entrar en juego, presumiblemente un material granular entre ambos materiales.

En cuanto la adherencia por acuñamiento, tenemos un proceso algo más complejo. En este caso, es importante destacar dos fases, la primera es cuando la corrosión es relativamente escasa, por lo que no se han corroído todavía las corrugas. Entonces en este caso el comportamiento del conjunto presenta una bajada de la adherencia pero no una reducción drástica de la misma, ya que todavía tenemos un cierto acuñamiento, y el hormigón no rompe por tracción resistiendo las tracciones aparecidas por el óxido y por el empuje de las corrugas

En una segunda situación, mucho más desfavorable, la oxidación ha deteriorado totalmente las corrugas. En este punto de corrosión más avanzada, tenemos dos consecuencias inmediatas. La primera de ellas, es que la pérdida de las corrugas convierte la barra en una barra tipo lisa, por lo que la única adherencia que se moviliza ante las solicitaciones sobre la estructura es la adherencia por rozamiento, que es sustancialmente inferior a la combinación de adherencia por acuñamiento más adherencia por rozamiento. En segundo lugar, otra importante consecuencia es la fisuración del hormigón por tracciones excesivas. En este punto de corrosión las tracciones sobre el mismo son ya insoportables, por lo que éste fisura como se ha descrito anteriormente, en sentido longitudinal, dejando descubierta la armadura, y además disminuyendo la capacidad adherente del conjunto por pérdida de confinamiento de la barra.

Se puede decir que en el proceso de corrosión tenemos dos puntos que caracterizan la adherencia de nuestra barra con el hormigón y que son determinantes para valorar su comportamiento, el primero de ellos es la pérdida total de las corrugas por corrosión de las mismas y el segundo es la abertura de fisuración o salto del recubrimiento (“spalling”) de los paramentos por tracciones excesivas. Estos dos instantes delimitan el comportamiento adherente de las barras en el hormigón.

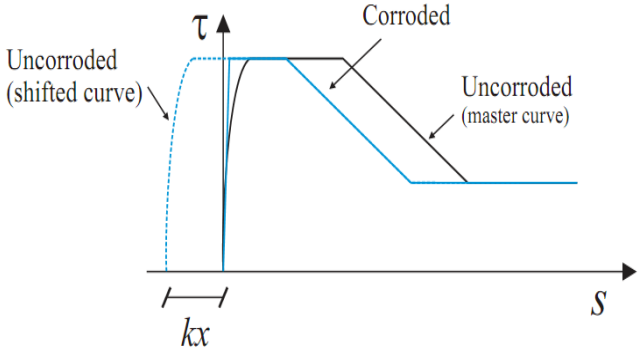

Ilustración II-14. Curva bond – slip para un acero con corrosión y otro sin corrosión [45]

La Ilustración II-14 muestra una curva tensión-deslizamiento, del comportamiento de un hormigón armado sin corroer y con corrosión en las armaduras, para un grado de corrosión específico. Este tipo de curvas se obtienen mediante ensayo de corrosión acelerada tipo pull-out.

Se aprecia claramente en la Ilustración II-14 el efecto positivo de la corrosión en las armaduras en la primera fase, donde aumenta la tensión aplicable reduciendo el deslizamiento. Sin embargo para fases más avanzadas se describe perfectamente, la disminución de la capacidad adherente de las barras, desplazando la curva de tensiones-deslizamiento hacia la izquierda.

Es cierto que hay factores externos que condicionan también la capacidad adherente de las barras en presencia de óxido. Uno de ellos, destacable ya que es muy usual, es la presencia de armadura transversal. Este tipo de armadura, generalmente dispuesta para otro tipo de solicitaciones, tiene un efecto importante sobre la adherencia de las barras. Esto se debe a que ejercen una especie de efecto confinamiento, que aumenta la capacidad del hormigón a resistir las tracciones producidas por el óxido, lo que retrasa la aparición de las fisuras o splitting, y aumenta la adherencia por confinamiento. Además la presencia de cercos dificulta también la aparición de fenómenos como el "spalling". Se ha registrado mediante numerosos ensayos que este incremento de adherencia se puede cuantificar hasta en un 20% respecto al mismo ensayo sin armadura transversal [47,48].

II.6.1.4 Efectos estructurales asociados a la pérdida de adherencia

Evidentemente la pérdida de adherencia tiene una serie de repercusiones a nivel estructural. En primer lugar, gracias a la adherencia entre el acero y el hormigón tenemos una compatibilidad de deformaciones entre ambos materiales. La mayoría de los modelos de cálculo empleados hoy en día contemplan una situación de adherencia perfecta, por lo que queda garantizada la hipótesis de compatibilidad de deformaciones. Si esta situación de por sí ya no es cierta, tal y como ha quedado reflejado, en una situación de corrosión de armaduras lo es menos. Por lo tanto, en este aspecto, el tener en cuenta en los modelos la pérdida de adherencia se antoja importante para poder reflejar los fenómenos con mayor rigor.

Se podría englobar en tres grupos los efectos derivados de la pérdida de adherencia entre el acero y el hormigón, ya sea de manera natural por la aplicación de cargas o por procesos de deterioro, como la corrosión de armaduras. Estos efectos son:

- Estado límite de servicio:
  - Flechas: La compatibilidad de deformaciones entre ambos materiales permite que el comportamiento de nuestra estructura no se asemeje al de una serie de dovelas ancladas mediante un acero pasante. Al cargar la pieza la tensión de adherencia queda movilizada por lo que las tracciones en el acero son variables, y decrecientes hacia los extremos. La movilización de esta interacción mecánica a igualdad de condiciones de carga que en la situación sin adherencia, reduce significativamente la deformación global, flechas, la abertura de las fisuras, así como la distribución de las mismas que es ahora más uniforme y distribuida.
  - Longitud de transferencia: este es otro parámetro que se ve afectado por la pérdida de adherencia. La longitud de transferencia de tensiones en armaduras queda completamente afectada si el hormigón y el acero no transmiten correctamente estas tensiones. La degradación de dicha adherencia disminuye esta capacidad por lo que aumentan las longitudes necesarias para asumir cierto valor en la tensión de adherencia.
  - Fisuras: relacionado con el punto anterior, si no se ha fisurado la estructura, se producirá un incremento en la separación de fisuras y a su vez una mayor abertura de las mismas. En cambio si la estructura ya está fisurada cuando se inicien los procesos de corrosión y pérdida de adherencia, la separación entre fisuras se mantendrá, pero el ancho de las mismas se verá notablemente incrementado.
- Estado límite último:
  - Solapes y anclajes: pérdida en la capacidad de los anclajes y solapes por el deterioro de los mecanismos de adherencia. No se pueden transmitir las tensiones necesarias para desarrollar la capacidad de anclaje necesaria por lo que se deterioran. Quizás este sea el efecto más importante en cuanto a corrosión de armaduras, ya que produce un fallo de carácter frágil y modifica el tipo de fallo esperado de la estructura.

Robustez: debido a la pérdida de la adherencia la robustez de la estructura se ve mermada, la transferencia de tensiones no se produce correctamente, el comportamiento entre acero y hormigón se deteriora de tal manera que las barras no son capaces de asumir la tensión que les corresponde por lo que se incrementan las deformaciones en el hormigón. En general se

pasa a un comportamiento más parecido al de dovelas cosidas por el acero, lo que disminuye en cierta manera la capacidad última de la estructura.

II.6.2 Modificación de las propiedades mecánicas del acero

Por último la modificación de las propiedades mecánicas del acero tiene también un fuerte impacto sobre el comportamiento estructural. Existen en la literatura estudios experimentales que hablan sobre la modificación de las propiedades mecánicas del acero debido a la corrosión [49,50].

Las barras de acero están constituidas por hierro y una pequeña parte de carbono, lo que le da unas ciertas propiedades y a lo que llamamos acero. Los procesos de fabricación de las barras y los tratamientos a los que se someten las mismas, confieren una microestructura específica a las barras. Si se estudia el comportamiento de cada una de las fases del acero, se comprueba que cada una tiene unas propiedades mecánicas diferentes y en función de cómo los porcentajes de las fases que conforman el conjunto el acero tendrán un comportamiento global u otro [49].

Actualmente en Europa se puede hablar de un sistema de conformación del acero que es el TEMPCORE. Dicho sistema de preproducción barras corrugadas para estructuras de hormigón armado, cosiste esencialmente, en aplicar un tratamiento superficial a base de vapor de agua a temperatura constante, que enfría de forma diferencial la sección de acero. La aplicación de dicho tratamiento para acelerar la producción dota al acero resultante de una microestructura peculiar. Al tener una distribución de temperaturas diferentes hacia el interior de la barra la microestructura del acero frio no es uniforme.

Generalmente debido al tratamiento, las barras de armar están constituidas por un núcleo central de ferrita y un recubrimiento de martensita. Ambas fases se caracterizan por comportamiento mecánicos diferentes. El núcleo, que se conforma a mayor temperatura, tiene una microestructura más dúctil en general. Este es capaz de alcanzar grandes deformaciones antes de romper. En contra partida, el resto de propiedades mecánicas, como el límite elástico, el módulo de elasticidad o la tensión de rotura, son relativamente bajos en comparación al valor medio que tífica el fabricante. Por otro lado, las capas más exteriores de la barra, tienen un comportamiento que se podría considerar opuesto. A cambio de un sacrificio en términos de ductilidad, se obtienen valores mucho mayores en cuanto a límite elástico o tensión de rotura, ver Ilustración II-15. Evidentemente la distribución de fases en la sección de acero no directa martensita-ferrita, Ilustración II-16. Existe también una fase

de transición entre ambos materiales, con propiedades intermedias. A efectos prácticos, dado que la fase intermedia no representa una parte significativa de la barra se puede considerar un material bicapa, martensita-ferrita.

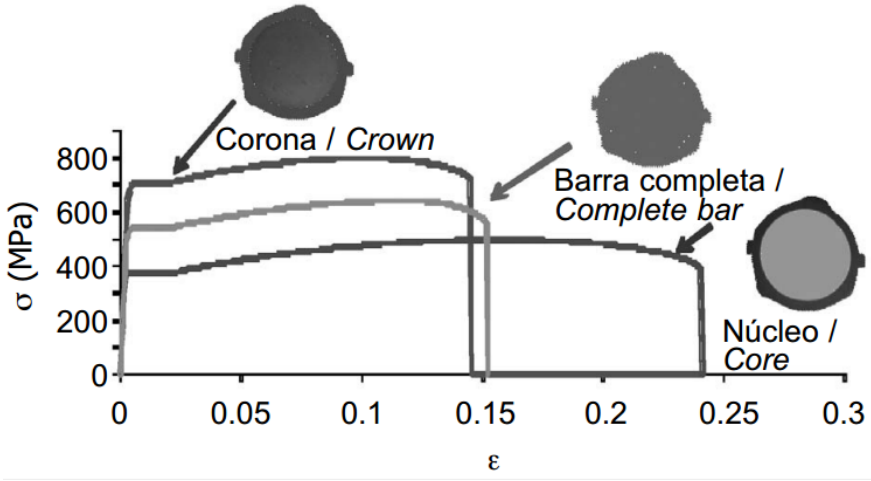

Ilustración II-15. Curvas tensión deformación para las distintas zonas de material [49]

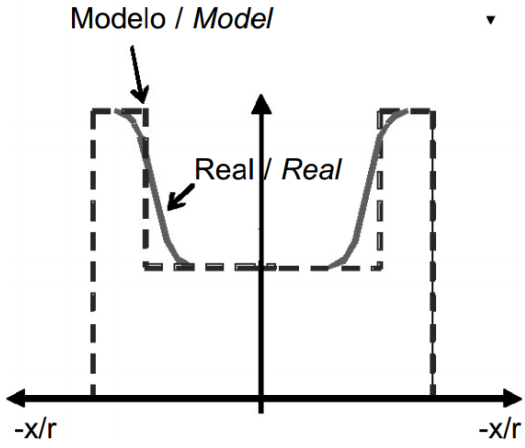

Ilustración II-16. Modelo material bi fase [49]

El valor medio del comportamiento conjunto de ambos materiales es el que resulta en las propiedades conocidas del material que se utilizan en diseño, Ilustración II-17.

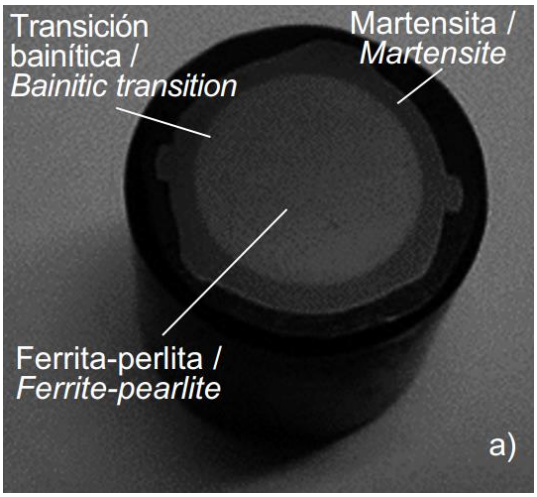

Ilustración II-17. Distribución de fases barra corrugada [49]

Generalmente para aceros convencionales la distribución de ambas fases es, la ferrita en el centro de la barra, y la martensita que envuelve a la ferrita, con lo que durante la corrosión de las mismas lo primero que se deteriora es la martensita. Este deterioro tiene unas consecuencias inmediatas en cuanto al comportamiento mecánico de la barra. No solo en términos de pérdida de área, sino que también en variación de las propiedades mecánicas medias del material. Teniendo en cuenta que la corona exterior es la encargada de dotar de resistencia al conjunto y que la corrosión actúa directamente sobre esta capa, la reducción de comportamiento ante cualquier solicitación sobre la barra, tendrá un efecto mayor que la pérdida de área propiamente.

Aunque se hable de corrosión generalizada como un fenómeno de corrosión uniforme en toda la sección de la barra, la realidad dista mucho de ser así. La corrosión generalizada no deja de ser un fenómeno de corrosión por picadura local a lo largo de toda la superficie. Esto más allá de una distribución de picaduras uniformemente repartidas tiene la implicación de que habrá zonas de la barra con un cierto valor de profundidad de picadura mayor que otras, porque las condiciones de formación de la pila habrán sido más favorables, por ejemplo. Debido a dicha distribución y pérdida de sección semiuniforme en la sección, localmente se produce un desplazamiento del centro de gravedad con respecto a la solicitación. Esto provoca una flexión local en la misma que si se suma al factor de concentración de tensiones que se produce de manera natural en el pico de las picaduras resulta en una reducción aún mayor del comportamiento mecánico de la barra.

Todos estos fenómenos deben considerarse a la hora de evaluar los efectos estructurales de la corrosión en una estructura. Más si se pretende modelar dichos fenómenos y predecir el comportamiento de una estructura en el tiempo, bajo condiciones de deterioro.

II.7 Simulación numérica del deterioro

El comportamiento estructural de las estructuras de hormigón armado bajo niveles de carga avanzados, difiere de manera importante del comportamiento elástico-lineal clásico, asumido como válido. Para niveles de carga últimos el comportamiento de dichas estructuras es altamente no-lineal, consecuencia de varios fenómenos. La fisuración en tracción, la fluencia y retracción del hormigón, la plastificación del acero, la adherencia imperfecta y sobretodo la no-linealidad de los materiales, principalmente del hormigón. Por otro lado fenómenos en elementos esbeltos, también pueden dar lugar a fenómenos de 2º orden y comportamiento geométricamente no lineal. Además estos fenómenos no actúan aisladamente sino que se producen durante la vida útil de una estructura de manera conjunta, interaccionando entre sí, afectando de forma importante el estado tensional, esfuerzos y deformaciones.

En el diseño de una estructura es importante satisfacer las condiciones de seguridad necesarias además de las condiciones de servicio. Ambos parámetros deben cumplirse satisfactoriamente en el proyecto de cualquier estructura. En cuanto a las condiciones de servicio, es importante predecir con exactitud los desplazamientos, tensiones y deformaciones, etc… durante su vida útil bajo cargas de servicio. Para las condiciones de seguridad frente a fallo, es importante una precisa estimación del comportamiento de la estructura a través de los rangos, elástico, plástico y último para obtener fiablemente la carga última.

Para el estudio estructural básicamente se dispone de dos caminos; el estudio experimental y el estudio analítico. Ambos métodos se deben considerar complementarios el uno del otro. A pesar de ello, el desarrollo tecnológico vivido a lo largo de los últimos años ha desembocado en un aumento importantísimo de las posibilidades a nivel de cálculo computacional. El desarrollo de métodos numéricos, sobre todo los elementos finitos (EF), juega un papel crucial en el análisis de estructuras de hormigón armado.

Desde las primeras aplicaciones de elementos finitos, diferentes estudios han ido cubriendo los diferentes aspectos del comportamiento estructural de las estructuras de hormigón. Estos estudios se podrían englobar en tres grandes grupos:

- Modelización de las propiedades del material: ecuaciones constitutivas, estados de tensión multiaxial, comportamiento dependiente del tiempo, etc…
- Estudios a nivel micro estructural: bond-slip, transferencia del cortante, tensión stiffening, efectos locales, etc…

- Estudios a nivel macro estructura: que pretenden modelar el comportamiento estructural global preferiblemente a efectos locales.

En el campo de estructuras de hormigón armado, la mayoría de estudios se han centrado en la modelización de estructuras mediante estructura de barras planas. Muchos autores han incorporado en dichos modelos, los fenómenos de fluencia y retracción, bond-slip, no linealidad geométrica, etc… así como modelos que incorporan la no-linealidad de los materiales y de la geometría conjuntamente.

Más adelante se añaden a la lista modelos basados en barras tridimensionales, que incorporan también los fenómenos citados.

II.7.1 Modelos locales

Los modelos locales, a grandes rasgos, son aquellos que pretenden desarrollar y modelar comportamientos concretos de fenómenos específicos en la estructura. En general lo que pretenden es dar una respuesta precisa y completa a un fenómeno determinado.

Este tipo de modelos son importantes ya que permiten analizar singularidades y comportamientos locales muy complejos, que a su vez pueden servir para entender el comportamiento general de una estructura. Hay muchos fenómenos que se pueden estudiar mediante modelos locales complejos, en los cuales se tienen en cuenta muchos parámetros que caracterizan los sucesos, o mediante modelos globales más sencillos, pero que recogen el comportamiento general del fenómeno.

Un claro ejemplo de esto se da en el estudio de la fisuración. La fisuración por flexión de una estructura se puede estudiar, como fisuración distribuida de manera global, caracterizando un ancho de fisura y una separación media entre ellas. Así mismo se podría analizar el fenómeno a partir del comportamiento local del material, simulando la abertura de la misma en función de las tensiones sobre el hormigón y la energía de fractura, por ejemplo.

II.7.1.1 Modelos de adherencia hormigón-acero

Dentro del campo de la adherencia en el hormigón, se han desarrollado un gran número de modelos, los cuales pretenden dar respuesta a los fenómenos que suceden en el contacto entre ambos materiales. Como se ha visto este contacto es muy complejo e intervienen muchos factores, que caracterizan el comportamiento adherente.

Además de desarrollarse modelos para simular la adherencia, también existen otros modelos más complejos aún, para incorporar el deterioro de las barras de acero por corrosión de las mismas. Ya se ha visto que la corrosión del refuerzo de acero tiene un efecto directo sobre la adherencia, por lo tanto es importante estudiarlo a fondo.

Un gran número de investigadores se han centrado en el desarrollo de modelos de carácter local, modelos complejos, generalmente en tres dimensiones, que caracterizan por completo las zonas afectadas, la interface hormigón-acero, la fisuración, el cambio de las propiedades del acero por corrosión, la aparición del óxido, la dispersión del mismo entre los poros y fisuras del hormigón, etc…

Un modelo propuesto por [51] considera el fallo de adherencia por "splitting". Posteriormente fue modificado por [52] para tener en cuenta a corrosión de las armaduras. El modelo presentado por [51] propuesto para barras no corroídas, asume el fallo por adherencia de las mismas cuando la tensión cortante en la interface supera la fricción y la adhesión entre la corruga y el hormigón. En la Ilustración II-18 se muestran las fuerzas que intervienen en la cara de la corruga.

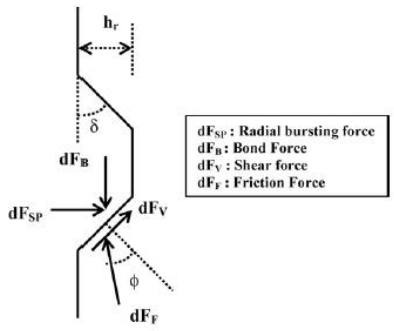

Ilustración II-18. Esfuerzos sobre la corruga [53]

La evaluación de la tensión última de adherencia en el modelo planteado es función de la presión máxima en fallo por adherencia y una constante que depende de las características de los materiales, como rozamiento interno del hormigón y corruga, área de la misma, etc…

El modelo para barras no corroídas es modificado posteriormente por [52] para incluir los efectos de la corrosión de las armaduras. La corrosión modifica todos los parámetros que afectan a la corruga, ya que modifica su geometría, además de que también tiene efectos sobre las tensiones de adhesión y fricción.

Con posterioridad [54][55] modifican el modelo propuesto por [51] añadiendo nuevos parámetro para la evaluación de la tensión de adherencia última.

En trabajos posteriores realizados por [56], se proponen metodologías para la evaluación de los diferentes parámetros que intervienen en la fuerza de adherencia. Se propone una metodología para predecir la presión causada por la expansividad de los productos de corrosión y a través de la capa microfisurada entorno a la barra. También como modelar el comportamiento de la tensión del hormigón fisurado, evaluando la presión máxima en fallo por adherencia.

[57], plantea un modelo teórico para simular la adherencia mediante un modelo friccional, añadiendo elementos de interface entre el hormigón y el acero, basados en la teoría elasto-plástica para describir las tensiones y deformaciones. Estos elementos "layer" están caracterizados por las tensiones normal y tangencial y los desplazamientos normal y tangencial. Las líneas de plastificación se determinan mediante funciones de plastificación que describen por un lado la fricción entre la los materiales y por el otro las tensiones derivadas del cono de tensiones resultante de la adherencia. Dicho estudio también plantea añadir una tercera componente al modelo, una tensión en dirección alrededor de la barra independiente del resto, para el modelado en 3D. El modelo propone unas zonas definidas como zonas deformadas dañadas/no dañadas, que contemplan la variación del valor del rozamiento con la barra, por "crushing" de las zonas de hormigón situadas en el entorno de la corruga, debido a acciones actuando en las dos direcciones.

Poco después de nuevo [58], incorpora al modelo presentado anteriormente los efectos del deterioro por corrosión. Para incorporar dicho efecto divide el desplazamiento normal a la barra en dos componentes, una debido a la adherencia y la otra a la corrosión (óxido expansivo). Así divide la capa de adherencia en dos, una capa que sería la planteada en el modelo original de adherencia, y otra nueva que sería la de corrosión. El incremento de volumen del acero por su corrosión se caracteriza mediante dicha tensión normal. La caracterización mecánica del óxido se adopta como un conjunto de cristales sin cohesión aunque apunta la dificultad de encontrar en la bibliografía una caracterización de este material. [59], emplean modelos de fisuración de otros ensayos tipo pull-out recogidos en la bibliografía y establecen una relación entre la fisuración y la deformación del óxido, que suponen en equilibrio con el hormigón circundante. Como la rigidez del acero es mucho mayor que la del hormigón consideran que este no se deforma por lo que toda la deformación por el incremento de volumen es absorbida por el hormigón.

Más adelante [58] ofrece una mejora del modelo para corregir ciertos problemas en casos de carga y descarga cíclicos.

[41] añade al modelo propuesto por Lundgren, el fenómeno de dispersión del óxido entre las fisuras y poros. Esto permite tener en cuenta el fenómeno de "despresurización" de la zona circundante a la armadura por la salida de dichos productos de corrosión hacia el exterior a través de las fisuras. También permite tener en cuenta de una manera más precisa el proceso de corrosión hasta fisuración.

En otro orden de modelos encontramos los modelos globales, o modelos más generales que pretenden la evaluación estructural de una manera conjunta, evaluando la interacción de diferentes fenómenos y encajándolos en un comportamiento general. Con este tipo de modelos se puede analizar los efectos que provoca sobre una estructura un episodio concreto de corrosión de armaduras, conjuntamente a otros fenómenos como fluencia retracción, etc…

Se pueden destacar entre este tipo de modelos, los que caracterizan la adherencia como una serie de muelles no lineales con una constante k de muelle, equivalente a la curva bond-slip, ver Ilustración II-19. Entre los más interesantes en este campo el propuesto por [60], destaca especialmente. Posteriormente una modificación del modelo propuesta por [61] incorpora mejoras en la formulación.

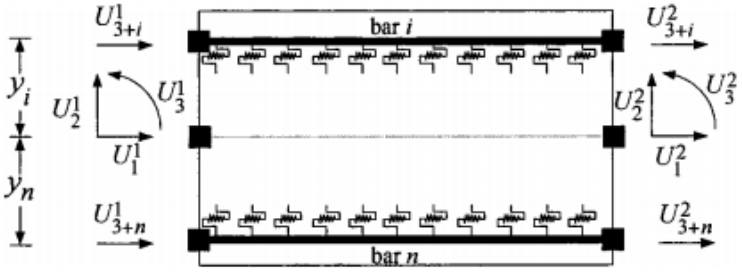

Ilustración II-19. Modelo de muelles bond-slip [62]

Claramente un modelo u otro implicarán un comportamiento diferente de la estructura, a pesar de que ésta solo se pueda comportar de una única forma.

Otro ejemplo de esto sería el estudio de la adherencia entre la barra y el hormigón, o lo que también es llamado como "bond-slip". En este caso un modelo local permitiría el estudio específico en el entorno de la barra. Permitiría conocer el comportamiento con precisión del hormigón que rodea la barra, determinar el estado tensional, multiaxial, del mismo y predecir la posible aparición de microfisuras por tracciones excesivas. Con un modelo local se podría introducir la geometría de la barra y estudiar exactamente la distribución de tensiones que provoca, por ejemplo en un ensayo pull-out.

El principal inconveniente de este tipo de modelos es su alto coste computacional y la complejidad de los modelos. El hecho de tratarse de modelos tan complejos, añade un gran número de variables, que de alguna manera dificultan la solución del problema. Así pues el empleo de este tipo de modelos generalmente queda relegado a estudios específicos de zonas concretas de la estructura, de los cuales sea de especial interés obtener información más completa y detallada de los fenómenos que se producen. Si bien es cierto que con el tiempo la evolución de la tecnología informática permite el desarrollo de modelos aún más complejos que se resuelven mucho más rápido, el uso de estos modelos no siempre resulta óptimo si lo que se quiere es evaluar una estructura en su conjunto o conocer el comportamiento global de la misma.

II.7.2 Modelos globales

Por otro lado están los modelos globales. Este tipo de modelos en contraposición de los modelos locales, procuran estudiar de manera general el comportamiento de una estructura. No pretenden centrarse en efectos locales producidos por fenómenos concretos, sino que integran de manera general el efecto estructural de los diferentes fenómenos para compatibilizarlos y mostrar el comportamiento global de la estructura.

El desarrollo de este tipo de modelos es importante ya que de alguna manera permiten estudiar el comportamiento de una estructura bajo diferentes estados de carga y bajo diferentes condiciones, ofreciéndonos una predicción muy ajustada del comportamiento a todos los niveles. La ventaja que ofrecen este tipo de modelos es, generalmente, que no son tan complejos como los modelos locales, por lo que permiten evaluar estructuras grandes, bajo estados de carga complejos, variables en el tiempo por ejemplo, y obtener resultados suficientemente aproximados como para considerarlos válidos. Como consecuencia el coste computacional requerido por estos modelos es a priori inferior, permitiendo su uso de manera más cómoda y sencilla. Además estos modelos pueden utilizar modelos locales de determinados fenómenos para incorporar en los resultados los efectos sobre la estructura de fenómenos específicos.

Por lo general la pretensión de dichos modelos es la evaluación estructural en términos globales, el estudio de deformaciones, esfuerzos, cargas, pérdida de adherencia, etc… y conocer los efectos estructurales de los mismos sobre las estructuras de hormigón armado. Así pues no se pretende evaluar los fenómenos localmente sino que se pretende integrar sus efectos sobre el conjunto de una estructura y con ello predecir su comportamiento y evaluar

por ejemplo su seguridad frente al fallo, capacidad, cumplimiento de los Estados Límite, etc…

Por lo general serán este tipo de modelos los que se emplearán a la hora de analizar estructuras complejas, y se respaldarían mediante modelos locales de algún fenómeno del que fuera especialmente interesante conocer su comportamiento más exacto a nivel micro, por su relevancia en la estructura.

II.8 Descripción del modelo CONS disponible en la actualidad

El modelo CONS es un modelo numérico para el análisis de estructuras de hormigón armado que tiene en cuenta la no linealidad geométrica, la no linealidad de los materiales y la dependencia del tiempo. Es un modelo que se puede llamar de "barras", donde la geometría de la estructura se esquematiza mediante barras en tres dimensiones, con sección arbitraria, y teniendo en cuenta los efectos de la dependencia de la historia de cargas, historia de temperaturas, fluencia, retracción, envejecimiento del hormigón, relajación del acero así como deterioro de las armaduras. El modelo permite la evaluación de la estructura y la predicción de la respuesta de la misma a través de su vida útil bajo una historia de cargas en su rango elástico, inelástico y carga última.

El modelo CONS emplea barras de hormigón armado esquematizadas mediante un conjunto de filamentos. El elemento empleado tiene 6 grados de libertad en cada uno de los extremos y un grado de libertad extra interno, en el centro del elemento que se elimina por condensación. Este elemento puede definirse con cualquier sección tipo, definida mediante una matriz de forma especial.

Los filamentos de acero, que representan las armaduras, se consideran sujetos a un estado de deformación uniaxial. Para el hormigón, se emplea una aproximación de la tensión-deformación parabólica-lineal. Para el acero se emplea una aproximación bilineal.

Para la solución del problema mediante las ecuaciones no lineales se puede emplear control por carga o control por desplazamiento, lo que permite trazar la curva completa de carga-desplazamiento.

II.8.1 Modelación de las propiedades del material

El comportamiento de los materiales que conforman las estructuras de hormigón armado, es muy complejo. Las principales causas de esta complejidad son:

- La heterogeneidad del hormigón
- La no linealidad in la tensión-deformación de los materiales, además de la diferencia en el comportamiento del hormigón para compresiones y tracciones.
- La dependencia del tiempo y del entorno para el hormigón.
- Las características de carga y descarga del hormigón y acero.
- La adherencia imperfecta entre los materiales.
- Comportamiento discreto de la fisuración, efecto "tension stiffening".

- Fricción entre las caras internas de las fisuras, etc…

El modelo CONS hace una serie de suposiciones en cuanto a la modelación de los materiales.

El hormigón se considera un material homogéneo a nivel macroscópico, del cual se pueden determinar las propiedades. El acero, es un material homogéneo a todos los efectos, el cual además tiene sus propiedades generalmente bien definidas.

En una primera instancia el modelo supone adherencia perfecta entre el acero y el hormigón, así que el campo de desplazamientos se puede considerar continuo en toda la sección.

Las deformaciones en el hormigón se consideran uniaxiales. Estas deformaciones están compuestas por una parte de la deformación mecánica y otra parte de la deformación no mecánica:

Ecuación II.3 $$\boldsymbol{\varepsilon(t) = \varepsilon^{m}(t) + \varepsilon^{nm}(t)}$$

Donde $\varepsilon^{nm}(t) = \varepsilon^{c}(t) + \varepsilon^{s}(t) + \varepsilon^{a}(t) + \varepsilon^{t}(t)$

La deformación mecánica depende directamente de la tensión y se puede obtener mediante la ecuación constitutiva del hormigón:

Ecuación II.4 $$\boldsymbol{\sigma(t) = f(\varepsilon^{m}(t))}$$

Las deformaciones no mecánicas corresponden a:

$\varepsilon^{c}(t)$, deformación debida a la fluencia

$\varepsilon^{s}(t)$, deformación debida a la retracción

$\varepsilon^{a}(t)$, deformación debida a la edad o envejecimiento

$\varepsilon^{t}(t)$, deformación debida a la temperatura

La relación tensión-deformación o también llamada ecuación constitutiva del hormigón que emplea el modelo es la sugerida por Hognestad.

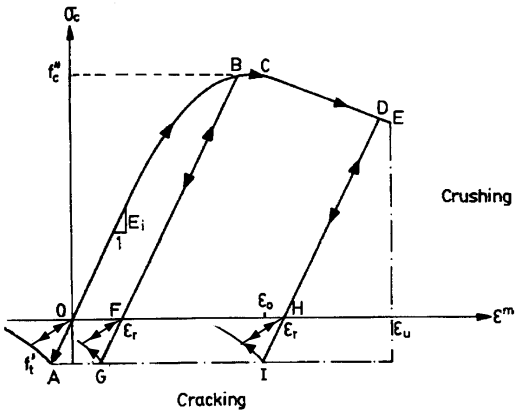

Ilustración II-20. Curva tensión deformación para el hormigón modelo CONS [63]

Esta ecuación constitutiva no contempla los efectos dinámicos de cargas como la sísmica o el viento. Si considera por eso, la carga y descarga de una historia de cargas activa, o por ejemplo de la temperatura. Esto se hace mediante un modelo reversible de carga simple de la curva tensión-deformación. La Ilustración II-20 muestra el modelo empleado en el CONS.

El modelo presentado asume las siguientes hipótesis:

1- La pendiente en el camino de descarga es idéntica a la carga, con el mismo módulo de elasticidad.
2- La tensión de rotura o de fisura del hormigón ocurre cuando la tensión excede su máximo f_{ct}.
3- La ruptura por compresión excesiva o "crushing" del hormigón ocurre cuando la deformación en el hormigón es superior a su máxima ε_u.
4- Una vez fisurado el hormigón este ya no puede absorber ninguna tensión a tracción. Sin embargo si puede resistir a compresión cerrándose la fisura y recargando. Lo que es lo mismo, se asume que la fisura se cierra en compresión y se abre en tracción sin oponer resistencia alguna.

El acero, a diferencia del hormigón no modifica sus propiedades a lo largo del tiempo, ni por el entorno. Además su comportamiento es aproximadamente simétrico en compresión y tracción por lo que su ecuación constitutiva será simétrica. Para simplificar se puede asumir que el comportamiento del acero es bilineal, con una rama elástica y otra plástica. En la Ilustración II-21 se puede observar el modelo constitutivo empleado para el acero en el CONS:

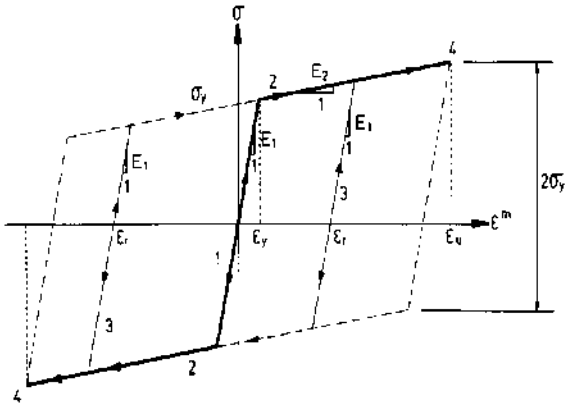

Ilustración II-21. Curva tensión deformación acero modelo CONS [63]

La pendiente del camino de regreso se supone idéntica al módulo de deformación inicial. Además el camino de regreso para la carga permanece siempre dentro de la envolvente punteada en la Ilustración II-21.

II.8.2 Modelación de la geometría

Como se ha anunciado con anterioridad el modelo CONS, es un modelo de barras en tres dimensiones. La idealización de la estructura consiste en barras unidimensionales, interconectadas entre sí mediante nudos. Cada elemento se supone prismático de longitud L y tiene una sección aleatoria definida por el usuario. La geometría del elemento se puede ver en la Ilustración II-22:

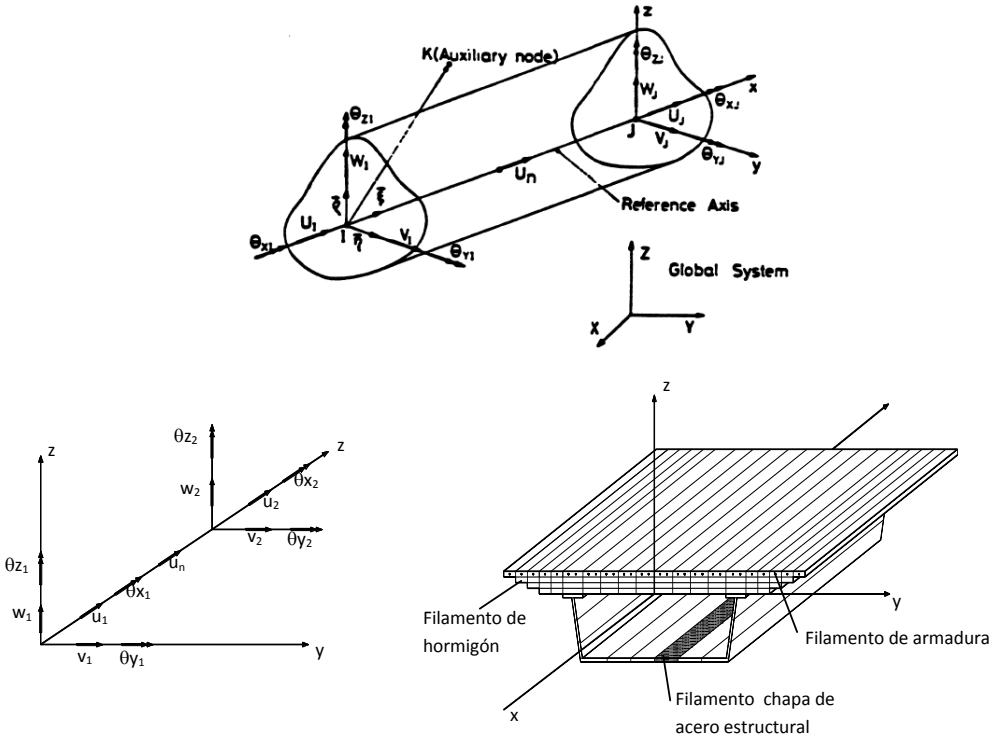

Ilustración II-22. Definición geométrica del modelo CONS [63]

La sección del elemento como se ha descrito puede ser arbitraria, sólida o con huecos. Para su definición se divide en un número discreto de trozos de hormigón, trapezoidales. Cada uno de estos trapecios a su vez se discretiza por un número finito de filamentos, que se posicionan en función de las coordenadas de los trapecios. Finalmente se obtienen un conjunto de filamentos a lo largo de la sección que definen completamente a ésta.

II.8.3 Formulación del elemento finito

El campo de desplazamiento del elemento viga se aproxima mediante funciones polinómica de orden tres, tanto para los desplazamiento transversales y rotacionales, como corresponde al elemento Hermitiano. Para los desplazamientos axiales la aproximación del campo de desplazamientos es mediante una función parabólica, pudiendo así representar la variación lineal de deformaciones axiales, como corresponde a casos donde hay fisuración (con el correspondiente desplazamiento del eje neutro) o cuando no se utiliza el centro de gravedad de la sección como eje de referencia. Para ello es necesario emplear un grado de libertad adicional en el centro del elemento, que se elimina por condensación estática posteriormente.

Las deformaciones axiales de cada una de las fibras se obtiene a partir de las deformaciones seccionales generalizadas (una deformación axial en el eje de referencia y dos curvaturas) mediante la hipótesis de deformación plana de las secciones. Por compatibilidad de deformaciones se considera que la adherencia entre los materiales es perfecta.

Así la matriz de rigidez elástica resultante del elemento, mediante la técnica de los elementos finitos resulta der:

$$\boldsymbol{K_e = \iiint_V \; B^T \cdot E \cdot V \cdot dV} \quad \textbf{(ec.) 1}$$

Dónde, E representa el módulo tangente de cada material, que depende de su estado deformacional (fisuración, plastificación o agotamiento) y B es la matriz que relaciona desplazamientos nodales y deformaciones en los puntos de Gauss y σ son las tensiones en cada fibra.

El vector de cargas internas en el elemento equivalentes al estado tensional en el hormigón y el acero puede evaluarse a través de:

$$\boldsymbol{R^i = \iiint_V \; B^T \cdot \sigma \cdot dV} \quad \textbf{(ec.) 2}$$

El vector de cargas equivalente debido a deformaciones no mecánicas ε^{nm}, se calcula mediante la expresión:

$$\boldsymbol{R^{nm} = \iiint_V \; B^T \cdot E \cdot \varepsilon^{nm} \cdot dV} \quad \textbf{(ec.) 3}$$

Las propiedades de los materiales para cada instante y nivel de carga dependen de las relaciones tensión-deformación no lineal mostrada anteriormente, de la existencia de fisuración, plastificación, agotamiento o de los estados de carga y descarga. Estos vectores y matrices se obtienen integrando numéricamente la contribución de cada uno de los filamentos, avaluando la función a integrar en las dos secciones de Gauss consideradas.

El modelo permite también considerar los efectos de la no linealidad geométrica, actualizando las coordenadas de los nodos a medida que se deforma la estructura e introduciendo la matriz de rigidez geométrica.

II.8.4 Estrategia para la solución del problema no lineal en el tiempo

Para captar el comportamiento no lineal durante construcción y a lo largo de toda la vida útil de la estructura, el dominio de tiempo se divide en diferentes intervalos que se utilizan para realizar un proceso de avance paso a paso en el tiempo, en el que los incrementos de

desplazamientos y deformaciones se van acumulando sobre los obtenidos en los escalones anteriores. Para realizar este proceso se definen cuatro grupos de ciclos que permiten la determinación de dichos desplazamientos y deformaciones. Cada uno de los ciclos encierra al anterior:

- Etapas constructivas, que son operaciones que implican cualquier modificación en el esquema estructural o sistema de cargas, como son la colocación o retirada de apeos o tirantes provisionales, el tesado de tendones, hormigonados sucesivos de la sección, etc. Ello se consigue permitiendo cambios en las condiciones de apoyo, en las vinculaciones entre elementos, colocación y retirada de elementos, armaduras o partes de sección, tesado o destesado de tirantes y tendones de pretensado. De esta manera pueden reproducirse los procesos de construcción más usuales y también posteriores modificaciones durante su vida útil.
- Pasos de tiempo, que es cada uno de los subintervalos en que se divide el período de tiempo transcurrido entre etapas constructivas. En cada paso de tiempo se actualizan las propiedades de los materiales, la matriz y el vector de cargas. Asimismo se evalúan los incrementos de deformaciones diferidas $\Delta\varepsilon_{nm}$ que han tenido lugar durante el intervalo de tiempo de t_{n-1} a t_n, y mediante la expresión (1), el vector de incremental de cargas equivalentes ΔR^{nm} en el instante t_n, se obtiene añadiendo el vector incremental de cargas nodales exteriores ΔR_{in}, el vector de cargas desequilibradas R^{u}_{n-1} procedente del intervalo de tiempo anterior t_{n-1} y el vector incremental de cargas debido a deformaciones no mecánicas $\Delta R_n{}^{nm}$.

$$\Delta R_n = \Delta R_n^i + \Delta R_n^{nm} + R_{n-1}^u \text{ (ec.) 4}$$

- Escalones de carga o de desplazamiento controlado, que permiten introducir la carga gradualmente y trazar la respuesta estructural (curva P-δ) en los rangos elástico, fisurado y de prerotura. Los factores de carga pueden ser diferentes para acciones directas, pretensado y desplazamientos impuestos. Este sistema, unido a las etapas constructivas, permite introducir secuencias de carga predeterminadas, como es el caso de peso propio inicial y sobrecarga después.

Iteraciones, orientadas a satisfacer las condiciones de equilibrio, compatibilidad y relaciones constitutivas de los materiales. En cada iteración se introducen sobre la estructura unas cargas residuales o desequilibradas procedentes de los efectos no lineales, al comparar la solicitación con la respuesta interna. Se establecen diversas estrategias de análisis no lineal

orientadas a lograr la convergencia del proceso iterativo y a disminuir el tiempo de cálculo y un criterio de convergencia basado en consideraciones estratégicas.

II.8.5 Modelo de deterioro: consideraciones de los efectos del deterioro e intervenciones para refuerzo

La reparación y el refuerzo de una estructura son intervenciones en la misma que suelen implicar modificaciones en su geometría, en las cargas, en el comportamiento de los materiales o en las vinculaciones. El planteamiento paso a paso del modelo matemático desarrollado permite tener en cuenta estas intervenciones. Para ello se especifican algunos aspectos en la lectura de datos, como son:

- Cada trapecio de una sección transversal puede ser de un hormigón diferente, del cual se define el día en que se fabrica, el día en que se demuele y el día en que se repara inyectando las fisuras.
- Para cada armadura pasiva se define el día en que se coloca en las estructuras y el día que se demuele o retira.
- De cada elemento se especifica qué día se ensambla en la estructura y qué día se retira.
- Las condiciones de apoyo, así como las vinculaciones entre elementos pueden cambiar en cada etapa constructiva.
- Cada tendón de pretensado puede tesarse, destensarse o retesarse a lo largo del tiempo. Por tanto, en cada etapa constructiva se definen aquellos tendones que se tesan, retesan o destensan.

La colocación de una nueva armadura, filamento de hormigón o barra estructural implica únicamente incorporar su rigidez a la estructura y activar algunos grados de libertad. La retirada o demolición de un elemento estructural requiere la introducción, como cargas, de los esfuerzos en extremos de la barra que se retira, y la desactivación de algunos grados de libertad. A partir de estos principios, se pueden simular, entre otros los siguientes procesos de deterioro y de intervención:

- **Degradación de las propiedades de los materiales**. Al igual que en casos sin degradación, el hormigón va envejeciendo y modificando su resistencia y su rigidez, puede definirse una ley de degradación de las propiedades mecánicas y tener en cuenta la ecuación constitutiva en cada instante para obtener las

tensiones bajo nuevas cargas aplicadas, así como los efectos de estos cambios a través de la deformación ficticia de "envejecimiento".

- **Saneado de recubrimientos**. Suele implicar no solo una pérdida de sección de hormigón sino también de acero de las armaduras pasivas. Su simulación consiste en especificar que el hormigón del recubrimiento se elimina a una edad determinada. La pérdida de sección de armadura se simula eliminando la porción de área de acero eficaz correspondiente.
- **Inyección de fisuras**. Si un hormigón fisurado se repara con esta técnica se supone que vuelve a resistir tracciones. Por tanto se trata de una modificación de la ecuación constitutiva.
- **Recrecido con mortero y armaduras o mediante encolado de chapa metálica o laminado de FRP**. Puede simularse especificando que un conjunto de filamentos de hormigón y armaduras se colocan a una determinada edad. La chapa se considera una armadura más, de un acero de calidad distinta a las barras corrugadas. Si se trata de un laminado de fibra de carbono, lo único que varía son las propiedades mecánicas a introducir para ese material.
- **Pretensado exterior**. Se simula especificando que ciertos tendones se introducen y tensan en un instante determinado. El pretensado introduce un sistema de cargas autoequilibrado que puede cerrar fisuras y modificar el estado de tensiones, deformaciones y reacciones de la estructura.
- **Apeos, desapeos y movimientos impuestos**. Se simulan gracias a la posibilidad de modificar a lo largo del proceso paso a paso, las condiciones de vinculación de la estructura.

Referencias

[1] Tutti K. Corrosion of steel in concrete 1997:6–15. doi:10.4324/9780203414606_chapter_2.

[2] Broomfield J. Corrosion of steel in concrete: understanding, investigation and repair. 2nd Ed. Abingdon, United Kingdom: Taylor & Francis; 2002.

[3] Bertolini L, Elsener B, Pedeferri P, Polder R. Corrosion of Steel in Concrete. Prevention, Diagnosis, Repair. Weinheim, Germany: Wiley-VCH Verlag GmbH & Co. KGaA; 2004.

[4] Anstice DJ, Page CL, Page MM. The pore solution phase of carbonated cement pastes. Cem Concr Res 2005;35:377–83. doi:10.1016/j.cemconres.2004.06.041.

[5] Fontana G, Greene ND. Corrosion Engineering. New-York: McGraw-Hill; 1967.

[6] Pourbaix M. Atlas of electrochemical equilibria in aqueous solutions,. Oxford ;New York: Pergamon Press; 1966.

[7] Montemor M., Simões AM., Ferreira MG. Chloride-induced corrosion on reinforcing steel: from the fundamentals to the monitoring techniques. Cem Concr Compos 2003;25:491–502.

[8] Angst UM, Elsener B, Larsen CK, Vennesland Ø. Chloride induced reinforcement corrosion: Electrochemical monitoring of initiation stage and chloride threshold values. Corros Sci 2011;53:1451–64.

[9] Model Code 2010. Final Vers. 2012.

[10] Costa A, Appleton J. Chloride penetration into concrete in marine environment—Part I: Main parameters affecting chloride penetration. Mater Struct 1999;32:252–9.

[11] SHERMAN MR, MCDONALD DB, PFEIFER DW. Durability aspects of precast prestressed concrete. Part 2: Chloride permeability study. PCI J n.d.;41:76–95.

[12] Angst U, Elsener B, Larsen CK, Vennesland Ø. Critical chloride content in reinforced concrete — A review. Cem Concr Res 2009;39:1122–38. doi:10.1016/j.cemconres.2009.08.006.

[13] Ann KY, Song H-W. Chloride threshold level for corrosion of steel in concrete. Corros Sci 2007;49:4113–33. doi:10.1016/j.corsci.2007.05.007.

[14] Stansbury E, Buchanan R. Fundamentals of electrochemical corrosion. Ohio, USA: ASM International; 2000.

[15] Caré S, Nguyen QT, L'Hostis V, Berthaud Y. Mechanical properties of the rust layer induced by impressed current method in reinforced mortar. Cem Concr Res 2008;38:1079–91. doi:10.1016/j.cemconres.2008.03.016.

[16] Zhao Y, Ren H, Dai H, Jin W. Composition and expansion coefficient of rust based on X-ray diffraction and thermal analysis. Corros Sci 2011;53:1646–58. doi:10.1016/j.corsci.2011.01.007.

[17] Andrade C, Alonso C, Molina FJ. Cover cracking as a function of bar corrosion: Part I-Experimental test. Mater Struct 1993;26:453–64. doi:10.1007/BF02472805.

[18] Yalciner H, Eren O, Sensoy S. An experimental study on the bond strength between reinforcement bars and concrete as a function of concrete cover, strength and corrosion level. Cem Concr Res 2012;42:643–55. doi:10.1016/j.cemconres.2012.01.003.

[19] Val D V., Chernin L, Stewart MG. Experimental and Numerical Investigation of Corrosion-Induced Cover Cracking in Reinforced Concrete Structures. J Struct Eng 2009;135:376–85. doi:10.1061/(ASCE)0733-9445(2009)135:4(376).

[20] Lundgren K. Bond between Corroded Reinforcement and Concrete. Göteborg: 2001.

[21] Llorca MÁC, Terradillos PG, Gómez EZ. Corrosión de armaduras en estructuras de hormigón armado. vol. 5. Editorial Club Universitario; 2008.

[22] Zhu W, François R, Coronelli D, Cleland D. Effect of corrosion of reinforcement on the mechanical behaviour of highly corroded RC beams. Eng Struct 2013;56:544–54. doi:10.1016/j.engstruct.2013.04.017.

[23] Torres-Acosta AA, Navarro-Gutierrez S, Terán-Guillén J. Residual flexure capacity of corroded reinforced concrete beams. Eng Struct 2007;29:1145–52. doi:10.1016/j.engstruct.2006.07.018.

[24] Chung L, Najm H, Balaguru P. Flexural behavior of concrete slabs with corroded bars. Cem Concr Compos 2008;30:184–93. doi:10.1016/j.cemconcomp.2007.08.005.

[25] Rodriguez J, Ortega L, Casal J. Load carrying capacity of concrete structures with corroded reinforcement. Constr Build Mater 1997;11:239–48. doi:10.1016/S0950-0618(97)00043-3.

[26] Malumbela G, Moyo P, Alexander M. Behaviour of RC beams corroded under sustained service loads. Constr Build Mater 2009;23:3346–51. doi:10.1016/j.conbuildmat.2009.06.005.

[27] Malumbela G, Alexander M, Moyo P. Steel corrosion on RC structures under sustained service loads - A critical review. Eng Struct 2009;31:2518–25. doi:10.1016/j.engstruct.2009.07.016.

[28] Malumbela G, Alexander M, Moyo P. Variation of steel loss and its effect on the ultimate flexural capacity of RC beams corroded and repaired under load. Constr Build Mater 2010;24:1051–9. doi:10.1016/j.conbuildmat.2009.11.012.

[29] Muñoz Noval A. Comportamiento de vigas hiperestáticas de hormigón armado corroídas y reparadas con mortero : pérdida de propiedades mecánicas del acero de refuerzo y fisuración del recubrimiento de hormigón por corrosión 2009.

[30] Lundgren K, Tahershamsi M, Zandi K, Plos M. Tests on anchorage of naturally corroded reinforcement in concrete. Mater Struct 2014. doi:10.1617/s11527-014-0290-y.

[31] Tahershamsi M, Zandi K, Lundgren K, Plos M. Anchorage of naturally corroded bars in reinforced concrete structures. Mag Concr Res 2014;66:729–44. doi:10.1680/macr.13.00276.

[32] Williams Portal N, Fernandez Perez I, Nyholm Thrane L, Lundgren K. Pull-out of textile reinforcement in concrete. Constr Build Mater 2014;71:63–71. doi:10.1016/j.conbuildmat.2014.08.014.

[33] Eiras López, J., Seara Paz, S., González Taboada, I., Vieito Raña I. COMPORTAMIENTO ADHERENTE EN HORMIGÓN CON ÁRIDO. Comport. Adherente en Hormigón con Árido Reciclado. Curva Tensión Adherente-Deslizamiento, Madrid: ACHE - Asociación cientificotécnica del hormigón estructural; 2014, p. 1–10.

[34] Golafshani EM, Rahai A, Sebt MH, Akbarpour H. Prediction of bond strength of spliced steel bars in concrete using artificial neural network and fuzzy logic. Constr Build Mater 2012;36:411–8.

[35] Dahou Z, Mehdi Sbartaï Z, Castel A, Ghomari F. Artificial neural network model for steel–concrete bond prediction. Eng Struct 2009;31:1724–33.

[36] Amleh L, Ghosh A. Modeling the effect of corrosion on bond strength at the steel–concrete interface with finite-element analysis. Can J Civ Eng 2006;33:673–82.

[37] Abosrra L, Ashour AF, Youseffi M. Corrosion of steel reinforcement in concrete of different compressive strengths. Constr Build Mater 2011;25:3915–25.

[38] Choi YS, Yi S-T, Kim MY, Jung WY, Yang EI. Effect of corrosion method of the reinforcing bar on bond characteristics in reinforced concrete specimens. Constr Build Mater 2014;54:180–9.

[39] Losberg A. Cracks in continuous concrete road slabs and other concrete structures locked against movements from temperature and shrinkage. 1962.

[40] Ruiz MF, Muttoni A, Gambarova PG. Analytical Modeling of the Pre- and Postyield Behavior of Bond in Reinforced Concrete 2007:1364–72.

[41] Hanjari KZ, Utgenannt P, Lundgren K. Experimental study of the material and bond properties of frost-damaged concrete. Cem Concr Res 2011;41:244–54.

[42] Al-Sulaimani G, Kaleemullah M, Basunbul I. Influence of corrosion and cracking on bond behavior and strength of reinforced concrete members. ACI Struct J 1990.

[43] Alonso C, Andrade C, Rodriguez J, Diez J. Factors controlling cracking of concrete affected by reinforcement corrosion. Mater Struct 1998;31:435–41.

[44] Lundgren K, Gylltoft K. A model for the bond between concrete and reinforcement. Mag Concr Res 2000:53–63.

[45] Lundgren K, Kettil P, Hanjari KZ, Schlune H, Roman ASS. Analytical model for the bond-slip behaviour of corroded ribbed reinforcement. Struct Infrastruct Eng 2012;8:157–69. doi:10.1080/15732470903446993.

[46] FiB Bulletin 10 - Bond of reinforcement in concrete. 2000.

[47] Torre-Casanova A, Jason L, Davenne L, Pinelli X. Confinement effects on the steel–concrete bond strength and pull-out failure. Eng Fract Mech 2013;97:92–104. doi:10.1016/j.engfracmech.2012.10.013.

[48] Al-Hammoud R, Soudki K, Topper TH. Confinement effect on the bond behaviour of beams under static and repeated loading. Constr Build Mater 2013;40:934–43. doi:10.1016/j.conbuildmat.2012.09.081.

[49] Bairan JM, Marí a. R, Ortega H, Rosa JC. Efecto del enrollado y enderezado en las propiedades mecánicas de barras de acero de diámetro medio y grande fabricadas en rollo. Mater Construcción 2011;61:559–81. doi:10.3989/mc.2011.60110.

[50] Garcia MD, Alonso MC, Andrade MC, Rodríguez J. Influencia de la corrosión en las propiedades mecánicas del acero. Hormigón Y Acero 1998;210:11–21.

[51] Cairns J, Abdullah RB. Bond strength of black and epoxy-coated reinforcement—a theoretical approach. ACI Mater J 93 1996;4:362–9.

[52] Coronelli D. Corrosion cracking and bond strength modeling for corroded bars in reinforced concrete. ACI Struct J 2002;99:267–76.

[53] Fang C, Lundgren K, Plos M, Gylltoft K. Bond behaviour of corroded reinforcing steel bars in concrete. Cem Concr Res 2006;36:1931–8. doi:10.1016/j.cemconres.2006.05.008.

[54] Wang X, Liu X. Modeling bond strength of corroded reinforcement without stirrups. Cem Concr Res 2004;34:1331–9.

[55] Liu XL, Wang XH. Modelling effects of corrosion on cover cracking and bond in reinforced concrete. Mag Concr Res 2004;56:191–9. doi:10.1680/macr.2004.56.4.191.

[56] Bhargava K, Ghosh A. Analytical model for time to cover cracking in RC structures due to rebar corrosion. Nucl Eng … 2006;236:1123–39. doi:10.1016/j.nucengdes.2005.10.011.

[57] Ã KL, Ã KG. A model for the bond between concrete and reinforcement 2010:53–63.

[58] Lundgren K. Bond between ribbed bars and concrete. Part 2: The effect of corrosion. Mag Concr Res 2005;57:383–95.

[59] Fang C, Lundgren K, Chen L, Zhu C. Corrosion influence on bond in reinforced concrete. Cem Concr Res 2004;34:2159–67. doi:10.1016/j.cemconres.2004.04.006.

[60] Monti G, Spacone E. Reinforced concrete fiber beam element with bond-slip. J Struct Eng 2000:654–61.

[61] Limkatanyu S, Spacone E. Reinforced Concrete Frame Element with Bond Interfaces . and Mixed Formulations. J Struct Eng 2002:346–55.

[62] Salari MR, Spacone E. Finite element formulations of one-dimensional elements with bond-slip. Eng Struct 2001;23:815–26. doi:10.1016/S0141-0296(00)00094-8.

[63] Marí AR. Numerical simulation of the segmental construction of three dimensional concrete frames. Eng Struct 2000;22:585–96.

Chapter III

STRUCTURAL EFFECTS OF STEEL REINFORCEMENT CORROSION ON STATICALLY UNDETERMINED REINFORCED CONCRETE BEAMS. Serviceability and ultimate capacity

III.1 Introduction

In the state of the art of the present work, it was reported the lack of experimental studies involving complex concrete structures such as statically undetermined beams, submitted to deterioration phenomena. This chapter aims to extend the existing database of corroded concrete members and define the capacity of statically undetermined beams to answer in front of steel corrosion and its effects.

The analyses of the structural response of statically undetermined beams submitted to accelerated corrosion of steel reinforcement are presented in the next points. The structural assessment was performed along different phases in order to capture the structural behaviour under its whole entire service life. The first part of the presented work, Part 1, consists of the study of the serviceability response under deterioration phenomena. Two span continuous beams were cast and subjected to impressed current on its reinforcement. Some of the

specimens were permanently loaded during the corrosion exposure time; with the underlying propose to assess the influence of the service loads on the structural response of actively deteriorated beams. The observed behaviour is compared with uncorroded specimen. Internal forces redistributions, steel stresses evolution and overall deflections are presented to understand the structural effects of the deterioration phenomena of this kind of structures.

The second part of the work, Part 2, describes the structural response at ultimate limit state. After the corrosion process had been finished, the same statically undetermined beams were loaded up to failure. Several structural parameters were measured such us deflections, reactions, concrete strains and the total applied load. The effect of steel corrosion is analysed by comparing the results of the corroded specimens with respect to the uncorroded ones. The reduction of bending capacity as well as the internal forces redistribution were assessed and presented here. In addition, the identification of determinant structural parameters affected by corrosion, which define the final structural behaviour, was performed and analysed in further chapters of the thesis.

III.2 Structural effects of steel reinforcement corrosion on statically undetermined reinforced concrete members. Serviceability

Ignasi Fernandez*[1], Manuel F. Herrador[2], Antonio R. Marí[1], Jesús Miguel Bairán[1]

[1] Department of Construction Engineering, Polytechnic University of Catalonia, Jordi Girona, 1-3, Barcelona 08034, Spain.

[2] Department of Construction Technology, University of A Coruña, Campus de Elviña, s/n, A Coruña 15172, Spain.

*corresponding author: ignasi.fernandez-perez@upc.edu

Highlights:

- Corrosion effects on statically undetermined beams
- Modelling deterioration effects
- Internal forces redistribution due to steel corrosion

Abstract: Understanding the structural deterioration effects on complex structures such as statically undetermined beams and thereafter implement them in non-linear models, which help us describe the structural behaviour during the whole service life, is crucial for a safer and better structural design. In this work, an experimental study of statically undetermined beams is presented. Thirteen two-span continuous beams were cast, divided into four groups of three beams each. Each group was submitted to a defined corrosion level except for one group, which was left uncorroded as a benchmark. Different dead weights were applied during the corrosion phase to assess its effect in final deflections. A substantial increment of the observed deflections was registered. The applied load had an amplified nonlinear effect on the observed deflection. Natural internal forces redistribution was produced by steel corrosion, which kept the maximum stress in the steel reinforcement below the maximum stress registered for uncorroded specimens in the same steel bars.

Keywords: Corrosion; reinforced concrete structures, Steel reinforcement; tests; statically undetermined beams;

III.2.1 Introduction and objectives

The repair of structures as well as better execution of new, more durable ones takes a particular relevance in the actual frame of knowledge, becoming a spearhead for councils and governments to rationalize existing resources and for their better investment. Broad knowledge of structural behaviour, as well as the deterioration phenomena in which structures could be involved, becomes really necessary. Projects should account for the appearance of these deterioration phenomena in order to guarantee durability and service life. Engineers often have to assess and quantify the structural damage with the aim to decide, at the end of the structure's service life, what means are needed for its demolition, or whether it is more convenient to have it repaired and strengthened, investing towards its extension.;all of this, under the strictest safety and cost control criteria.

In this frame, deterioration models are presented as a powerful tool to assess and predict the structural behaviour under the influence of different deterioration phenomena, also improving the structural design in project phase. These models should be capable of predicting reliably and accurately the structural behaviour. With the help of a set of variables, these models should provide enough information to quantify structural deterioration and to define proper criteria to take the decision whether to demolish or strengthen.

During their service life, structures can suffer changes in their geometry, structural configuration and material properties, as well as deferred effects. Also, evolutive constructive procedures usually cause changes in the cross-section, longitudinal configuration, supports and loads that may generate different stress states depending on the construction procedure followed. Additionally, concrete mechanical properties change during setting and hardening, although they are also modified because of environmental effects (carbonation, chemical attack). All those aspects, as well as instantaneous or deferred non-linear material behaviour (due to cracking, yielding, non-linear stress-strain behaviour, etc…) and second order effects, must be considered to assess with sufficient reliability and scientific rigour the bearing capacity of the structure during its service life regarding possible strengthening or demolition. In addition, deterioration effects on the structure can entail structural changes, which may dramatically reduce its service life.

Instantaneous or deferred non-linear analysis lets us consider in a realistic way the previously mentioned phenomena. Many non-linear models have been developed over the last years. However, beam models that consider the combination of non-linearity, deferred analysis, evolutive construction and deterioration phenomena are much less developed. The most

relevant models formulated in this field are [1–4], applied in plane regular structures and also used on 3D typical structures.

Corrosion of steel reinforcement is one of the main problems in reinforced concrete structures that directly affect its service life. Study of corrosion effects is crucial for a better understanding of the structural behaviour of existing impaired concrete structures. The most severe reinforcement corrosion effect is the change in bond properties between steel and concrete [5,6]. Also, volumetric expansion of corrosion products causes serious problems inducing splitting stresses along corroded reinforcement, which might be harmful to the surrounding material. Generally, the splitting stresses are not tolerated by concrete, and that leads to cracking and eventually spalling of the cover. As the reinforcement becomes more exposed, the corrosion rate may increase and facilitate the deterioration process [7,8].

Many researchers have performed the study of corrosion effects for several years. Despite the size of the database of experimental studies, they mostly encompass simple specimens, reduced in dimensions and statically determined. Thus, the structural effect on statically undetermined beams is presented as a relevant investigation to improve the database and to observe the effect of corrosion in this type of structures, widely employed in construction around the world. The impact of corrosion on statically undetermined beams may be different because of their natural internal forces redistribution capacity; for example, bending moments shift from the weaker zones to the stiffer ones and vice versa [9]. This capability might result in better behaviour regarding reinforcement corrosion and its effects if, for instance, such an internal forces redistribution shifts naturally from the corroded zones to the uncorroded ones.

An experimental campaign, consisting of impressed corrosion tests of two-span statically undetermined beams with the objective of studying the effects of corrosion on this configuration is presented in this paper. Four groups of three beams were cast. Three different corrosion levels were achieved as a result of an impressed current applied on the reinforcement, defined using second Faraday's Law theory [10–12]. One group of beams was left uncorroded to compare their response with that of the corroded ones. In addition, the effect of the load during the corrosion procedure was studied because in the literature, there is a lack of experimentation involving specimens under constant load. Some researchers [13–15] claim that there is a relationship between the load level and the deterioration: for a fixed corrosion level, the higher the load, the stronger the deterioration effects. In order to investigate this hypothesis, in this study each specimen within a given group was assigned a different constant load level. The beams were loaded either at 2P,

which means load over design service load; loaded at level P, which is load under design service load or self-weight loaded only. Different parameters of the structure were measured and compared during the corrosion process.

Finally, an extension of a pre-existing non-linear analysis model [16] is also presented to consider in a simplified way the deterioration effects due to corrosion of steel. The reduction of steel area is implemented, as well as the loss of concrete cover due to expansiveness of corrosion products (spalling effect). In this manner, redistribution of stresses between reinforcement and concrete and redistributions of internal forces along the structure produced by deterioration are captured by the model through the decrease in steel area and section stiffness. A comparison between the results predicted by the model with those measured experimentally is presented, discussing the main differences among them and the suitability of this kind of models.

III.2.2 Materials and experimental program and test setup

III.2.2.1 Cement

Type I Portland cement, CEM I 42.5R, was used in concrete mixtures with the characteristic rapid hardened strength of 42.5 MPa. The chemical properties of cement are given in Table III-1.

Table III-1. Chemical composition of the cement used

Composition	SiO_2	Fe_2O_3	Al_2O_3	CaO	MgO	K_2O	Na_2O	SO_3	LOI
%	19.16	3.56	5.04	62.9	1.66	0.75	0.15	3.54	3.25

Natural limestone fine (FA, 0/4 mm) and coarse aggregates (two fractions; CA1, 4/12 mm and CA2, 12/20 mm) were used for concrete production. Physical properties, density and absorption, and the grading distributions are described in Table III-2 and Figure III-1, respectively. . The properties of the fine and coarse aggregates were determined according to EN specifications. All fractions of natural aggregates satisfy the requirements specified by the Spanish Standard of Structural Concrete, EHE-08 [17].

Table III-2. Dry density and water absorption capacity of aggregates

Properties	**CA2 12/20mm**	**CA1 4/12mm**	**FA 0/4mm**
Dry density (kg/dm^3)	2.65	2.64	2.58
Water absorption (%)	0.67	0.87	1.68

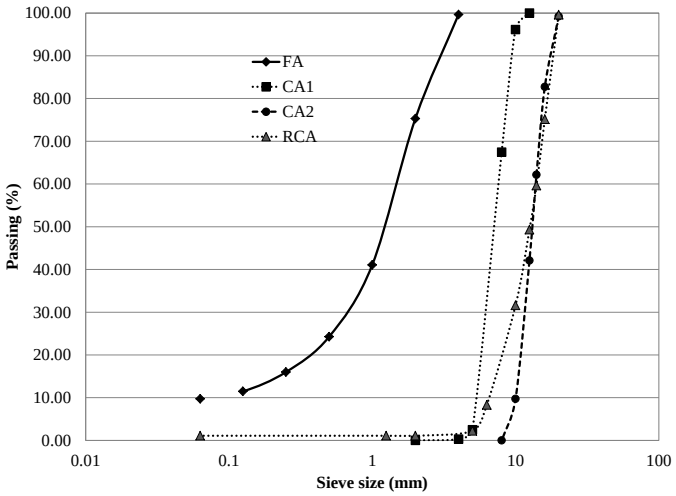

Figure III-1. Particle size distribution of fine and coarse aggregates

High ductility B500S steel was disposed as reinforcement steel. Two different diameters were used, 10 mm and 12 mm.

III.2.2.1.1 Concrete mix proportions

The mix was prepared and cast in the Structures Technology Laboratory, Universitat Politècnica de Catalunya (UPC) – Barcelona Tech (LTE).

The mix proportion of conventional concrete produced with 300 kg/m^3 of cement and a total water/cement ratio of 0.5 is the one specified for concretes exposed to marine and chloride environment described by Spanish Structural Concrete code [17]. The effective w/c ratio on CC concrete was 0.44 and it was determined removing from the total water (150 litres) the effective absorption capacity of raw aggregates, determined by the absorption capacity at 20 min submerged and defined as the 80% and 20% of total absorption capacity for fine and coarse raw aggregates, respectively.

Concrete mix proportions were defined according to their maximum volumetric compaction. This mix proportion for conventional concrete (CC) was defined as 50% of fine aggregates and 50% of coarse aggregate. The distribution of coarse aggregate was 30% CA1 4/12mm and 70% of CA2 12/20mm.

Table III-3 shows the mix proportions used. The represented weight of aggregates is dry. Total water includes the 80-90% of humidity that recycled aggregates had at the time of concrete production.

4% of NaCl over cement weight was also included in the mix. NaCl guarantees the depassivation of the steel inside the concrete and provides a conductive medium for the corrosion process.

Table III-3. Proportioning of the concrete mixtures

Material (1000 litres)	Dosification
Cement (kg)	300
Total Water (kg)	150.00
Effective w/c	0.446
FA 0/4mm	976.00
CA1 4/12mm	210.00
CA2 12/20mm	765.00
NaCl (weight of cement)	4%
Superplastizicer (weight of cement)	1%
Retarder (weight of cement)	0.8%

III.2.2.2 Test specimens description

Twelve continuous two-span beams were cast. The beams had 5000 mm total length and two symmetric spans of 2400 mm between support axes. The cross-section was rectangular with 250 mm width by 125 mm depth. Concrete cover was 15 mm on all four faces.

Only longitudinal steel reinforcement was placed, trying to avoid the direct connection between the top and bottom steel faces in order to prevent interference in the corrosion process. Two 10 mm diameter rebars were placed on the top face, plus two extra 10 mm diameter rebars across the maximum negative bending moment zone. In the bottom face two 12 mm diameter rebars were placed along the whole length.

Figure III-2 describes the geometrical specifications of the specimens, steel disposition of the reinforcement and the cross-section definition.

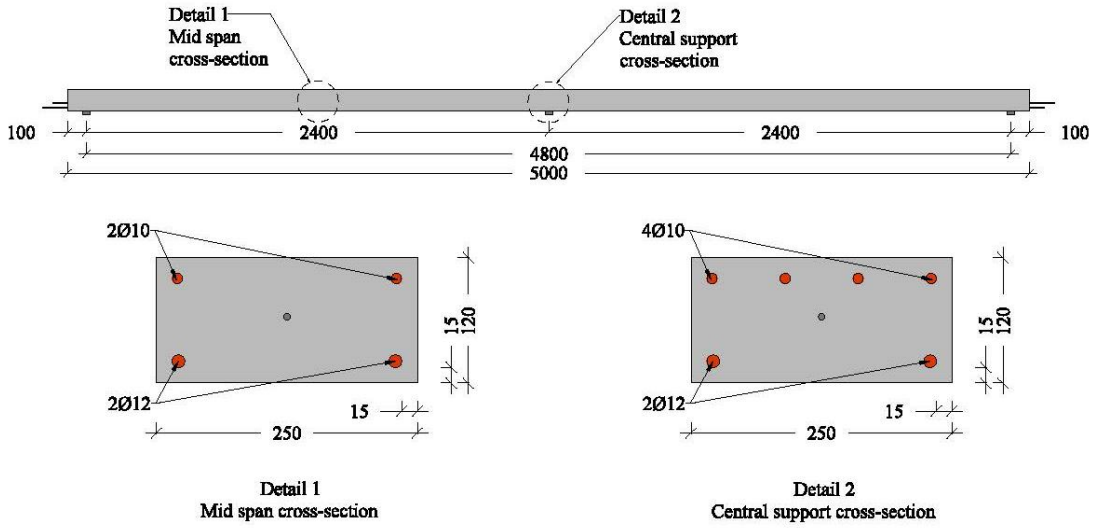

Figure III-2. Geometrical specs of the specimens

III.2.2.2.1 Test setup

Each one of the four groups comprised three specimens aimed at a different corrosion level. Three different corrosion levels were defined, plus a control group with no corrosion conditioning.

Within each group, every beam was burdened with a different permanent load to evaluate its effect during the corrosion process. One beam was left self-weighted, another beam saddled with a load P, representative of a service load level, and the last one with a value of 2P, over the service load level.

Figure III-3 describes the test setup where it can be seen how the permanent load is applied over each beam. Table III-4 describes the final load values for each specimen.

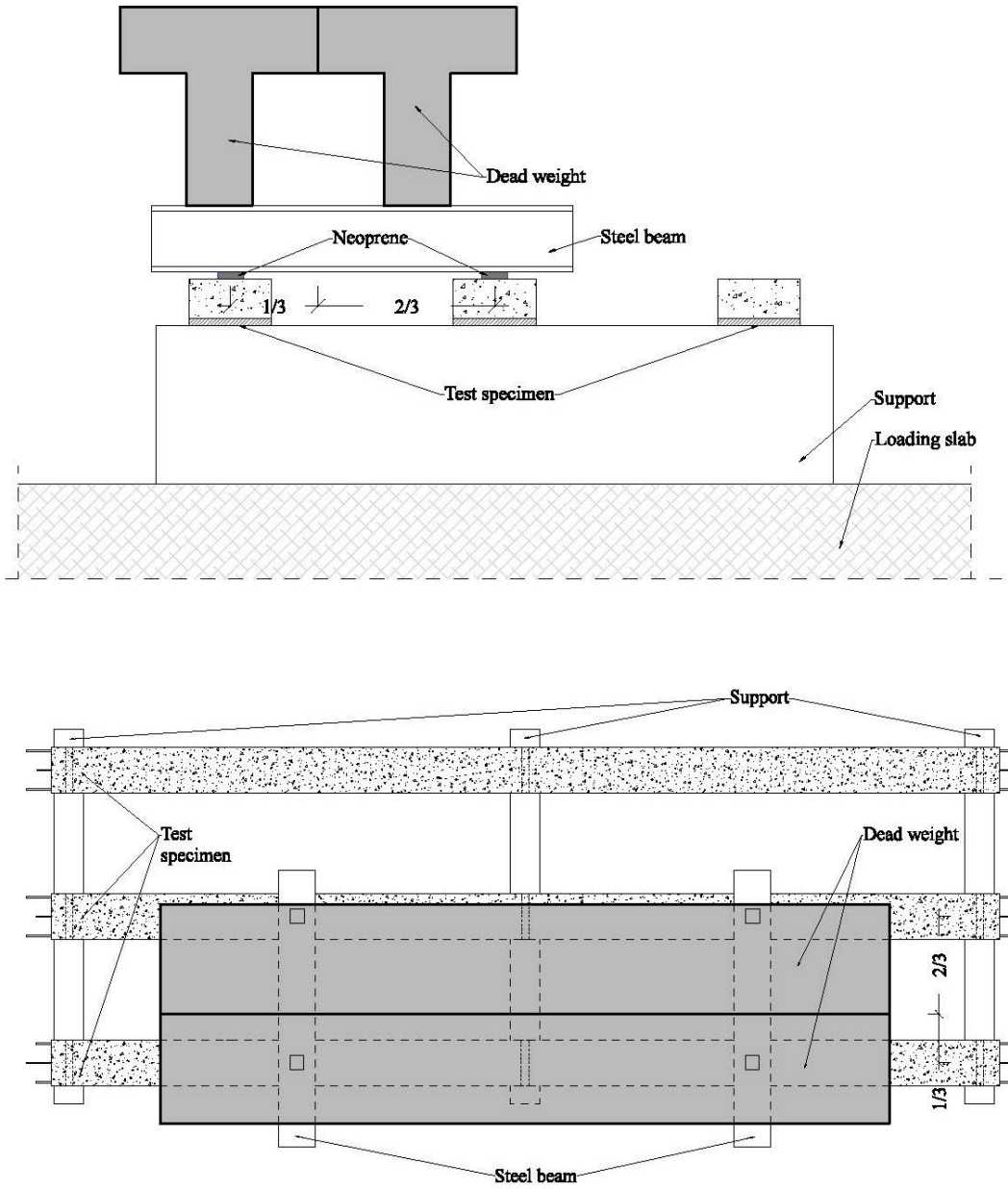

Figure III-3. Test configuration during corrosion procedure

III.2.2.3 Concrete properties. Compression, modulus and tensile tests

The compressive strength of concrete was determined using a compression testing machine with a loading capacity of 3000 kN. The compressive strength was measured at the age of 28 days following UNE-EN 12390-3 standards. Three cylindrical specimens (150mm diameter and 300 mm length) were used for each type of concrete produced.

The modulus was determined using the same machine by applying three cycles in the concrete elastic range, as prescribed by UNE-EN 12390-3 standards. The modulus was measured at the age of 28 days.

The splitting tensile stress was obtained by means of the Brazilian test, which involves indirect tensile measurement. The compressive strength was measured at the age of 28 days following UNE-EN 12390-3. The specimens were the same as for the other tests..

III.2.2.4 Tensile steel test

The tensile steel behaviour was determined using a fatigue tensile machine with a loading capacity of 5000 kN. The tensile steel behaviour was measured from a sample of the same steel employed in the specimens. A 40 cm specimen length was tested following the prescriptions defined in UNE-EN-ISO-15630-01 [18]. Three displacement transducers were used to obtain the strains according to the applied load and consequently the modulus of elasticity of the material in the elastic range, and the load-strain curve was recorded up to failure.

Additionally, tensile steel tests were performed on the corroded bars recovered from the beams at the end of the test series. The test was carried out following the same prescription as for uncorroded ones. The stress-strain curves for corroded steels were obtained up to failure by means of the displacement transducer.

III.2.2.5 Accelerated corrosion

Accelerated corrosion methods open the possibility to reproduce corrosion episodes over structures in very short periods, as compared to natural corrosion. Obviously, this form of corrosion mechanism has some drawbacks compared to natural corrosion testing. Some researches found that common methods may influence bond capacity and change the anchorage behaviour [19–21]. Further, the corrosion procedure for accelerated corrosion method resulted in homogeneous corrosion along the bar, while natural corrosion produces heterogeneous corrosion. They are nevertheless necessary to investigate the effects on

structures and materials over time within an appropriate investigation period. With this kind of methods, it is possible to reproduce a 20-30 years phenomenon in a few months with a reasonable agreement between the natural and induced corrosion effects.

III.2.2.5.1 Corrosion method

Corrosion of steel reinforcement was forced using impressed current. Following Faraday's law Equation III-1, it is possible to estimate the weight loss of steel due to corrosion, knowing the applied intensity along time, I(t), and the geometrical bar properties such as diameter and exposed length.

Equation III-1 $$\boldsymbol{E = \frac{m_{Fe} \cdot \int I \cdot dt}{V \cdot F}}$$

In Equation III-1Fe is the atomic mass, V is the steel valence that is taken as equal to two and F is Faraday's constant. As the applied intensity was an input during the test and it is also constant along time, it is possible to rewrite Faraday's law as Equation III-2

Equation III-2 $$\boldsymbol{\Delta m = \frac{m_{Fe} \cdot I \cdot t}{V \cdot F}}$$

Many researchers have observed [10,22] that, using corrosion current densities below 350 μA/cm^2 for accelerated corrosion, the difference between the corrosion rate estimated by means of Faraday's law and the corrosion rate registered from gravimetric methods (steel weight measure after accelerated corrosion) ranges between 5-10%. Thus, by applying corrosion current density values below this threshold, it is possible to accurately estimate the achieved corrosion level. Furthermore, current densities above this threshold imply moving the test further away from a natural corrosion process, inducing earlier cracking as well as (probably) differences between corrosion products. Also, bond between steel and concrete is affected by the corrosion rate [20]. In the presented work, corrosion rates below 350 μA/cm^2 were applied in order to corrode the specimens. The proposed goal was 10% steel weight loss in 28 days, which means a corrosion current density of 335 μA/cm^2 and an equivalent current of 1.26 A for each beam. Taking these values into account, it was possible to estimate the different exposure times for each specimen according to the goal corrosion level and the current value. Each group of beams was supposed to be exposed to current during 28 days, 32 days and 56 days respectively. Accordingly, the estimated corrosion level for each group was 10% (for 28 days), 15% for (32 days) and 20% for (56 days).

Accelerated corrosion methods based on impressed current need depassivated steel for proper development. This means that it is necessary to previously depassivate steel bars. As mentioned above, in the present study a 4% sodium chloride (NaCl) solution in the water

used for concrete casting was chosen in order to eliminate the passive layer by means of chloride attack.

III.2.2.5.2 Corrosion procedure

The groups to be corroded were placed over two pools located under the free span areas. In the middle of the cross-section a 6 mm diameter stainless steel wire was placed along the beam length to play the role of cathode in the corrosion circuit, the steel rebar being the anode. An irrigation system was set over the top face of the beams by means of a porous tube, which was used to keep the beams wet during all the exposure time. Concrete moisture had to be higher than usual in order to make possible the corrosion process, reducing the resistivity of the concrete and interacting with the NaCl put in the mixture as an electrolyte for the corrosion cell. Additionally, to ensure a high level of moisture in the beam, reducing water and power consumption, every beam was wrapped individually in plastic sheets and burlap. The irrigation was programmed to take place for 5 minutes every 120 minutes. It was possible to connect different specimens in series, guaranteeing the same current circulation over every specimen. Figure III-4 describes the connection setup for one group of beams between the various elements.

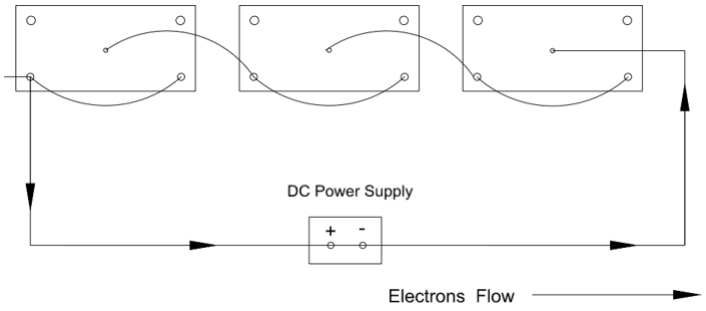

Figure III-4. Connection setup

III.2.2.6 Measurement equipment

Three kinds of measuring equipment were used during the corrosion procedure:

III.2.2.6.1 Displacement transducers.

Displacement transducers were placed to register beam deflections during the corrosion procedure. Deflections were measured in mid-span beam, two deflection records for beam. Additional displacement transducers were placed at the free steel bar-end to register bond-slip due to steel corrosion, one transducer per beam end. Figure III-5 describes the position of the different transducers.

III.2.2.6.2 Load transducers.

Each beam had five load transfer points: three reactions and two load application points. In order to gather enough information to determine the bending moment law along the beam at any given time, four load cells were placed, obtaining the fifth unknown by equilibrium, (the symmetry condition was avoided because of possible construction imperfections). Thus, reactions and applied load over every beam were known during the whole corrosion procedure. Figure III-5 shows the load cell measurement points.

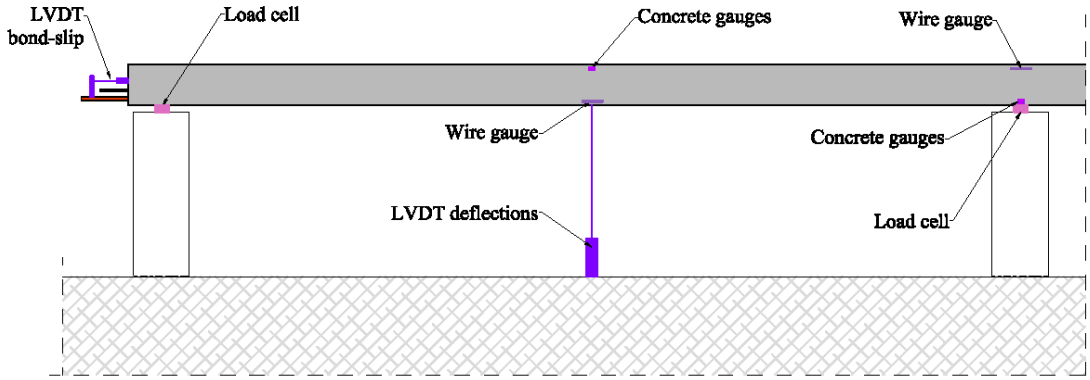

Figure III-5. Equipment position

III.2.2.6.3 Strain gauges.

The steel stress/strain redistribution due to the corrosion process was supposed to be registered by means of resistive strain gauges glued on the steel bars at different points of the beam. Tensile and compressive steel stress in mid-span cross-section and tensile steel stress in middle-support cross-section were measured. However, the extremely aggressive medium due to NaCl and the applied current in addition to water made data acquisition difficult. Many gauges became useless in a few days, some other read few data but anyone resisted the whole corrosion procedure. Figure III-6 shows the strain gauges placed onto the steel reinforcement bars.

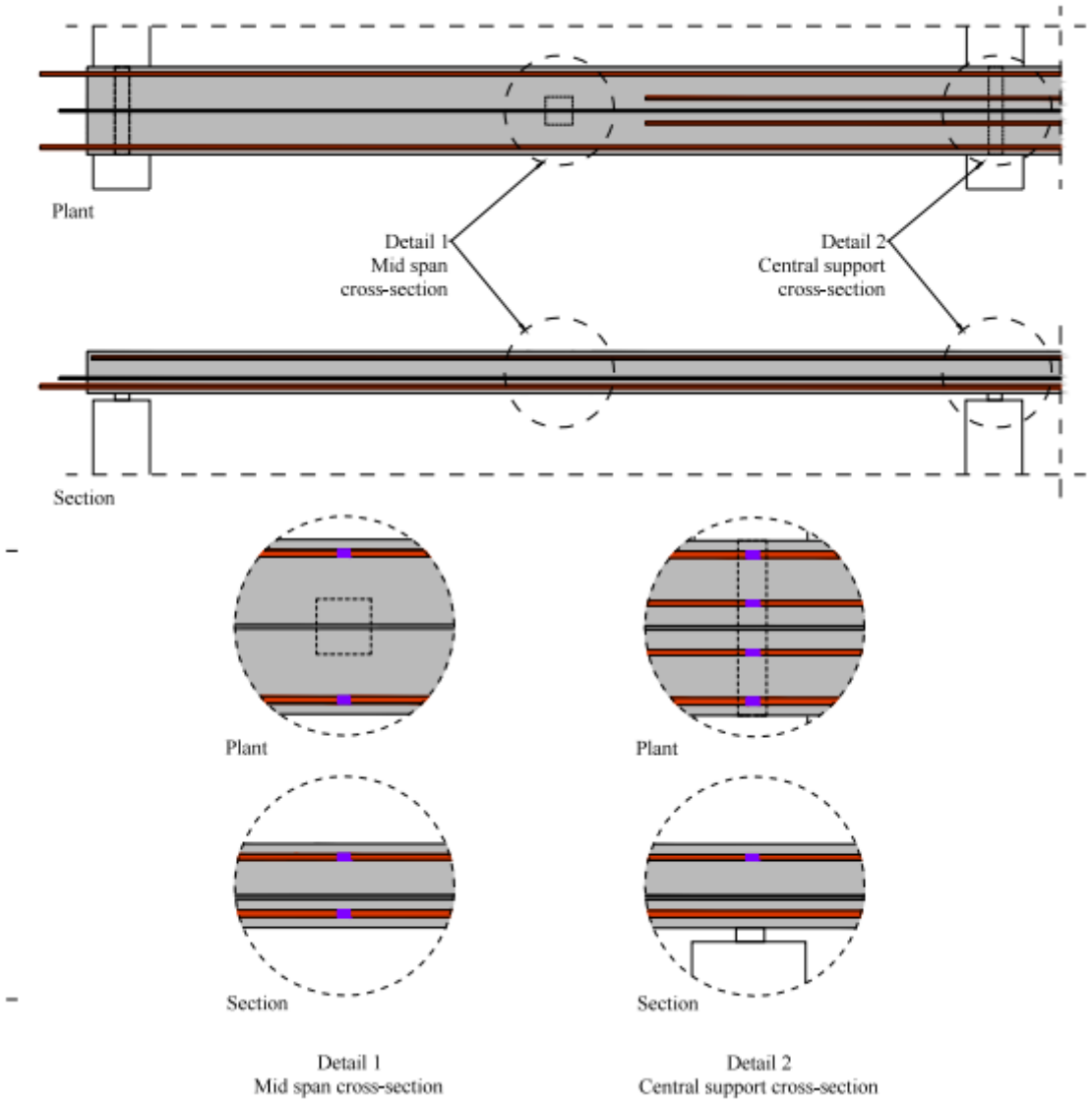

Figure III-6. Placed strain gauges

III.2.3 Deterioration model implementation

III.2.3.1 Existing non-linear model

A previously developed non-linear and time-dependent analysis model was modified to include the effects of steel and concrete deterioration due to the corrosion phenomenon [16]. The internal organization of the model, designed to perform step-by-step analyses of segmentally erected structures as well as to deal with any subsequent changes, allowed to implement the effects of deterioration in a straightforward manner.

A filament beam element with arbitrary cross-section and 13 degrees of freedom is used by the model together with non-linear constitutive equations for the steel and concrete filaments to account for the non-linear response under increasing loading levels. These capabilities, together with a the time-dependent scheme taking into account load and temperature histories, creep, shrinkage, aging and steel relaxation, enable the model to assess existing deteriorated structures at any time of its structural service life (as well as, of course, newly built structures).

III.2.3.2 Loss of steel area and cover cracking

The non-linear model CONS was modified to reproduce the reinforcement steel cross-section reduction by uniform corrosion in the bars. Pitting or localized corrosion has not been included in the model for the time being. On the other hand, the model does not include any features related to the external aggressive agent penetration. This means that the model needs as an input an estimation of time-to-corrosion. Previous deterioration processes, as well as transport through the cover of aggressive agents, are not modelled.

In order to account for the effects of the reinforcement deterioration, the following parameters defining the damage evolution (in terms of geometry of the reinforcing bars) are provided to the structural analysis model. These are:

- Initiation time (T_i): The starting time of the deterioration phenomena in terms of reinforcement cross-section reduction (time-to-corrosion).
- Final time (T_f): Is the initial time plus the time elapsed, in which the analysis is performed.
- Percentage of corroded cross-section of the reinforcement in the considered element: this parameter, together with initial time and final time, determines corrosion velocity. It is possible to express this value in terms of velocity in mm/day (diameter reduction) or in terms of the percentage of total cross-section reduction during the defined exposure time. In the last case, the model will compute the value of velocity of corrosion from the introduced values.
- Rebar diameter: in the original model, only the amount of steel per filament is needed. In this case, since the development of corrosion phenomena depends on rebar diameter, this parameter has to be provided.

The evolution of cross-section over time is expressed as a function of the described parameters according to Equation III-3.

Equation III-3 $\boldsymbol{A_s(t) = n_{bar} \cdot \frac{\pi}{4} \cdot (\emptyset_0 - v \cdot \Delta t)^2 = \frac{4 \cdot A_{so}}{\pi \cdot \emptyset_o^2} \cdot \frac{\pi}{4} \cdot (\emptyset_0 - v \cdot \Delta t)^2 = A_{so} \left(1 - \frac{v \cdot \Delta t}{\emptyset_0}\right)^2}$

Where:

v, is obtained from the equation $v = \frac{\emptyset_0 \cdot (1 - \sqrt{\%_{acorr}})}{Tfin - Tini}$, in mm/day

Δt, is the increment of time from T_i

$\emptyset_0$, is the nominal diameter of the steel bars

A_{so}, is the amount of initial Steel in the section, corresponding to the initial filament area.

Following Equation III-3, the model incorporates the steel area value in each time step and proceeds to compute the structural state. The loss of steel area results in a reduction in capacity and in stiffness of any cross section affected by corrosion. Thus, when performing the computation of internal forces, by integration of the stresses at the sections placed at the element's Gauss points, the external forces will not be balanced by the internal ones. Then, these unbalanced forces will be automatically introduced in the non-linear iterative scheme, until equilibrium is obtained. As a consequence of corrosion, increments of stresses and strains in concrete and steel, increments of deflections (due to the loss of stiffness) and redistribution of internal forces takes place to satisfy equilibrium and compatibility conditions for the current state of the materials.

III.2.4 Evolution of the experimental phase

The provided voltage suffered some variations during the first days until the environmental condition where stable (due to watering system and beam wrapping after aged). The current was applied by means of different power supplies fixing the desired current limit. The power supply was programmed to regulate the voltage value to keep the design current constant. Thanks to the beam wrapping, it was possible to keep the beams at a high and roughly constant degree of humidity. During the test, the voltage was approximately between 20-30 V for each beam, which means that a power supply capable of providing at least 90 V for each group was needed.

In the beginning, only bottom reinforcement steel was aimed to be corroded. Eventually, some factors produced an extension of corrosion to the top reinforcement steel too. The corrosion of top reinforcement was observed for all the tested specimens, but at different

exposure times. Figure III-7 depicts the initial (left) and final (right) resistance corrosion scheme that was finally formed and caused the corrosion of the top reinforcement steel.

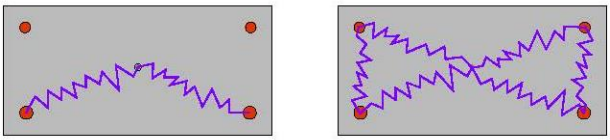

Figure III-7. Initial and final resistance scheme during corrosion procedure

The final deterioration state for group 1 beams, which attained corrosion levels up to 14 % steel loss in the bottom reinforcement, is shown in Figure III-8. For this group of beams, top steel reinforcement corrosion was not as conspicuous as it was for the other groups. Despite this, it was possible to observe longitudinal cracks in different zones along the beam with corrosion stains on the concrete that revealed corrosion of both top and bottom bars.

Figure III-8. Final corroded beams aspect. Group 1

All the specimens presented longitudinal cracking along the bottom steel reinforcement in the first five days, counting from the beginning of the impressed current procedure. This type of cracks was also observed along the top reinforcement. Corrosion stains were very evident in the specimens and the corrosion products seeped through the longitudinal cracks.

After the beams had reached the defined exposure time, the corroded steel was extracted to determine the actual steel loss. Each corroded beam was demolished. Top and bottom reinforcement bars were cut into 50 cm long pieces, which were later carefully cleaned by means of a mechanical cleaning system. The average mass loss of each reinforcement was estimated by the difference in its original weight, estimated from a same 1 meter uncorroded steel bar piece. The final corrosion values for each beam, including top and bottom

reinforcement, are described in Table III-4. The corrosion level presented is averaged over the whole reinforcement length.

Table III-4. Corrosion levels achieved, exposure days and applied load on span centre

Group	Encompassed Beams	Corroded Reinforcement	Steel loss (%)			Exposure time (days)	Applied load (kN)		
1	1-2-3	Top reinforcement	6	6	9	56	16,50	6,74	0,00
		Bottom reinforcement	14	12	11				
2	4-5-6	Top reinforcement	6	6	7	48	17,70	0,00	8,34
		Bottom reinforcement	15	10	15				
3	7-8-9	Top reinforcement	15	17	10	100	0,00	8,47	17,50
		Bottom reinforcement	15	20	24				
Ref	10-11-12		0			0	15,40	7,98	0,00

III.2.5 Test results

III.2.5.1 Concrete Properties

Table III-5 describes the compressive strength at 28 days of curing for all types of concretes produced as well as the modulus of elasticity.

Table III-5.Concrete compressive strength, tensile strength and modulus. Steel fy and modulus

	Compressive strength	Tensile strength	Elasticity modulus
Concrete	40 MPa	3.5 MPa	35000 MPa
ϕ 10 steel	--	550 MPa	200000 MPa
ϕ 12 steel	--	545 MPa	195000 MPa

III.2.5.2 Steel properties

Table III-5 shows the properties (yield stress and modulus of elasticity) of the 10 mm and 12 mm diameter bars used for reinforcing steel used to cast the beams.

Additionally, tensile tests on corroded steel bars were performed. Figure III-9 shows the σ-ε curves for uncorroded steel as well as corroded specimens. A substantial variation of the main steel properties was observed.

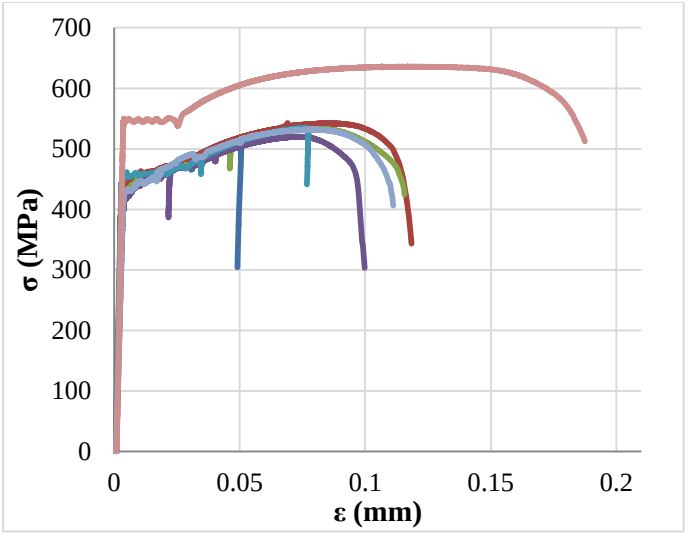

Figure III-9. Stress-strain curves corroded (12% corrosion level) and uncorroded steel

III.2.5.3 Deflections

Figure III-10 depicts the measured deflection for all the tested specimens. It is possible to observe the three groups and the behaviour of each one during the corrosion exposure time.

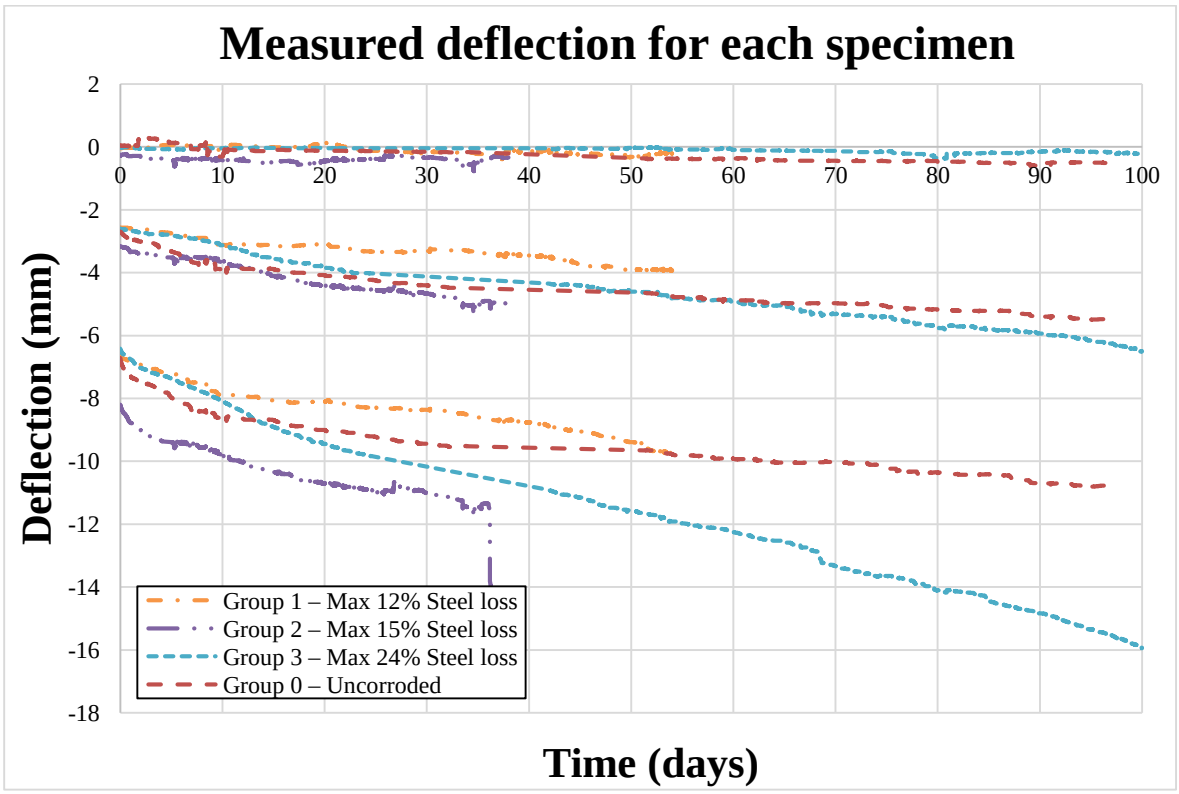

Figure III-10. Registered deflections for all tested beams

The following procedure has been used to study the effect of load level on the corrosion process. Firstly, for each load level, a normalized deflection value is obtained by dividing total deflection by instantaneous deflection. Then, the ratio between normalized deflection under load 2P and normalized deflection under load P is computed. This ratio is obtained for each corrosion group, and the results are plotted in Figure III-11. It can be seen that deferred deflections are more pronounced in the groups, which underwent corrosion. Also, deferred deflection amplification due to corrosion is greater in the case of 2P-loaded specimens than in P-loaded specimens. In the long term, it seems that trend shapes for all groups tend to be similar.

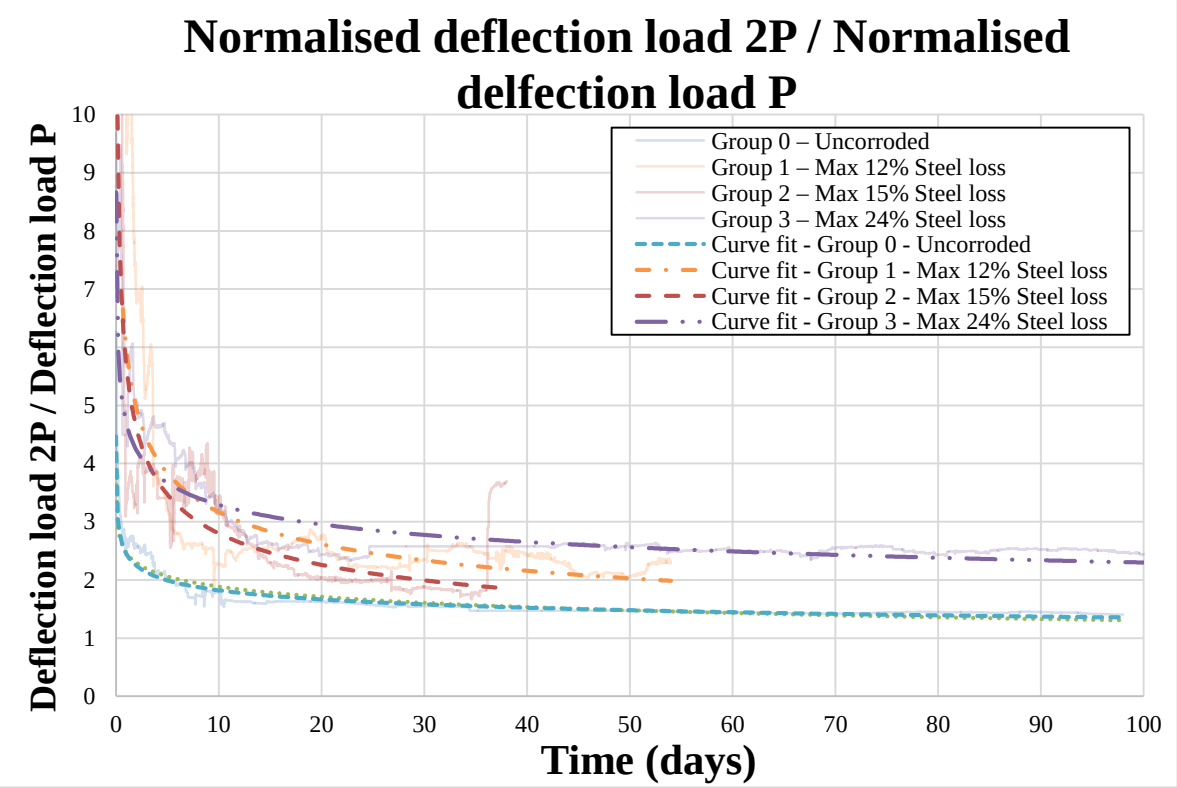

Figure III-11. Deflection ratio: evolution of normalized deflection under 2P load divided by normalized deflection under P load, with respect to time

Figure III-12 shows a summary of the aforementioned effect. The normalized deflection ratio for each group of beams, as measured at the end of their respective corrosion processes, is compared to the normalized deflection ratio for uncorroded beams. It can be seen that the ratio is significantly higher for all groups, with an increase between 20% and 40% against the uncorroded beam, depending on the corrosion level attained.

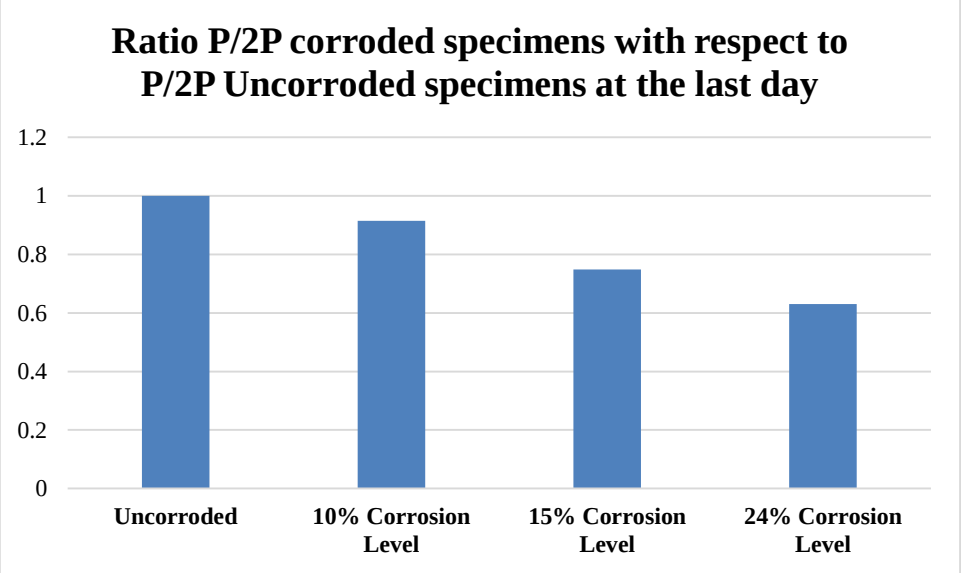

Figure III-12. Comparison of the deflection ratio (deflection under 2P load divided by normalized deflection under P load) of corroded beam groups against uncorroded beam group at the end of their respective corrosion processes time

III.2.5.4 Reactions

All beams showed load redistribution between the central support and the end support reactions in both directions. However, as expected, uncorroded specimens only presented redistribution at very early time because of the initial effect of creep and shrinkage; after that, each reaction remained almost constant over time. Figure III-13 depicts the average registered reaction at the beam-ends for all specimens. All graphs have been translated so that the reaction value at day 0 is the same for each load level and, therefore, the evolution of redistribution is more easily interpreted.

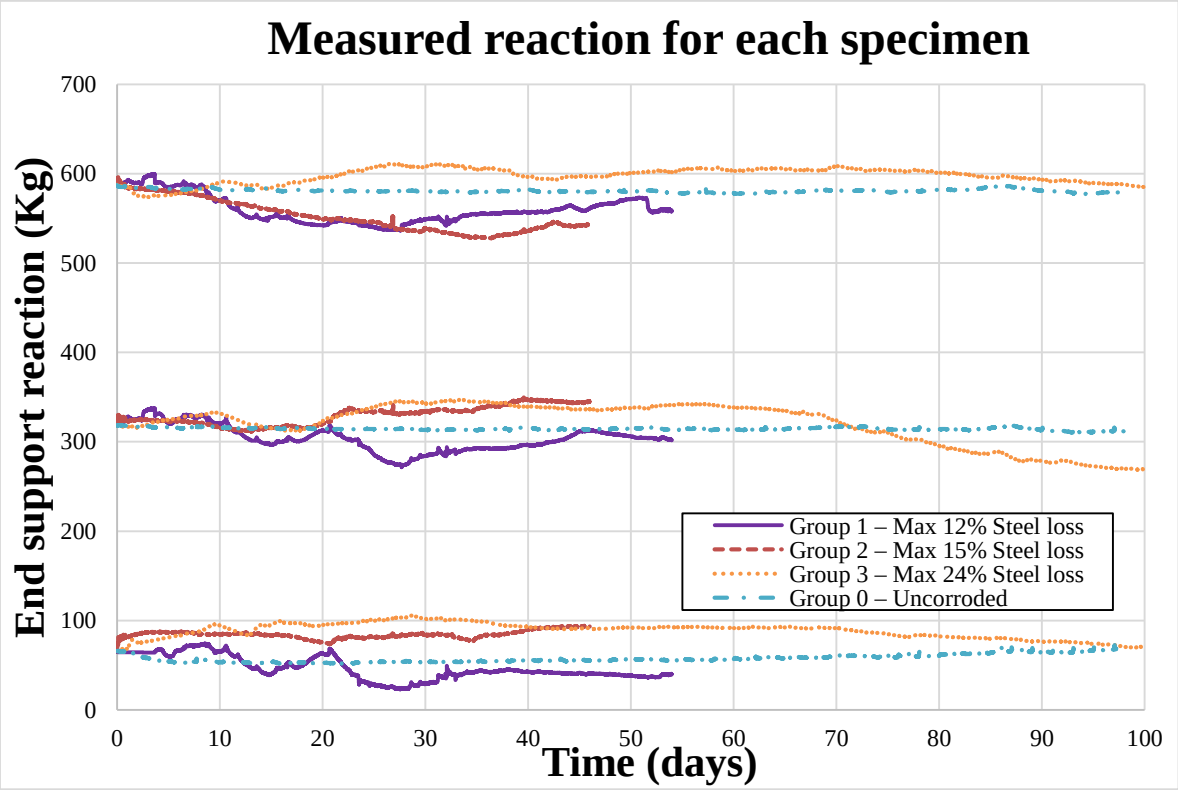

Figure III-13. Overall evolution of reaction forces for all the specimens

The observed load redistribution directly influenced the bending moment distribution in the beams. Using load balance calculations, it was possible to obtain the bending moment at the critical cross-sections (midspans and central support), which represented the maximum positive and the highest negative bending moment respectively. Figure III-14 describes the evolution of the bending moment at the aforementioned sections. It seems that the relative effect of redistribution was actually lower at higher loads. Despite this, all the beams presented some bending moment redistribution. It can be seen that the evolution of the bending moment did not follow a constant trend, but instead increased and decreased over time. Table III-6 describes maximum and minimum redistribution values at the central cross-section(shown as a percentage of load redistribution with respect to initial load) for all specimens, comparing the maximum and minimum bending moment observed.

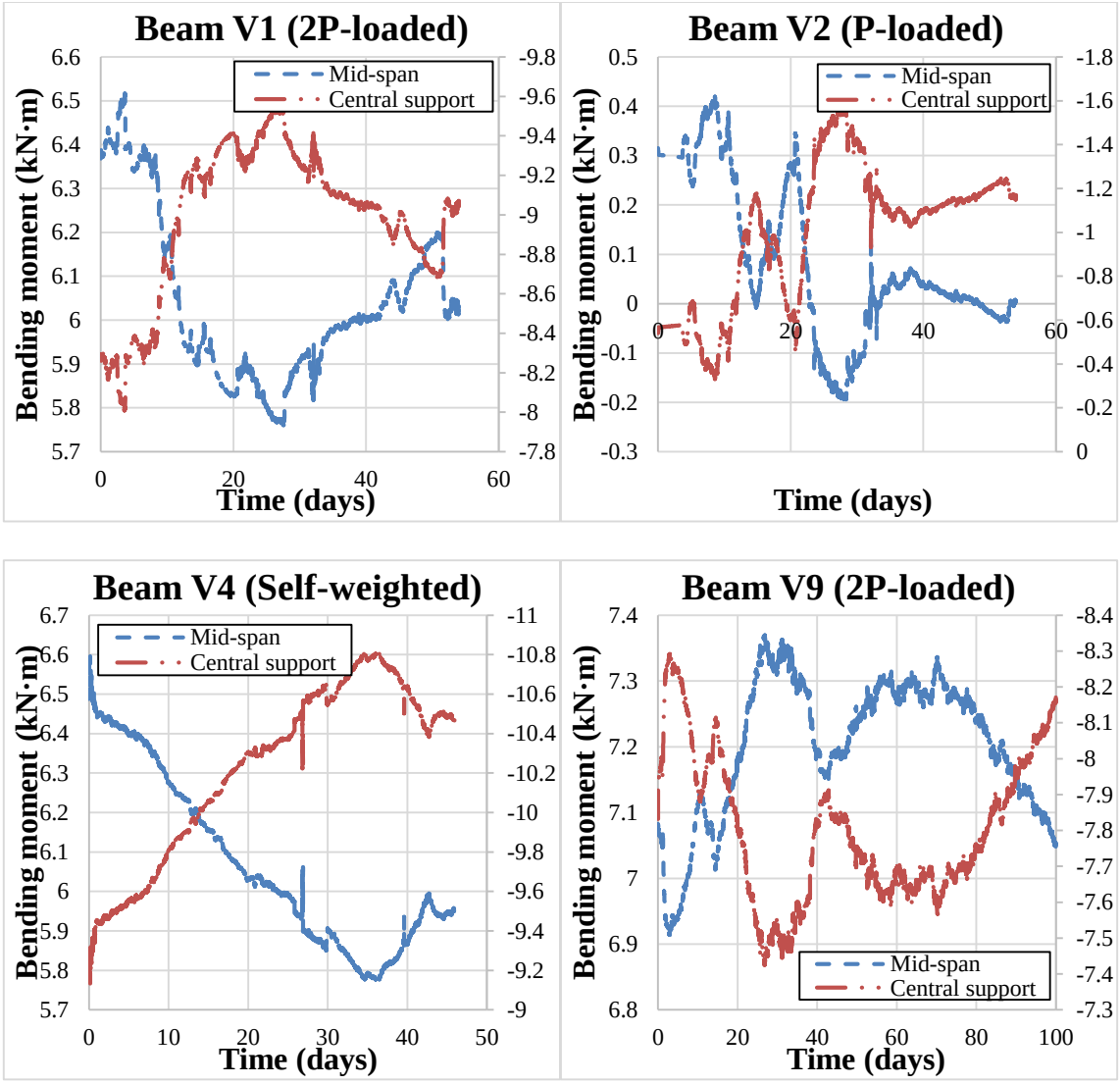

Figure III-14. Bending moment evolution at mid-span and central support cross-sections. . A) Beam V1 (2P-loaded) b) Beam V2 (P-loaded) c) Beam V4 (self-weighted) d) uncorroded beam V9 (2P-loaded)

Table III-6. Bending moment redistribution at central support cross-section (actual values and value as a percentage of bending moment at t = 0)

	Self-weight		Load P		Load 2P	
	Max. (kN·m)	Min. (kN·m)	Max. (kN·m)	Min. (kN·m)	Max. (kN·m)	Min. (kN·m)
Uncorroded	-1.03	-0.68	-4.54	-4.39	-8. 03	-7.77
	49.28%	1.45%	2.48%	0.90%	3.35%	0.00%
Group 1	-1.57	-0.33	-4.38	-3.24	-9.59	-8
	190.74%	38.89%	30.19%	12.67%	15.60%	3.26%
Group 2	-0.3	-0.29	-4.79	-3.8	-10.81	-9.13
	69.07%	70.10%	4.13%	17.39%	17.12%	1.08%
Group 3	-0.85	0.12	-5.41	-3.47	-8.29	-7.77
	0.00%	114.12%	27.00%	18.54%	5.87%	5.24%

The maximum and minimum variations in Table III-6 were attributed to corrosion of top and bottom steel reinforcement starting at different times i.e. if the top reinforcement started corroding several days after the bottom reinforcement the bending moment redistributed to mid-span cross-section, and vice-versa.

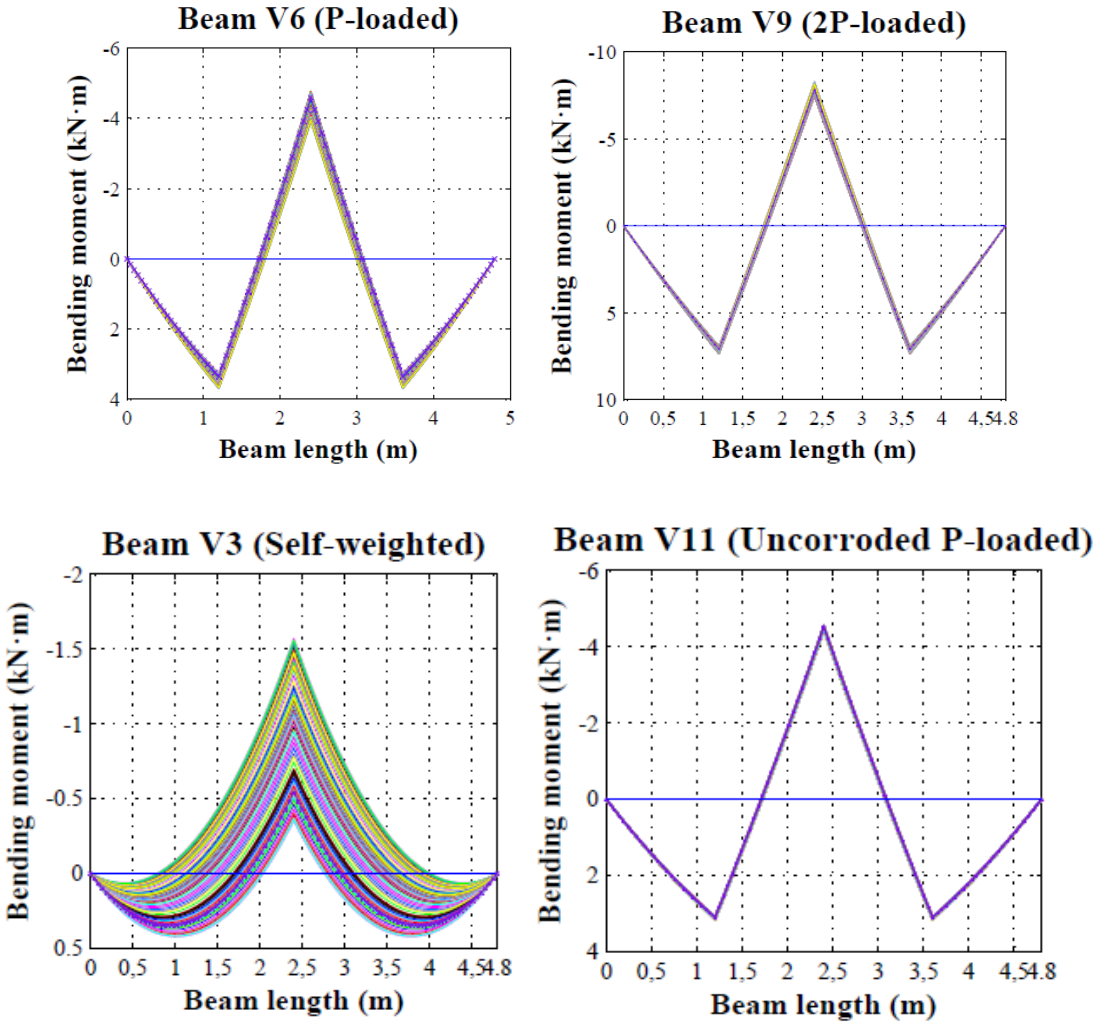

Figure III-15. Bending moment distribution along the beam. A) Beam V6 (Load P) b) Beam V9 (Load 2P) c) Beam V3 (self –weight only) d) Beam V11, uncorroded (Load P)

A description of the global bending moment distribution is depicted in Figure III-15 for some beams. Creep strains translated into an increase of the negative bending moment at the central support section for uncorroded specimens, Figure III-15c. Internal forces redistribution in self-weighted, corroded beams proceeded in the direction opposite to the self-weighted, uncorroded beam in all cases. The effect of reinforcing steel corrosion produced load redistribution in the sense opposite to the one expected under usual circumstances because of the increment of steel stress due to loss of cross-section at the

bottom reinforcement. If the bottom steel is corroded, the cross-section curvature becomes more negative (lower stiffness, hence higher compressive strains in the bottom fibre). Conversely, if the top reinforcement is corroded the curvature becomes more positive.

Group 1 and Group 3 beams under P load showed redistribution from the less stiff to the stiffer sections and vice versa with respect to the initial bending moment law. That behaviour as described for self-weighted only beams was attributed to the top reinforcement steel undergoing different corrosion levels. The Group 2 beam under load P showed redistribution towards positive bending moment zone only, indicating less corrosion of the top reinforcement.

In general all 2P-loaded beams underwent less redistribution than their P-loaded companions, pointing out that the bending moment capacity redistribution of statically undetermined beams is inhibited by the load. A possible explanation for observed such behaviour could be the stress level of the reinforcement. However, it is possible to observe some redistribution towards the central support cross-section.

As expected, uncorroded beams under P and 2P loads did not present any significant redistribution with respect to the initial bending moment law. The self-weighted control beam gave the expected redistribution due to creep.

III.2.5.5 Steel stress

Some of the gauges recorded information about the steel strains despite the extremely aggressive environmental conditions due to the NaCl solution and the current itself, although all the gauges stop working before the end of the test. With the data that were actually registered, it was possible to observe the steel behaviour due to corrosion. Figure III-16 shows the stress in reinforcement steel for the same sections described in Figure III-14 to make easier to compare effort redistribution, steel stress and corrosion level.

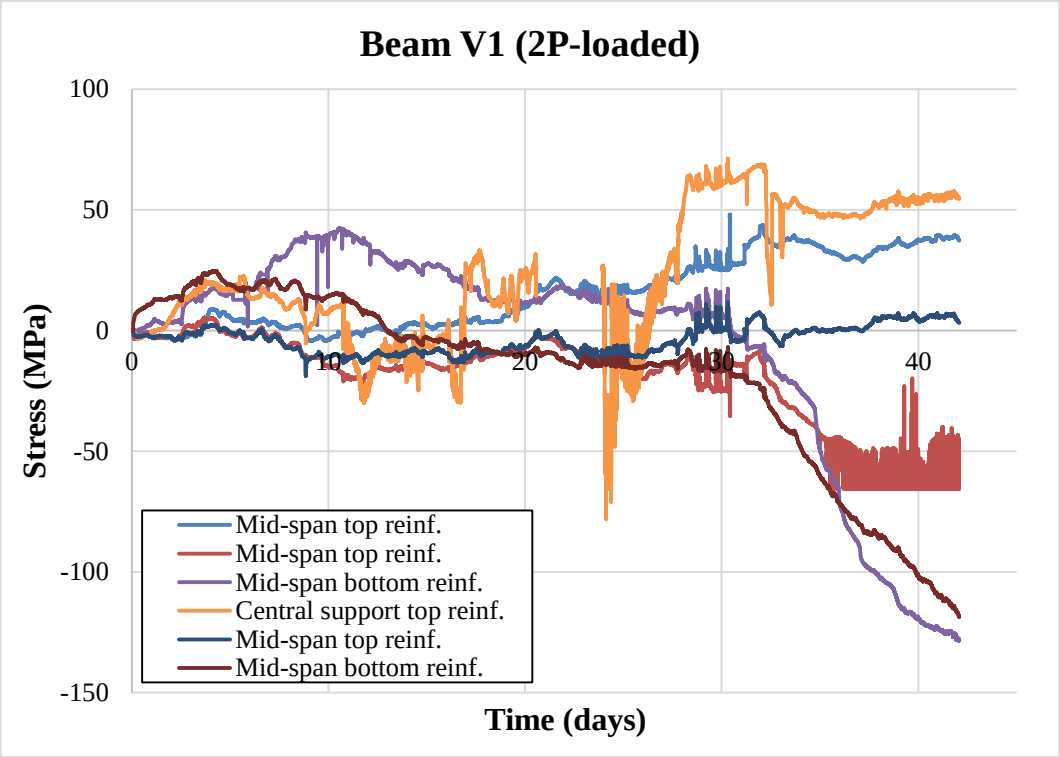
Beam V1 (2P-loaded)
Stress (MPa)
100
50
0
-50
-100
-150
0
10
20
30
40
Time (days)
Mid-span top reinf.
Mid-span top reinf.
Mid-span bottom reinf.
Central support top reinf.
Mid-span top reinf.
Mid-span bottom reinf.

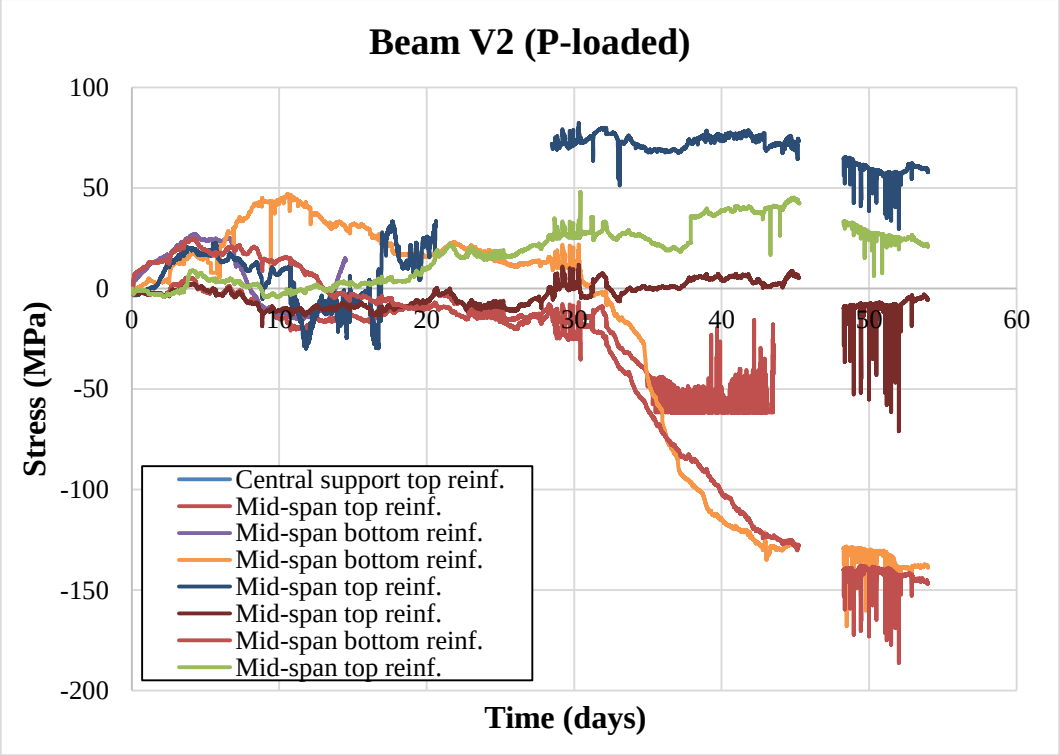
Beam V2 (P-loaded)
Stress (MPa)
100
50
0
-50
-100
-150
-200
0
10
20
30
40
50
60
Time (days)
Central support top reinf.
Mid-span top reinf.
Mid-span bottom reinf.
Mid-span bottom reinf.
Mid-span top reinf.
Mid-span top reinf.
Mid-span bottom reinf.
Mid-span top reinf.

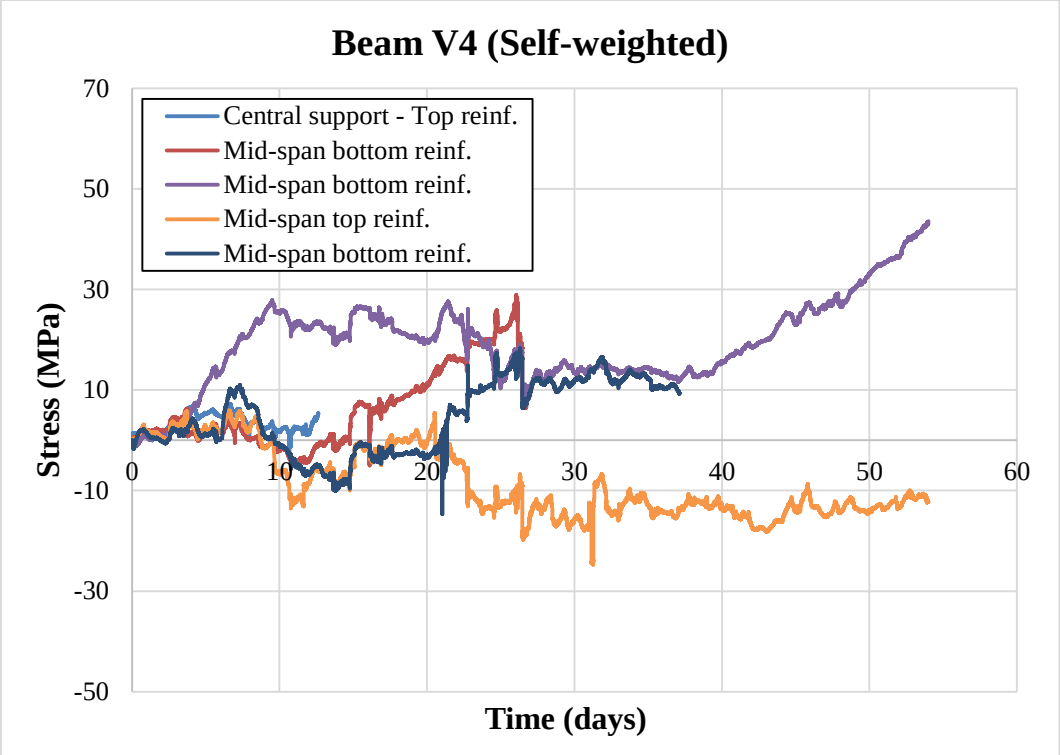
Beam V4 (Self-weighted)
Central support - Top reinf.
Mid-span bottom reinf.
Mid-span bottom reinf.
Mid-span top reinf.
Mid-span bottom reinf.
Stress (MPa)
70
50
30
10
-10
-30
-50
0
10
20
30
40
50
60
Time (days)

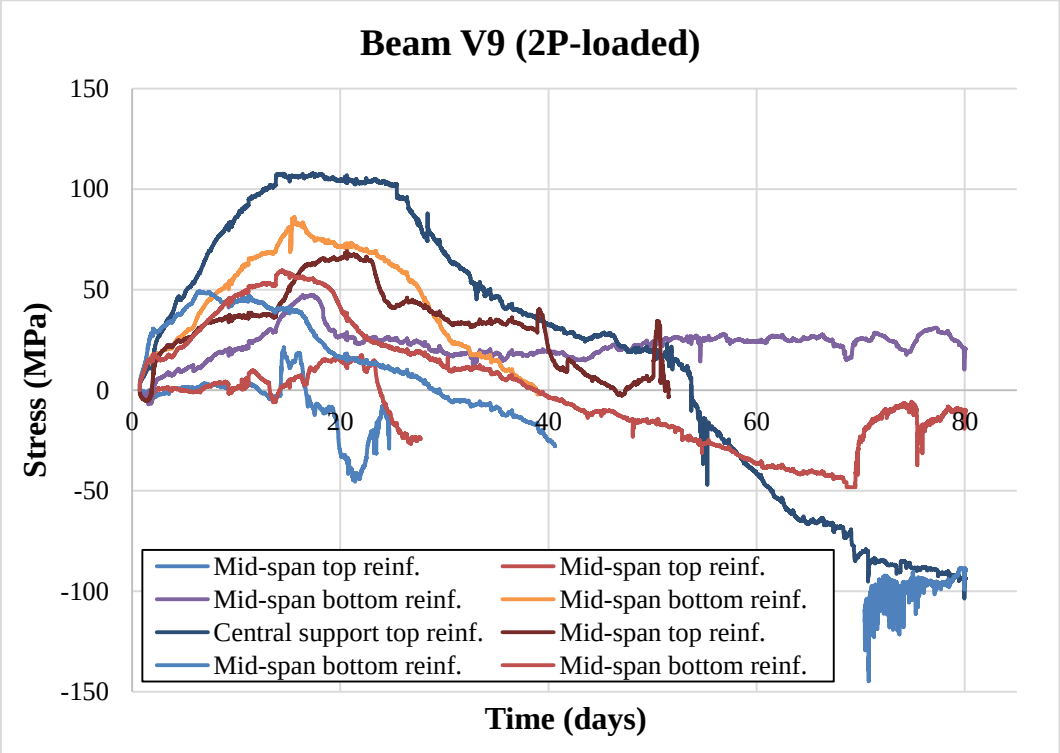
Beam V9 (2P-loaded)
Stress (MPa)
150
100
50
0
-50
-100
-150
0
20
40
60
80
Mid-span top reinf.
Mid-span top reinf.
Mid-span bottom reinf.
Mid-span bottom reinf.
Central support top reinf.
Mid-span top reinf.
Mid-span bottom reinf.
Mid-span bottom reinf.
Time (days)

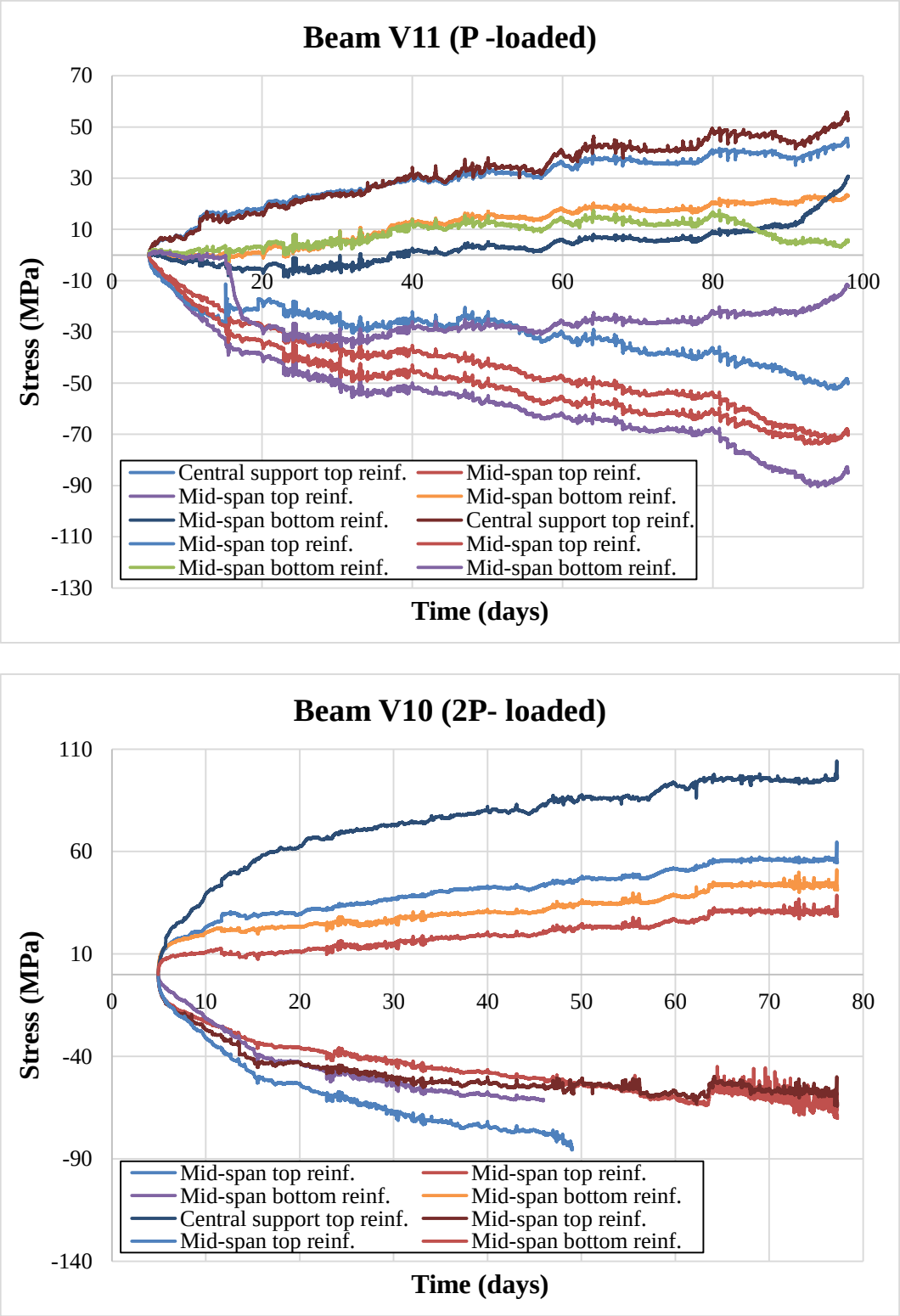

Figure III-16. Steel stress evolution during corrosion procedure

Stress on steel reinforcement described several fluctuations too, not just following loss of steel cross-section but also because of the forces redistribution. According to the stress evolution, the maximum stress increment was usually below the stress expected due to the loss of cross-section itself, as one would have in the case of an isostatic beam, for example. This means that the redistribution phenomenon typical of statically undetermined structures reduced the stress level on corroded steel bars reducing the possibility of premature failure.

In Figure III-16 - Beam V10 (2P-loaded), uncorroded beam, it can be seen that the natural stress increment on the top reinforcement of the central support cross-section is at least about 100 MPa after 80 days, due to creep. On the other hand Figure III-16 - Beam V9 (2P-loaded), which represents the same load case (2P-loaded beam), depicts roughly the same stress increment for the same reinforcing layer but after 20 days, describing a descending trend from there to last measurement at 80 days. Thus, the maximum stress level was observed for both specimens at the same cross-section, but at different times. The same behaviour was registered for the tensile reinforcement at the mid-span cross-section. The same response can be inferred when comparing Figure III-16 - Beam V11 (P-loaded), uncorroded beam, with Figure III-16 - Beam V2 (P-loaded): the tensile stresses hardly exceeded the maximum stress increment with respect to the uncorroded specimen.

Regarding mid-span top reinforcement, Figure III-16 shows that, in general, they were relieved of stress, presenting positive stress increments.

III.2.5.6 Slips

No significant variations of the slips were observed for any specimen during the corrosion procedure. No influence of the corrosion level and the relation between the applied load and the registered slip at the bar end of the bottom reinforcement steel was observed either.

III.2.5.7 Comparison between the predicted and the test results

A comparison between the theoretical and the experimentally obtained results was performed in order to assess the capacity of the structural analysis model to predict the structural effects of deterioration. Results for some specimens are presented to show the capabilities of the model.

Figure III-17 represents the delayed deflection for uncorroded beams and for Beam V6 (2P-loaded), Beam V8 (P-loaded) and Beam V3 (self-weighted only).

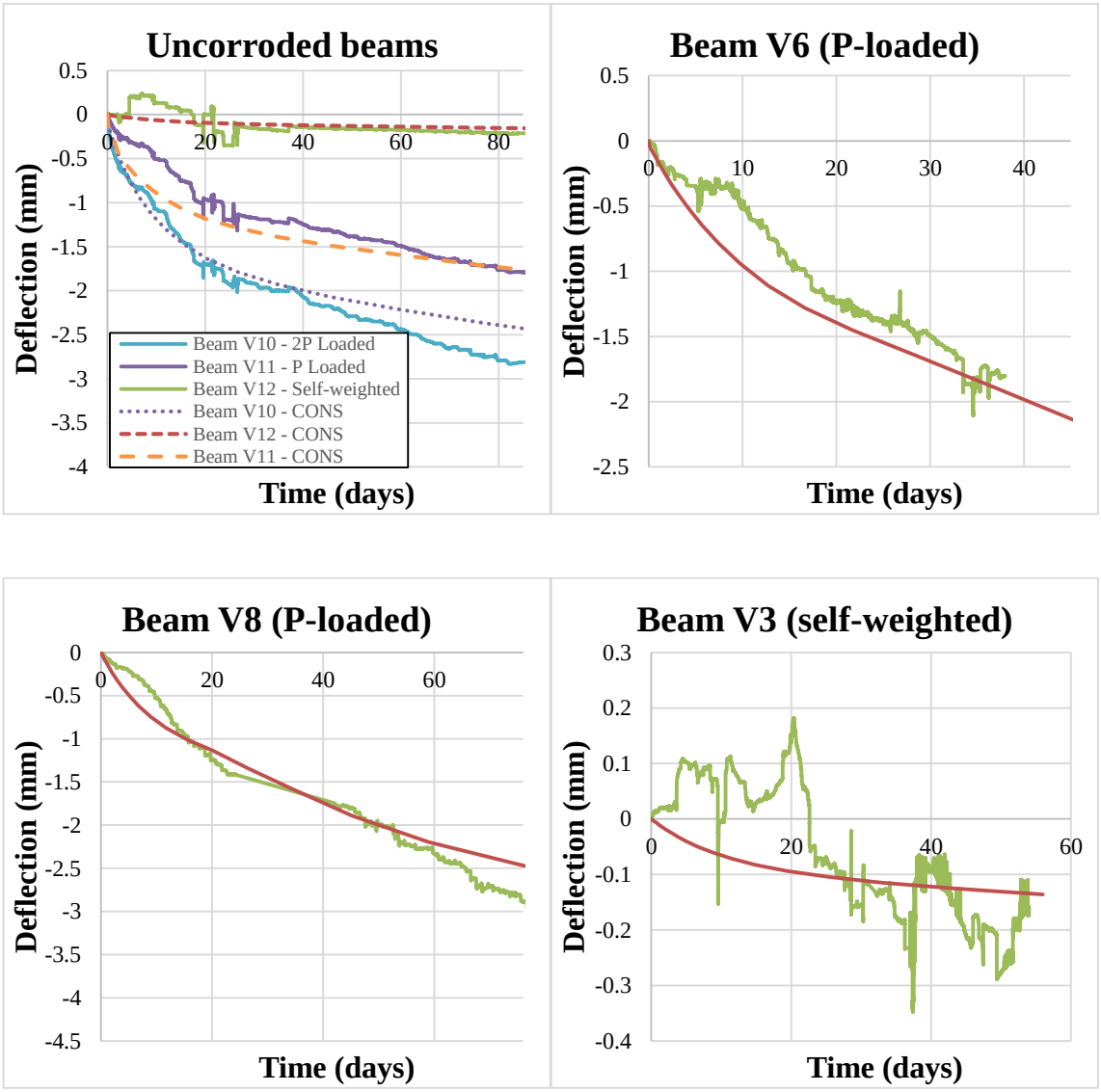

Figure III-17. a) Uncorroded specimens b) Beam V6 (P-loaded) c) Beam V8 (P-loaded) d) Beam V3 (self-weighted only)

The model adjusts quite accurately the deflections along time in the case of uncorroded beams. On the other hand, corroded specimens present more dispersion. The dispersion increases with the corrosion level, as it can be observed in Figure III-17b, for example. There are significant differences between predicted load redistribution values and experimental registered data.

III.2.6 Discussion

Four factors were identified as the main reasons for the corrosion of top reinforcement. Firstly, the reduced depth of the designed cross-section forces a spacing of less than 10 cm between upper and lower reinforcement. Secondly, since the cathode was placed in the middle of the cross-section, the distance from top and bottom reinforcement to the cathode was the same. Thirdly, the beam was saturated because of the irrigation system. Finally, both the top and the bottom reinforcement were depassivated because of the NaCl solution added during concrete mixing. These factors translated into a change of the initial corrosion scheme, switching to one where the top reinforcement took part, and started to corrode when humidity conditions were optimal.

It is extremely difficult to estimate initiation time of top reinforcement corrosion in each beam since many factors (such as beam humidity, pore mesh or cracking)... A potential initiation time of the top reinforcement has been nevertheless estimated through the analysis of reaction redistribution measurements. However, it is hard to confirm this parameter, even after the corroded rebar was extracted and cleaned to measure actual corrosion level, since not all specimens showed top reinforcement corrosion, and in some cases, only the outer top reinforcement was corroded (being the layer more exposed to irrigation water).

As described above, deflections are strongly influenced by corrosion of steel. In general terms, a significant increment of deflection was observed, severely reducing structure serviceability. Some factors could explain the increment of deflections in the structure. The main reason is the loss of stiffness because of steel cross-section reduction. An increase in stresses due to steel loss translated directly into a rise of deflections. In addition, other authors have stated the increment of the longitudinal strains as a reason for higher deflections [14,23]. The reduction of concrete cross-section could be another reason for increasing deflections, contributing to the overall stiffness reduction.

Another interesting phenomenon observed during the steel corrosion process was the effect of load. As previously noted, higher loads produced nonlinear amplification of deflections. In addition to the influence of creep, other phenomena induced an increment of deflections with the increase of corrosion level. It could be attributed to an amplification effect of the loss of cross-section stiffness with the applied load.

A significant impact of steel corrosion on load redistribution was observed. The reduction of steel cross-section and the modification of its mechanical properties is also observed on load redistribution. Each group of beams submitted to the same theoretical corrosion level

described quite a similar behaviour on load redistribution, which indicated that the corrosion on top and bottom steel was produced at a similar time. Since strain gauges did not survive the full corrosion procedure, steel stress remains mostly unknown, which renders difficult the interpretation of the load distribution. In spite of this, the capacity of statically undetermined beams to redistribute loads made possible to observe some effects.

The increase in stress detected in corroded elements is almost always smaller than the increase observed in uncorroded beams with the same reinforcement and the same load level. This means that the structure remains safe until very high corrosion levels are reached. For instance, beam V9, which attained a high corrosion degree, collapsed at the end of exposure time under the effect of the permanent load applied. Failure took place at the intermediate support, where negative moments are strongest and maximum local corrosion was observed *a posteriori* (local steel loss up to 40%). It can be seen, through the study of the evolution of bending moment in the intermediate support section, which there is indeed a moment redistribution towards the end supports, keeping the beam in a safety zone. The same phenomenon takes place in other tested elements in the opposite sense: concentrated corrosion in the bottom reinforcement produced redistribution towards the intermediate support.

Modelling the evolution of deterioration due to reinforcing steel corrosion is a difficult task. Many variables are affected by corrosion in addition to steel cross-section reduction. The preliminary tensile test for corroded steel showed a variation of the mechanical steel properties compared to uncorroded steel. Decreases of the modulus of elasticity, yield strength, tensile strength and maximum and ultimate strains were observed. Furthermore, the relation between this decrease and corrosion level is nonlinear, which indicates a degradation of steel at high corrosion levels; this behaviour has already been observed by other researchers [24].

The influence of other corrosion-dependent mechanic factors, such as stress concentration in pitting crack tips or local bending due to center of gravity shifts, produces non-uninform stress distributions throughout the section [22]. Also, material non-uniformity due to modern manufacturing procedures such as TEMPCORE tends to exacerbate these phenomena [22]. A more detailed description of material properties is necessary to better adjust model response. In addition, a more complex representation of splitting phenomena would be needed to discern which parts of the concrete section contribute to total resistance at each moment in time. Other authors have observed variations in mechanical properties of the concrete surrounding corroded bars [25,26]. This should also be included in the model to

take into account the full effect of corrosion if the goal is to accurately reproduce deterioration processes in statically undetermined structure.

III.2.7 Conclusions

Based on the results of the study, the following conclusions can be drawn:

(1) Higher deflections were observed for corroded specimens. Furthermore, the applied load produce higher deflections for the same corrosion levels, as shown by the comparison between normalized deflections under 2P and P loads.

(2) Internal forces redistribution between the different parts of the structure was observed, more pronounced at lower load levels. Up to 20% forces redistribution in the main cross-section under 2P load and 40% for P load took place only due to steel corrosion.

(3) The stress levels measured by means of the strain gauges described significant variations not only due the loss of cross-section itself but also due to the above-mentioned internal forces redistributions. However, the maximum increase in stress level observed for corroded specimens was roughly the same to those of uncorroded samples.

(4) The natural capability for forces redistribution of statically undetermined beams renders this type of structures safer under corrosion and deterioration phenomena.

(5) The mechanical properties of corroded steel bars are one of the main things to take into account during corrosion of steel. All the defining properties of steel were modified by corrosion. Furthermore, the degradation does not follow the corrosion degree linearly, becoming more intense with the increase in corrosion level.

(6) Modelling deterioration phenomena is a difficult task. Many factors have to be included in the model to take into account all the deterioration variables involved. The presented model can predict quite accurately the structure deflection; however, it did not properly reproduce effort redistribution.

Acknowledgments

The authors wish to acknowledge the financial support of The Ministry of Economy and Competitiveness of the Government of Spain (MINECO) for providing funds for project BIA2009-11764. The financial support of Infrastructures de Catalunya (ICAT) is also highly appreciated.

III.3 Effects of steel corrosion on the structural behaviour of reinforced continuous beams. Ultimate load capacity

Ignasi Fernandez*[1], Manuel F. Herrador[2], Antonio R. Marí[1], Jesús Miguel Bairán[1]

[1] Department of Construction Engineering, Polytechnic University of Catalonia, Jordi Girona, 1-3, Barcelona 08034, Spain.

[2] Department of Construction Technology, University of A Coruña, Campus de Elviña, s/n, A Coruña 15172, Spain.

*corresponding author: ignasi.fernandez-perez@upc.edu

Highlights:

- Corrosion effects on structural behaviour
- Load carrying capacity of corroded statically undetermined beams
- Anchorage failure due to steel corrosion

Abstract: Steel reinforcement corrosion is presented as the primary cause of structure deterioration, which may considerably reduce structural serviceability and safety. Focus on the behaviour of statically undetermined beams submitted to a synthetic corrosion procedure is interesting to study how this deterioration phenomenon affects complex structures. Tests on four groups of three two-span statically undetermined beams each are presented in this work. Three groups were submitted to different corrosion levels. For comparison purposes, the last one was left uncorroded. In addition, the study of the effect of confinement by external transverse strengthening of beam end is presented. Strengthened specimens described better structural response, shown as higher load capacity and ductility at failure in spite of higher corrosion levels. On the other hand, unstrengthened specimens showed clear anchorage failure mode with up to 55% decrease in load capacity. In any case, all the specimens presented a remarkable load capacity reduction even higher that only considering steel cross-section reduction.

Keywords: Corrosion; Steel reinforcement; Experimental tests; Bond-slip; statically undetermined beams;

III.3.1 Introduction and objectives

Structural safety is one of the most important factors in reinforced concrete structure design. A good understanding of the structural behaviour is essential to improving the designs and develop safer structures under different loading combinations and environmental situations. Many factors involving concrete, steel or both can initiate the structure deterioration, but the corrosion of steel reinforcement is the most severe of all possible deterioration phenomena. It has been reported as the first natural cause of structural failure, affecting a large number of structures in different situations [8]. Corrosion affects the structure in many ways, for instance, changing the structure serviceability by increasing deflections and producing new cracks, by reducing the steel cross-section (which translates into a change of its mechanical properties [24,27]), or it could directly affect structure safety strongly reducing its carrying capacity [28], changing the failure mode, developing other unexpected failure for which the structure has not been designed, or reducing the ductility producing brittle failures.

Many researchers have widely studied corrosion in concrete structures [13,29–32]. Some experimental campaigns involving steel corrosion have been performed, but concerning generally simple structures such statically determined beams or particular structure parts to consider local effects. The complexity of the phenomenon as well as the test setup required to perform accelerated corrosion methods tests have actively determined the development of experimentation in this field.

Furthermore the complexity of the phenomenon drives towards a lack of reliability in the existing models to adequately describe the corrosion phenomenon, mainly because most of them do not include all the effects involved in structure deterioration due to corrosion. The study of different modelling approaches to corrosion is relevant to simplify the phenomenon as much as possible without losing accuracy in model response.

The work hereby presented is the second and last phase of the analysis of two-span continuous beams under corrosion effects. Twelve statically undetermined beams, divided into four groups of three beams, submitted to impressed current are presented in this research to study the effects of corrosion on the ultimate state limit after the corrosion procedure took place. Different corrosion levels were achieved as a result of an impressed current applied to the reinforcement, defined using second Faraday's Law theory [10–12]. One group was left uncorroded as a benchmark. Additionally, the effect of steel confinement was studied. Three beams were tested up to failure without any strengthening, and the other set were externally strengthened with transverse reinforcement in order to provide some confinement

to the longitudinal steel bars, which deeply increases bond capacity. Different parameters of the structure were measured, and their evolution compared during loading up to failure.

III.3.2 Experimental programme and test setup

III.3.2.1 Materials

Type I Portland cement, CEM I 42.5R, was used in concrete mixtures with the characteristic strength of 42.5 MPa and rapid hardening. The specifications of the cement used are given in Fernandez et al. [33].

High ductility B500S steel bars were placed as reinforcement steel. Two different diameters were used, 10 mm and 12 mm.

III.3.2.1.1 Concrete mix proportions

The mixt was prepared and cast in the Structures Technology Laboratory, Universitat Politècnica de Catalunya (UPC) – Barcelona Tech (LTE).

The mix proportion of conventional concrete with 300 kg/m^3 of cement and a total water/cement ratio of 0.50 is the one specified for concretes exposed to marine and chloride environment described by Spanish Structural Concrete code [16]. The dosage is also described in Table III-7.

Table III-7.Proportioning of the concrete mixtures

Material (1000 litres)	Dosification
Cement (kg)	300
Total Water (kg)	150.00
Effective w/c	0.446
FA 0/4mm	976.00
CA1 4/12mm	210.00
CA2 12/20mm	765.00
NaCl (weight of cement)	4%
Superplastizier (weight of cement)	1%
Retarder (weight of cement)	0.8%

III.3.2.2 Concrete properties. Compression, modulus and tensile tests

The compressive strength of concrete was determined using a compression test machine with a loading capacity of 3000 kN. The compressive strength was measured at the age of 28 days

following UNE-EN 12390-3. Three cylindrical specimens (150 mm diameter and 300 mm length) were used for each type of concrete produced.

The modulus was determined using the same machine applying cycles in the concrete elastic range on cylinder of 150x300 mm, as prescribed by UNE-EN 12390-3. The modulus was measured at the age of 28 days. The tensile stress parameter was obtained by means of the Brazilian test using the same specimens, which involves indirect tensile measurement.

III.3.2.3 Tensile steel test

The tensile strength was determined using a test machine with a loading capacity of 5000 kN. The tensile steel behaviour was measured from a sample of the same steel used in the beams. Different 40 cm length specimens were tested following standards [18]. A displacement transducer was used to obtain the modulus of elasticity of the material in the elastic range, and the load-displacement curve was recorded up to failure.

III.3.2.4 Test specimens description and test setup

Twelve continuous two-span beams were cast. The beams had 5 m total length with two symmetric clear spans of 2.4 m. The cross-section was rectangular with 250 mm width and 125 mm depth. Concrete cover was 15 mm on all four faces.

Reinforcement steel was arranged longitudinally only, trying to avoid direct connection between the top and bottom steel faces to prevent interference in the corrosion process. Two 10 mm diameter rebars were placed on the top face, plus two extra 10 mm diameter rebars across the maximum negative bending moment zone. In the bottom, face two 12 mm diameter rebars were placed along the whole length.

Figure III-18 describes the geometrical specifications of the specimens, steel disposition of the reinforcement and the cross-section definition.

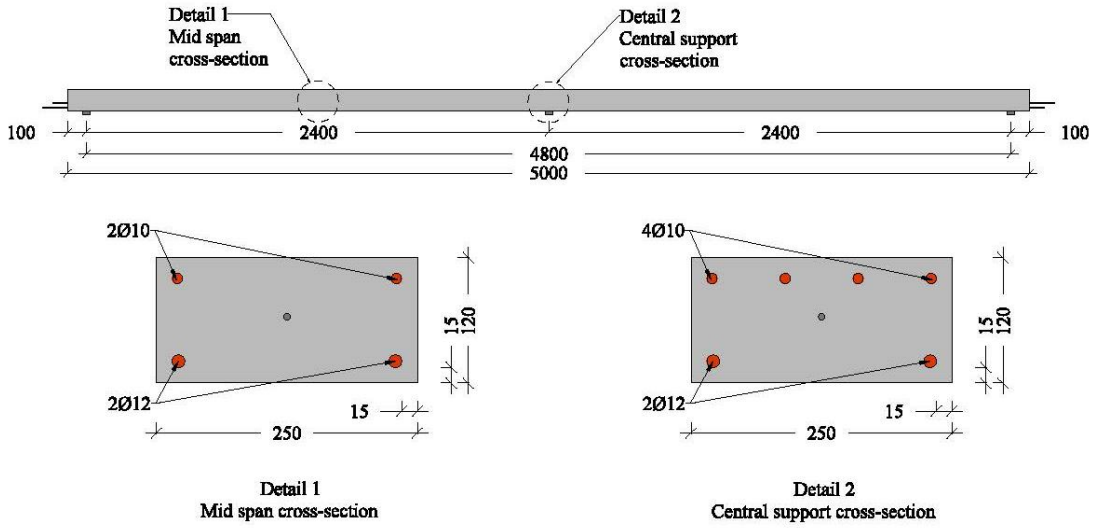

Figure III-18. Geometrical specs of the specimens

III.3.2.4.1 Test setup

Two load frames affixed to the test slab were disposed over the two mid-span points. Two identical hydraulic jacks were used to introduce the applied load on the beams until failure. The load was applied by means of displacement control of one of the jacks. The same pressure was applied in both load points during the test since both hydraulic jacks were connected to the same pressure supply. The applied load was recorded using two load cells. Figure III-19 shows the loading setup.

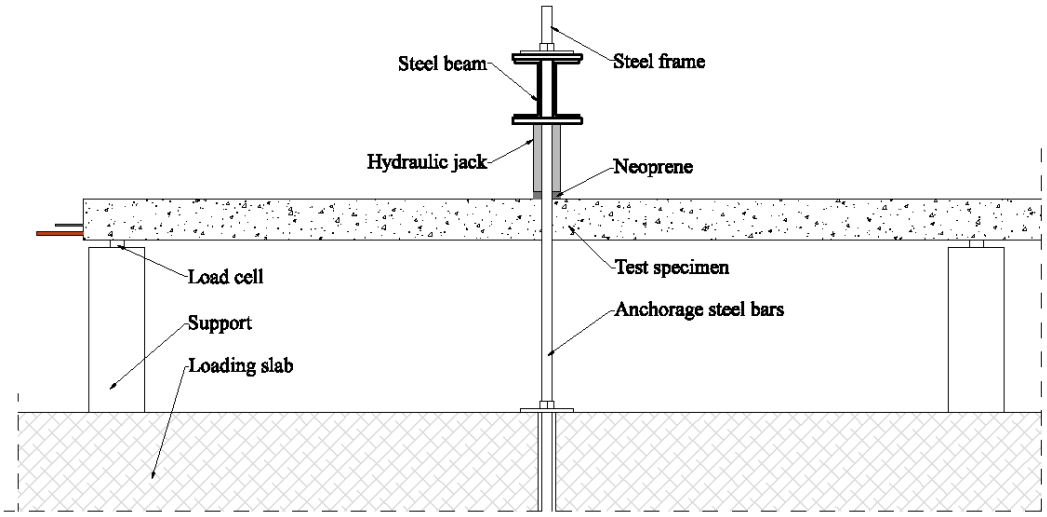

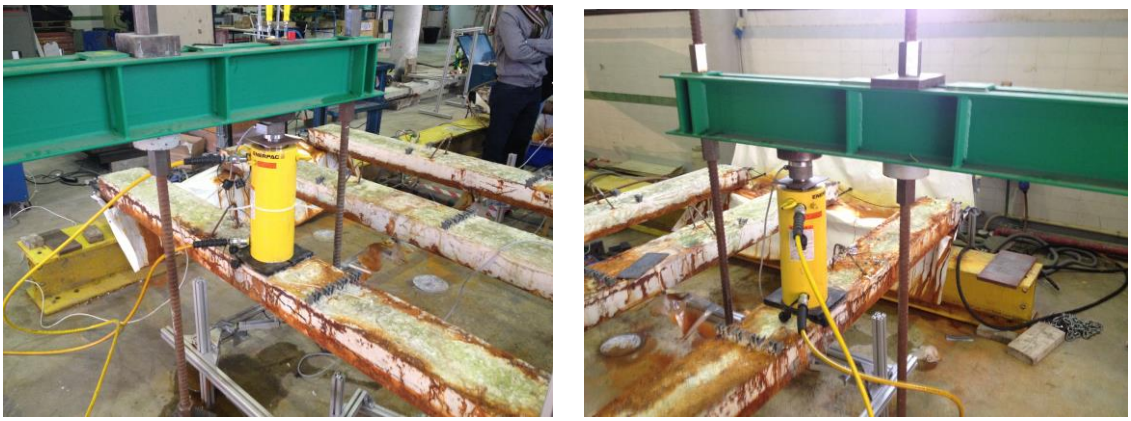

Figure III-19. Test configuration during load to failure

Neoprene bearings of 20 mm depth were placed under the two applied load points as well as under the support. A characterization of the mechanical properties of the neoprene to consider its effect on the total displacement was done.

III.3.2.4.2 Strengthening

Three of the twelve beams were left unstrengthened to assess the failure mode of unconfined corroded structures without transversal steel.

On the other hand, the rest of specimens were strengthened with an external passive strengthening simulating the presence of transverse steel in the structure. Due to the corrosion procedure adopted, the configuration of the reinforcing steel was arranged without transverse steel, which is not a common situation. Passive strengthening was proposed and applied to simulate more real structural conditions of corroded members. A detail of the strengthening configuration can be seen in Figure III-20.

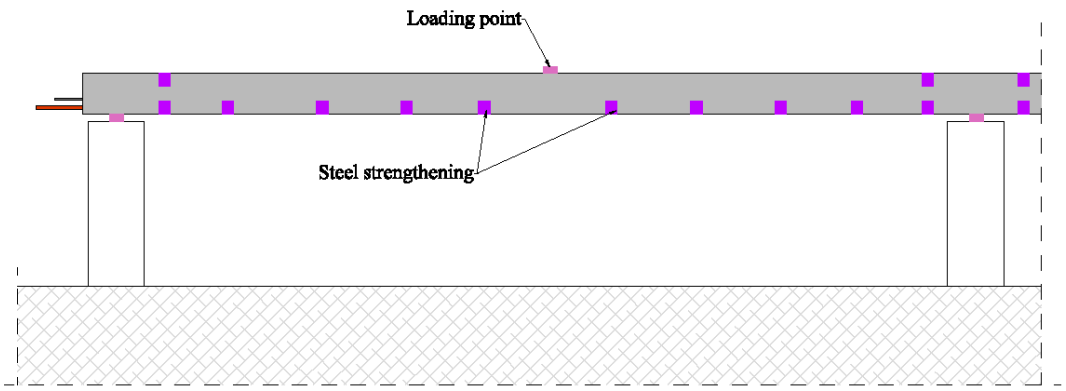

Figure III-20. Placed strengthening

III.3.2.5 Accelerated corrosion

Accelerated corrosion methods open the possibility to reproduce corrosion episodes in structures over very short periods of time, as compared to natural corrosion. Obviously, this kind of corrosion mechanism has some drawbacks compared to natural corrosion testing. They are nevertheless necessary to investigate the effects in structures and materials over time within an appropriate investigation period. With this kind of methods, it is possible to reproduce a 20-30 years phenomenon in a few months with a reasonable agreement between the natural and induced corrosion effects.

III.3.2.5.1 Corrosion method

Corrosion of steel reinforcement was forced by means of impressed current. Following Faraday's law (Equation III-4), it is possible to estimate the weight loss of steel due to corrosion, knowing the applied intensity along time, I(t), and the geometrical bar properties such as diameter and exposed length.

Equation III-4 $$\boldsymbol{E = \frac{m_{Fe} \cdot \int I \cdot dt}{V \cdot F}}$$

Where, m_{Fe} is the atomic mass, V is the steel valence that is taken as equal to two and F is Faraday's constant. As the applied intensity was an input during the test and it is also constant along time, it is possible to rewrite Faraday's law as Equation III-5.

Equation III-5 $$\boldsymbol{\Delta m = \frac{m_{Fe} \cdot I \cdot t}{V \cdot F}}$$

Further details of the corrosion method performed are described in Fernandez et al. [33]

III.3.2.6 Measuring equipment

Four kinds of measuring equipment were used during the loading process:

III.3.2.6.1 Displacement transducers.

Displacement transducers were placed to register beam deflections during the loading phase. Deflections were measured at mid-span, two deflection records per beam. Additional displacement transducers were placed at the free steel bar-end to register bond-slip due to steel corrosion, one transducer at each beam end. Figure III-21 describes the position of the different transducers.

III.3.2.7 Load transducers.

Each beam had five load transfer points: three reactions and two load application points. In order to gather enough information to determine the bending moment law along the beam at any given time, 4 load cells were placed, obtaining the 5th unknown by equilibrium (the symmetric condition was avoided because of possible construction imperfections). Thus, reactions and applied load on every beam were known during the whole corrosion procedure as well as in failure tests. Figure III-21 shows the load cell measurement points.

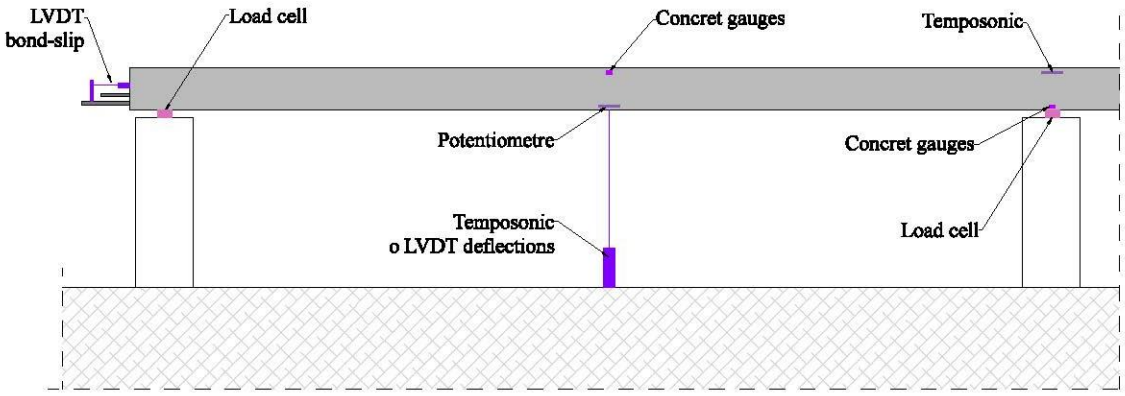

Figure III-21. Displacement transducers

III.3.2.7.1 Strain gauges.

Strain gauges were placed to record the steel stress variation during the beam loading. Very few gauges survived the corrosion procedure. Nevertheless, some data were collected.

The strain gauges were placed on the tensile reinforcement, both in the negative and the positive bending moment zones, as well as in the compressed steel bars in the mid-span cross-section. The gauges were placed in both spans. See Figure III-22.

Uncorroded specimens were also instrumented with strain gauges placed on the concrete surface.

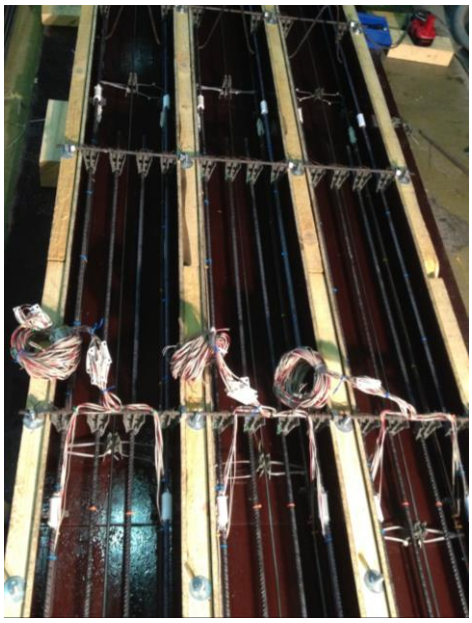

Figure III-22. Strain gauges

III.3.2.7.2 Wire strain gauges

The initial bending cracks were instrumented with wire strain gauges to register the crack width during the test. Only the main initial cracks were instrumented: the positive bending moment cracks in both spans and the negative bending crack over the middle support.

III.3.3 Test results

Table III-8 describes the ultimate load for each beam and the corrosion degree reached at the end of the corrosion procedure. Beam V9 failed under the service load applied during the corrosion phase presenting a significant reduction in the ultimate load with respect to the other specimens. The corrosion in this beam was very severe achieving up to 24% steel loss. In addition, a localization of the corrosion was observed in the tensile reinforcements after the cleaning process in the central support cross-section. A cut formed in the two rebars due to loss of cross-section resulted in the structure failure. The registered deflections just before the failure did not describe any significant increment, so the failure was brittle. Figure III-23 shows the final state after the beam failure and the steel cross-section reduction suffered.

Table III-8. Corrosion levels achieved, exposure days and applied load on span centre at failure

Group	Beams	Corroded Reinforcement	Steel loss (%)			Ultimate load (kN)		
1	V1-V2-V3	Top reinforcement	6	6	9	24,50	16,50	11,40
		Bottom reinforcement	14	12	11			
2	V4-V5-V6	Top reinforcement	6	6	7	25,75	21,00	24,75
		Bottom reinforcement	15	10	15			
3	V7-V8-V9	Top reinforcement	15	17	10	21,80	21,00	8,40*
		Bottom reinforcement	15	20	24			
Ref	10-11-12			0		31,60	36,59	36,42

Figure III-23. Beam V9 after failure

III.3.3.1 Concrete, uncorroded steel bars and neoprene properties

Table III-9 describes the compressive strength at 28 days of curing and the steel tensile test results that include yielding tensile strength and modulus of elasticity.

Table III-9. Concrete compressive strength, tensile strength and modulus. Steel fy and modulus

	Compressive strength	Tensile strength	Elasticity modulus
Concrete	40 MPa	3.5 MPa	35000 MPa
ϕ 10 steel	--	550 MPa	200000 MPa
ϕ 12 steel	--	545 MPa	195000 MPa
Neoprene	--	--	30000 MPa

III.3.3.2 Damage description before testing

Due to induced steel corrosion, beams presented a highly deteriorated aspect. Longitudinal cracks along the bottom and top reinforcements were observed for all the specimens due to rust expansivity. Beams loaded during the induced corrosion procedure presented three transverse cracks: two of them in each mid-span, under the applied load point, and the other one in the negative bending moment zone. Corrosion products were highly visible in the beams presenting stains along the member, see Figure III-24.

Figure III-24. Damage before testing. Longitudinal and transverse crack

III.3.3.3 Confined specimens results

III.3.3.3.1 Uncorroded beams

Uncorroded beams presented bending failure. Both the top reinforcement and the bottom reinforcement yielded showing high ductility at failure. The ultimate applied load was around 36 kN. Figure III-25 displays the load - displacement curves for the three uncorroded members.

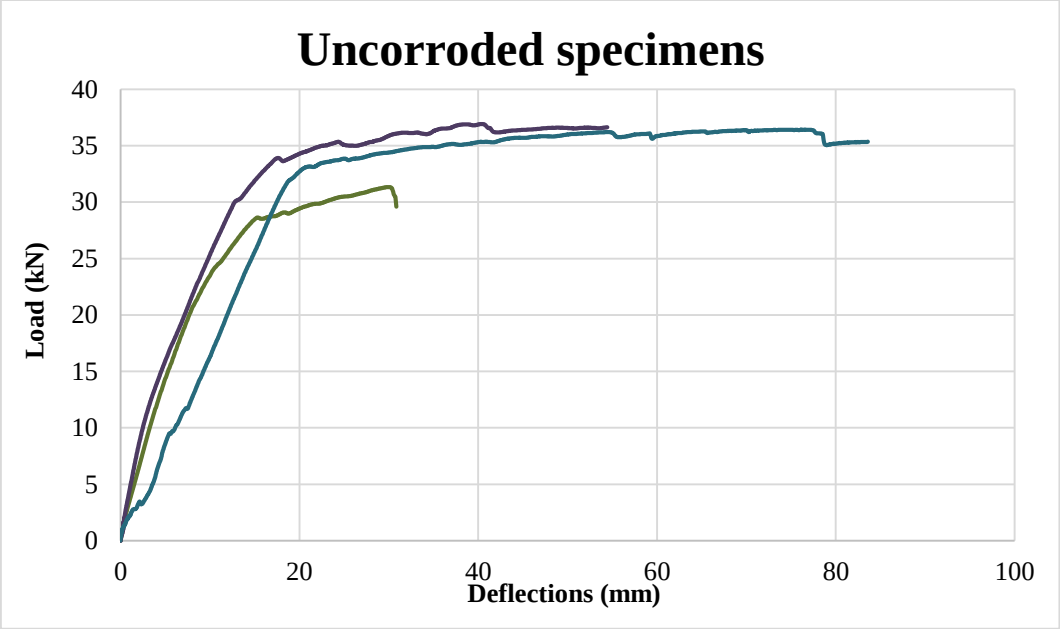

Figure III-25. Load displacement curves for the three uncorroded specimens

Steel disposed amount made no significant internal forces redistribution between critical cross-sections before failure. Only at the very end of the load process, the specimens showed redistribution, as see in Figure III-26.

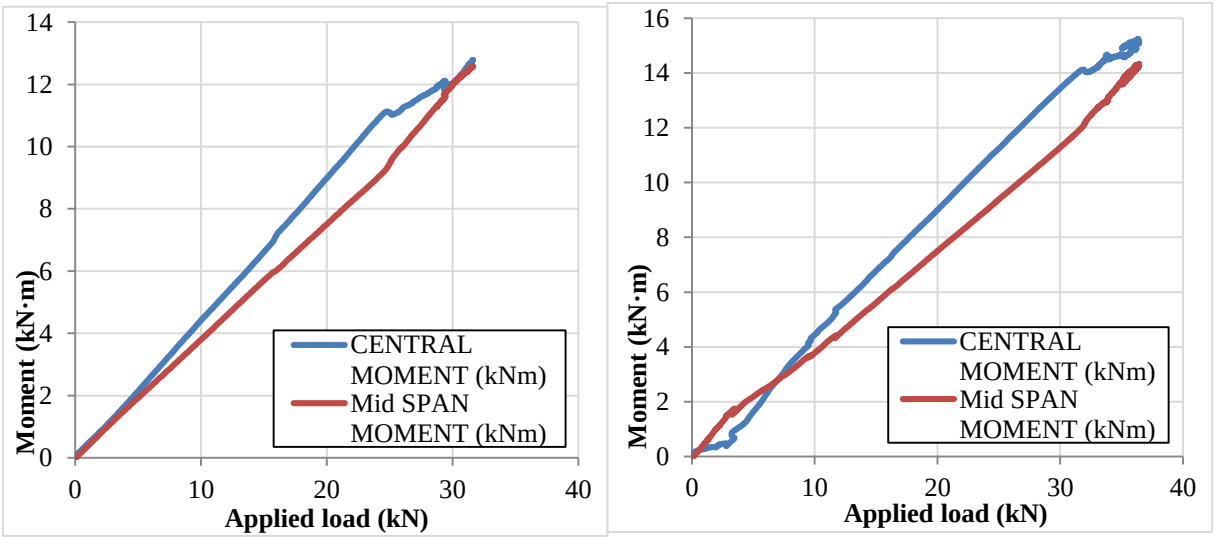

Figure III-26. Beam 12 Bending moment – Applied load. Internal forces redistribution at the very end of the applied load

Figure III-27 shows the steel reinforcement stress in the sections under the applied load and above the central support. Both critical cross-sections presented steel yielding.

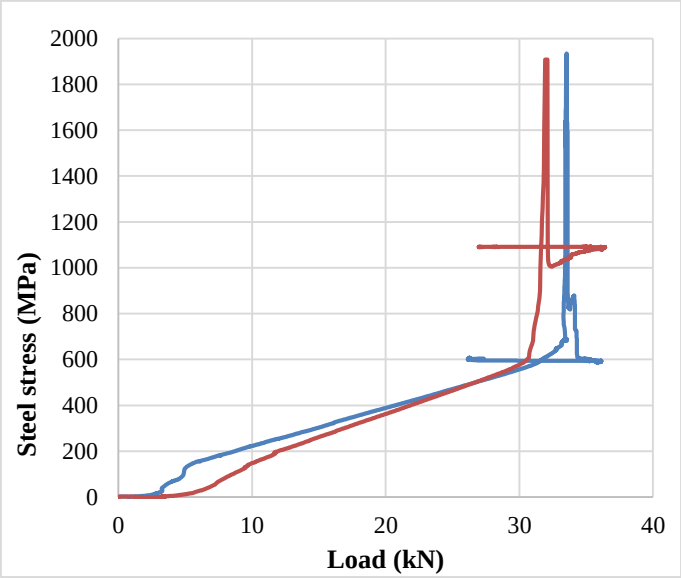

Figure III-27. Steel stress reinforcement mid-span and central support cross-sections

III.3.3.3.2 Corroded beams

All corroded specimens presented similar behaviour. All the specimens, independently from their corrosion levels, showed similar load capacity. The failure load ranged between 20 kN and 25 kN, which is a load reduction between 46% and 30% respectively compared to that of uncorroded specimens. Despite the reduction in bearing capacity, the external strengthening provided some ductility at failure as it is shown in Figure III-28. Half of the specimens presented the same displacement at ultimate load as the uncorroded benchmarks. However, the other specimens presented less ductility at ultimate load.

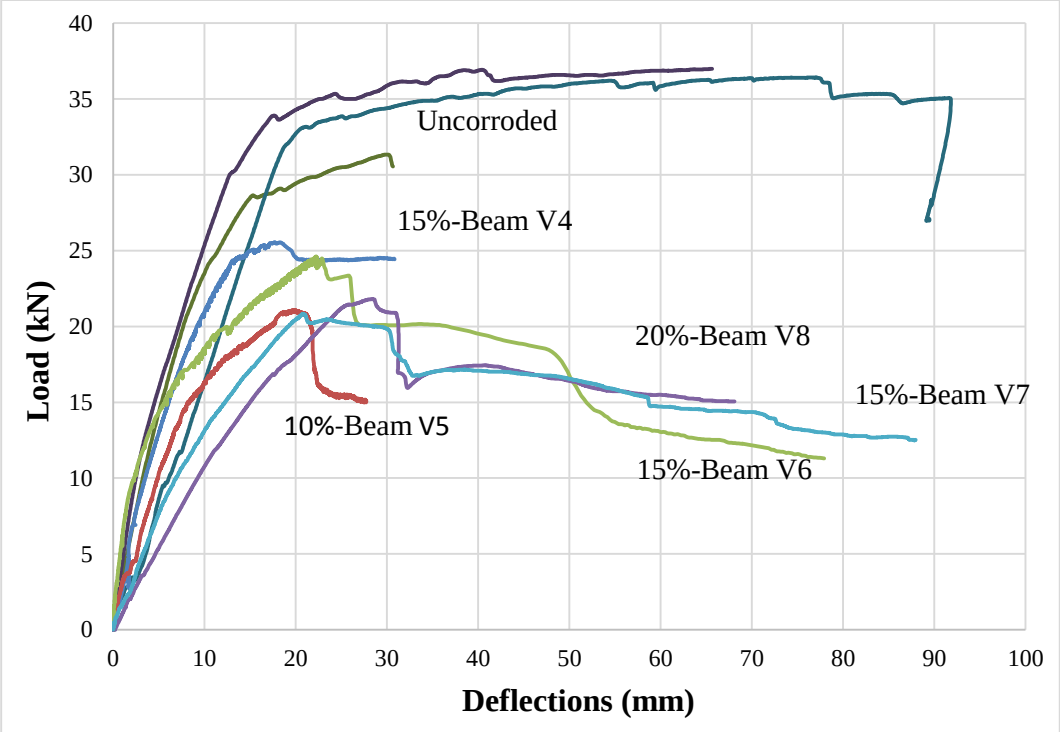

Figure III-28. Load - displacement confined corroded and uncorroded beams.

Redistribution of internal forces for corroded specimen was observed in some cases as it is depicted in Figure III-29. The corrosion effects due to cross-section reduction and corroded steel mechanical properties degradation are also observed in the same figure. The difference between the moment at the central support and the mid-span moment was more pronounced than in uncorroded specimens, which indicates that the capacity and the stiffness of the specimens had been reduced.

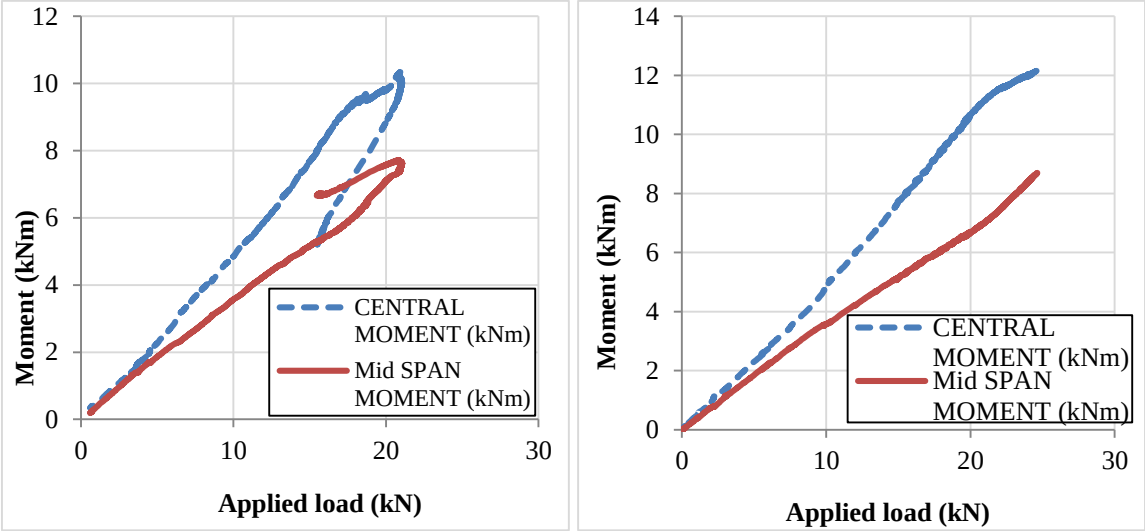

Figure III-29. Bending moment – Applied load. Internal forces redistribution at the very end of the applied load.

Beams Beam V5 and Beam V6

Nevertheless, Beam V6 and Beam V7 presented important slipping at the bottom reinforcement as shown in Figure III-30. High deterioration levelled to an anchorage failure, which produced a reduction of load capacity of the member. Beam V7 presented reinforcement slip at very low load levels, indicating bond reduction capacity due to corrosion and lower effectiveness of the provided confinement. On the other hand, Beam V6 presented brittle bond failure. The slip for very low load levels was tiny but when the load reached 25 kN the bond between concrete and steel dropped drastically, triggering severe reinforcement slipping and reducing load capacity.

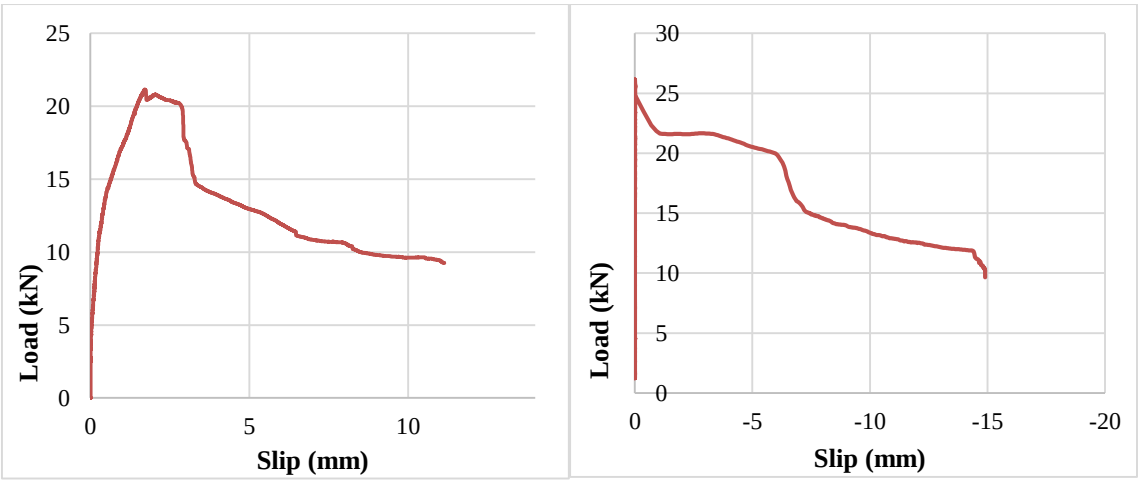

Figure III-30. Slip curves for beams Beam V7 and Beam V6

III.3.3.4 Unconfined specimens

All the unconfined members presented anchorage failure. In Figure III-31, the final state of the unconfined beams (Beam V1, Beam V2 and Beam V3) is shown. Splitting as well as concrete cover spalling was observed. Even though this group was the less corroded, the achieved corrosion level was enough to change the failure mode. All the beams presented anchorage failure. Figure III-32 describes the evolution of the stress in the bottom reinforcement with respect to the deflection. The second axis represents the load evolution with respect to the total deflection too. After the applied load reached 10 kN, the slip of the bottom reinforcement steel took place, leading to the aforementioned anchorage failure. The remaining residual bond capacity let to a constant stress value in steel. The beam capacity significantly dropped with respect to those uncorroded specimens, which registered up to 45% reduction of load capacity. Failure was premature and more brittle, so the expected beam ductility was also significantly reduced.

Figure III-31. Final beam state after splitting and spalling

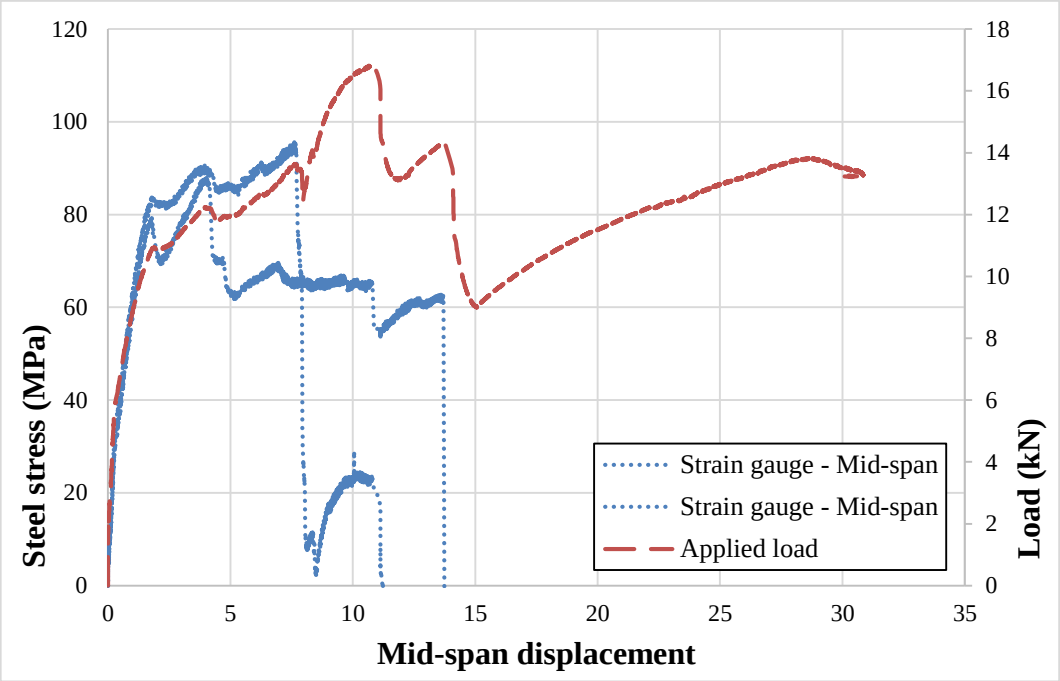

Figure III-32. Beam V2 described failure. Steel stress in left axis and load in right axis vs deflection

In Figure III-33a a more detailed description of the anchorage failure of Beam V2 is shown. The discharging effect on the bottom reinforcement (until the residual bond capacity is reached) while the slip of the reinforcement increases can be observed. Figure III-33b depicts the anchorage failure of the Beam V3. In this case, the remaining bond capacity allowed the recovery of some load capacity after bond failure.

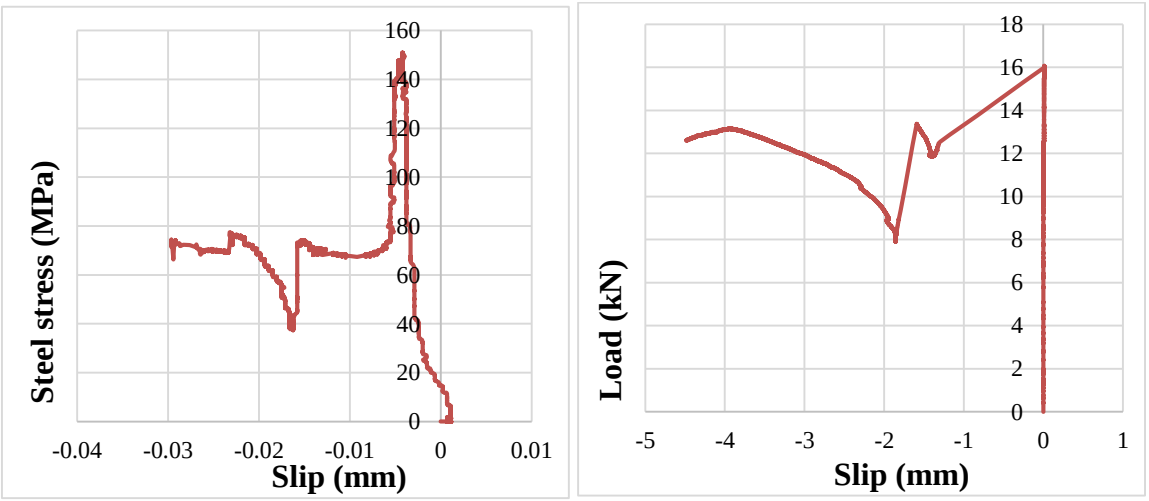

Figure III-33. a) Slip at the end bar vs stress steel, beam 2. B) Slip at the end bar vs applied load, beam 3

The overall behaviour of unconfined corroded specimens compared to uncorroded beams is shown in Figure III-34.

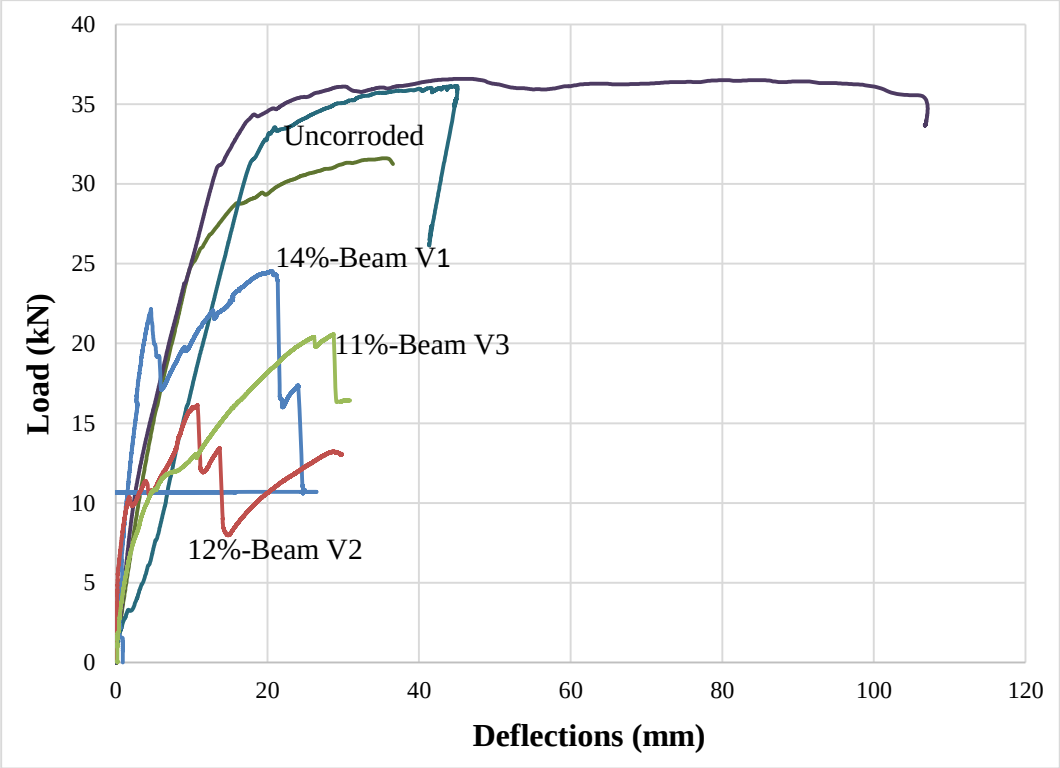

Figure III-34. Load- displacement registered for unconfined specimens as well as uncorroded members

III.3.3.5 Discussion

Corrosion of steel reinforcement produced a clear reduction of the ultimate capacity of the different tested members. A brittle and premature failure due to anchorage failure took place in unstrengthened corroded specimens; splitting and cover spalling were mainly observed. The lack of transverse steel produced local splitting failure in the bottom reinforcement with a subsequent bond drop. The remaining bond capacity was not enough to bear the applied load and the load capacity of the beams was strongly reduced.

On the other hand, strengthened specimens described better overall behaviour. An increase of the total load capacity with respect to the unconfined specimens was observed in spite of greater corrosion levels. The confinement provided by the disposed strengthening produced an increase of the bond capacity even for higher corrosion levels than measured for unstrengthened specimens.

All the confined beams described roughly the same failure loads independently of their corrosion level. A change of the failure mode took place for in all the specimens towards bond failure, which indicates that effects such as the reduction of steel cross-section and the degradation of corroded steel mechanical properties did not influence the structural behaviour as much as bond, for high corrosion levels. Hence, the failure is mainly governed by the reduction of bond capacity. Very high confinement conditions are needed to avoid anchorage failure for very high corrosion levels. Other corrosion effects such as concrete cover spalling, concrete mechanical properties degradation, steel cross-section reduction or steel mechanical properties degradation may have much more influence at low corrosion levels where the bond between concrete and steel is not as deteriorated.

The crack pattern was also modified by corrosion of steel. The steel stresses were not well transferred to the concrete and the bending cracks were reduced. The specimens only showed one or two wide-open cracks which points toward this effect. It was not possible to develop a third crack in a single specimen.

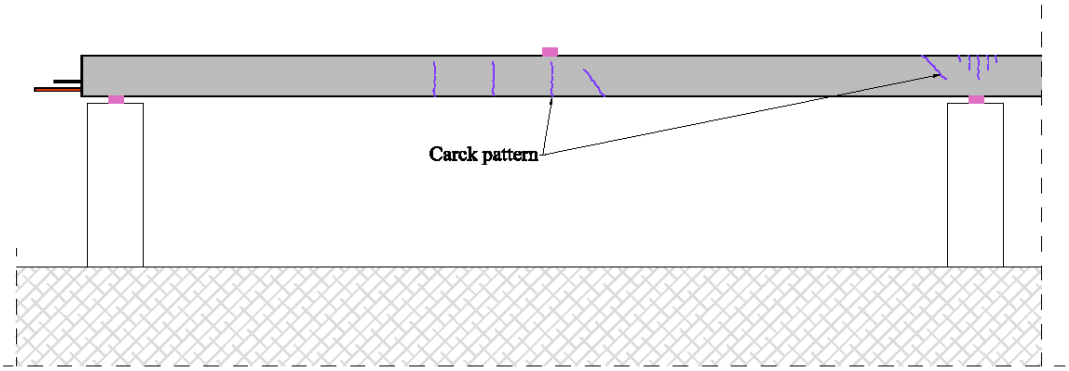

Figure III-35. Crack pattern uncorroded specimen

III.3.4 Conclusions

Based on the results of the study, the following conclusions can be drawn:

(1) Corrosion of steel reinforcement strongly reduces the load-bearing capacity of the structure. The reduction of load capacity is higher than the reduction that would take place considering only reinforcement steel cross-section reduction, which means that other local phenomena have to be taken into account to study the structural response.

(2) Unconfined conditions produced premature, brittle anchorage failure due to splitting. On the other hand, confined members had an increased overall structure response, with higher load bearing capacity despite higher corrosion levels. However, failure load reductions between 30% and 46% with respect to uncorroded members were observed.

(3) Bond between concrete and steel is considered as the main parameter that affected the structural response. Very high corrosion levels produced a severe drop in bond, which mainly controls the failure mode and load bearing capacity of the specimens in all the cases. Other local effects such as corroded steel mechanical properties degradation are more significant for low corrosion levels or more confined specimens.

Acknowledgments

The authors wish to acknowledge the financial support of The Ministry of Economy and Competitiveness of the Government of Spain (MINECO) for providing funds for project BIA2009-11764. The financial support of Infrastructures de Catalunya (ICAT) is also highly appreciated.

References

[1] E. Spacone, F.C. Filippou, F.F. Taucer, Fibre Beam-Column Model for Non-Linear Analysis of R/C Frames: Part I. Formulation, Earthq. Eng. Struct. Dyn. 25 (1996) 711–725. doi:10.1002/(SICI)1096-9845(199607)25:7<711::AID-EQE576>3.0.CO;2-9.

[2] A.R. Marí, Numerical simulation of the segmental construction of three dimensional concrete frames, Eng. Struct. 22 (2000) 585–596. doi:10.1016/S0141-0296(99)00009-7.

[3] D.C.S. Ferreira, A model for the nonlinear, time-dependent and strengthening analysis of shear critical frame concrete structures, (n.d.). http://www.tdx.cat/handle/10803/116540 (accessed September 10, 2014).

[4] S. Mohr, J.M. Bairán, A.R. Marí, A frame element model for the analysis of reinforced concrete structures under shear and bending, Eng. Struct. 32 (2010) 3936–3954. doi:10.1016/j.engstruct.2010.09.005.

[5] G. Al-Sulaimani, M. Kaleemullah, I. Basunbul, Influence of corrosion and cracking on bond behavior and strength of reinforced concrete members, ACI Struct. J. (1990). http://www.concrete.org/Publications/InternationalConcreteAbstractsPortal.aspx?m=details&i=2732 (accessed July 3, 2014).

[6] C. Alonso, C. Andrade, J. Rodriguez, J. Diez, Factors controlling cracking of concrete affected by reinforcement corrosion, Mater. Struct. 31 (1998) 435–441. http://link.springer.com/article/10.1007/BF02480466 (accessed July 3, 2014).

[7] K. Tutti, Corrosion of steel in concrete, (1997) 6–15. doi:10.4324/9780203414606_chapter_2.

[8] J. Broomfield, Corrosion of steel in concrete: understanding, investigation and repair, 2nd Ed., Taylor & Francis, Abingdon, United Kingdom, 2002.

[9] A. Muñoz Noval, Comportamiento de vigas hiperestáticas de hormigón armado corroídas y reparadas con mortero : pérdida de propiedades mecánicas del acero de refuerzo y fisuración del recubrimiento de hormigón por corrosión, (2009). http://oa.upm.es/2488/1/ALEJANDRO_MUNOZ_NOVAL.pdf (accessed March 26, 2015).

[10] T.A. El Maaddawy, K.A. Soudki, Effectiveness of Impressed Current Technique to Simulate Corrosion of Steel Reinforcement in Concrete, (2003) 41–47.

[11] S. Caré, Q.T. Nguyen, V. L'Hostis, Y. Berthaud, Mechanical properties of the rust layer induced by impressed current method in reinforced mortar, Cem. Concr. Res. 38 (2008) 1079–1091. doi:10.1016/j.cemconres.2008.03.016.

[12] C. Lu, W. Jin, R. Liu, Reinforcement corrosion-induced cover cracking and its time prediction for reinforced concrete structures, Corros. Sci. 53 (2011) 1337–1347. doi:10.1016/j.corsci.2010.12.026.

[13] G. Malumbela, P. Moyo, M. Alexander, Behaviour of RC beams corroded under sustained service loads, Constr. Build. Mater. 23 (2009) 3346–3351. doi:10.1016/j.conbuildmat.2009.06.005.

[14] G. Malumbela, M. Alexander, P. Moyo, Steel corrosion on RC structures under sustained service loads - A critical review, Eng. Struct. 31 (2009) 2518–2525. doi:10.1016/j.engstruct.2009.07.016.

[15] G. Malumbela, M. Alexander, P. Moyo, Variation of steel loss and its effect on the ultimate flexural capacity of RC beams corroded and repaired under load, Constr. Build. Mater. 24 (2010) 1051–1059. doi:10.1016/j.conbuildmat.2009.11.012.

[16] A.R. Marí, Numerical simulation of the segmental construction of three dimensional concrete frames, Eng. Struct. 22 (2000) 585–596. http://www.sciencedirect.com/science/article/pii/S0141029699000097 (accessed June 18, 2014).

[17] Instrucción de hormigón estructural - EHE-08, 2008.

[18] UNE-EN-ISO-15630-01, Acero para el armado y pretensado del hormigón - Métodos de ensayo. Parte 1: Barras, Alambre y Alambrón para el hormigón armado, (n.d.).

[19] Y. Yuan, Y. Ji, S. Shah, Comparison of Two Accelerated Corrosion Techniques for Concrete Structures, ACI Struct. J. 104(3) (207AD) 344–347.

[20] M. Saifullah, L.A. Clark, Effect of corrosion rate on the bond strength of corroded reinforcement, in: S.A. Press (Ed.), Proc. Int. Conf. Corros. Corros. Prot. Steel Concr., University of Sheffield, 1994: pp. 591–600.

[21] S. a. Austin, R. Lyons, M.J. Ing, The Electrochemical Behaviour of Steel Reinforced Concrete During Accelerated Corrosion Testing, (n.d.).

[22] M. Badawi, K. Soudki, Control of Corrosion-Induced Damage in Reinforced Concrete Beams Using Carbon Fiber-Reinforced Polymer Laminates, J. Compos. Constr. 9 (2005) 195–201. doi:10.1061/(ASCE)1090-0268(2005)9:2(195).

[23] G. Malumbela, M. Alexander, P. Moyo, Interaction between corrosion crack width and steel loss in RC beams corroded under load, Cem. Concr. Res. 40 (2010) 1419–1428. doi:10.1016/j.cemconres.2010.03.010.

[24] I. Fernandez, J. Bairán M., A. Marí R., Corrosion effects on the mechanical properties of reinforcing steel bars. Fatigue and σ-ε behaviour, Constr. Build. Mater. (2015).

[25] M. Quagliaroli, From Bidimensional towards Monodimensional Modeling of Sound and Damaged Reinforced Concrete Structures, 2014.

[26] F. Biondini, F. Bontempi, D.M. Frangopol, P.G. Malerba, Cellular Automata Approach to Durability Analysis of Concrete Structures in Aggressive Environments, J. Struct. Eng. 130 (n.d.) 1724–1737. http://cedb.asce.org/cgi/WWWdisplay.cgi?143874 (accessed May 25, 2015).

[27] C.A. Apostolopoulos, M.P. Papadopoulos, S.G. Pantelakis, Tensile behavior of corroded reinforcing steel bars BSt 500s, Constr. Build. Mater. 20 (2006) 782–789. doi:10.1016/j.conbuildmat.2005.01.065.

[28] Y. Ballim, J.C. Reid, Reinforcement corrosion and the deflection of RC beams—an experimental critique of current test methods, Cem. Concr. Compos. 25 (2003) 625–632. doi:10.1016/S0958-9465(02)00076-8.

[29] J.G. Cabrera, Deterioration of concrete due to reinforcement steel corrosion, Cem. Concr. Compos. 18 (1996) 47–59.

[30] A.A. Torres-Acosta, S. Navarro-Gutierrez, J. Terán-Guillén, Residual flexure capacity of corroded reinforced concrete beams, Eng. Struct. 29 (2007) 1145–1152. doi:10.1016/j.engstruct.2006.07.018.

[31] J. Rodriguez, L. Ortega, J. Casal, Load carrying capacity of concrete structures with corroded reinforcement, Constr. Build. Mater. 11 (1997) 239–248. doi:10.1016/S0950-0618(97)00043-3.

[32] M. Tahershamsi, K. Zandi, K. Lundgren, M. Plos, Anchorage of naturally corroded bars in reinforced concrete structures, Mag. Concr. Res. 66 (2014) 729–744. doi:10.1680/macr.13.00276.

[33] I. Fernandez, M.F. Herrador, A.R. Marí, J.M. Bairán, Structural effects on serviceability due to reinforcement steel bars corrosion of statically-undetermined concrete members, (2015).

Chapter IV

LOCAL CORROSSION EFFECTS

IV.1 Introduction

Corrosion of steel reinforcement leads to different local effects on the structure, which may have a non-negligible effect on the structural response. Essentially, two of these phenomena have been studied in this thesis: mechanical steel properties and bond capacity reduction due to corrosion of steel. The first aspect presented in this chapter is the change of mechanical steel properties. The traditional approach to consider steel corrosion on the structural models has been including the degree of corrosion of steel as a direct reduction of the cross-section. Some researchers claimed that a modification of the steel properties is produced during steel corrosion. An extensive experimental study with more than 140 steel specimens was performed which encompassed test of steel bars under cyclic or monotonic loads with the underlying porpoises of extend the sparse existing database of fatigue test of corroded steel bars and extend and calibrate a previously developed model. From the experimental study, a significant variation of the mechanical properties was observed for corroded steel rebars.

In addition, a nonlinear relationship between the loss of cross-section and the steel properties reduction has been defined. A geometrical description of the corrosion phenomenon was performed describing the critical pit in the failure cross-section. Different relationships were established relating the geometrical pit characteristics and the mechanical properties of corroded steel.

The second phenomenon studied is the modification of bond properties between steel and recycled aggregates concrete. Recycled aggregates concrete has claimed by many researchers as a good alternative to reduce the impact of the wastes coming from construction. Nevertheless, the existing codes restrict its use by replacing only 20% of the coarse aggregates because the durability issues associated with them. Mainly an increment of porosity and permeability might lead to a higher deterioration velocity of the structure. The aim of this work is to define the bond behaviour after a reinforcing steel corrosion episode. Corrosion of steel reinforcement produces high expansive products which damage the surrounding concrete. Due to rust between concrete and steel the bond between both might be deteriorated. The porosity of Recycled Concrete Aggregates, what is stated as the major weak point in this kind of concretes, might improve bond performance because an internal and external cracking reduction due to a greater capacity to absorb corrosion products. Some concrete specimen were cast with different amounts of recycled coarse aggregate, 20%, 50% and 100%. Thereafter by means of accelerated corrosion methods steel embedded bars were corroded until three different corrosion levels were reached. A comparison between the uncorroded and corroded specimens is done observing a significant bond increment as higher amount of recycled coarse aggregate was employed for low corrosion levels. However high corrosion levels produced similar bond strength.

IV.2 Corrosion effects on the mechanical properties of reinforcing steel bars. Fatigue and σ-ε behaviour.

Ignasi Fernandez*[1], Jesús Miguel Bairán[1], Antonio R. Marí[1]

[1] Department of Construction Engineering, Polytechnic University of Catalonia, Jordi Girona, 1-3, Barcelona 08034, Spain.

*corresponding author: ignasi.fernandez-perez@upc.edu

Highlights:

- An experimental study on fatigue and monotonic test with corroded an uncorroded steel bars.
- Study of corroded steel mechanical properties with respect to the generalized corrosion level
- Pitting characterization in the critical cross-section.
- Study of the geometrical pit parameters with respect to the corrosion level in the fatigue life.

Abstract: Corrosion of steel reinforcement is one of the most severe problems of durability in reinforced concrete structures. A good understanding of the corroded steel mechanical properties is necessary to assess impaired structures adequately. A study of the mechanical response of corroded reinforcement subjected to monotonic and fatigue loading is presented. An experimental study consisting of more than 190 corroded specimens, 40 monotonic and 140 fatigue tests was performed. Relationships between corrosion level and the mechanical properties are identified. In addition, a study of the pit geometry influence on the fatigue life is conducted, which includes the effect of the different geometrical parameters on the fatigue life. Severe non-linear reduction in all the mechanical properties considered according to the corrosion level is observed. These phenomena result in relevant information for the assessment of existing structures and in life cycle evaluation.

Keywords: Corrosion, Tensile properties, Mechanical properties, Fatigue, Durability

IV.2.1 Introduction

Corrosion of the reinforcement steel bars is one of today's most frequent and significant types of damage in existing reinforced concrete structures. Therefore, the study of the structural effects of bars corrosion is crucial for determining the structural performance and residual strength of impaired structures. Volumetric expansion of corrosion products causes severe problems inducing splitting stresses along corroded reinforcement, with possible resulting damage to the surrounding material. Generally, the splitting stresses are not well tolerated by concrete, resulting in cracking and eventually spalling of the concrete cover. As the reinforcement becomes more exposed, the corrosion rate may increase and facilitate the deterioration process.

One significant steel corrosion effect is the change in mechanical properties of steel. Although most of the investigations are not mainly focused on this effect, steel reinforcement corrosion yields into material mechanical properties changes [1–4]. The study of the local impacts of corrosion is critical to defining the new steel bars properties due to corrosion in structural models to adequately assess the structural behaviour and safety in local or global levels. The change in steel behaviour can become into an unexpected structural response, even producing undesired brittle failures.

The classical approach to consider corrosion of steel reinforcement in the response of concrete structures has been to consider a reduction of nominal cross-section area proportionally to the corrosion level. However, both generalized corrosion and pitting corrosion are subjected to another effects than just the loss of steel area. Phenomenon such as distributed pitting along the steel bar becomes in a stress concentration at the notch tip. Also, the displacement of the centre of gravity of the cross-section due to a non-uniform corrosion or because of the pitting itself produces a non-uniform stress distribution along the pitted cross-section. Further, some modern production systems of reinforcing bars, such as TEMPCORE®, produces heterogeneous material properties throughout the steel cross-section, being the apparent σ-ε characterization of the bar, the mean response of the heterogeneous section. Specifically annular distribution of the mechanical properties takes place for this steel manufacture system [5–9]. Obviously the loss of part of the cross-section modifies the balance of the mechanical properties distribution not only because of the reduction of steel cross-section itself but because of the loss of the external crowns of material which provides higher load capacity to the outfit.

Several experimental studies were performed during the last years to evaluate the relationship between the degrees of corrosion of the steel bars embedded in concrete on their mechanical properties [1,3,10–17]. A smaller number of studies have been undertaken on the evaluation of corroded steel bars subjected to low-cycle loads [10,18,19]. Even fewer investigations are found in the literature studying the corroded steel behaviour under high-cycle loads [17].

In this research work, a study of the mechanical reinforcing steel properties, either corroded or uncorroded, using monotonic tensile tests and cyclic loading fatigue tests is presented. Two experimental phases were carried out in order to define the parameters that are necessary to understand the modification of corroded steel properties, testing specimens of two different diameters, (10 mm and 12 mm) of artificially corroded steel. The tests results of these specimens were compared with those obtained from the uncorroded reinforcement specimens tested.

Experimental Phase 1 encompassed monotonic test performed to get the main parameters defining the σ-ε curves of corroded steel. 40 specimens of 310mm to 320 mm length with a range of 8% to 22% corrosion levels were satisfactorily tested.

At Phase 2, 140 specimens of 310 to 320 mm length with corrosion levels ranging from 8% to 28% were tested under several cycling loads. Three different stress ranges (ΔS) were defined, 150 MPa, 200 MPa and 300 MPa in order to evaluate the influence of the stress range on the fatigue life of corroded bars. The applied load for the different specimens was obtained by means of the nominal diameter of the corroded specimen, measuring the fatigue life reduction at the service load level with respect to the uncorroded steel. The characteristic pitting was measured on all the tested specimens in order to evaluate its influence on the reduction of fatigue life.

IV.2.2 Uncorroded steel properties

B500SD reinforcing steel was used in the monotonic and fatigue test for corroded and uncorroded specimens. Uncorroded steel properties are described in Table IV-1. Figure IV-1 shows the measured σ-ε behaviour for the two steel diameters used in this work.

Table IV-1. Steel characterization of B500SD bars

Diameter	Yielding Load (kN)	Ultimate Load (kN)	ε_{max}	ε_u	Modulus of elasticity	f_y	f_{max}
ϕ10	42.62	51.01	0.151	0.189	208590	542.56	649.50
ϕ12	62.02	72.11	0.13	0.189	197207	548.35	637.58

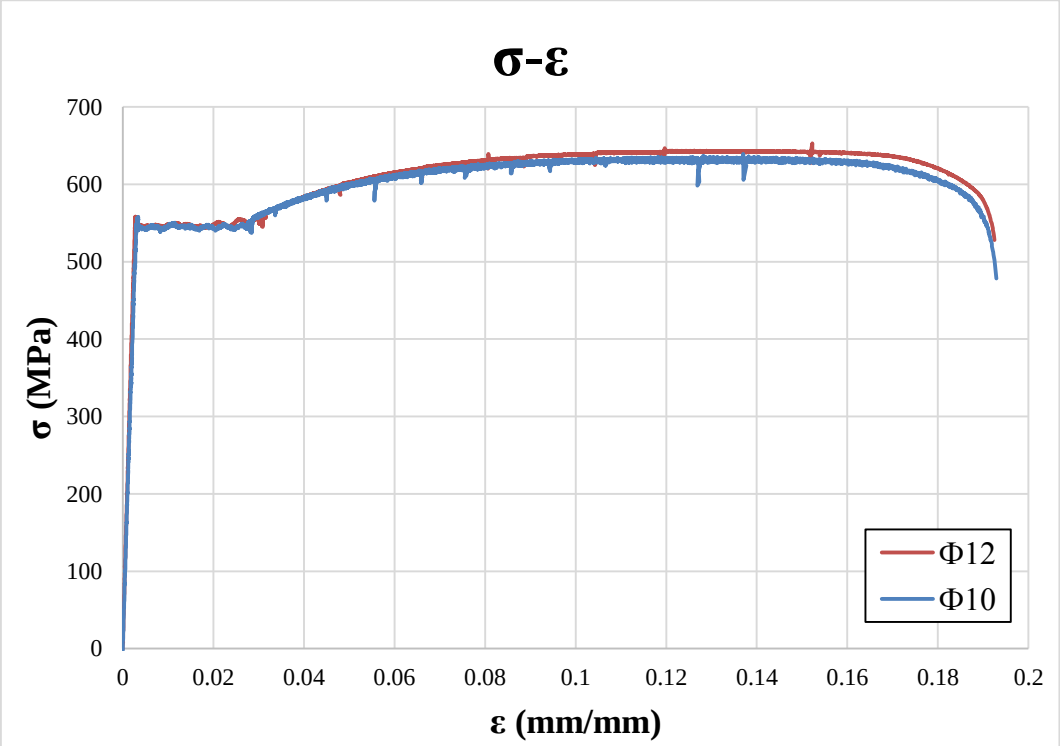

Figure IV-1. Stress-strain behaviour of uncorroded B500SD bars

IV.2.3 Cyclic and monotonic test of corroded steel bars

IV.2.3.1 Test setup and execution

The tests presented next are part of a larger experimental campaign , conducted at the Universitat Politècnica de Catalunya – Barcelona Tech (UPC), which encompassed tests of statically indeterminate beams under different corrosion levels to assess the structural effects due to steel reinforcement corrosion, Figure IV-2. This work focuses on direct monotonic and cyclic tests of the corroded reinforcement bars extracted from the above mentioned beams having the underlying purpose to extend the existing database of monotonic test of corroded steel bars and contribute to a new significant database of corroded specimens tested under cyclic loads.

Figure IV-2. Statically indeterminate corroded beams and extracted steel reinforcement

Steel bars were extracted from beams exposed to different corrosion levels by means of induced corrosion procedure [20–22]. The beams were casted incorporating in the mixture 4% NaCl in cement weight, breaking the steel passive protective layer. A particular current density was applied to assure the desired corrosion level. This was done through a DC power supply with an ammeter to monitor and fix the current intensity. The current direction was defined fixing the reinforcing steel as anode and the stainless steel bar as the cathode. A schematic representation of the accelerated corrosion test setup is presented in Figure IV-3a. Each beam had two different bar diameters (ϕ10 mm and ϕ12 mm). Monotonic load tests were carried out in the continuous beams. Finally, bars were carefully extracted from the non-critical section of the beams in order to perform the characterization of the corroded bars under monotonic and fatigue loads.

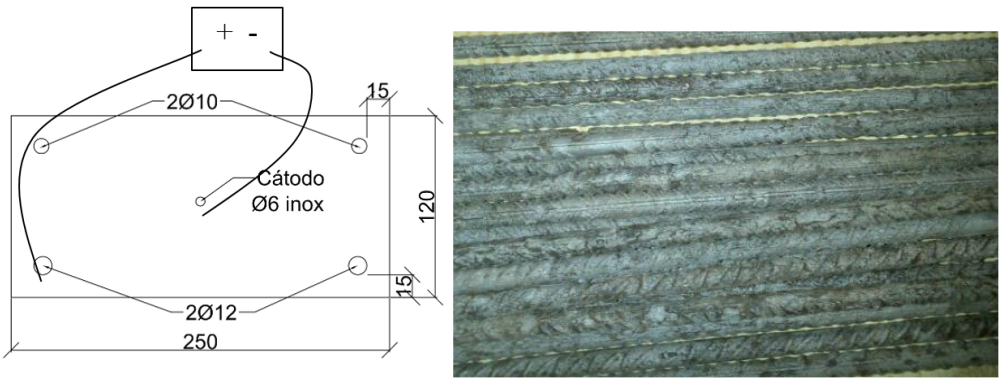

Figure IV-3. a) Corrosion scheme, b) Cleaned bars by means of sand cleaner

Using gravimetric methods, the loss in weight of the specimens was determined according the ASTM code. A pressure sand cleaning method was applied in order to remove both rust

and bonded cement, Figure IV-3b. In total 241 specimens were obtained covering corrosion rates from 3% to 28% for both the 10 mm and the 12 mm diameter bars, see Figure IV-4.

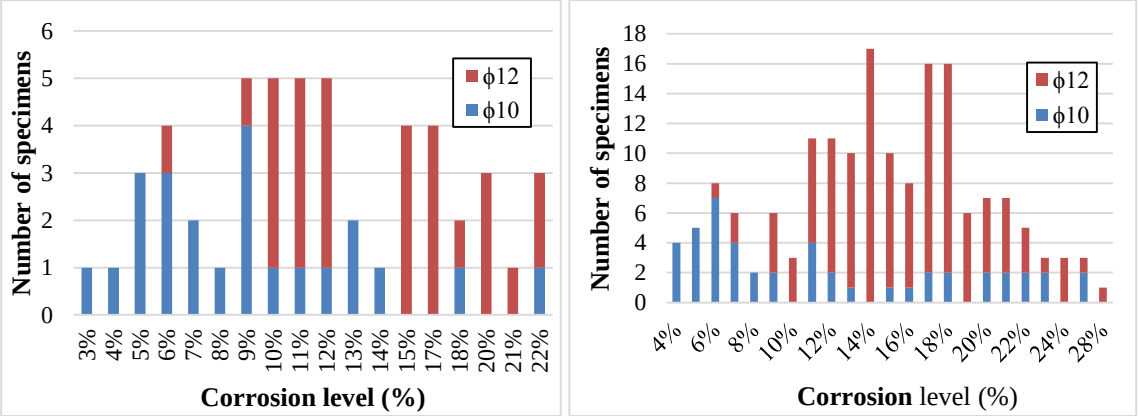

Figure IV-4. Test member distribution with respect to the corrosion level, a) monotonic test b) fatigue test

IV.2.3.2 Monotonic test

The tests were carried out following the code recommendations [23] and an INSTRON 8803 Universal Testing machine.

The specimens employed for monotonic testing had between 310 mm and 320 mm length. The ends of the test specimen were affixed by two clamps, which were used to transfer directly the load to the specimen. The tested free length was for all the specimens 170 mm letting 70/75 mm length for each clamp. Monotonic tests were conducted by means of displacement control. The load was applied directly to the bar controlled by the load cell placed on the top of the hydraulic jack. Total displacement, as well as deformation, were registered too. Specimen deformation was measured using a displacement transducer of 50 mm length positioned in the middle of the specimen (see Figure IV-5). The test was conducted until specimen failure. Each measurement was stored every half second by means of a data logger. Uncorroded specimens also were tested to compare and assess the influence of the degree of corrosion on the mechanical properties. In total, 40 specimens were tested satisfactorily. The weakest section, where most likely would fail, was identified for all the specimens by means of the definition of the pitting geometry using a Vernier calliper.

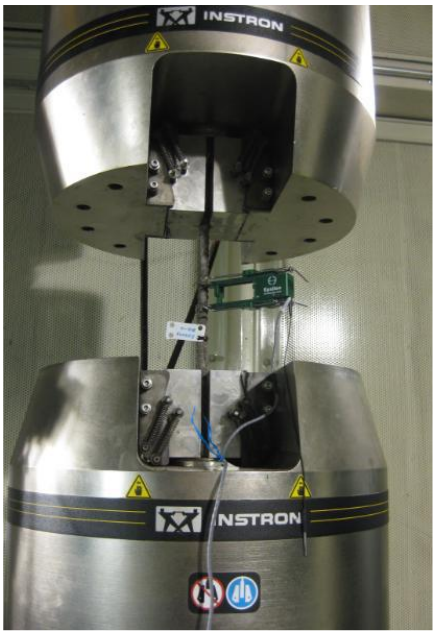

Figure IV-5. Test setup description monotonic

IV.2.3.3 Fatigue test

Fatigue specimens were between 310 mm and 320 mm large. The ends of the test specimen were affixed by two clamps, which were used to transfer directly the load to the specimen. The tested free length was for all the specimens 170 mm letting 70/75 mm length for each clamp. In the case of fatigue test, it was conducted by means of load control. The load was applied directly to the bars controlled by the load cell placed on the top of the hydraulic jack. Total displacement, as well as deformation, were registered too. Specimen deformation was measured using a displacement transducer of 30 mm length positioned in the middle of the specimen. Each measurement was stored every half second by means of a data logger, see Figure IV-6. Some specimens were discarded due to an induced failure in the clamps zone because stress localization effects. Also, the characterization of the most probably failure cross-section was done by means of the definition of the pitting geometry using a Vernier calliper.

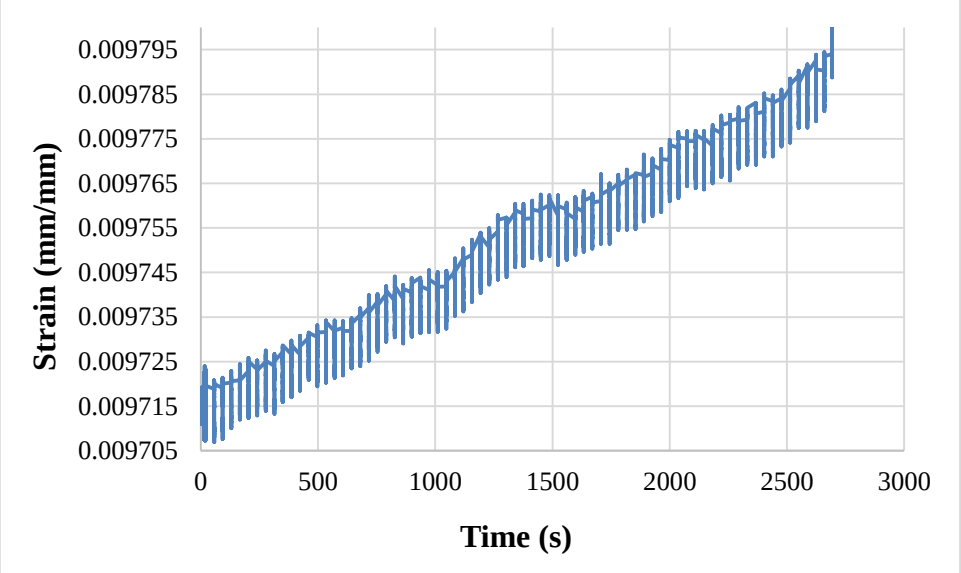

Figure IV-6. Strain recorded vs time by means of the disposed transducer. Accumulative damage on the bar

Three different stress ranges were defined for fatigue tests, 150 MPa, 200 MPa and 300 MPa ($\Delta S = S_{max} - S_{min}$). The stress range was defined based on the uncorroded section steel. A non-zero minimum stress was used to avoid compression in the bar and its possible buckling effects. The maximum stress (S_{max}) was for uncorroded specimens lower than $0.6 * f_{y,}$ which is the theoretical threshold for which there is no influence on the fatigue life due to the maximum stress. Considering the nominal diameter of uncorroded specimens and the stress range chosen, the maximum and minimum applied loads were defined. The applied load range for corroded specimens was the same as for uncorroded specimens, taking into account the uncorroded nominal diameter, see Equation IV-1.

Equation IV-1

$$\Delta S = S_{max} - S_{min} = \frac{F_{max}}{A_0} - \frac{F_{min}}{A_0}$$

Using these load ranges it was possible to compare the effect of corrosion level and loss of cross-section in a corroded structure with the same design loads. The applied loads considering the three mentioned stress ranges are described in Table IV-2, No specimens of 10 mm diameter were tested with ΔS= 150 MPa. The load was applied in same wave shape cycles of 15 Hz frequency (see Figure IV-7). In the same figure, the main variables for the fatigue problem are stated, S_{max}, S_{min}, S_m, S_a and ΔS. The specimens were tested at room temperature.

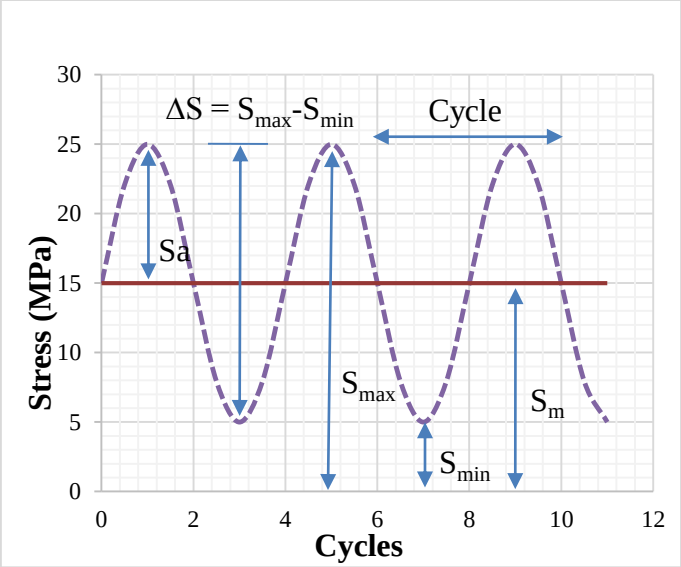

Figure IV-7. Sinusoidal loading curve for fatigue test

A total of 142 specimens were tested with a range of corrosion levels between 8% and 28%. Some specimens were discarded due to an induced failure in the clamps zone because stress localization effects, see Table IV-3

.

Table IV-2. Stress range and applied load to each diameter

Stress Range [MPa]	Diameter [mm]	Max Load [kN]	Min Load [kN]
300	10	23.4	0
	12	33.9	0
200	10	23.4	7.8
	12	33.7	11.3
150	10	-*	-*
	12	25	8.5

*No specimen tested

Table IV-3. Specimen list

Specimens	Number
Failed tests	10*
Monotonic test	40
Fatigue tests	142
Total valid specimens	143
Total specimens	192

*Member failed inside the clamps

IV.2.4 Test results

The results of the satisfactory tested specimens are described in the next points.

IV.2.4.1 Effect of corrosion on the reinforcing steel mechanical properties

Table IV-4 shows the results of monotonic tested specimens. In the table it is presented the nominal diameter of tested bars, the yielding load in kN, the ultimate load in kN (maximum resisted load by the specimen), the strain corresponding to the maximum load ε_{max}, the registered strain on failure ε_u and the modulus of elasticity, E, in N/mm^2 for each specimen. In addition, for easier comparison between corroded and uncorroded specimens, the apparent yielding stress f_y^* (elastic limit stress in MPa), the apparent strength f_{max}^* (maximum resisted stress in MPa), which means the stress obtained with respect to the theoretical corroded diameter (due to generalized corrosion), are also included.

Equation IV-2.
$$g = 1 - \frac{A_c}{A_0}; \qquad f = \frac{1}{1-g}$$

Where Ac is the generalized corroded steel area and A_o is the nominal area.

The characterization of the critical pitting observed in each specimen is described by means of the depth and length of itself. Figure IV-8a depicts a typical σ-ε curve for 10 mm and 12 mm diameter bars with varying the degree of corrosion (8-10%). This figure shows the high scatter in measured strains for all the test, even considering the same corrosion level specimen. Figure IV-8b compares the measured strain with the test machine with respect to the extensometer, which had a 50 mm base measurement. It can be seen that in uncorroded specimens, higher strains were registered by the machine than by the extensometer, as it was expected (it is included machine deformation, slip in the clamps, etc..). Instead, corroded members showed the opposite behaviour. These phenomena indicated the strong influence of local effects on the pitting during the tensile test.

Table IV-4. Monotonic test results

Specimen #	Corrosion (%)	Nominal Diameter	Yielding Load (kN)	Ultimate Load (kN)	ε_{max}	ε_u	Modulus of Elasticity (GPa)	fy*	fmax*	Pitting depth	Pitting length
BS-B10-01	0.0%	10	42.9	51.3	0.152	0.192	208	545.7	652.96	-	-
BS-B10-03	0.0%	10	42.4	50.7	0.150	0.185	209	539.5	646.04	-	-
B10-02	8.4%	10	34.2	43.4	0.117	0.144	180	474.6	603.52	1.00	6.000
V7-B10-01	8.7%	10	33.6	41.2	0.064	0.078	201	468.6	573.66	2.00	5.000
V8-B10-17	8.8%	10	32.1	39.7	0.062	0.078	199	448.4	554.73	2.00	9.000
V7-B10-12	9.3%	10	33.1	41.4	0.086	0.107	202	464.0	580.85	1.50	13.00
V7-B10-10	9.5%	10	32.1	39.4	0.056	0.066	186	451.7	553.31	1.50	9.000
B10-06	10 %	10	31.6	39.3	0.059	0.077	204	446.2	555.37	2.50	9.000
V9-B10-08	11.1%	10	32.6	40.1	0.069	0.080	206	466.7	574.63	0.50	8.000
V7-B10-07	12.6%	10	30.1	38.1	0.061	0.095	205	438.1	554.73	1.00	7.000
V8-B10-02	12.9%	10	27.5	34.6	0.041	0.052	185	401.7	504.97	2.00	12.00
V8-B10-10	14.3%	10	32.1	40.5	0.101	0.105	163	477.0	600.66	2.00	9.000
V7-B10-06	18.5%	10	22.9	29.2	0.037	0.050	132	358.1	456.18	4.00	9.000
BS-B12-01	0.0%	12	61.5	72.2	0.126	0.179	206	544.1	638.34	-	-
BS-B12-02	0.0%	12	61.4	72.3	0.137	0.191	190	542.5	639.26	-	-
BS-B12-03	0.0%	12	63.2	71.8	0.127	0.196	196	558.5	635.14	-	-
BN-01	9.1%	12	51.2	62.4	0.076	0.101	201	498.6	607.54	1.00	7.000
V2-B12-11	9.6%	12	45.6	57.0	0.107	0.135	153	445.8	557.50	1.50	17.00
V2-B12-13	9.7%	12	45.1	55.3	0.080	0.103	150	441.8	541.64	1.50	22.00
V7-B12-21	9.7%	12	45.4	55.0	0.071	0.073	175	445.1	538.37	1.00	9.000
V7-B12-15	10.7%	12	46.5	57.1	0.090	0.130	161	460.3	565.58	1.00	10.00
V2-B12-03	10.8%	12	45.6	56.7	0.069	0.098	173	452.3	561.62	2.00	17.00
B12-03	11.1%	12	45.4	58.8	0.090	0.156	134	451.7	585.05	1.50	16.00
V7-B12-26	11.3%	12	46.6	57.1	0.079	0.086	161	464.3	569.05	1.00	10.00
V7-B12-06	12.0%	12	48.0	57.8	0.086	0.088	158	482.9	580.97	1.50	10.00
V8-B12-03	12.1%	12	44.7	54.0	0.070	0.100	161	449.5	542.82	2.50	14.00
V7-B12-13	12.2%	12	44.8	53.7	0.066	0.085	166	451.0	541.13	1.50	7.000
V2-B12-10	12.4%	12	43.0	54.2	0.071	0.094	138	433.8	546.83	2.50	26.00
V2-B12-24	14.6%	12	44.9	55.9	0.073	0.100	186	464.5	578.72	0.50	7.000
B12-07	14.9%	12	45.1	55.5	0.070	0.105	196	468.4	576.68	2.00	24.00
B12-04	15.0%	12	40.4	51.4	0.063	0.087	170	420.4	534.09	1.80	21.00
V3-B12-03	16.8%	12	36.9	47.6	0.054	0.073	145	392.0	506.21	2.00	12.00
V9-B12-07	16.9%	12	39.2	48.7	0.062	0.081	151	416.9	518.88	2.00	12.00
V3-B12-11	17.5%	12	38.1	44.9	0.032	0.040	161	408.3	481.01	3.00	21.00
V8-B12-23	17.9%	12	40.1	50.1	0.074	0.114	158	431.6	539.70	1.50	6.000
V8-B12-18	19.6%	12	38.2	44.8	0.037	0.037	157	420.3	492.62	2.50	11.00
V8-B12-24	19.7%	12	34.5	42.0	0.040	0.059	147	379.3	462.02	3.50	8.000
V3-B12-19	19.7%	12	36.5	44.2	0.058	0.076	131	402.2	487.23	3.00	73.00
V7-B12-24	21.4%	12	34.9	42.3	0.037	0.059	223	392.7	475.93	3.00	18.00
V3-B12-01	21.5%	12	35.0	39.2	0.027	0.036	165	394.0	442.14	3.00	17.00

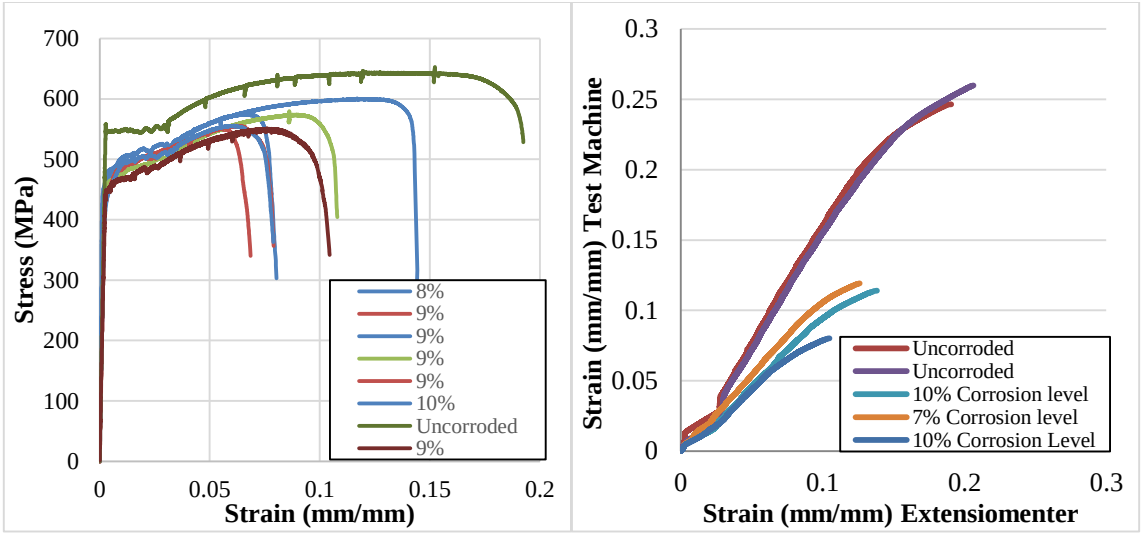

Figure IV-8. a) σ-ε curve corroded specimens, b) strains measured,

IV.2.4.1.1 Yielding and ultimate load capacity

Figure IV-10 describes the evolution of some parameters presented in Table IV-4 with respect to the measured corrosion level. As expected, there was a significant drop of all of the parameters studied with respect to that of uncorroded steel bars due to different causes. Yielding stress and maximum stress presented a polynomic decreasing tendency with respect to the corrosion level. The adjustment of the results for 12 mm diameter bars described a polynomic trend with 0.647-0.749 of correlation coefficient showing a good goodness of the adjustment. The correlation coefficient for 10 mm diameter specimens was reduced to 0.54-0.61 most, probably because there were much less tested specimens, especially for high corrosion levels. In any case, the polynomic trends adjusted correctly in both cases 10 mm diameter and 12 mm diameter, which indicated that the behaviour of these parameters decreased polynomially with respect to the corrosion level.

Previous studies [1,3,11,13] already reported a decreasing behaviour of the elastic and ultimate stresses of corroded bars, however, in those studies a linear relationship with the corrosion level was stated. Those works also noticed that the reduction of the tensile properties slightly decrease respect to those of uncorded specimens. In this work, the tensile stresses were obtained using an equivalent corroded cross-section area of the bar, which represented the generalised corrosion level measured. Using that value allows to establish a trustworthy relationship between corrosion level and reduction of cross-section. So it is considered that corrosion level is a global variable of the specimen, not the particular corrosion level of the critical cross-section which should be higher than generalized because of the local pitting in the critical cross-section. Using the generalised corroded cross-section

area hypothesis, the effective stress value decreased with respect to that of the value obtained using the real cross-section diameter. See Figure IV-9, obtained by means of a 3D scan technique.

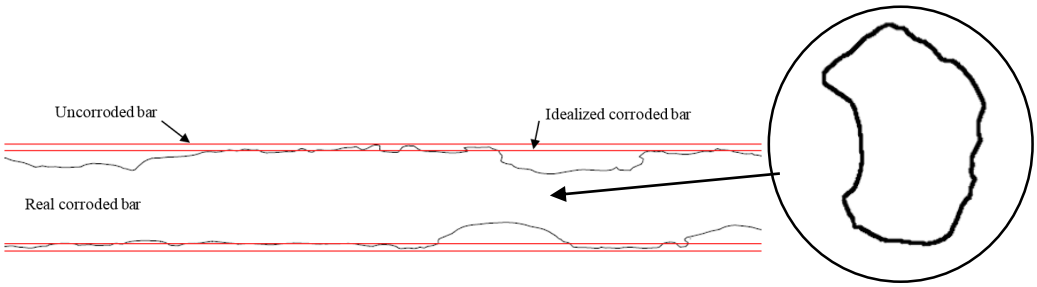

Figure IV-9. a) Pitting distribution. Idealized and nominal cross-section b) Real critical cross-section

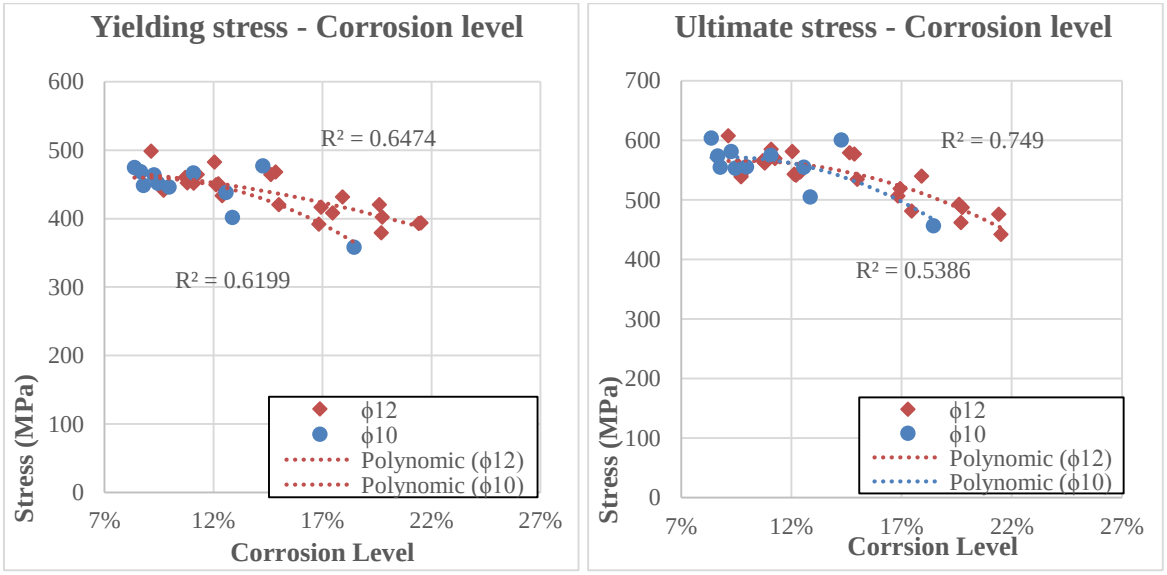

Figure IV-10. Elastic limit load and ultimate load vs. corrosion level

IV.2.4.1.2 Modulus of elasticity and ductility

The elastic modulus and the measured strains at maximum load (ε_{max}) showed higher scatter than f_y* and f_u*, see Figure IV-11. It was very difficult to establish a good correlation between these values with respect to the corrosion level. However, the observed values also decreased with the corrosion level. The lack of 10 mm diameter tested specimens for high corrosion levels resulted in greater dispersion than for 12 mm diameter specimens. In any case the correlation coefficient for 12 mm diameter it was always lower than 0.65 for the three parameters. Mechanical fracture theory could justify that registered dispersion. In general, a reduction of ductility was observed for all the specimens becoming in mostly tests in a less ductile failure, behaviour which was also observed by other researchers [13,24].

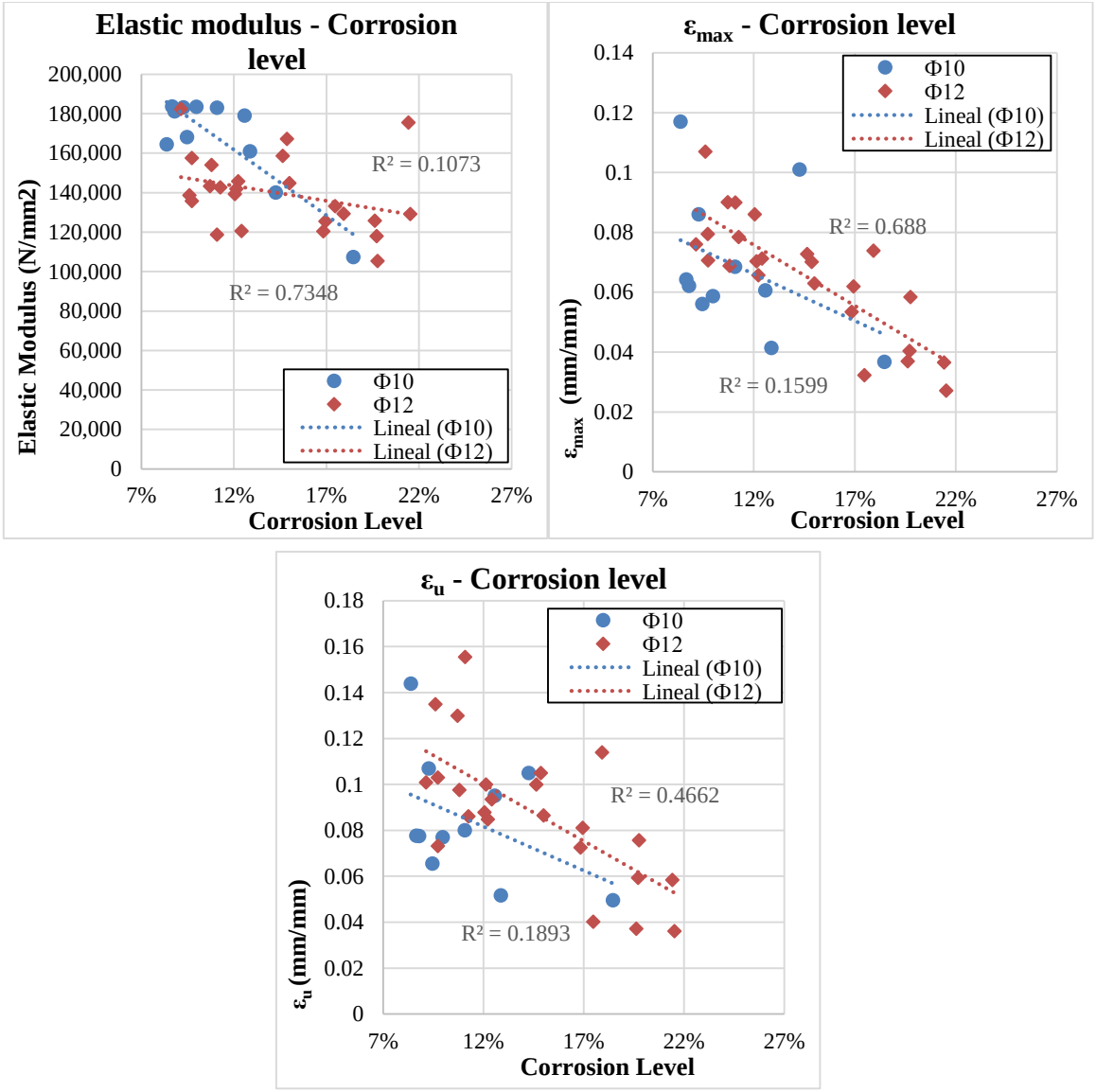

Figure IV-11. Elastic modulus, maximum ε and ultimate ε with respect to the corrosion level

IV.2.4.1.3 Discussion

Figure IV-12 describes the variation of the maximum stress, elastic limit stress and modulus of elasticity with respect to those of uncorroded steel. In both the 10 mm diameter and the 12 mm diameter, it is possible to observe a different growing rate between the corrosion level and the ratio of both parameters. This fact means that the reduction of capacity was not constant to the corrosion level either to the reduction of cross-section. Other phenomena, such as stress concentration in the pit [12] and non-homogeneity of the steel bar cross-section (because of the production procedures [6,8,10]) have to be taken into consideration. Both 10 mm diameter and the 12 mm diameter described the same behaviour.

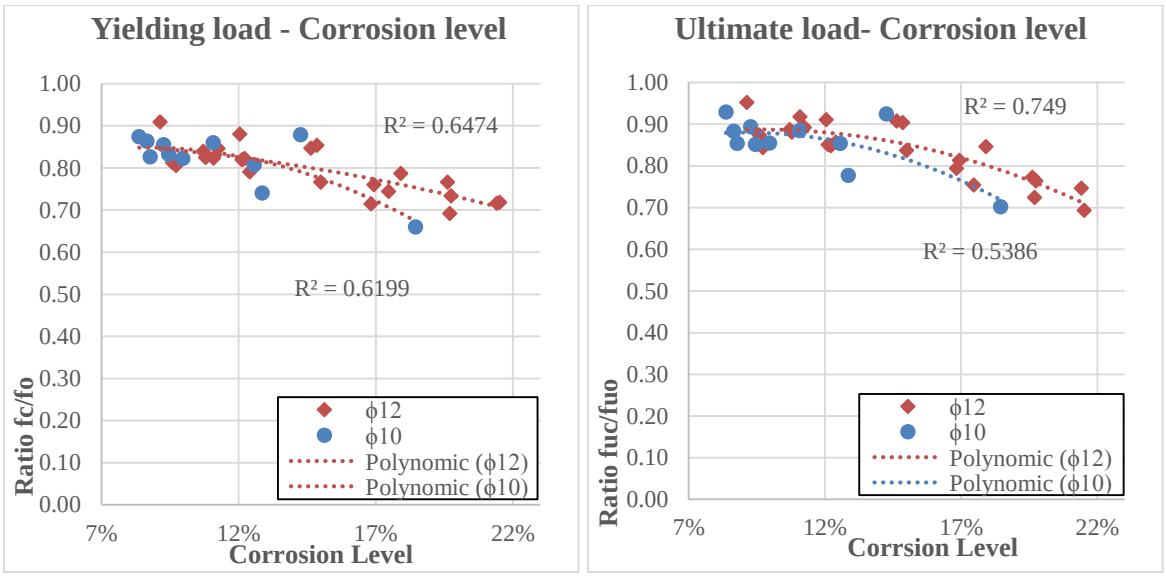

Figure IV-12. Reduction of ultimate stress and yielding stress ratios with respect to those of uncorroded steel and corrosion level for ϕ12 and ϕ10

IV.2.4.2 Effect of corrosion on the fatigue behaviour

The results of cycling load test in terms of total resisted cycles for the corroded specimens extracted and characterised from the beams are shown in Table IV-5. The characterization pit parameters such depth (p) and length (l) are also included, whit half mm precition, as well as the stress range to which the bar was submitted (ΔS), corresponding to the applied load of Table IV-2.

Table IV-5. Fatigue test results and pitting characterization

Specimen #	Corrosion Level (%)	Nominal diameter (mm)	Pitting description		Stress range (MPa)*	Resisted cycles
			Depth (mm)	Length (mm)		
V3-B10-05	10%	10	1.50	17.00	200	102,030
V3-B10-06	9.2%	10	1.00	12.00	300	99,027
V9-B10-10	10.7%	10	1.00	6.000	300	82,951
V9-B10-09	10.8%	10	2.00	14.00	200	192,984
V8-B10-08	11.1%	10	2.00	10.00	200	74,703
V8-B10-09	11.3%	10	1.00	21.00	300	122,934
V7-B10-11	12.3%	10	1.00	14.00	300	55,970
V7-B10-09	12.4%	10	1.00	4.000	300	44,883
V7-B10-05	12.5%	10	1.00	5.000	200	254,568
V8-B10-04	15.1%	10	2.00	8.000	200	167,236
V8-B10-18	15.7%	10	0.50	6.000	300	64,691
V8-B10-01	17.2%	10	2.50	14.00	200	31,959
V8-B10-16	17.2%	10	2.00	16.00	300	5,715
V8-B10-11	17.7%	10	1.50	27.00	200	146,670
V8-B10-15	17.9%	10	1.50	22.00	300	8,603
V7-B10-04	20.3%	10	2.50	21.00	200	5,706
V8-B10-03	20.3%	10	2.00	37.00	200	55,508
V8-B10-12	20.5%	10	2.50	19.00	300	3,157
V7-B10-08	20.6%	10	3.00	11.00	300	99
V8-B10-14	21.8%	10	1.00	8.000	300	12,959
V8-B10-06	21.8%	10	2.50	15.00	200	16,346
V7-B10-03	22.8%	10	2.00	53.00	200	35,988
V8-B10-05	23.2%	10	2.00	82.00	200	68,742
V7-B10-13	25.1%	10	2.50	47.00	300	2,649
V8-B10-13	25.2%	10	2.50	23.00	300	1,785
V2-B12-05	8.6%	12	1.50	77.00	200	266,070
V2-B12-17	8.7%	12	1.50	9.000	300	134,401
V2-B12-01	8.7%	12	1.50	17.00	150	943,043
BN-02	9.7%	12	1.00	8.000	200	325,922
V2-B12-18	10.3%	12	1.50	27.00	300	94,433

V3-B12-16	10.4%	12	1.50	23.00	200	325,956
V2-B12-08	10.8%	12	1.50	6.000	200	438,070
V2-B12-06	10.8%	12	2.00	36.00	200	267,542
V2-B12-20	10.9%	12	2.00	36.00	200	153,870
V2-B12-21	10.9%	12	1.50	44.00	300	64,620
V3-B12-13	11.2%	12	2.00	13.00	200	264,010
V7-B12-17	11.2%	12	2.00	60.00	150	372,276
BN-04	11.5%	12	1.50	24.00	200	374,083
V2-B12-16	11.6%	12	2.00	27.00	200	245,160
V3-B12-07	11.6%	12	1.50	12.00	300	91,536
V2-B12-23	11.6%	12	1.50	70.00	300	87,416
V7-B12-22	11.7%	12	1.50	14.00	200	256,383
V7-B12-14	11.7%	12	1.00	10.00	300	108,497
B12-02	12.2%	12	2.00	8.000	300	28,050
B12-20	12.2%	12	2.00	11.00	150	583,245
B12-21	12.6%	12	2.00	15.00	200	126,155
V3-B12-14	12.7%	12	1.00	4.000	300	60,355
V3-B12-10	13.0%	12	2.00	15.00	200	343,394
V7-B12-20	13.1%	12	2.00	10.00	300	29,815
B12-09	13.2%	12	2.00	31.00	300	56,650
V7-B12-08	13.3%	12	2.00	27.00	200	132,471
V2-B12-12	13.4%	12	1.50	13.00	300	62,138
B12-19	13.4%	12	2.00	14.00	200	90,750
V3-B12-23	13.6%	12	2.00	43.00	200	129,033
V3-B12-27	13.6%	12	1.50	13.00	300	63,818
V2-B12-02	13.7%	12	2.00	52.00	300	18,182
V2-B12-04	13.7%	12	2.00	16.00	200	395,720
B12-01	13.7%	12	2.00	6.000	200	112,996
V7-B12-03	14.1%	12	2.00	15.00	200	40,007
V7-B12-12	14.1%	12	1.00	13.00	300	51,259
V8-B12-17	14.2%	12	1.50	14.00	300	24,711
V7-B12-25	14.3%	12	1.50	7.000	200	151,373
V7-B12-16	14.3%	12	3.00	19.00	300	11,548

V3-B12-25	14.4%	12	1.00	7.000	200	283,849
V3-B12-12	14.4%	12	1.50	10.00	300	42,910
V3-B12-09	14.5%	12	2.00	11.00	200	132,905
V3-B12-22	14.5%	12	2.00	14.00	200	179,672
V7-B12-09	14.5%	12	1.00	8.000	300	64,468
V3-B12-26	14.5%	12	2.00	21.00	300	11,751
B12-15	14.5%	12	2.00	12.00	200	160,378
V7-B12-04	14.6%	12	2.00	29.00	200	99,873
V8-B12-29	14.8%	12	1.50	12.00	200	149,582
B12-05	14.9%	12	2.00	12.00	200	155,094
V3-B12-24	14.9%	12	2.00	11.00	200	99,365
V8-B12-08	15.0%	12	1.50	54.00	300	68,504
V8-B12-25	15.0%	12	2.50	16.00	200	39,134
V3-B12-21	15.2%	12	1.50	33.00	300	92,051
V3-B12-18	15.2%	12	2.50	21.00	200	111,312
V7-B12-01	15.6%	12	2.00	12.00	200	178,298
V7-B12-18	15.8%	12	1.50	8.000	300	48,224
B12-10	16.1%	12	2.00	12.00	150	556,891
B12-17	16.1%	12	2.00	12.00	200	266,610
B12-11	16.1%	12	2.00	12.00	300	12,100
B12-06	16.2%	12	2.00	19.00	150	574,851
V8-B12-26	16.3%	12	3.00	29.00	200	23,509
B12-12	16.6%	12	2.00	22.00	200	54,991
V8-B12-15	16.6%	12	1.50	13.00	300	42,581
B12-14	16.8%	12	2.50	49.00	300	13,192
V3-B12-05	17.1%	12	2.00	12.00	200	81,724
V8-B12-16	17.2%	12	2.50	31.00	200	48,511
V7-B12-10	17.2%	12	2.50	72.00	300	42,505
V7-B12-19	17.3%	12	2.50	58.00	200	78,338
V3-B12-20	17.3%	12	2.00	20.00	300	27,798
V7-B12-05	17.3%	12	2.00	32.00	200	146,772
V8-B12-12	17.3%	12	1.50	11.00	200	109,014
B12-22	17.5%	12	3.00	44.00	200	73,150

V8-B12-09	17.5%	12	1.50	11.00	300	40,084
V8-B12-13	17.5%	12	2.00	51.00	200	49,011
V8-B12-01	17.5%	12	2.00	32.00	300	54,870
B12-18	17.6%	12	2.00	16.00	300	13,494
V7-B12-07	17.7%	12	3.00	23.00	150	324,138
V8-B12-02	17.7%	12	2.00	19.00	300	22,164
V9-B12-15	17.8%	12	3.00	31.00	300	3,095
V8-B12-10	17.9%	12	2.50	31.00	300	11,582
V9-B12-08	17.9%	12	3.00	20.00	200	95,451
B12-08	17.9%	12	2.50	28.00	150	119,620
V8-B12-19	17.9%	12	2.00	7.000	200	32,852
V9-B12-06	17.9%	12	1.00	30.00	300	147,678
V8-B12-27	18.2%	12	2.00	12.00	200	159,922
V8-B12-06	18.3%	12	2.00	12.00	300	12,353
V8-B12-11	18.3%	12	3.00	34.00	300	7,405
V8-B12-22	18.4%	12	1.50	17.00	200	79,579
V3-B12-15	18.6%	12	1.50	52.00	300	43,900
V3-B12-17	18.9%	12	2.50	18.00	200	117,108
V9-B12-1	19.0%	12	4.00	39.00	150	14,767
V8-B12-28	19.1%	12	2.50	53.00	200	18,025
V8-B12-07	19.3%	12	2.00	23.00	300	10,613
V9-B12-04	19.3%	12	3.50	27.00	200	2,780
V8-B12-20	19.5%	12	3.00	27.00	200	37,538
V8-B12-04	19.6%	12	2.00	23.00	300	18,255
V9-B12-13	19.6%	12	3.00	24.00	200	13,850
V9-B12-23	20.1%	12	2.50	24.00	150	200,597
V9-B12-11	20.3%	12	3.00	31.00	300	898
V9-B12-21	20.6%	12	3.00	57.00	200	5,909
V7-B12-02	21.0%	12	3.00	40.00	300	10,490
V8-B12-14	21.1%	12	2.00	29.00	300	10,010
V7-B12-23	21.2%	12	2.50	23.00	200	51,428
V7-B12-11	21.4%	12	2.50	27.00	200	63,863
V8-B12-21	21.5%	12	3.00	62.00	200	7,485

V9-B12-09	21.7%	12	2.50	27.00	300	3,453
V9-B12-05	22.5%	12	4.00	13.00	200	156
V9-B12-16	23.2%	12	3.00	66.00	200	25,064
V9-B12-19	23.8%	12	4.00	24.00	150	11,208
V9-B12-12	23.9%	12	3.00	82.00	150	26,411
V9-B12-03	24.1%	12	3.00	39.00	200	887
V9-B12-22	25.3%	12	2.00	21.00	300	3,200
V9-B12-02	27.6%	12	4.00	41.00	150	6,459

*Stress range considering the nominal diameter

IV.2.4.2.1 Influence of pit geometry

Figure IV-13a describes the evolution of the pitting depth with respect to the corrosion level measured. It is possible to observe a large scatter of the obtained results. However, a clear trend of the values was depicted indicating the higher pitting depth the higher corrosion level was. That trend is described by the linear adjustment defined in Figure IV-13a. The goodness of that correlation was 0.4517, consistent with the observed dispersion. Despite, the trend was clear. To compare the different diameter specimen tested the pit characteristic were divided by the nominal diameter obtaining a dimensionless parameter. The same comparison is stated in Figure IV-13b for the pitting length. Also, the length value was divided by the nominal bar diameter to obtain a dimensionless parameter and make easier the comparison between all the specimens. Again a correlation between the corrosion level and length/diameter value was observed. In that case, the adjustment showed a worst goodness. A linear or polynomic second-order adjustment described well the specimen behaviour. In any case, the pitting length increment is lower with respect to the corrosion level than for pitting depth. In Figure IV-13c it is reproduced a comparison between the pitting depth and the pitting length showing that the pitting depth is a parameter more sensible to corrosion level than pitting length. In addition the effect of stress concentration has less influence than the loss of steel area, because that effect is more sensitive to the longitudinal pitting angle (figuring out the pitting geometry like an elypsse where the long diameter is the length and the other diameter is the depth).

Lastly, Figure IV-13d describes the overall behaviour of the corroded specimens depicting the total resisted cycles respect with its corrosion level. As it is shown in that figure, the number of recycled cycles decrease fastly with corrosion level.

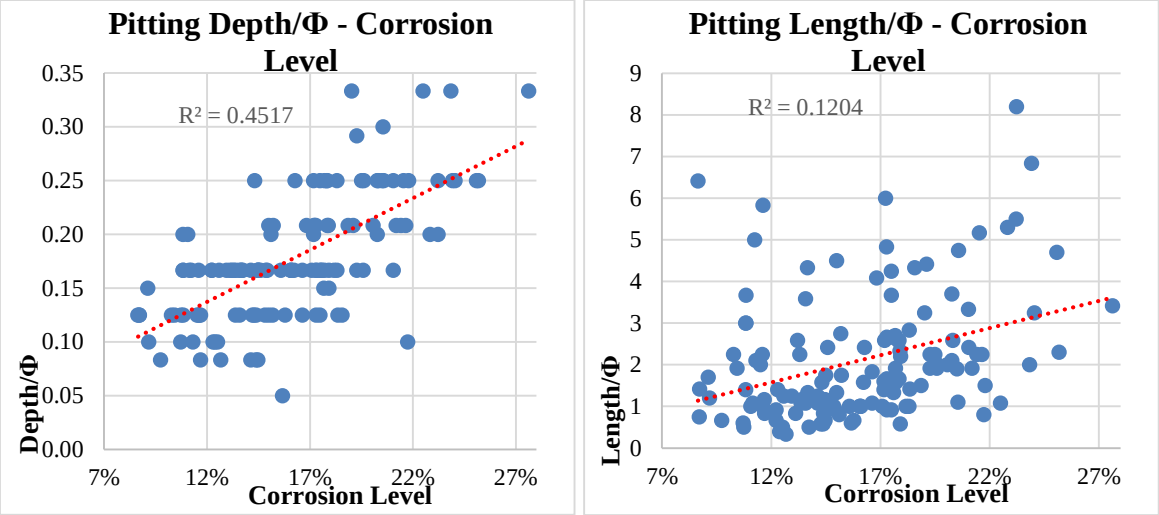

Figure IV-13. Pitting characterization with respect to corrosion level and fatigue life results

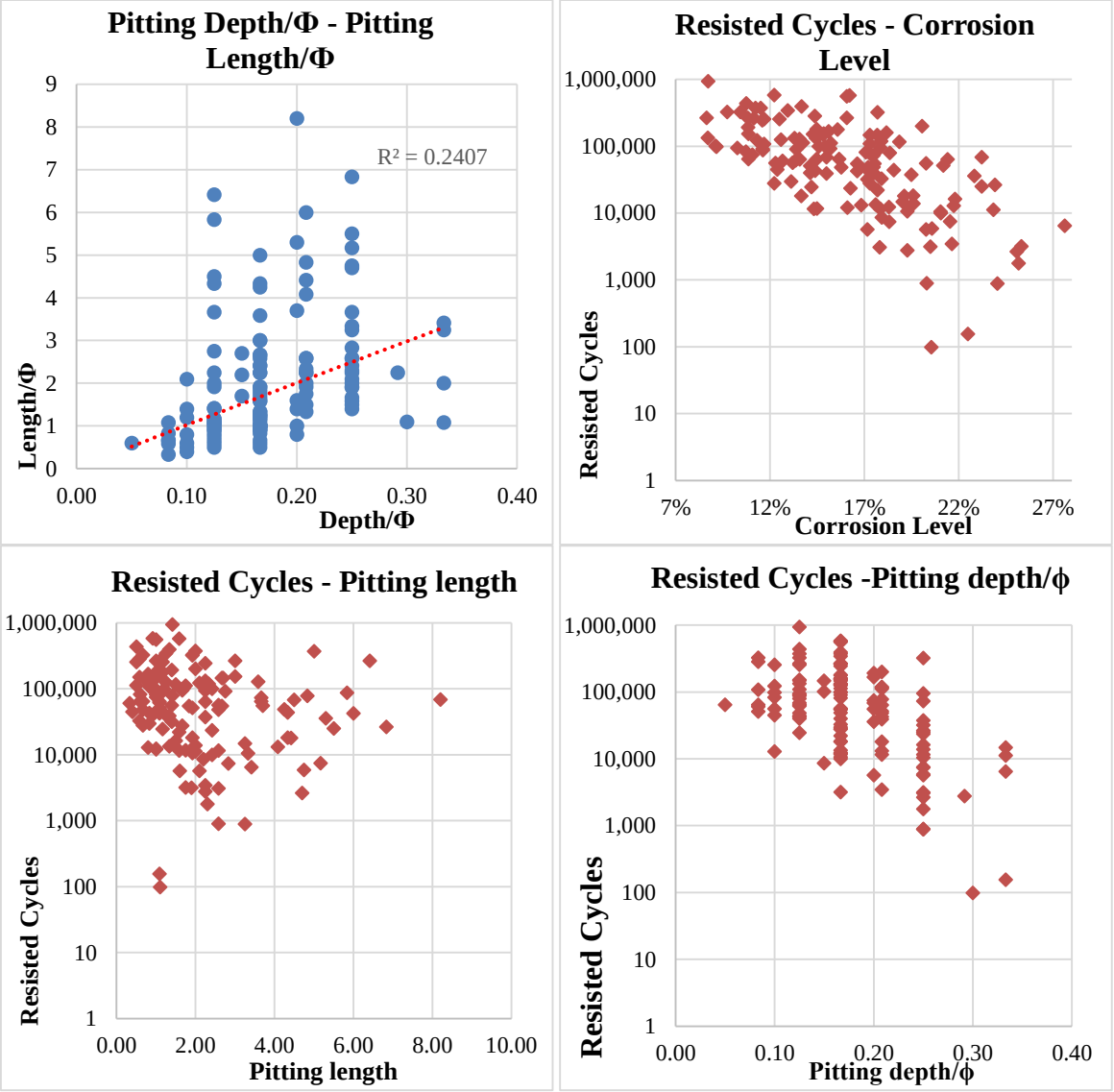

Figure IV-14. Registered fatigue life with respect to pitting parameters

Figure IV-14a shows that the effect of the pitting length on fatigue life, N, was practically constant for ratios length/diameter higher than two. For those, the effect on fatigue life can be considered constant, not reducing the number of the resisted cycles of the specimen. However, as it is shown in Figure IV-14b 14b the fatigue life always decreased with the ratio p/ϕ (ratio between pitting depth and nominal diameter).

IV.2.4.2.2 Influence of stress range

As it is shown in Figure IV-15a and Figure IV-15b, the fatigue life of corroded specimens is reduced significantly with respect to that of uncorroded steel. The reduction of fatigue life of corroded specimens could be adjusted quite accurately following a negative exponential adjustment. An attenuation rate is observed with a decrease in the stress level, as it is

observed in both figures and mainly in Figure IV-15a for the stress range 300, 200 and 150. A similar behaviour was also documented by other authors [1,17] for naturally corroded specimens submitted to different stress ranges, however in this work it was noticed that all the specimens described the same behaviour despite the stress range applied.

The results obtained suggested that corrosion of steel reinforcement has no significant effect on fatigue life for very low corrosion levels, although for higher corrosion level a severe reduction of fatigue life was observed.

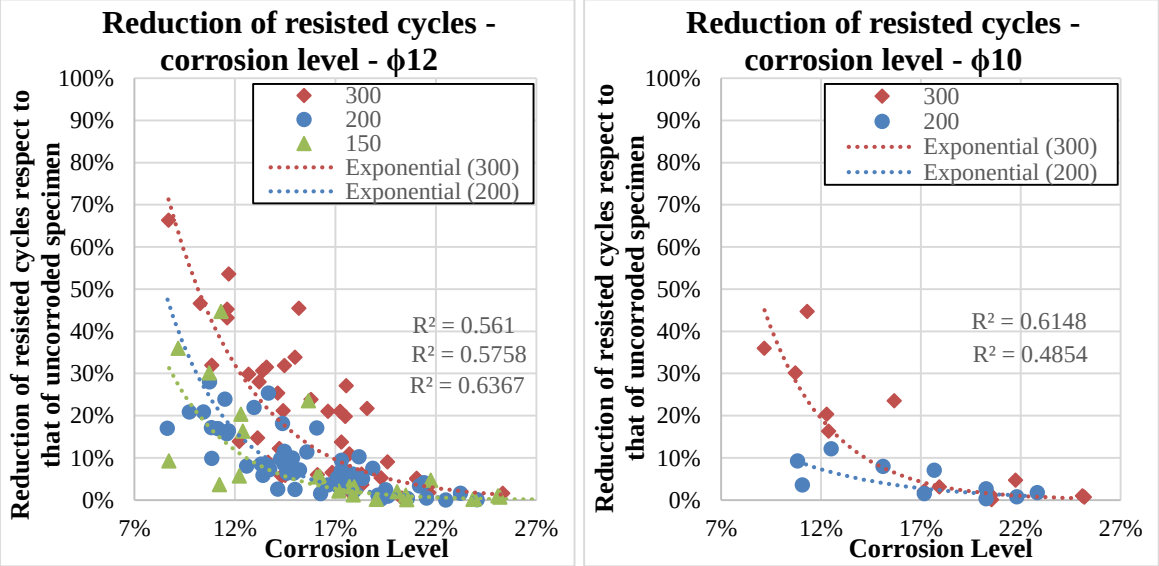

Figure IV-15. Fatigue life of corroded specimens ϕ12 and ϕ10 bars

IV.2.5 Conclusions

Based on the results of the study performed, the following conclusions can be drawn:

(1) Yield and ultimate stresses measured in the monotonic test were found strongly dependent on corrosion level. Corrosion of steel highly reduces the yielding and ultimate stresses.

(2) Modulus of elasticity and measured strains present a very high dispersion with respect to that of yield stresses and strength. In addition, a premature failure is observed becoming in a severe reduction in ductility.

(3) The reduction of all the mechanical properties is not proportional to the corrosion level, while they show a strong influence of other parameters such as stress

concentrations at the top of the pits, non-homogeneity of steel bar properties (due to TEMPCORE® production system) or the displacement of the center of gravity due to a non-uniform loss of mass. The relationship mechanical properties/corrosion level has showed to be parabolic with the corrosion level for both yield stress and ultimate stress when the stresses are referred to the idealized generalized corroded diameter.

(4) Pitting depth has a higher influence on fatigue life behaviour than pitting length. Effect of pitting length has no effect on fatigue life for length/diameter ratios higher than 2. Instead, the impact of the ratio depth/diameter is bigger as deeper the pitting is.

(5) Fatigue life for corroded bars is severely reduced with respect to that of uncorroded steel bars. For very little corrosion levels, the effect is entirely negligible. Higher corrosion level describe a negative exponential decreasing behaviour in terms of resisted cycles. In addition, very high corrosion levels present a severe reduction of fatigue life independent of the stress range applied.

Further studies on the effects of low corrosion levels, from 0% to 8% would be desirable. In addition, to studying naturally corroded specimens would be interesting to confirm the effect of pitting characteristics on fatigue and tensile properties.

Acknowledgments

The authors wish to acknowledge the financial support of The Ministry of Economy and Competitiveness of the Government of Spain (MINECO) for providing funds for projects BIA2009-11764, as well as BIA2012-36848. The financial support of Infrastructures de Catalunya (ICAT) is also highly appreciated.

IV.3 Bond behaviour of recycled aggregate concrete with corroded and uncorroded reinforcing steel bars

Ignasi Fernandez[1], Miren Etxeberria*[1], Antonio R. Marí[1]

[1] Department of Construction Engineering, Polytechnic University of Catalonia, Jordi Girona, 1-3, Barcelona 08034, Spain.

*corresponding author

Abstract: The use of recycled aggregates for concrete production may result in a worsening of certain key properties such as compressive strength or durability, also affecting steel-concrete bond. The aim of this experimental study was to assess the bond performance of recycled aggregate concretes, which were cast using different percentages of coarse recycled aggregates (20%, 50% and 100%), with embedded corroded and uncorroded steel bars. The assessment was carried out performing pull-out tests. The uncorroded specimens presented comparable bond strength for all concretes due to their similar compressive strength values. However, the slip suffered by recycled aggregate concretes made with 100% of recycled aggregates was higher. The low corroded recycled aggregate concrete specimens presented better bond performance and later superficial cracking in comparison to those of conventional concrete. At higher corrosion levels, the bond strength capacity of all concretes was similar, although recycled aggregate concrete consistently presented slightly better bond capacity.

Keywords:

Bond strength, Slip, Recycled aggregate concrete, steel corrosion; Compressive strength; initial cracking; Pull-out; Bond-slip.

IV.3.1 Introduction

Corrosion of the steel bars is one of the today's most frequent and significant type of damage, in existing reinforced concrete structures. Therefore, the study of the structural effects of bars corrosion is crucial for determining the structural performance and residual strength of impaired structures. One of the most severe reinforcement corrosion effects is the change in bond properties between steel and concrete. Moreover, volumetric expansion of corrosion products causes serious problems inducing splitting stresses along corroded reinforcement, with possible resulting damage to the surrounding material. Generally, the splitting stresses are not tolerated by concrete, resulting in cracking and eventually spalling of the cover. As the reinforcement becomes more exposed, the corrosion rate may increase and facilitate the deterioration process.

Steel reinforcement unconfinement due to cover cracking or spalling of concrete cover, as well as rust between both materials, quickly decreases the bond strength, thus changing the structural behaviour and inducing anchorage failures. Many researchers have studied the effect of the corrosion process on bond deterioration extensively. Several studies have investigated parameters that may influence the bond and anchorage capacity of corroded structures [25–29]. Models studying the interaction between both materials, and numerous experimental studies identifying and studying this phenomenon can be found in the literature [30–33]. Even though, the literature on works covering bond behaviour on recycled aggregates is very sparse [34–40].

The increasing amount of construction wastes coming from old and deteriorated structures at the end of their service life has a relevant environmental impact in the construction sector due to the economic benefits of using the wastes produced in the form of recycled concrete aggregates (RCA) in the concrete employed in reinforced concrete production. Wastes from older structures yield fragments in which the aggregate is contaminated with various different substances such as gypsum, asphalt, etc. A proper treatment of the recycled aggregate, as well as an accurate production process, results in recycled aggregate concrete (RAC) being a very suitable option to reduce the overall cost in the construction sector [41]. Over the past 50 years, the use of RCA has been profoundly studied for concrete production [41–50] and the resulting studies maintain that the primary weakness of RCA is its high porosity, which could directly influence a decrease in the compressive strength and durability of concretes produced with those aggregates.

Recent studies have tried to determine the bond between both the RAC and the steel with respect to that of conventional concrete (CC) and steel [37]. These studies manifest that a reduction of bond strength could be associated with the amount of recycled aggregate used in the mixture. Several authors [37,39,40] reported reductions of 6-8% up to 30% of bond capacity, nevertheless other researchers' work [34] noted differences of approximately 1% of the bond strength of recycled aggregate concrete with respect to that of CC concrete. Although the reduction in bond strength is strongly related to concrete compressive strength, it is also dependent on other parameters such as steel bar rib geometry and the position and orientation of the bars during casting. The amount of concrete cover also has an important influence on this phenomenon [34,51–56].

In this experimental study of the bond strength and bond behaviour between recycled aggregate concrete and reinforcement steel, either corroded or uncorroded, using the direct pull-out tests was presented. Two experimental Phases were conducted, one with uncorroded and another with corroded steel bars embedded in RAC and CC concrete cube specimens. For that purpose, four different concrete mixtures were cast in each Phase by replacing 0% or CC (using 100% of natural aggregates, CC concrete), 20% (RAC-20), 50% (RAC-50) and 100% (RAC-100) of natural coarse aggregates by coarse recycled concrete aggregates. The obtained results for RAC concretes were compared with those obtained from the CC concrete.

At Phase 1, bond behaviour of the four types of concretes with steel reinforcement bars of ϕ12 mm was characterised. 100 mm cubic concrete specimens with embedded steel bars were produced in order to carry out the pull-out test. In accordance with the pull-out test specifications [57], the uncorroded steel reinforcement bars completely crossed the concrete specimens.

Experimental Phase 2 was performed in order to determine the influence of steel corrosion on the bond strength of RA concretes and CC concrete. In this case, ϕ10 mm steel bars were used. In order to control the corrosion procedure, the steel bars were partially embedded in concrete and did not fully cross the entire length of the cubic concrete specimen This configuration ensured the same corrosion level guaranteed in all the embedded section of the steel bar. Three different corrosion levels were achieved as a result of an applied electrical current on the steel bars in all of the four types of concretes specimens, after which the pull-out test was carried out on each sample. The instant of the first cracking appearance on the surface of the specimens and the cracking evolution was determined for the four types of concretes during the corrosion process.

IV.3.2 Materials

IV.3.2.1 Cement

Type I Portland cement, CEM I 42.5R, was used in concrete mixtures with rapid hardening and 42.5 MPa characteristic strength cement. The chemical properties of cement are given in Table IV-6.

Table IV-6. Chemical composition of cement

Composition	SiO_2	Fe_2O_3	Al_2O_3	CaO	MgO	K_2O	Na_2O	SO_3	LOI
%	19.16	3.56	5.04	62.9	1.66	0.75	0.15	3.54	3.25

Natural limestone, fine (FA, 0/4 mm) and coarse aggregates (two fractions; CA1, 4/12 mm and CA2, 12/20 mm) were used for concrete production. Physical properties, density and absorption, and the grading distributions are described in Table IV-7 and Figure IV-16, respectively. The properties of the fine and coarse aggregates were determined according to EN specifications. All fractions of natural aggregates satisfy the requirements specified by Spanish Standard of Structural Concrete [58].

Table IV-7. Dry density and water absorption capacity of aggregates

Properties	CA2 12/20mm	CA1 4/12mm	FA 0/4mm	RCA
Dry density (kg/dm^3)	2.65	2.64	2.58	2.30
Water absorption (%)	0.67	0.87	1.68	5.91

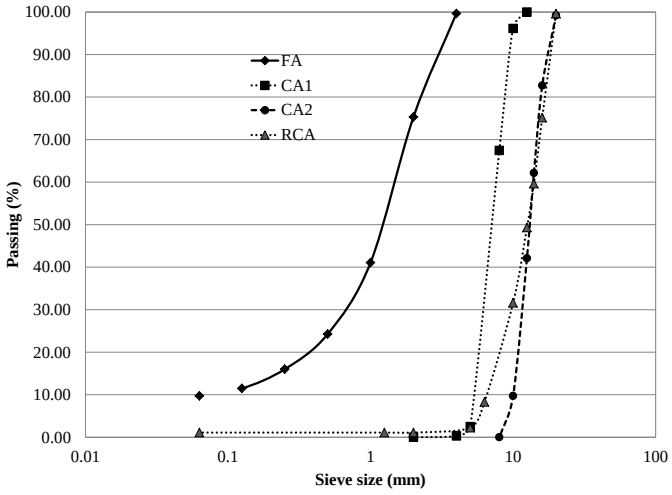

Figure IV-16. Grading distribution of fine natural aggregates (FA) and coarse natural (CA1 and CA2) and recycled aggregates (RCA)

RC aggregates were obtained by crushing rejected 40 MPa compressive strength concrete produced by a precast concrete company. The properties of RCA of density-absorption and grading size are shown in Table IV-7 and Figure IV-16, respectively. The density of RCA was found to be lower than that of the natural aggregates and the absorption capacity higher. The porosity of RA determined by MIP of 8.63% and its average pore diameter was of 0.048 µm.

The quality of the recycled aggregates obtained from the 40 MPa strength original waste concrete signified that, it was adequate for structural concrete production. The grading was defined by 4/20 mm, it was adequate with respect to Spanish Standard of Structural concrete [58], in its employment for recycled concrete production and it was used in substitution of CA1 and CA2 natural aggregates.

At concrete production 4% NaCl in weight of cement was added to the mixture; its aim was the depassivation of the steel inside the concrete and the causing of a conductive medium to facilitate the corrosion procedure. Superplasticizer was also used to provide the desired workability to the mixture.

IV.3.2.2 Concrete mix proportions

The four mixtures (Conventional concrete, CC; concrete produced with 20% of RCA, RAC-20; concrete produced with 50% of RCA, RAC-50; concrete produced with 100% of RCA, RAC-100) were prepared and cast. The replacement of raw, coarse aggregates by recycled coarse aggregates was carried out according to the volume.

The mix proportion of CC concrete was defined with 300 kg of cement and a total water-cement ratio of 0.5 for concretes exposed to a marine and chloride environment described by the Spanish Structural Concrete code [58]. The effective water-cement ratio of CC concrete was determined and maintained constant in all RAC concretes, due to the higher water absorption capacity of RCA the total w/c ratio of RAC was higher than for CC [47]. The effective w/c ratio on CC concrete was approximately of 0.45, this was determined by removing from the total water amount the effective absorption capacity of raw aggregates (the absorption capacity determined the effective absorption capacity at 20 min submerged, being defined as 80% and 20% of the total absorption capacity for fine and coarse raw aggregates, respectively).

In order to control the concrete production, recycled coarse aggregates were wetted the day before use by means of a sprinkler system and then covered with a plastic sheet so as to maintain their humidity until used in concrete production. A recommended level of moisture

is 80% of their total absorption capacity [47]; however the most important factor was that the aggregates employed were wet in order to reduce their absorption capacity [49]. Due to moderate initial moisture content, recycled aggregate absorb a certain amount of free water and lowered the initial w/c ratio in the ITZ, consequently improving the interfacial bond between the aggregates and cement [50]. However, recycled aggregates should not be completely saturated [50], as that would probably result in the failure of an effective interfacial transition zone between both the saturated recycled coarse aggregates and the new cement paste. In line with these recommendations, the compressive strength of concrete made with saturated aggregate was lower than concrete made with air dried aggregates due to the adverse effect of the bleeding of the saturated aggregates [46].

Concrete mix proportions were defined according to their maximum volumetric compaction. This mix proportion for conventional concrete (CC) was defined as 50% of fine aggregates and 50% of coarse aggregate. The distribution of coarse aggregate was 30% CA1 4/12mm and 70% of CA2 12/20mm. The same volume of CA1 and CA2 was replaced by RCA for each recycled aggregate concrete production.

Table IV-8 shows the mix proportions used. The weight of aggregates is given as their dry weight. The total amount of water was considered, including the 80-90% of humidity of aggregates at concrete production and the absorbed water by aggregates. 4% of NaCl and 1% of superplasticizer were used in all concretes with respect to cement weight.

Table IV-8. Mix proportions of the concrete mixtures

Material (1000 litres)	CC	RCA-20	RCA-50	RCA-100
Cement (kg)	300	300	300	300
Total Water (kg)	150	159	172	194
Effective w/c	0.45	0.45	0.45	0.45
FA 0/4mm	976	976	976	976
CA1 4/12mm	210	168	105	-
CA2 12/20mm	765	612	383	-
RCA	-	171	428	855
NaCl (weight of cement)	4%	4%	4%	4%
Superplasticizer (weight of cement)	1%	1%	1%	1%

IV.3.3 Experimental campaign and test procedure

Concrete compressive strength was determined for all concrete types. Bond strength between concrete and steel bars both corroded and uncorroded were analysed by means of two experimental Phases.

IV.3.3.1 Compression test

The compressive strength of concrete was determined using a compression machine with a loading capacity of 3000 kN. The compressive strength was measured at the age of 28 days following the UNE-EN 12390-3. Three cylindrical specimens (100mm of diameter and 200 mm of length) were used for each type of concrete produced.

IV.3.3.2 Pull-out test

The experimental work presented here focuses on the direct pull-out test of natural aggregate concrete, and the recycled aggregate concretes, reinforced with steel bars. The underlying purpose of that being to characterise the corresponding bond behaviour. Pull-out test was stated as a useful test to obtain the local bond behaviour for short embedded length steel specimens. The typical assumption for short pull-out tests with ribbed steel reinforcement bars, defined by embedment length of less than five times the bar diameter, is that the distribution of bond stresses is uniform along the bonded section [59,60]. Accordingly, the uniform bond stresses hypothesis was assumed, such that the local bond stress could be estimated as:

Equation IV-3 $$\tau = P / \pi \Phi L$$

where, P is the applied load, Φ is the nominal diameter of the steel bar, and L is the embedded length.

The experimental study was divided into two Phases. In experimental Phase 1 the test was performed according to the code recommendations [57]. In experimental Phase 2, some concrete specimens were summited to accelerated corrosion and consequently the embedded bar design was modified with respect to the criteria defined by the code. The pull-out test were carried out through the use of 100x100 mm cubic specimens which had embedded steel in the upper face. For the purpose of this study the top, bottom and sides of the concrete cube shall be known as upper face, the bottom face and lateral faces.

IV.3.3.2.1 Pull-out test: Phase 1

The experimental setup was conducted following the code recommendations [57] and using a specific fatigue machine INSTRON 8800.

Steel bars of ϕ12 mm were embedded in the centre of the 100x100 mm cubic concrete specimens. The steel bars completely crossed the cube section of 100 mm. A piece of plastic tube was used to debond 50 mm of steel bar from the concrete, leaving the other 50 mm to bond with the concrete (see Figure IV-17a). In total were cast 16 cubic specimens, four for each concrete type.

The total slip between both the concrete and the steel was measured during the test. An LVDT was affixed to the concrete cube at the specimen's bottom in order to register the total rebar slip.

The hydraulic jack clamps were attached to the steel bar-end. The load was applied directly to the bar by means of control displacement, in order to achieve results on the pre and post peak behaviour up to failure, as well as the residual bond capacity. The applied load and the LVDT readings were recorded every half a second by means of a DAQ. The test was conducted using a constant velocity of 0.2 mm/min. Figure IV-17b shows the experimental setup.

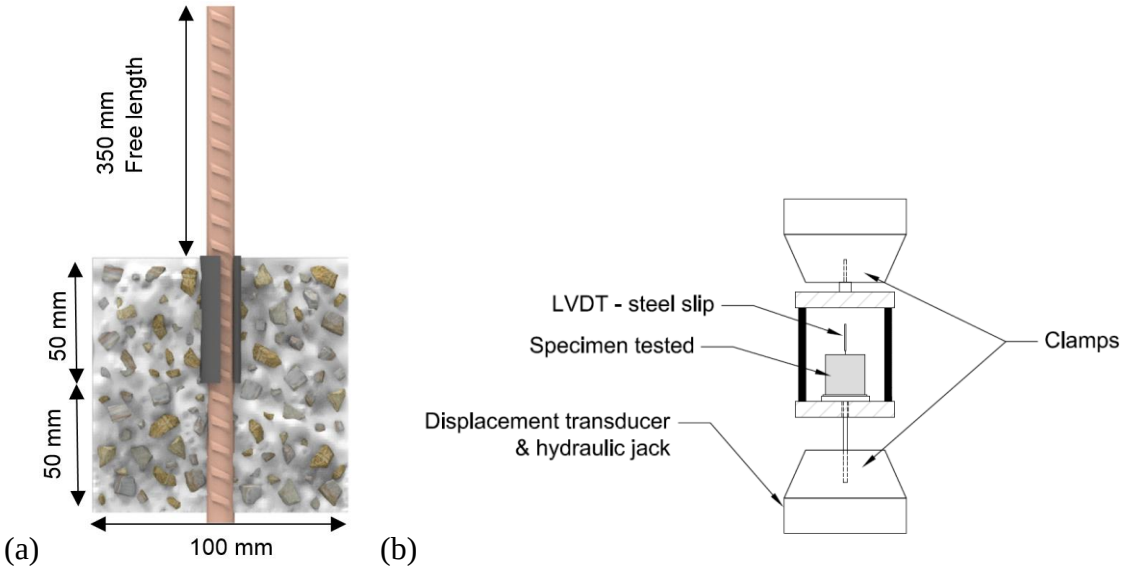

Figure IV-17. (a) Concrete specimen description (phase 1) (b) Test setup, direct pull-out test

IV.3.3.2.2 Pull-out test: Phase 2

The Phase 2 test specimen design was modified with respect to that defined by the code [57] in order to facilitate a simpler and more reliable method of the steel corrosion procedure. 16

cubic specimens of 100 mm were cast for each designed concretes. ϕ10 mm steel bar diameter were used in the experimental Phase 2 and the bars, as Figure IV-18 shows, did not fully cross the whole concrete section of 100 mm. The free steel length for all the specimens, was 350 mm and the bonded section was 50 mm.

The bars were embedded from the centre of the upper surface of the cubic specimens to a length which was equivalent to five times the steel bar diameter. The moulds used were specially designed in order to ensure that the bars were fixed at the same position in all the specimens. Figure IV-18 describes the test specimens and the established setup. 45 mm of concrete covered the embedded bar in all directions. This configuration ensured the same corrosion level guaranteed in all the embedded section of the steel bar.

(a) 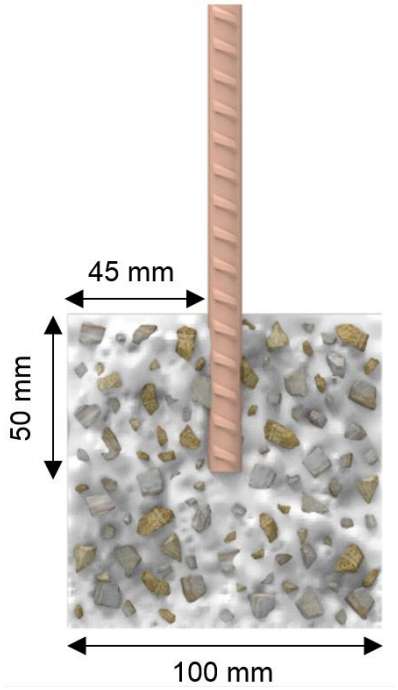

(b) 

Figure IV-18. (a) Concrete specimens description (Phase 2) (b) Pull-out test setup

In this case, the hydraulic jack clamps also were attached to the steel bar-end in order to pull the bar out of the concrete. The tests were conducted by means of displacement control, of 0.2 mm/min, until failure or until the residual bond load was reached.

The load was applied directly to the bar via a hydraulic jack controlled by a load cell. The total displacement, as well as the applied load, were registered. Each measurement was recorded and stored every half a second by means of a DAQ. The registering of the real slip between both materials was impossible to carry out as the bar did not completely cross the specimens. Thus, the displacement values expressed included all the other external deformations such as slip in the clamps, neoprene compression, concrete deformation, free

length steel bar deformation, etc. Consequently, the slip values obtained in Phase 1 and Phase 2 were not directly comparable. The τ_{max} was the only comparable data.

IV.3.3.3 Accelerated corrosion

IV.3.3.3.1 Corrosion method

Corrosion of steel reinforcement was induced by means of the passing of an electrical current. Following Faraday's law, Equation IV-4, it is possible to determine the weight loss of steel at any given time through corrosion, due to the applied intensity of the electrical current I(t), together with the diameter and exposed length of bar.

Equation IV-4

$$E = \frac{m_{Fe} \cdot \int I \cdot dt}{V \cdot F}$$

Where, m_{Fe} is the atomic mass, V is the steel Valence that is equal to two and F is the Faraday's constant. The applied intensity being a determined, fixed, known factor remained constant. Consequently, it was possible to rewrite Faraday's law as Equation IV-5, in order to determine the weight loss of steel.

Equation IV-5

$$\Delta m = \frac{m_{Fe} \cdot I \cdot t}{V \cdot F}$$

Many researchers have claimed [21,61] that the use of current densities below 200 μA/cm^2 for accelerated corrosion tests causes a similar (5-10% difference) loss of weight in the steel to weight loss of bars estimated by Faraday's law.

Thus, it is possible accurately to estimate the corrosion level achieved by applying electrical current density values below this threshold. Furthermore, current densities above this threshold cause earlier cracking as well as a notable difference with the real corrosion procedure and resulting corrosion products. It is known that the bond between steel and concrete is affected by the corrosion rate [22]. In the present work, 1% loss of weight of steel bar by corrosion procedure, at ten days was estimated and consequently 130 μA/cm^2 of electrical current density was applied. The same electrical current density was also maintained over a period of 20 and 30 days in order to produce 2% and 3% of weight loss of steel bar due to the corrosion procedure.

In order to produce accelerated corrosion of embedded steel bars by means of impressed current, the steel bars must be depassivated. In this experimental study, as mentioned above, sodium chloride was added to the concrete mixing water in order to eliminate the passive layer by means of chloride attack.

IV.3.3.3.2 Corrosion procedure

The specimens produced in Phase 2 were placed into plastic recipients and approximately 90% of their volume immersed (90 mm) in water, which contained 5% of NaCl solution (electrolyte). A copper plate was located under the concrete specimens, see Figure IV-19. The copper plate was used as a cathode during the corrosion process, and the steel bar was used as anode. The steel bar and copper plate were connected to the power supply equipment, which provided the specified current as defined earlier. A different number of specimens was connected in series guaranteeing the same intensity (see Figure IV-20 Figure IV-19).

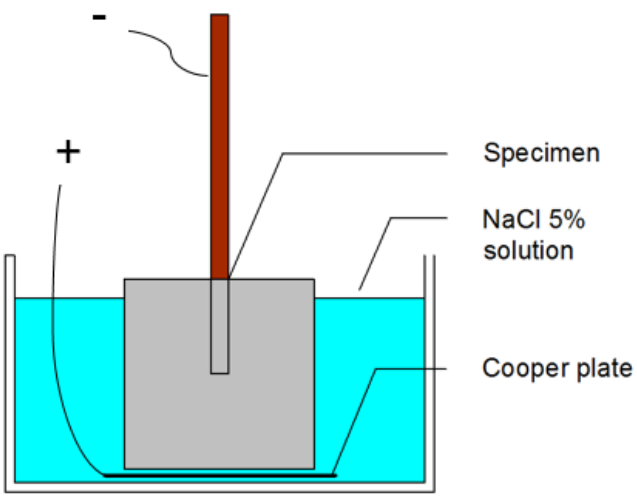

Figure IV-19. Test setup induced corrosion

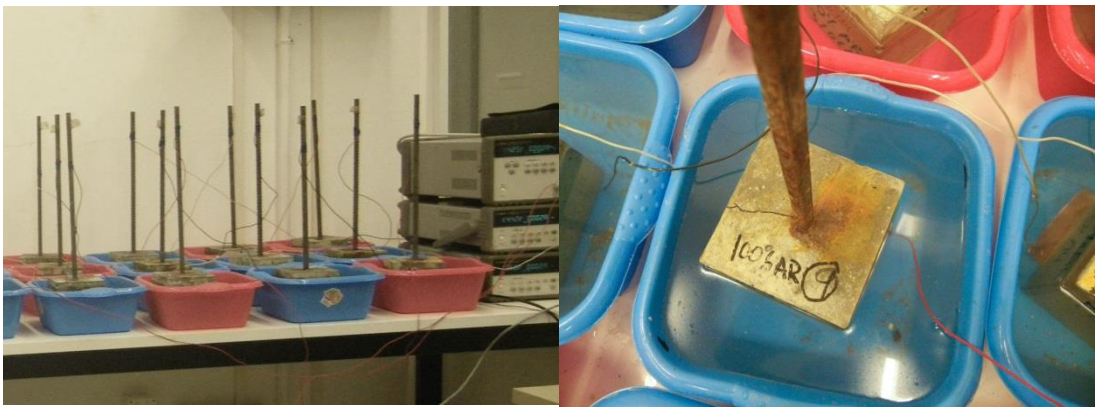

Figure IV-20. Series connection scheme for corrosion procedure

The instant of the first cracking appearance on the surface of the different types of concrete specimens during corrosion process was evaluated.

Three specimens of each type of concrete (CC, RAC-20, RAC-50 and RAC-100) were exposed to the corrosion process at three different ages, 10 days (1% estimated corrosion level by Faraday's law), 20 days (2% estimated corrosion level by Faraday's law) and 30

days (3% estimated corrosion level by Faraday's law). All the specimens were tested by employing the pull-out test described previously (Phase 2). The % of mass loss was measured and compared with the Faraday's law prediction, in each type of concrete. Chemical cleaning of corroded steel specimens was performed to calculate the steel mass loss, following the specifications [62]. The cleaning procedure was conducted using a solution of hydrochloric acid.

IV.3.4 Test results

IV.3.4.1 Concrete properties

Table IV-9. Compressive strength and experimental and theoretical Bond strength (τ_{max}) obtained in phase 1 and phase 2 uncorroded specimens for the four concretes cast describes the compressive strength at 28 days of curing and the standard deviation of the values for all types of concretes produced.

As expected, there was no significant drop in the compressive strength of the RAC specimens with respect to that of CC concrete specimens due to the adequate compressive strength (40MPa) of the parent concrete. The weak point of medium–high strength concretes made with coarse recycled aggregates can be determined by the strength of the recycled concrete and its attached mortar [41,47].

IV.3.4.2 Pull-out test results. Type of concrete influence

IV.3.4.2.1 Pull-out test results: Phase 1

The results of direct pull-out test in terms of τ_{max} (maximum bond capacity) for the specimens produced at Phase 1 are shown in Table IV-9. The value of τ_{max} was very similar in all the concretes with lower than 10% variation with respect to the maximum bond capacity of CC. That variation was in accordance with the compressive strength obtained by RAC and CC concretes, as already reported by other researchers [34,63].

Table IV-9. Compressive strength and experimental and theoretical Bond strength (τ_{max}) obtained in phase 1 and phase 2 uncorroded specimens for the four concretes cast

Concrete Type	Compressive strength (MPa)		τ_{max}-Pull Out test	
	Average	Std.	Phase1 Exp.	Phase2 Exp. (un.)
HC	51.2	0.92	28.64	34.36
RCA-20	48.28	0.66	29.69	35.78
RCA-50	47.8	0.21	27.14	32.57
RCA-100	49.95	3.05	30.31	35.63

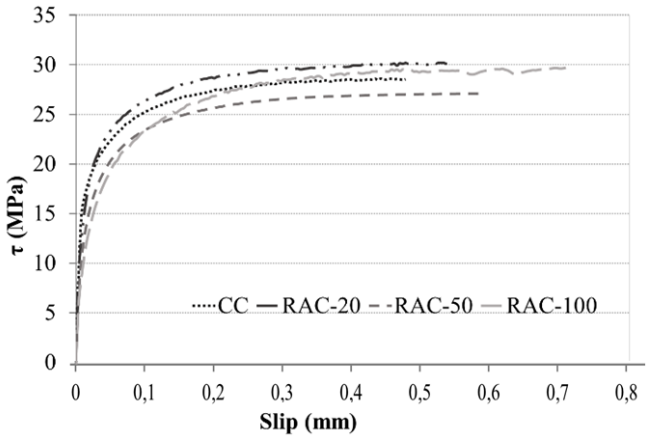

Figure IV-21. Direct bond τ (MPa)-slip (mm) curves of the four types of concrete

The LVDT placed underneath the specimen was able to monitor and register the actual direct slip between the concrete and steel bar. Figure IV-21 shows the direct bond-slip curves of the four types of concretes. It shows that the maximum slip registered was higher in RAC concretes, and it increased when higher percentages of recycled aggregates were used. Figure IV-22 illustrates the pull-out test picture of CC concrete.

Figure IV-22. Specimen after pull-out test

Figure IV-23 shows the average values of the instant τ with respect to τ_{max} ratio for each type of concrete according to the instant slip respect to $slip_{max}$ ratio. The CC, RCA-20, RCA-50 concretes showed almost the same stiffness with smooth variations in the curves. However, RCA-100 presented higher slips for the same τ_{max}. There was a considerable reduction in stiffness, more than 30%, in the RAC-100 concrete when compared to other concretes. A behaviour fact which has also been documented by other authors [38]. It is also known that the modulus of elasticity is reduced with the employment of RCA for concrete production [43,47] and it is coherent with the behaviour observed in Figure IV-21 Figure IV-21 and Figure IV-23. The higher porosity registered for RCA concretes could correctly explain this behaviour in concretes produced with 100% of RCA.

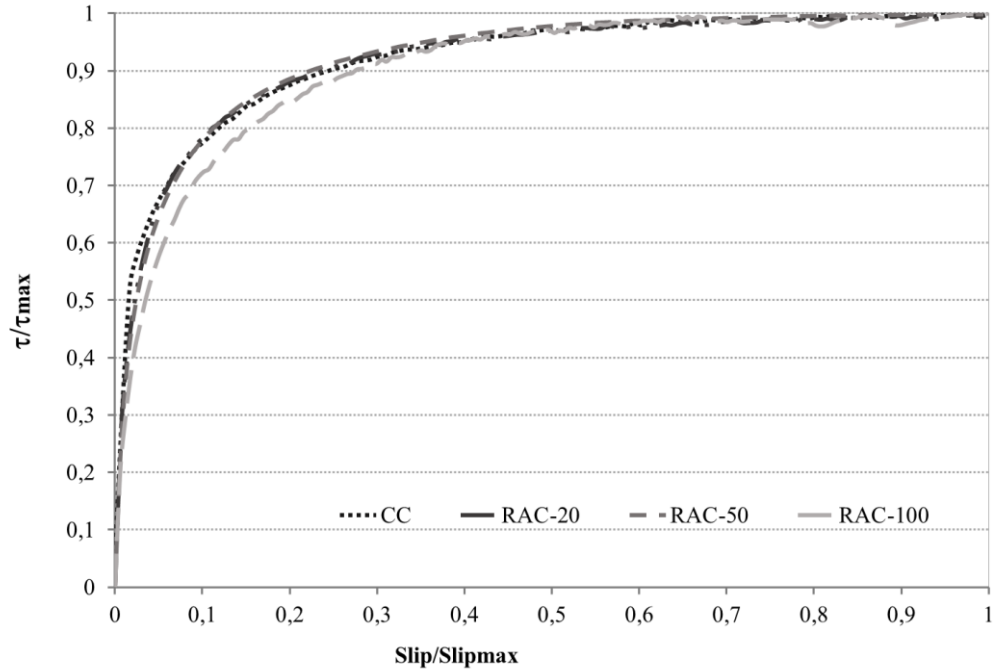

Figure IV-23. Unitary τ /τ_{max} respect to slip/slip$_{max}$ curves of the four types of concrete

IV.3.4.2.2 Pull-out test results: Phase 2 (uncorroded)

The τ_{max} value for the four types of concrete specimens, with uncorroded bars, are shown in Table IV-9. τ_{max} value for recycled aggregate concretes was similar to that obtained for CC concrete. RAC-20 concrete presented a slightly higher τ_{max}, when RAC-50 suffered a lower reduction than 10% with respect to the value of conventional concrete. The RCA-100 obtained a similar value to that of CC concrete. These values were in accordance with those obtained in Phase 1 and also in accordance with the similar compressive strength results obtained by all the concretes. As mentioned by some researchers [64,65] bond between reinforcing steel and concrete depends on the geometric properties of both steel and concrete as well as of the concrete properties. Regarding concrete properties, its compressive strength is stated as the most important parameter. Kim and Yun [64] confirmed that the compressive strength was also the adequate parameter to be used for bond strength characterization for concretes made employing fine recycled aggregates.

IV.3.4.2.3 Discussion

Figure IV-24 shows the ratio between the τ_{max} (Phase 1), τ_{max} (Phase 2) and the compressive strength for the three RA concretes produced with respect to the same values of CC concrete. As illustrated, the results obtained by recycled aggregate concretes were similar to those obtained by conventional concrete. The τ_{max} value for recycled aggregate concretes reached

or exceeded that of conventional concretes except for the concrete produced with 50% of recycled aggregates. In all cases, all the registered variations were attributed to the inherent high dispersion of the pull-out tests [57].

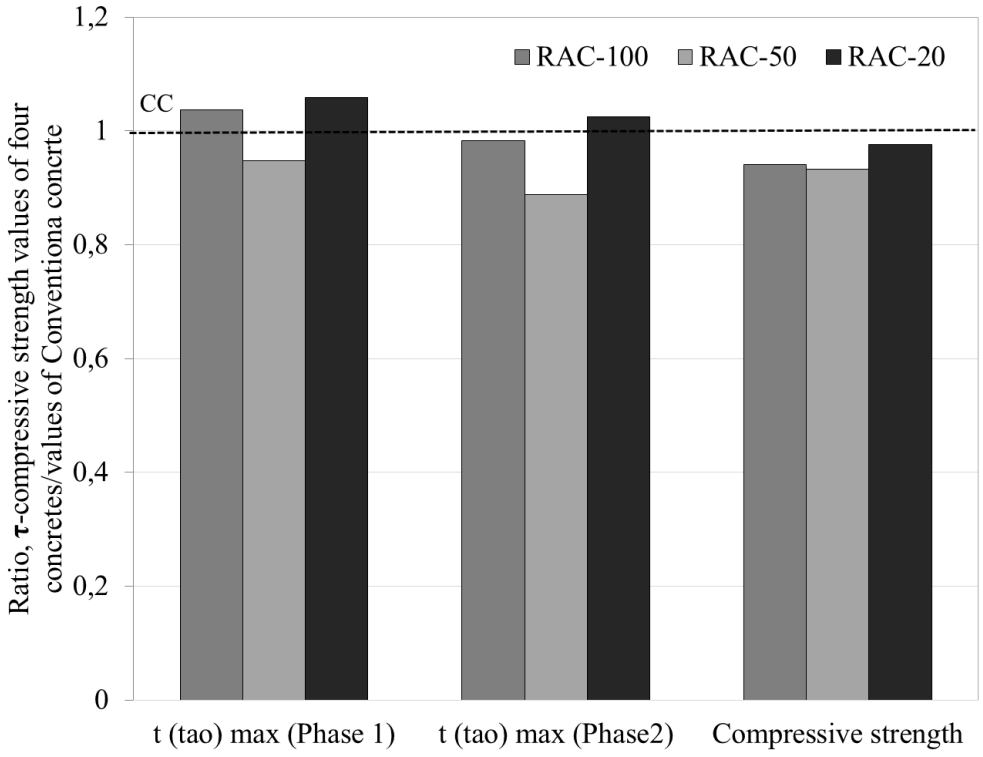

Figure IV-24. Ratio of τ_{max} (phase 1), τ_{max} (phase2) and compressive strength of all the concrete produced with respect to the same values of conventional concrete

Figure IV-25 shows the influence of compressive strength on τ_{max} values, determined by the ratio of $\tau_{max\text{-}RAC}/\tau_{max\text{-}CC}$ with respect to $f_{c\text{-}RAC}/f_{c\text{-}CC}$. All the values were approximately one due to the similar compressive strength of all the concretes studied and its influence on bond strength determination in any type of concretes, similar conclusions were obtained by other researchers [64–66].

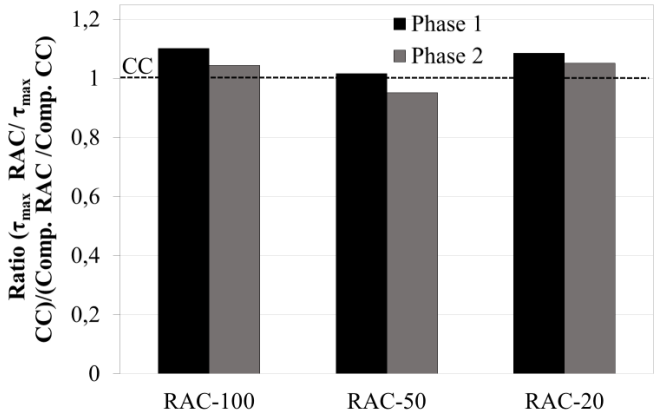

Figure IV-25. Ratio of $\tau_{max\text{-}RAC}/\tau_{max\text{-}CC}$ with respect to $f_{c\text{-}RAC}/f_{c\text{-}CC}$

IV.3.4.3 Phase 2 results. Corrosion level influence

IV.3.4.3.1 Weight loss determination

Table IV-10 shows the resulting mass loss for each specimen and the average weight loss of all bars at different exposition time. The weight loss obtained experimentally was a little higher than that determined by Faraday's law at 10 day and 20 days of exposure. However, at 30 days of exposure the real mass loss was higher probably due to the influence of concrete cracking on the accelerating of corrosion process. In any case as it was described in Maadaway et al. [20], experimental results of acelerated corrosion method always produced higher mass loss than theretical estimation. In Figure IV-26 it is possible to see the steel bars before and after the cleaning was performed.

Table IV-10. Determined corrosion levels by mass loss

Type of concrete	10 exposition days (1% mass loss according to Faraday's law		20 exposition days (2% mass loss according to Faraday's law)		30 exposition days (3% mass loss according to Faraday's law)	
	Corrosion level (%)	Average (%)	Corrosion level (%)	Average (%)	Corrosion level (%)	Average (%)
CC	--	1.65	1.86	2.6	5.71	5.75
	--		1.89		6.59	
	--		2.18		5.65	
	--					
RAC-20	1.66		2.42		5.40	
	0.83		2.54		5.75	
	1.58		2.40		4.99	
			2.61			
RAC-50	1.35		3.16		5.94	
	1.86		2.24		6.65	
	1.93		3.28		5.02	
RAC-100	2.23		2.91		6.35	
	1.69		3.04		5.43	
	1.70		3.04		5.60	
			2.87			

Figure IV-26. Steel bar specimens before and after cleaning procedure

IV.3.4.3.2 Surface cracking due to corrosion procedure

Cracks produced by corrosion are a major problem during the concrete deterioration process. The instant of the first surface cracking of each type of concrete during the electrical current exposition period was determined (see Table IV-11).

Table IV-11. Description of the exact time of the first cracking of each type of concrete and the ratio of required time by each RAC concretes with respect to that of CC in percentage

Concrete type	CC	RAC-20	RAC-50	RAC-100
First cracking time (in days)	4.75	6.15	7.66	6.55
Ratio of required time (%)	0	29.47	61.26	37.89

It was noted that the RAC concrete needed approximately 30% more exposure time than conventional concrete for the first surface cracking to appear. According to Yalciner et al. [56] the concretes produced with high water/cement ratio needed more time for the first outer cracking than concretes with low water/cement ratio due to lower porosity of later ones. The high porosity of concrete had similar adequate influence on the happening of the first cracking in all tested concretes. In this research work, the higher porosity of recycled aggregates, which had a greater capacity for absorbing the internal stresses caused by the corrosion products, delayed the surface cracking. A higher corrosion level was needed in order to achieve the same external cracking for RAC.

A description of surface crack pattern caused by corrosion cracking is described in Table IV-12 (Figure IV-27 illustrates the cracking of CC and RAC-100 at 1.6% and 5.75% of corrosion level). The first outer cracks appeared on the upper face of the concrete cubic specimens, in which the steel bar was embedded. The cracks became prolonged on the lateral faces due to the increase of corrosion level. Table IV-12 describes the total amount of cracks that appeared: the enumeration of the upper face cracks represents the order of occurrence, whilst the lateral face crack's enumeration corresponds to the number of the upper face crack prolongation. The τ_{max} of all the corroded samples is also described in the same Table IV-12.

Table IV-12. Description of the crack pattern caused by corrosion cracking

Concrete type	Estimated corrosion level	External Crack amount	Numeration of cracks on upper face (cms)			Numeration of Crack on lateral faces (cms)			τ_{max} (MPa)
			1	**2**	**3**	**1**	**2**	**3**	
CC	1%	3	6.0	5.0	4.5	-	3.0	5.5	5.53
		3	3.0	5.0	5.0	-	4.0	6.5	5.47
	2%	3	6.0	5.0	4.5	-	3.0	5.5	4.09
		3	3.0	5.0	5.0	-	4.0	6.5	5.37
	3%	2	4.5	4.5	-	8.0	9.0	-	3.47
		2	4.0	4.5	-	9.0	8.5	-	4.13
		3	4.0	4.5	4.0	10.0	8.5	5.5	4.39
RAC-20	1%	3	2.5	5.5	4.5	-	-	2.0	6.72
		2	4.4	4.5	-	1.0	5.5	-	7.13
	2%	2	4.0	4.5		7.0	5.0		6.61
		3	5.0	4.5	5.0	5.0	6.5	7.0	4.92
		3	6.0	5.0	4.0	4.5	3.5	8.0	5.28
		2	4.5	4.5	-	4.0	7.0	-	5.81
	3%	2	5.0	4.0	-	7.5	3.0	-	5.31
		2	5.0	4.5	-	5.5	6.0	-	4.32
RAC-50	1%	1	7.0	-	-	-	-	-	6.91
		2	4.0	4.0	-	1.5	6.0	-	6.24
	2%	3	4.0	5.5	6.0	4.0	5.0	-	5.20
		3	4.5	4.5	4.0	8.0	1.0	9.5	5.65
		3	5.0	4.5	5.0	8.0	8.0	6.0	6.30
	3%	1	5.5	-	-	6.0	-	-	5.04
		1	4.5	-	-	8.5	-	-	3.53
RAC-100	1%	3	4.7	4.0	4.0	-	-	-	8.40
		2	5.5	4.0	-	5.5	5.5	-	7.67
	2%	3	4.0	4.5	5.0	3.0	8.0	4.5	6.58
		3	4.2	5.5	4.0	1.0	4.0	4.5	6.30

	3	6.0	5.5	4.5	4.5	6.5	8.0	5.49
3%	2	4.5	4.5	-	7.0	9.0	-	3.90
	3	4.0	6.5	6.0	8.5	6.0	6.0	4.50

(a) CC concrete at 1.6% corrosion level

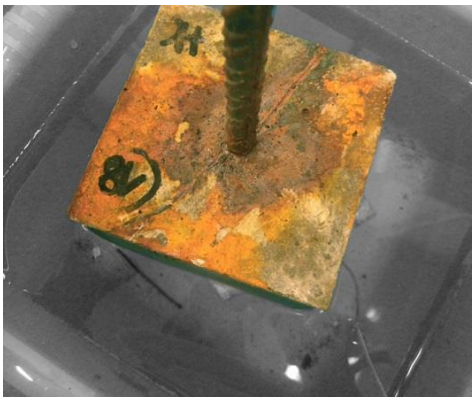

(b) CC concrete at 5.75% corrosion level

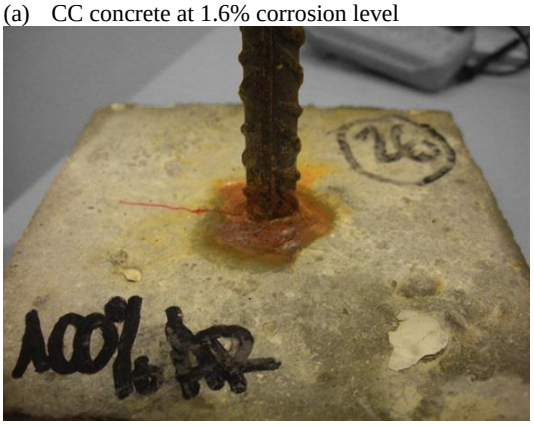

(c) RAC-100 concrete at 1.6% corrosion level

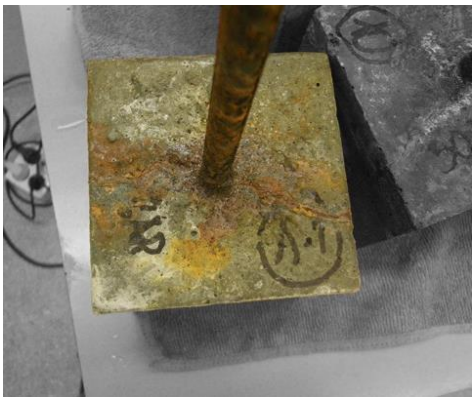

(d) RAC-100 concrete at 5.75% corrosion level

Figure IV-27. Cracking of different specimens after corrosion exposition

It must be considered as remarkable that there was no clear relationship between the values obtained by the visual crack measurements and the τ_{max} achieved for each concrete by means of the direct pull-out tests (Phase 2). A similar behaviour was stated by Yalciner et al. [56], where the bond strength capacity was not attributed to the number of cracks in conventional concretes. That phenomenon could most probably be attributed to the different internal damage on each specimen. Due to the impossibility of observing the internal damage via a visual inspection a post pull-out test examination was performed on the samples.

Figure IV-28. Surface cracking of RAC-50 at 5.75% of corrosion level

Nearly all the samples showed 2 or 3 upper surface cracks which later became prolonged on the lateral faces. However, with respect to the RAC-50 concrete it was noted that after 30 days of being induced by electrical current (of 130 $\mu A/cm^2$) it only suffered one crack on its upper surface, which later became prolonged on one of the lateral faces (see Figure IV-28. Surface cracking of RAC-50 at 5.75% of corrosion level). However, the pull-out test revealed severe internal damage, in accordance with the above-mentioned hypothesis. The corrosion products could fill the pours of concrete producing stress and changing the crack pattern. Consequently, specimens could not release those products causing internal damage. Figure IV-29 depicts other specimens with differing forms of internal damage, revealing different internal crack formations.

Figure IV-29. Internal damage cracking for RAC-100

IV.3.4.3.3 Corrosion level influence on bond-slip relationships

Table IV-13 describes the results of pull-out tests carried out with uncorroded and corroded steel bars (with 1.6%, 2.6% and 5.75% corrosion level). The standard deviation of the results is also described. As previously mentioned, CC concrete and RAC concretes had similar bond strength when they were not exposed to the corrosion effect. However, the bond strength for RAC after 10 days being submitted to an electrical current was higher than that of the CC concrete, and this difference was higher when a larger amount of RCA was employed in concrete production. Consequently, the concretes produced with a greater amount of RCA presented better behaviour in terms of bond capacity under initial corrosion procedures. Mainly, that trend was followed by the three tested corrosion levels. Nevertheless, this better response was significantly decreased as the specimen became more corroded, achieving similar τ_{max} values after 5.75% of corrosion level.

Table IV-13. Pull-out tests (τ_{max}) Results (average-Avg) carried out with none corroded and corroded steel bars (with 1%, 2% and 3% estimated corrosion level)

Concrete	Corrosion – Avg τ_{max} (MPa)							
	0%		1.65%		2.60%		5.75%	
	Avg	Std	Avg	Std	Avg	Std	Avg	Std
CC	32.38	1.75	5.36	0.04	4.73	0.90	4.00	0.47
RAC-20	34.94	3.13	6.93	0.29	5.65	0.73	4.81	0.69
RAC-50	28.77	0.21	6.57	0.47	5.72	0.55	4.29	1.07
RAC-100	31.84	3.63	8.03	0.52	6.12	0.57	4.20	0.43

Figure IV-30 describes the reduction (in %) of τ_{max} of each concrete at a different corrosion level with respect to its τ_{max} value when the steel was uncorroded. In general terms, it was possible to observe a better performance of RCA concretes which improved in concretes produced with high percentages of RCA at low corrosion level. However at high corrosion level, the bond capacity was quite similar in all concretes. It is also relevant to note that concrete produced with more RCA produced a larger drop of τ_{max}.

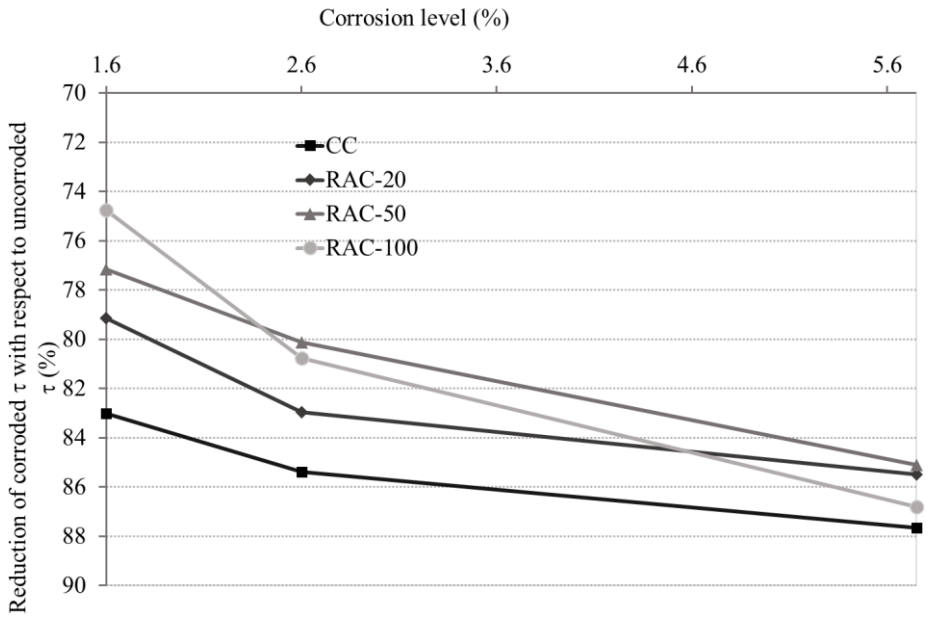

Figure IV-30. Reduction (in %) of τ_{max} of each concrete at a different corrosion level with respect to its τ_{max} value when the steel was uncorroded

Figure IV-31 shows the ratio of τ_{max} of recycled aggregate concretes with respect to that of conventional concrete at different corrosion levels. It can be asserted that τ_{max} was better in all of the RAC concretes than in the Conventional Concrete, independent of the percentages of recycled aggregates used for concrete production and the corrosion level of the steel bars.

Increases of up to 40% of bond capacity were registered for recycled aggregate concretes, with very low corrosion levels. The concrete produced with 100% of recycled aggregate achieved the highest τ_{max} value (see Figure IV-31). The improvement of performance for higher corrosion levels showed increases below those of 10% with which could be defined as being similar in behaviour to all of the corroded specimens.

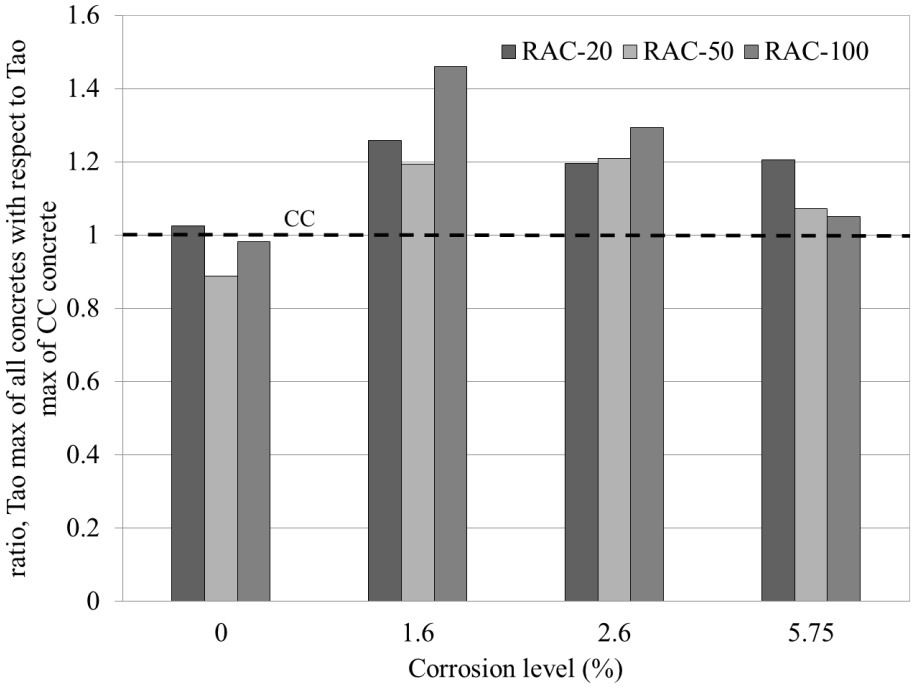

Figure IV-31. Ratio of τ_{max} (phase2) of all the concrete produced with respect to that value of conventional concrete at different corrosion level

Figure IV-32 describes the bond-displacement behaviour of all the tested corroded specimens (2-4 samples were used in each type of concretes). As mentioned above, the displacement showed corresponds to a total displacement which includes slip in the clamps, free steel bar length deformation, etc., as well as the slip between both materials. This is due to the configuration of the pull-out test in Phase 2. However, it is possible to observe the specimen's general behaviour in terms of τ-displacement**.** The concretes produced employing a higher amount of RCA a higher total deformation suffered, accord with the results described in Phase 1 where the RCA-100 showed stiffer bond-slip behaviour than the other specimens.

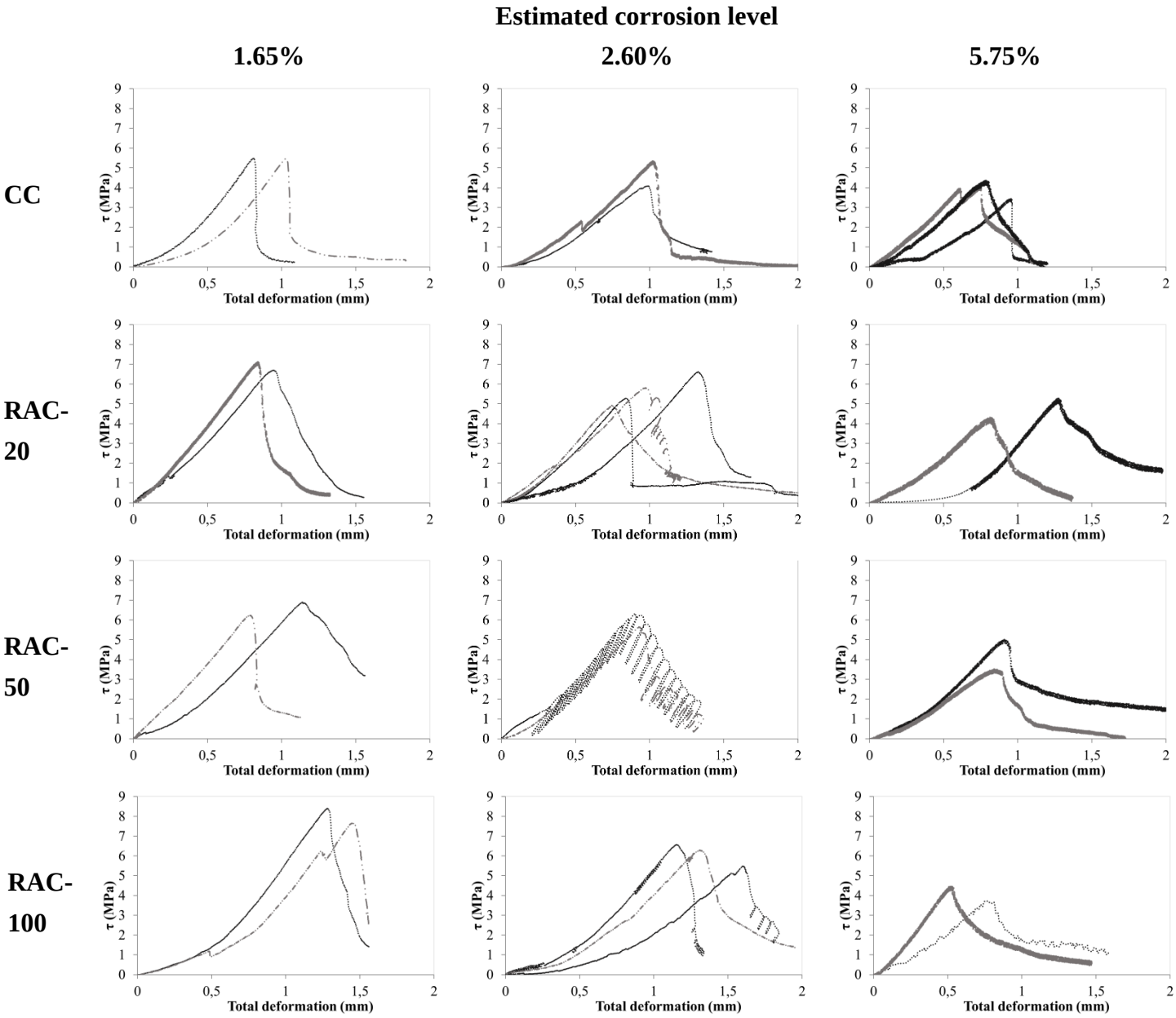

Figure IV-32. Bond (τ, MPa) –displacement (mm) behaviour of all the tested corroded specimens

The observed trend describes a decreasing bond capacity which was directly related to the extent of corrosion products through the specimens. In contrast, the higher the amount of RCA employed for concrete production the higher the bond capacity achieved at 1.6% and 2.6% of corrosion level. However at 5.75 % of corrosion level, RAC-50 and RAC-100 concretes produced the similar bond capacity to CC concrete. At low corrosion level, the RAC concretes produced with three different percentages of RCA presented a higher bond strength than CC concrete. The confinement effect that corrosion products produced due to its expansively for very low corrosion levels might be the responsible of that observed bond

strength increment for RAC concretes. According to other researchers [66–68] slight corrosion of the steel improves the bond strength due to the increase in steel bar surface roughness or friction which caused an increase in bond strength. Besides, the higher porosity of concrete [56] and consequently of RAC reduced the stress level in the surrounding concrete (due to its absorption capacity of that product) increasing the bond strength. However, for high corrosion levels, the absorption capacity of those concretes has no influence causing a significant bond strength reduction as it was described in this study.

Other researchers [68] claimed the reduction of performance of RAC in the whole service life, when chloride diffusion was also considered. In that case, the performance of RAC was worse due to higher chloride diffusion than CC concrete. However, due to the addition of chloride in the mixtures used in this research work and the depassivation of the reinforcement bars the chloride diffusion was not taken into account. RAC Concrete achieved 40% higher bond strength than CC concrete, thus clearly showing better performance at low corrosion level. At high corrosion level, all the concretes tend to have a similar bond strength. However, RAC concrete always has higher values, approximately 10% higher than CC concrete.

IV.3.4.4 Ultimate bond strength (τ_{max}) estimation models

It is possible to find in the literature few mathematical models which estimate/ predict the bond strength value for CC [56,69]. As expected, fewer models are designed to determine the bond strength for RAC concretes [35,37].

In accordance with bond strength prediction of CC concrete, the values obtained by Model Code [69] depends on the compressive strength of concrete and the model defined by Yalciner et al. [56] takes into account the compressive strength of concrete and the ratio between the concrete cover and steel bar diameter for pull-out test setup. The model defined by Kim &Yun [35] for RAC concretes, takes into account the compressive strength of conventional concrete, the ratio between the concrete cover and steel bar diameter for pull-out test setup and the influence of a percentage of RCA in the concrete.

Figure IV-33 shows the estimated bond strength values of the four types of concretes according to the three mathematical models described previously, defined by Kim &Yun [35], Model Code [69], and the model defined by Yalciner et al. [56]. The bond strength values predicted by Kim & Yun model [9] underestimated the real experimental values obtained by Recycled aggregates concretes because it considers the compressive strength of

RAC is lower than that of conventional concrete due to the presence of RCA and consequently also the bond strength.

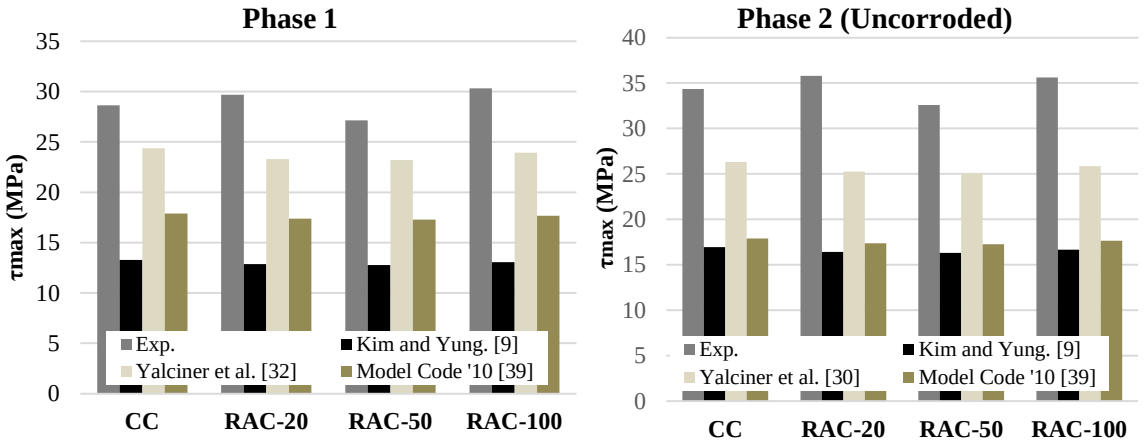

Figure IV-33. Phase 1 and Phase 2 experimental and numerical bond strength values

However, the model defined by Yalciner et al. [56], predicts more adequately the bond strength of all the concretes. It considers that the prediction of the bond strength of any concrete depends only on its compressive strength values and the ratio between the concrete cover and steel bar diameter for the pull-out test. It does not take into account the influence of a different percentage of RCA. The models defined for prediction of the bond strength of CC concretes could predict it adequately the bond strength of recycled aggregate concrete when those RAC concretes are produced with the similar compressive strength of the parent concrete of RCA. According to The Model Code [69], the only consideration of the compressive strength of concrete, underestimated the bond strength of RAC and CC concretes.

Yalciner et al. [32] proposed an analytical model for determination of bond strenth between concrete and different levels of corroded reinforcing steel. That model could be used when the ratio cover/diameter (c/D) was between 1 and 3.2. It has to be noticed that the ratio c/D for the tested specimens is 4.5, which it is outside the bounds defined in the model. Figure IV-34 shows the obtained results in this research work in comparison to the values calculated by the model mentioned above. According to the obtained results, the model overestimated the results achieved by the four types of concretes at low corrosion levels except for concretes produced employing 100% of recycled aggregates which was adequately predicted at low corrosion level. The model also predicted adequately the behaviour of all the concretes at 5.75% corrosion level. The trend described for both the experimental data and the numerical data was roughly the same. However, the real behaviour showed a pronounced drop in bond capacity for lower corrosion levels.

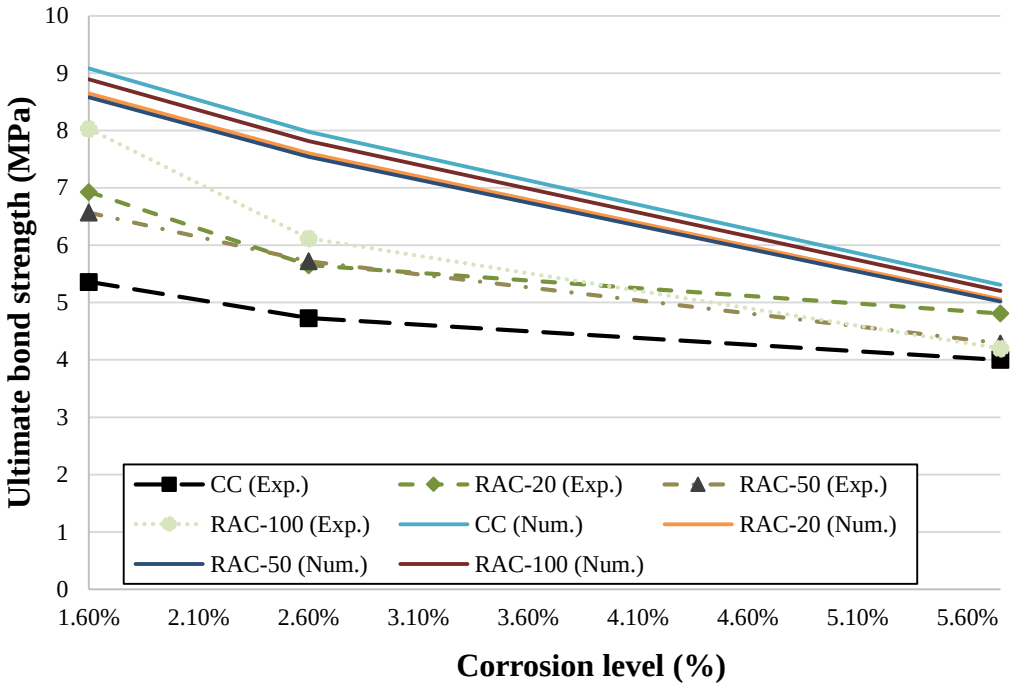

Figure IV-34. Experimental and numeral bond strength values for corroded specimens

IV.3.5 Conclusions

Based on the results of the study, the following conclusions can be drawn:

(1) The bond behaviour is strongly dependent on compressive strength values. The recycled aggregate concretes which had a similar compressive strength to that of conventional concrete obtained similar or better bond strength.

(2) Recycled aggregate concretes produced employing up to 50% of coarse recycled aggregates achieved similar slip and bond strength to those of conventional concrete. However, the recycled aggregate concrete produced with 100% of RCA suffered a substantial stiffness drop.

(3) On reaching the same corrosion level, it was noted that the initial cracking (visually detectable) of recycled aggregate concretes occurred later than conventional concrete. Furthermore, there is no determined relationship between the amount of cracks produced with RA replacement and the corrosion level, nor is there a relationship between the amount of cracks and maximum bond strength.

(4) The employment of a higher amount of RCA leads to better bond strength performance at very low corrosion levels due to higher absorption capacity that leads to a bond improvement. A higher corrosion level caused similar behaviour on RAC and CC concretes.

(5) An increase of the corrosion damage propagation Phase in the structural service life of RAC concrete takes place due to its capacity to reduce longitudinal cracking and development of better bond strength performance for low corrosion levels.

(6) The ultimate bond strength estimation models used for CC were adequate for the prediction of the bond strength of the RAC, when the compressive strength of the RCA parent concrete was found to be similar or higher to that of RAC. In order to validate an Ultimate bond strength, one must consider not only its compressive strength and the percentage of RCA but also parameters such as ratio cover/Diameter and the compressive strength of RCA parent concrete. The model presented by Yalciner et al. [56] described quite well the bond behaviour of the corroded specimen. However, a calibration with a more extended database is needed in order to adjust the real observed behaviour accurately.

It would be advantageous to produce a further work based on an analysis of lower corrosion rates in order to accurately compare the presented conclusions with those of naturally corroded concrete specimens. The resulting values obtained from RAC, which would have been subjected to corrosion over extended periods of time, simulating closer to natural corrosion procedure, are expected to be defined as behaving even better than those obtained in this research work, consequently improving their adequate property with respect to that of CC concrete.

Acknowledge

The authors wish to acknowledge the financial support of The Ministry of Economy and Competitiveness of the Government of Spain (MINECO) for providing funds for projects BIA2009-11764 as well as INNPACT project (IPT-2012-1093-310000) and European Regional Development Fund (FEDER). The financial support of Infrastructures de Catalunya (ICAT) for personnel expenses is also highly appreciated.

References

[1] W. Zhang, X. Song, X. Gu, S. Li, Tensile and fatigue behavior of corroded rebars, Constr. Build. Mater. 34 (2012) 409–417. doi:10.1016/j.conbuildmat.2012.02.071.

[2] C.A. Apostolopoulos, Mechanical behavior of corroded reinforcing steel bars S500s tempcore under low cycle fatigue, Constr. Build. Mater. 21 (2007) 1447–1456. doi:10.1016/j.conbuildmat.2006.07.008.

[3] C.A. Apostolopoulos, M.P. Papadopoulos, S.G. Pantelakis, Tensile behavior of corroded reinforcing steel bars BSt 500s, Constr. Build. Mater. 20 (2006) 782–789. doi:10.1016/j.conbuildmat.2005.01.065.

[4] C. a. Apostolopoulos, V.G. Papadakis, Consequences of steel corrosion on the ductility properties of reinforcement bar, Constr. Build. Mater. 22 (2008) 2316–2324. doi:10.1016/j.conbuildmat.2007.10.006.

[5] H. Çetinel, M. Toparlı, L. Özsoyeller, A finite element based prediction of the microstructural evolution of steels subjected to the Tempcore process, Mech. Mater. 32 (2000) 339–347. doi:10.1016/S0167-6636(00)00009-0.

[6] I. Sankar, K. Rao, A. Gopalakrishna, Optimization of steel bars subjected to Tempcore process using regression analysis and harmony search algorithm, J Sci Ind Res. 69 (2010) 266–270. http://nopr.niscair.res.in/handle/123456789/7713 (accessed July 10, 2014).

[7] J. Nikolaou, G.. Papadimitriou, Microstructures and mechanical properties after heating of reinforcing 500 MPa class weldable steels produced by various processes (Tempcore, microalloyed with vanadium and work-hardened), Constr. Build. Mater. 18 (2004) 243–254. doi:10.1016/j.conbuildmat.2004.01.001.

[8] P. Simon, M. Economopoulos, P. Nilles, Tempcore: a new process for the production of high quality reinforcing bars, Iron Steel Eng. 61 (198AD) 55–67.

[9] J.M. Bairan, a. R. Marí, H. Ortega, J.C. Rosa, Efecto del enrollado y enderezado en las propiedades mecánicas de barras de acero de diámetro medio y grande fabricadas en rollo, Mater. Construcción. 61 (2011) 559–581. doi:10.3989/mc.2011.60110.

[10] C.A. Apostolopoulos, Mechanical behavior of corroded reinforcing steel bars S500s tempcore under low cycle fatigue, Constr. Build. Mater. 21 (2007) 1447–1456. doi:10.1016/j.conbuildmat.2006.07.008.

[11] C.A. Apostolopoulos, V.G. Papadakis, Consequences of steel corrosion on the ductility properties of reinforcement bar, Constr. Build. Mater. 22 (2008) 2316–2324. doi:10.1016/j.conbuildmat.2007.10.006.

[12] A.A. Almusallam, A.S. Al-Gahtani, A.R. Aziz, F.H. Dakhil, Rasheeduzzafar, Effect of Reinforcement Corrosion on Flexural Behavior of Concrete Slabs, J. Mater. Civ. Eng. 8 (n.d.) 123–127. http://cedb.asce.org/cgi/WWWdisplay.cgi?101994 (accessed February 14, 2015).

[13] A. a. Almusallam, Effect of degree of corrosion on the properties of reinforcing steel bars, Constr. Build. Mater. 15 (2001) 361–368. doi:10.1016/S0950-0618(01)00009-5.

[14] J.M. Bairan, A.R. Marí, H. Ortega, J.C. Rosa, Efecto del enrollado y enderezado en las propiedades mecánicas de barras de acero de diámetro medio y grande fabricadas en rollo, Mater. Construcción. 61 (2011) 559–581. doi:10.3989/mc.2011.60110.

[15] M.D. Garcia, M.C. Alonso, M.C. Andrade, J. Rodríguez, Influencia de la corrosión en las propiedades mecánicas del acero, Hormigón Y Acero. 210 (1998) 11–21.

[16] E. Moreno Fernández, A. Cobo Escamilla, M. Fernández Cánovas, Ductility of reinforcing steel with different degrees of corrosion and the'equivalent steel'criterion, Mater. …. 57 (2007) 5–18. http://scholar.google.com/scholar?hl=en&btnG=Search&q=intitle:Ductility+of+reinforcing+steel+with+different+degrees+of+corrosion+and+the+?+equivalent+steel+?+criterion#0 (accessed July 11, 2014).

[17] S.L.W.Z.X.G.C. Zhu, Fatigue of Reinforcing Steel Bars Subjected to Natural Corrosion, Open Civ. Eng. J. (2011) Vol.5, p69. http://connection.ebscohost.com/c/articles/70458995/fatigue-reinforcing-steel-bars-subjected-natural-corrosion (accessed February 14, 2015).

[18] C. a. Apostolopoulos, M.P. Papadopoulos, Tensile and low cycle fatigue behavior of corroded reinforcing steel bars S400, Constr. Build. Mater. 21 (2007) 855–864. doi:10.1016/j.conbuildmat.2005.12.012.

[19] C.A. Apostolopoulos, M.P. Papadopoulos, Tensile and low cycle fatigue behavior of corroded reinforcing steel bars S400, Constr. Build. Mater. 21 (2007) 855–864. http://www.sciencedirect.com/science/article/pii/S0950061805003260 (accessed February 14, 2015).

[20] T. El Maaddawy, K. Soudki, Effectiveness of impressed current technique to simulate corrosion of steel reinforcement in concrete, J. Mater. Civ. …. (2003) 41–47. http://ascelibrary.org/doi/abs/10.1061/(ASCE)0899-1561(2003)15:1(41) (accessed July 3, 2014).

[21] M. Badawi, K. Soudki, Control of Corrosion-Induced Damage in Reinforced Concrete Beams Using Carbon Fiber-Reinforced Polymer Laminates, J. Compos. Constr. 9 (2005) 195–201. doi:10.1061/(ASCE)1090-0268(2005)9:2(195).

[22] M. Saifullah, L.A. Clark, Effect of corrosion rate on the bond strength of corroded reinforcement, in: S.A. Press (Ed.), Proc. Int. Conf. Corros. Corros. Prot. Steel Concr., University of Sheffield, 1994: pp. 591–600.

[23] UNE-EN-ISO-15630-01, Acero para el armado y pretensado del hormigón - Métodos de ensayo. Parte 1: Barras, Alambre y Alambrón para el hormigón armado, (n.d.).

[24] T.U. and S. Misra, Behavior of Concrete Beams and Columns in Marine Environment When Corrosion of Reinforcing Bars Takes Place, (1988) 127–146, Vol. 109 SP. doi:10.14359/2796.

[25] K.Z. Hanjari, K. Lundgren, D. Coronelli, Bond capacity of severely corroded bars with corroded stirrups, Mag. Concr. Res. 63 (2011) 953–968. doi:10.1680/macr.10.00200.

[26] I. Sæther, Bond deterioration of corroded steel bars in concrete, Struct. Infrastruct. Eng. 7 (2011) 415–429. doi:10.1080/15732470802674836.

[27] D. Coronelli, K.Z. Hanjari, K. Lundgren, Severely Corroded RC with Cover Cracking, J. Struct. Eng. 139 (2013) 221–232. doi:10.1061/(ASCE)ST.1943-541X.0000633.

[28] A. Muñoz Noval, C. Andrade, A. Torres, J. Rodríguez, Relation between Crack Width and Diameter of Rebar Loss Due to Corrosion of Reinforced Concrete Members, ECS Trans. 3 (2007) 29–36. doi:10.1149/1.2721428.

[29] C. Alonso, C. Andrade, J. Rodriguez, J.M. Diez, Factors controlling cracking of concrete affected by reinforcement corrosion, Mater. Struct. 31 (1998) 435–441. doi:10.1007/BF02480466.

[30] K. Lundgren, P. Kettil, K.Z. Hanjari, H. Schlune, A.S.S. Roman, Analytical model for the bond-slip behaviour of corroded ribbed reinforcement, Struct. Infrastruct. Eng. 8 (2012) 157–169. doi:10.1080/15732470903446993.

[31] K. Zandi Hanjari, K. Lundgren, M. Plos, D. Coronelli, Three-dimensional modelling of structural effects of corroding steel reinforcement in concrete, Struct. Infrastruct. Eng. (2011) 1–17. doi:10.1080/15732479.2011.607830.

[32] C. Fang, K. Lundgren, M. Plos, K. Gylltoft, Bond behaviour of corroded reinforcing steel bars in concrete, Cem. Concr. Res. 36 (2006) 1931–1938. doi:10.1016/j.cemconres.2006.05.008.

[33] M.R. Salari, E. Spacone, Finite element formulations of one-dimensional elements with bond-slip, Eng. Struct. 23 (2001) 815–826. doi:10.1016/S0141-0296(00)00094-8.

[34] J. Xiao, H. Falkner, Bond behaviour between recycled aggregate concrete and steel rebars, Constr. Build. Mater. 21 (2007) 395–401. doi:10.1016/j.conbuildmat.2005.08.008.

[35] S.-W. Kim, H.-D. Yun, Evaluation of the bond behavior of steel reinforcing bars in recycled fine aggregate concrete, Cem. Concr. Compos. 46 (2014) 8–18. doi:10.1016/j.cemconcomp.2013.10.013.

[36] S.-W. Kim, H.-D. Yun, Influence of recycled coarse aggregates on the bond behavior of deformed bars in concrete, Eng. Struct. 48 (2013) 133–143. doi:10.1016/j.engstruct.2012.10.009.

[37] S. Seara-Paz, B. González-Fonteboa, J. Eiras-López, M.F. Herrador, Bond behavior between steel reinforcement and recycled concrete, Mater. Struct. 47 (2013) 323–334. doi:10.1617/s11527-013-0063-z.

[38] I. Eiras López, J., Seara Paz, S., González Taboada, I., Vieito Raña, COMPORTAMIENTO ADHERENTE EN HORMIGÓN CON ÁRIDO, in: Comport. Adherente En Hormigón Con Árido Reciclado. Curva Tensión Adherente-Deslizamiento, ACHE - Asociación cientificotécnica del hormigón estructural, Madrid, 2014: pp. 1–10.

[39] FiB Bulletin 10 - Bond of reinforcement in concrete, 2000.

[40] L. Butler, J.S. West, S.L. Tighe, The effect of recycled concrete aggregate properties on the bond strength between RCA concrete and steel reinforcement, Cem. Concr. Res. 41 (2011) 1037–1049. doi:10.1016/j.cemconres.2011.06.004.

[41] S.W. Tabsh, A.S. Abdelfatah, Influence of recycled concrete aggregates on strength properties of concrete, Constr. Build. Mater. 23 (2009) 1163–1167. doi:10.1016/j.conbuildmat.2008.06.007.

[42] T. Hansen, Recycled aggregate and recycled aggregate concrete, Second State-of-the-art Report developments 1945–1985, Mater. Struct. RILEM. 111 (1986).

[43] T. Hansen, RILEM: recycling of demolished concrete and masonry, Report of Technical Comité 37-DRC: Demolition and Reuse of Concrete, London, 1992.

[44] M.C. Limbachiya, T. Leelawat, R.K. Dhir, Use of recycled concrete aggregate in high-strength concrete, Mater. Struct. 33 (2000) 574–580. doi:10.1007/BF02480538.

[45] K.K. Sagoe-Crentsil, T. Brown, A.H. Taylor, Performance of concrete made with commercially produced coarse recycled concrete aggregate, Cem. Concr. Res. 31 (2001) 707–712. http://www.sciencedirect.com/science/article/pii/S0008884600004762 (accessed October 16, 2014).

[46] C.S. Poon, Z.H. Shui, L. Lam, H. Fok, S.C. Kou, Influence of moisture states of natural and recycled aggregates on the slump and compressive strength of concrete, Cem. Concr. Res. 34 (2004) 31–36. doi:10.1016/S0008-8846(03)00186-8.

[47] M. Etxeberria, E. Vázquez, A. Marí, M. Barra, Influence of amount of recycled coarse aggregates and production process on properties of recycled aggregate concrete, Cem. Concr. Res. 37 (2007) 735–742. http://www.sciencedirect.com/science/article/pii/S0008884607000415 (accessed May 26, 2014).

[48] R.V. Silva, J. de Brito, R.K. Dhir, Properties and composition of recycled aggregates from construction and demolition waste suitable for concrete production, Constr. Build. Mater. 65 (2014) 201–217. http://www.sciencedirect.com/science/article/pii/S0950061814004437 (accessed August 29, 2014).

[49] C.. Poon, Z.. Shui, L. Lam, Effect of microstructure of ITZ on compressive strength of concrete prepared with recycled aggregates, Constr. Build. Mater. 18 (2004) 461–468. http://www.sciencedirect.com/science/article/pii/S0950061804000388 (accessed May 29, 2014).

[50] M. Barra, E. Vázquez, Properties of concrete with recycled aggregates: influence of properties of the aggregates and their interpretation., in: Proceeding Int. Symp. Sustain. Constr. Use Recycl. Concr. Aggreg., London, 1998: pp. 19–30.

[51] A. Ajdukiewicz, A. Kliszczewicz, Influence of recycled aggregates on mechanical properties of HS/HPC, Cem. Concr. Compos. 24 (2002) 269–279. http://www.sciencedirect.com/science/article/pii/S0958946501000129 (accessed October 24, 2014).

[52] J.R. Jiménez, J. Ayuso, A.P. Galvín, M. López, F. Agrela, Use of mixed recycled aggregates with a low embodied energy from non-selected CDW in unpaved rural roads, Constr. Build. Mater. 34 (2012) 34–43. http://www.sciencedirect.com/science/article/pii/S0950061812001195 (accessed October 28, 2014).

[53] J. a. Pérez-Benedicto, M. Del Río-Merino, J.L. Peralta-Canudo, M. De la Rosa-La Mata, Características mecánicas de hormigones con áridos reciclados procedentes de los rechazos en prefabricación, Mater. Construcción. 62 (2011) 25–37. doi:10.3989/mc.2011.62110.

[54] V. Corinaldesi, G. Moriconi, Influence of mineral additions on the performance of 100% recycled aggregate concrete, Constr. Build. Mater. 23 (2009) 2869–2876. http://www.sciencedirect.com/science/article/pii/S0950061809000713 (accessed October 7, 2014).

[55] F.M. de Almeida Filho, M.K. El Debs, A.L.H.C. El Debs, Bond-slip behavior of self-compacting concrete and vibrated concrete using pull-out and beam tests, Mater. Struct. 41 (2007) 1073–1089. doi:10.1617/s11527-007-9307-0.

[56] H. Yalciner, O. Eren, S. Sensoy, An experimental study on the bond strength between reinforcement bars and concrete as a function of concrete cover, strength and corrosion level, Cem. Concr. Res. 42 (2012) 643–655. doi:10.1016/j.cemconres.2012.01.003.

[57] N.E. UNE, UNE-EN_10080=2006, (2006).

[58] Instrucción de hormigón estructural - EHE-08, 2008.

[59] A. Losberg, Cracks in continuous concrete road slabs and other concrete structures locked against movements from temperature and shrinkage, 1962.

[60] M.F. Ruiz, A. Muttoni, P.G. Gambarova, Analytical Modeling of the Pre- and Postyield Behavior of Bond in Reinforced Concrete, (2007) 1364–1372.

[61] T.A. El Maaddawy, K.A. Soudki, Effectiveness of Impressed Current Technique to Simulate Corrosion of Steel Reinforcement in Concrete, (2003) 41–47.

[62] ASTM, ASTM G1-03, (n.d.).

[63] S.-W. Kim, H.-D. Yun, Influence of recycled coarse aggregates on the bond behavior of deformed bars in concrete, Eng. Struct. 48 (2013) 133–143. doi:10.1016/j.engstruct.2012.10.009.

[64] S.-W. Kim, H.-D. Yun, Evaluation of the bond behavior of steel reinforcing bars in recycled fine aggregate concrete, Cem. Concr. Compos. 46 (2014) 8–18. doi:10.1016/j.cemconcomp.2013.10.013.

[65] Z. Dahou, Z. Mehdi Sbartaï, A. Castel, F. Ghomari, Artificial neural network model for steel–concrete bond prediction, Eng. Struct. 31 (2009) 1724–1733. http://www.sciencedirect.com/science/article/pii/S0141029609000789 (accessed March 23, 2015).

[66] Y.S. Choi, S.-T. Yi, M.Y. Kim, W.Y. Jung, E.I. Yang, Effect of corrosion method of the reinforcing bar on bond characteristics in reinforced concrete specimens, Constr. Build. Mater. 54 (2014) 180–189. http://www.sciencedirect.com/science/article/pii/S0950061813012221 (accessed March 23, 2015).

[67] L. Abosrra, A.F. Ashour, M. Youseffi, Corrosion of steel reinforcement in concrete of different compressive strengths, Constr. Build. Mater. 25 (2011) 3915–3925. http://www.sciencedirect.com/science/article/pii/S0950061811001632 (accessed February 13, 2015).

[68] Y. Zhao, J. Dong, Y. Wu, H. Wang, X. Li, Q. Xu, Steel corrosion and corrosion-induced cracking in recycled aggregate concrete, Corros. Sci. 85 (2014) 241–250. http://www.sciencedirect.com/science/article/pii/S0010938X14001991 (accessed November 25, 2014).

[69] Model Code 2010-Final draft, The international federation for structural concrete, FIB. Bulletin No 52 Fib, 2; Lausanne, 2012.

Chapter V

MODELLING LOCAL CORROSION EFFECTS: Mechanical properties of corroded steel bars and anchorage behaviour in concrete

V.1 Introduction

This chapter focuses on modelling the local effects described in the previous chapter. Part of the present work was developed during a stage of the author at Chalmers University of Technology, Sweden. Modelling of local effects is an important and challenging task. The implementation of these models into global structural models allows assessing the structural response of corroded structures much more accurately and to take into account many variables that they are affected by reinforcing steel corrosion. The first part of the Chapter consists of modelling the mechanical properties of corroded steel. A previously developed model was extended and validated by means of different experimental test to include the corrosion steel phenomenon. A pitted critical cross-section approach is defined to describe corrosion of steel reinforcement either pitting or generalised corrosion. By means of the previously presented experimental fatigue study of corroded steel bars, a critical

characteristic pit is defined according to the overall corrosion level. Thereafter, in accordance a fibre discretization analysis of the pitted cross-section it is possible to describe the main mechanical steel properties under wide corrosion range levels. A validation of the model was performed using different studies found in the literature. In addition, the model allows considering not-homogeneous steel cross-section due to the new manufacturing procedures (mainly TEMPCORE). Furthermore, a validation of the proposed model is presented. By means of 3D scanning technique, some corroded steel bars with different corrosion levels were scanned. By postprocessing of the scanned bars, the critical cross-section was obtained and discretized in fibres. The corroded cross-section was analysed and compared with the experimental data obtained. The comparison showed an excellent agreement between the experimental results and model predictions in terms of ultimate strength and elastic limit values. In addition, some 3D analyses were performed processing the scanned data. A 3D solid mesh of elements were defined. Thereafter, monotonic and cyclic analyses were performed and compared with the results obtained by the sectional model.

The second part of the Chapter focuses on bond modelling in concrete members. The study of different methods to model the anchorage in concrete is performed. A comparison of three approaches to model the anchorage behaviour were done: (a) a one-dimensional analysis, where the bond-slip differential equation with a nonlinear bond-slip constitutive model is numerically solved, and where the mean bond strength as well as the required anchorage length to anchor the yield force are computed. (b) Finite element (FE) analyses were performed using 3D solid elements for concrete, and beam elements for reinforcement, where the interaction was explicitly described using the same bond-slip constitutive model as in alternative (a). (c) 3D FE analysis with 3D solid elements for both concrete and reinforcement, where a frictional model described the concrete/rebar interaction, and the effect of corrosion was taken into account by introducing the swelling action and the flow of rust through cracks. In both types of FE analyses, non-linear fracture mechanics, with a rotating crack model based on total strain, was used. The bond models used were previously developed in other works at Chalmers University of Technology. The results show differences between the three approaches. Each of the modelling alternatives had both drawbacks and advantages; while the more complicated modelling accounting for more variables yielded more realistic results compared to reality, the simple 1D analysis was very fast and efficient.

The last part of the Chapter encompasses the study of bond between concrete and textile reinforcement. From some pull-out test, the 1D local bond-slip relationship was obtained.

The use of a 1D bond-slip analytical model previously developed at Chalmers for steel bars permits to get such curves and implement them into a 3D models of the pull-out tests. Hence, a comparison between the 1D bond-slip model and the 3D model performed using finite element programme has been done, with the underlying purpose to extend and assess the suitability of the 1D bond-slip model with different materials.

V.2 Mechanical model to evaluate steel reinforcement corrosion effects on σ-ε and fatigue curves. Experimental calibration and validation.

Ignasi Fernandez*[1], Jesús Miguel Bairán[1], Antonio R. Marí[1]

[1] Department of Construction Engineering, Polytechnic University of Catalonia, Jordi Girona, 1-3, Barcelona 08034, Spain.

*corresponding author: ignasi.fernandez-perez@upc.edu

Highlights:

- Mechanical model to evaluate corroded steel mechanical properties
- Calibration and validation of a mechanical model to evaluate corrosion effect on σ-ε and fatigue curves
- An experimental study on material properties characterization for not corroded bars produced with TEMPCORE® system.
- Experimental data validates presented model from 0% up to 25% corrosion level.

Abstract: Corrosion of steel reinforcement is one of the main problems in reinforced concrete structures. Loss of cross-section is due to pitting along the bar either generalized corrosion or pitting corrosion. This phenomenon takes into non-uniform stress distribution throughout the steel cross-section due to local effects such as stress localization and local bending in pitted cross-section. Besides, in commonly used TEMPCORE® produced bars, the non-uniform material properties distribution leads to an aforementioned effect emphaticising. In this work, an experimental study to characterize the real material properties throughout the steel cross-section in 10 mm and 12 mm diameter TEMPCORE steel bars is presented. Thereafter a mechanical model which allows the corroded steel σ-ε and fatigue curves description is presented. The model is calibrated and validated with different experimental tests which encompassed more than 200 corroded and uncorroded specimens subjected to monotonic and cyclic loading with the underlying purpose to evaluate the behaviour of corroded steel bars.

Keywords: Corrosion; Steel reinforcement; Mechanical properties; Experimental tests; Fatigue; Stress-strain; Statistical variability; Pitted cross-section; TEMPCORE®

V.2.1 Introduction

The study of corrosion effects is crucial for a better understanding of the structural behaviour of existing impaired concrete structures. Effects such as the loss of bond between concrete and steel reinforcement, steel cross-section reduction or concrete longitudinal cracking due to rust expansiveness, which leads in splitting stresses on the surrounding concrete, have been widely studied [1–4]. However, other local corrosion effects that lead to a steel mechanical behaviour changes [5–8] are relevant too. Both pitting and generalized corrosion of reinforcement steel bars conduct to a change in the cross-section geometry. This changes turn into local effects in steel cross-section such as non-uniform stress distribution due to both stress localization in the top of the pits and local bending due to centre of gravity displacement.

On the other hand some modern production systems, such as TEMPCORE® production system, produces a heterogeneous material properties throughout the steel cross-section, being the apparent σ-ε characterization of the bar, the mean response of the heterogeneous section. Specifically annular distribution of the mechanical properties is defined for this steel manufacture system [9–13][6,9–13], in which the outer layers resist more than the inner core. Consequently, due to non-uniform cross-section reduction of steel corrosion, the non-uniform stress throughout the cross-section and the reduction of the bar capacity are emphasised.

In this work, an experimental study to define a realistic material distribution throughout the steel cross-section was performed. Different specimens with reduced cross-section diameters were tested by means of monotonic loads. After post-processing the experimental data, it was possible to define the mechanical properties throughout the cross-section, i.e. the diametrical yielding stress and ultimate stress profiles.

Thereafter, a mechanical model to evaluate steel reinforcement corrosion effects on σ-ε and fatigue curves is presented. The model takes into account the reduction of cross-section either generalized or localized due to pitting corrosion. Pitting corrosion is considered by means of a notch in the cross-section, associated to a corrosion level. Generalized corrosion is considered by means of the critical cross-section definition, in which is performed a double steel cross-section reduction, a reduction due to the generalized corrosion level besides a notch. In both cases notches are described as perfect ellipses.

On the other hand, material heterogeneity in the cross sections due to current production systems of reinforcing bars such as TEMPCORE®, is considered by discretizing the cross-

section in two different layers. The damage produced by load cycles is defined in accordance to the Palmgren-Miner damage law [14,15], by which fatigue curves for corroded steel bars can be obtained

A statistical model relating the pitting geometry with the corrosion level was developed and calibrated using different experimental data found in the literature [16,17]. Thereafter, the mechanical model was validated by means of monotonic and fatigue tests of corroded steel bars [16,18,19]

V.2.2 Material behaviour. TEMPCORE® reinforcement steel bars.

An experimental study was conducted in order to define the mechanical properties of uncorroded heterogeneous steel reinforcement bars. TEMPCORE® production system consists on the application of cold water after the steel conformation with the purpose to quickly decrease its temperature. The temperature of the applied water and the applied time defines the steel microstructure and thereafter the final mechanical properties. The common microstructure obtained is a ferrite core followed by a mix ferrite-martensitic crown. Finally an outer martensitic layer. The aim of the presented experimental study was the characterization of 12 mm diameter steel bars used for the calibration and validation of the given model.

V.2.2.1 Test setup

The tests aimed the characterization of the tensile mechanical steel properties distribution throughout the cross-section. By performing monotonic tests to uncorroded specimens with different cross-section reductions the different σ-ε curves were obtained (see Figure V-1a). The reduction of cross-section was performed by means of a milling machine. Different crowns thickness were removed from each specimen using a diamond tip. The actual diameter was checked using a vernier calliper in order to know the exact remaining cylindrical steel area.

Test were performed following the code [20]. The specimens were afixed to the clamps, and the load was directly applied to the bar via a hydraulic jack controlled with a load cell placed on the top. The same jack had an active displacement control system so the tests could be controlled by the total applied displacement. A 50 mm displacement transducer was placed at the reduced cross-section zone in order to register the real strain of the bar, avoiding machine deformations, slip in the clamps and complete cross-section bar deformation. All

the tested specimens failed in the middle of the reduced cross-section zone. Member length between clamps was 110 mm, and the reduced cross-section length was 70 mm, enough to assure uniform stress distribution. Monotonic tests were carried out by means of a test machine INSTRON 8803, see Figure V-1b.The diameters tested are described in Table V-1.

Figure V-1. a) Reduced cross-section specimens. b) INSTRON 8800 transducer

Table V-1. Tested diameter for material characterization

Steel reduced diameter [mm]
6
8
9
10
11/11.5 (only removing ribs)
Theoretical 12 (whole section)

V.2.2.2 Results of monotonic test

σ-ε curves of tested reduced diameter members are described in Figure V-2. The strains described corresponded to the ones recorded by means of a displacement transducer (50 mm range) placed on the bars. The stresses depicted in the figures resulted from the division of the load recorded by the DAQ by the steel reduced diameter, measured with the calliper.

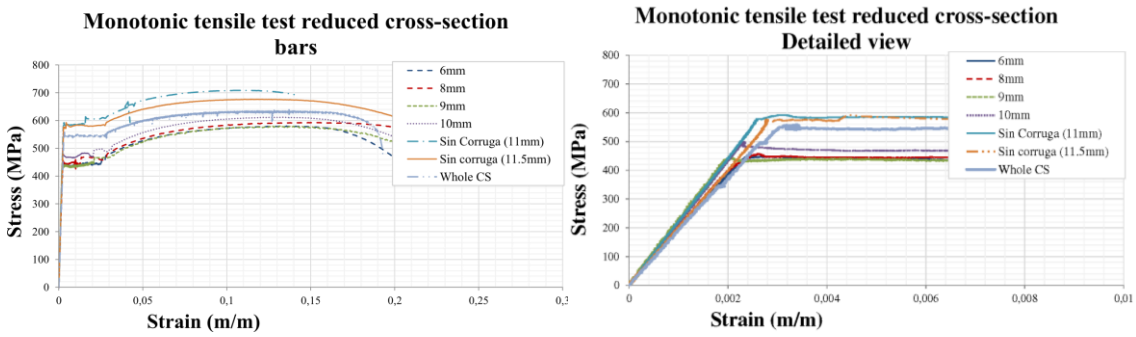

Figure V-2. σ-ε without corrosion a) up to failure b) up to the elastic limit

All the curves presented in Figure V-2 corresponded to the mean value between the ferrite core and the adjacent martensitic layers. A post-processing of the experimental data to obtain the real material properties of the layer itself was performed. Different specimens were tested to obtain the diameter of the ferrite core. From that successive crowns of 0.5 mm thickness were added until the complete steel bar was tested, see Figure V-3.

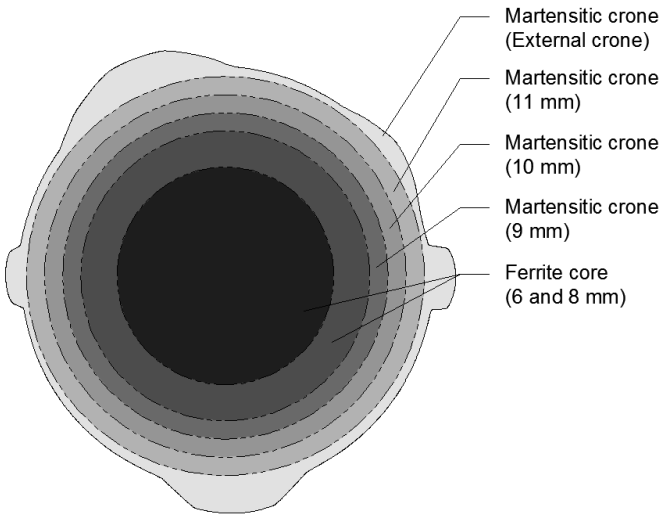

Figure V-3. Martensitic crowns up to whole cross-section and ferrite core

Applying the product-summation series described in Equation V-1 the material properties for each particular crown could be obtained. The final elastic limit and ultimate strength values for the different layers are shown in Table V-2.

Equation V-1 $$\sum \boldsymbol{A_i} \cdot \boldsymbol{f_{y_i}} = \overline{\boldsymbol{A}} \cdot \overline{\boldsymbol{f_y}}$$

The final profile of the elastic limit and ultimate strength along the cross-section is described in Figure V-4a, and the idealized σ-ε curve for each crown is described in Figure V-4b.

Table V-2. Real elastic limits and ultimate strength obtained after experimental data post-processing

Specimens (ϕ12)	External radius (mm)	fy (MPa)	fu (MPa)
Ferrite core	4	435	575
Crown 1 (Ferrite)	4.25	522	601
Crown 2	4.5	583	642
Crown 3	4.75	655	682
Crown 4	5	705	718
Crown 5	5.25	749	757
Crown 6	5.5	783	789
Crown 7	5.75	806	824
Outer crown	6	806	824

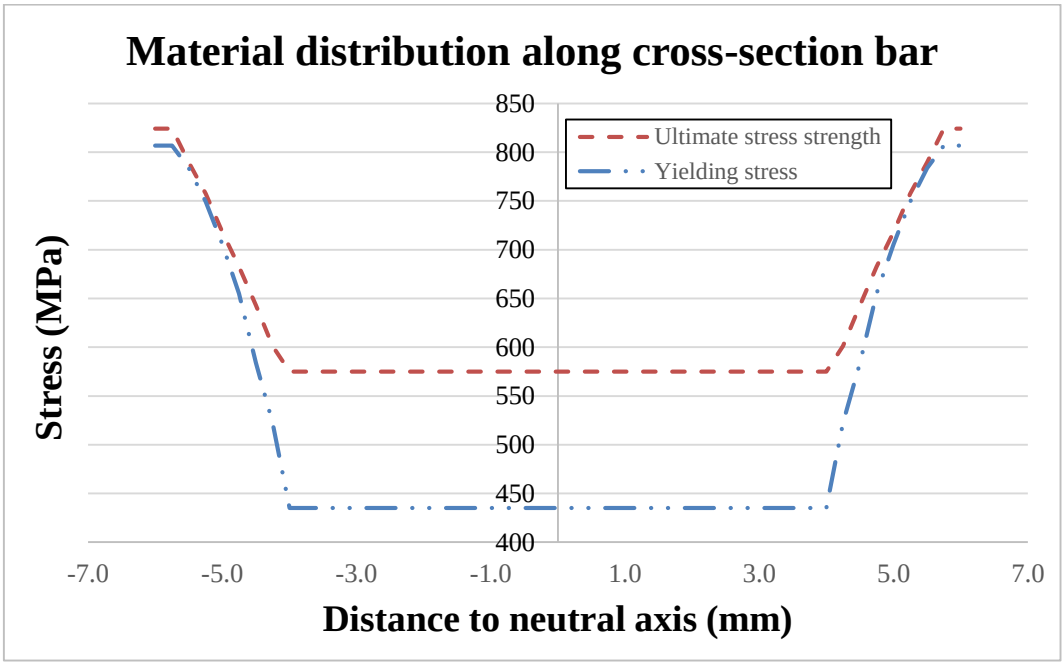

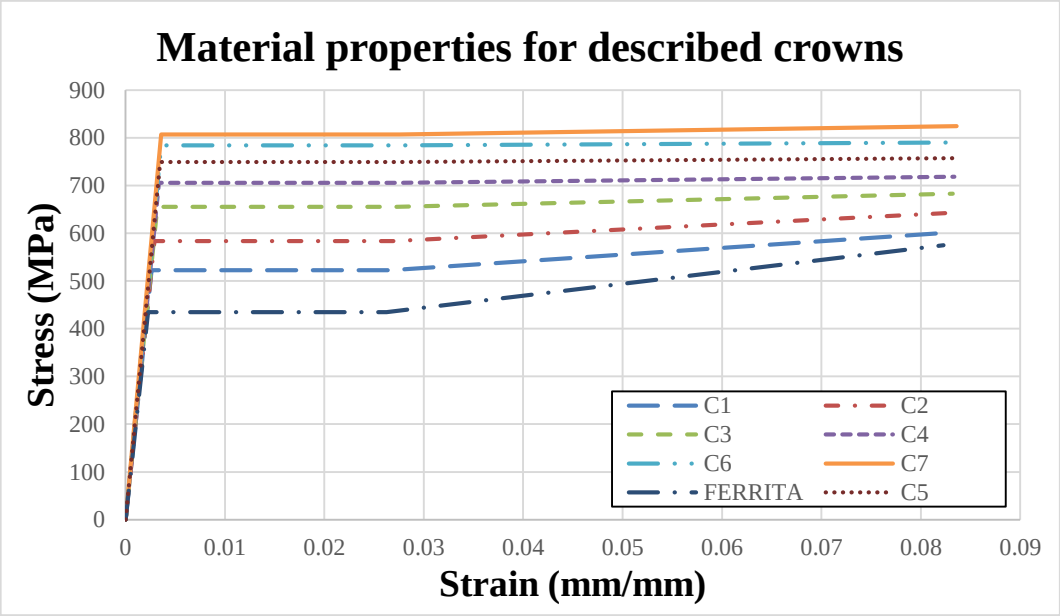

Figure V-4. a) Obtained stress profile from the tested bars. b) σ-ε final curves of each discretized layer

The measured capacity of the specimens on which only the ribs were removed, resulted higher than that of measured considering the whole bar. The influence of the ribs in the sectional behaviour resulted in a reduction of the mechanical properties. This phenomenon was due to 3D stress effects produced on the ribs, did not contribute as much as the other member section to the bar carrying capacity, see Figure V-5.

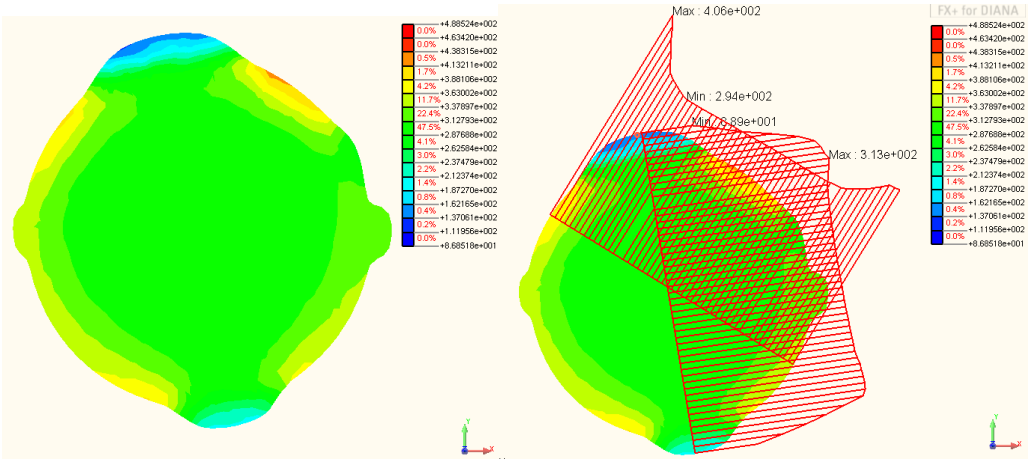

Figure V-5. Geometric effect of ribs (bar cross-section)

V.2.3 Description of the mechanical model

V.2.3.1 Material model

After the presented experimental study and taking into account the results obtained by Bairán et al. [13] a simplified bi-layer material model was chosen; an inner ferrite core and an outer martensitic crown, which described the average behaviour from all the remaining layers, see Figure V-6. The inner core diameter was calibrated by means of the experimental data.

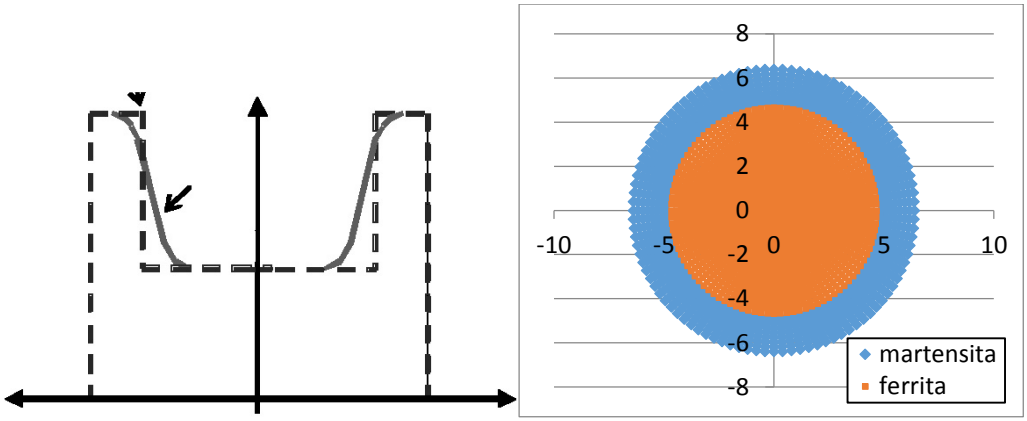

Figure V-6. Material properties distribution in the presented work

V.2.3.2 Cross-section definition and constitutive equation

The model uses a fibre discretization of the critical steel reinforcement cross-section in order to incorporate the variety of mechanical properties throughout the cross section. This approach can accurately describe the bar geometry as well as the material heterogeneity. This work is focused on this manufacturing process as far as it is the most extended production system for steel reinforcement bars in Europe.

The behaviour under large cyclic loading histories was controlled by means of material's hardening rules. The steel proposed material model is a mix of the two existing models in the literature: kinematic an isotropic hardening. Therefore, a mixed-hardening model was developed by Bairan et al. [13] an implemented in the mechanical model.

V.2.3.3 Implementation of corrosion phenomenon

Corrosion phenomenon was implemented into the model by means of the weakest section definition, where most likely would fail, which it was represented as a circular cross-section with an unique equivalent pit (circular idealized cross-section, see Figure V-7b). Both

generalized and pitting corrosion could be simulated considering this circular critical pitted cross-section.

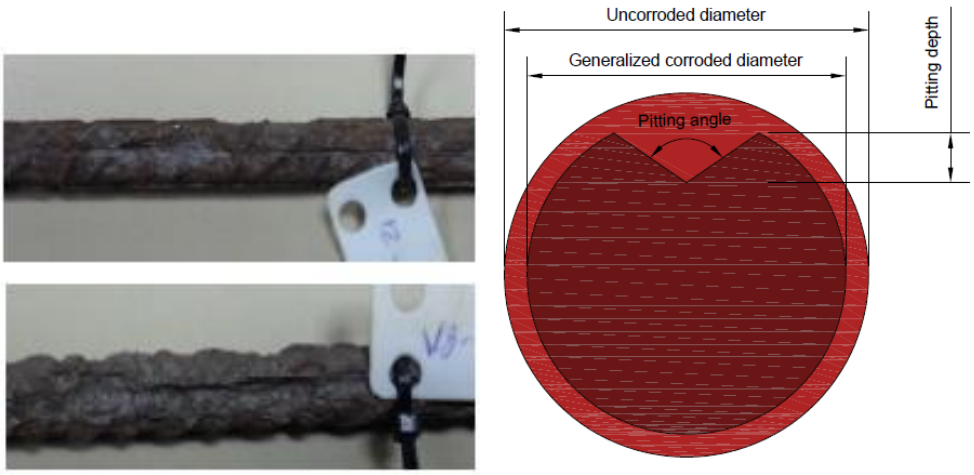

Figure V-7. Model of the critic pitted cross-section and pit definition (depth, angle and length)

By defining a pit, which includes the steel cross-section reduction due to corrosion, in the equivalent steel cross-section, the pitting corrosion was implemented. On the other hand, a double cross-section reduction for generalized corrosion was performed on the initial cross-section; a reduction of area equivalent to the generalized corrosion level was applied, see Figure V-7b. This reduction led to a new smaller diameter, $\phi_{cor} < \phi$. Thereafter a notch was performed to that new cross-section, which geometrical characteristics depended on the generalized corrosion level and were calibrated by means of the statistical model presented below.

A half ellipse hypothesis, defined by its major and minor axes, to reproduce the geometrical shape of the pit was idealized. Depth, length and angle in the section plane defined the main geometrical parameters of the pit. The critical cross-section was placed in the maximum depth of the ellipse, minor axis, whereas the major axis represented the pitting length in the longitudinal direction bar, see Figure V-7a.

Localization stresses factor over the notch tip and linear fracture mechanics criteria [21] were applied thanks to the ellipse hypothesis. Equation V-2 defined the stress at the notch tip (σ_p), where σ_n was the pressure under plain strain distribution hypothesis. L and p were the pitting length and depth respectively (see Figure V-8). Stress amplification in the different points of the cross-section was a function of the distance to the notch tip and it followed the Airy function [21].

Equation V-2 $\sigma_p = \sigma_n \cdot (1+4p/L)$

Because the assumptions made, the application of any stress and temperature histories to the bar are allowed by the model. Loading in monotonic test was applied by means of strain control. Fatigue test was a particular case in which it is possible to apply a desired load history; residual stresses or local yielding were possible to be simulated.

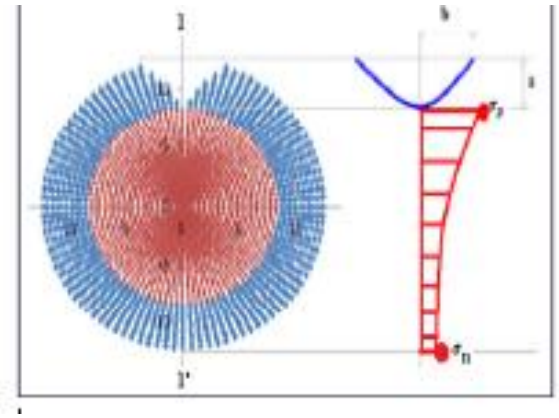

Figure V-8. Pitting effect in the steel cross-section: stress localization and local bending moment

V.2.3.4 Fatigue model description

Fatigue analyses was performed using a specific stress range, which was referred to the complete cross-section (using uncorroded nominal diameter). Raw materials were considered. The maximum and the minimum stresses at every fibre in the cross-section were determined after each analysis. Then, the number of resisted cycles of each fibre under the defined stress range could be obtained.

By modifying the number of cycles resisted by each fibre, the effect of the applied mean stress was considered, i.e. two fibres subjected to the same stress range resisted different number of cycles depending on the applied σ_m value. In addition, the reduction of the resisted cycles with the temperature, was also considered.

Palmgren-Miner, Equation V-3, was used to define the damage state of each fibre after every load step (i).

Equation V-3 $d_i = n_i / N_i$

Where N was the cycle resisted number, n the number of times the applied stress range was and d the fibre damage state index. The damage was accumulated during every load step. When the fibre achieved damage index 1, it was considered broken and it was removed from the cross-section for the next steps iteratively until the last group of fibres did not resist the

applied stress range. Thereafter the cycle resisted number, N, was stated as the fatigue life value.

V.2.4 Model calibration

V.2.4.1 Experimental data for the model calibration

An extensive database of corroded reinforcing steel bars submitted to monotonic and cycle loading [16] were used for calibration pourposes. That work focused on direct monotonic and cyclic tests of corroded reinforcement bars extracted from statically undetermined beams exposed to accelerated corrosion procedure with different corrosion levels.

The specimens employed for monotonic testing had in between 310 mm and 320 mm length. The ends of the test specimen were affixed by two clamps, which were used to transfer directly the load to the specimen. The tested free section was for all the specimens 170 mm letting 70/75 mm length for each clamp. Tests were conducted by means of displacement control. Uncorroded specimens also were tested to compare and assess the influence of degree of corrosion on the mechanical properties. In total 40 specimens were tested satisfactorily with a range of corrosion levels between 8% and 22%.

Fatigue test specimens also had in between 310 mm and 320 mm length. The ends of the test specimen were affixed by two clamps, which were used to transfer directly the load to the specimen. The tested free length was for all the specimens 170 mm letting 70/75 mm length for each clamp. In that case, tests were conducted by means of load control.

Three different stress ranges were defined for fatigue tests, 150 MPa, 200 MPa and 300 MPa ($\Delta S = S_{max} - S_{min}$). The minimum stress ($S_{min}$) was defined avoiding compressions in the bar and its possible buckling effects. The maximum stress (S_{max}) was lower than $0.6 * f_y$ (referred to uncorroded specimens). Corroded specimens were submitted to the same load range as uncorroded ones, which was obtained by means of the uncorroded nominal diameter. In total 142 specimens were tested with ranging from 8% up to 28% corrosion levels. The most probably failure cross-section were characterized by means of the definition of the pitting geometry using a Vernier calliper. Further information regarding the experimental work is described by Fernandez et al. [16].

Due to the reduced existing database of corroded specimens submitted to high-cycle loading, half of the above-mentioned specimens were employed for calibration purposes and the other

half for the model validation. The σ-ε corroded properties were validated by means of different experimental studies [5,6,18,19].

V.2.4.2 Calibration of the critical pit parameters

Model calibration consisted in the definition of the pit in the critical cross-section, which resulted in the same experimental fatigue life value. Different geometrical pitting parameters were tested, until good agreement between the experimental mesured pit and the model pit was obtained, see Figure V-9.

A bisectional iterative algorithm was performed, which applied different notch geometries until the convergence was reached (the same resisted number of cycles). Pitting length and pitting depth were compared. The defined pitting angle aperture strongly conditioned the model pitting depth, so different angle aperture relationships with respect to the corrosion level were tested to adjust this last parameter.

Figure V-9. Pitting depth-corrosion level. Experimental data and calibrated numerical model

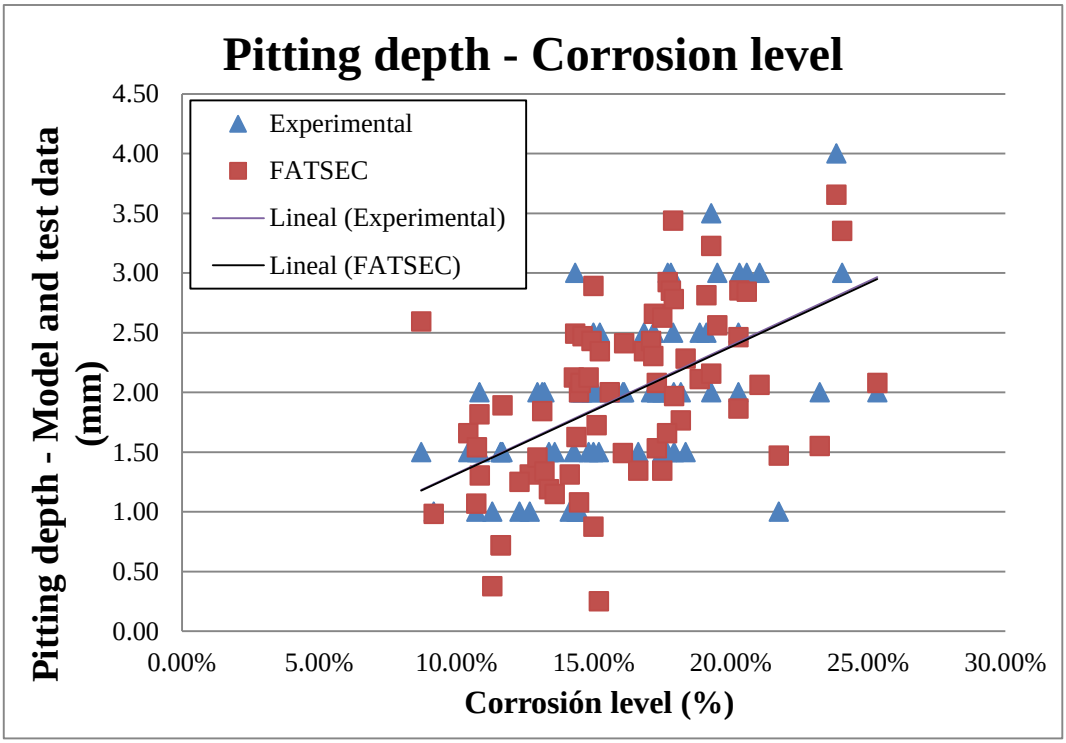

A dimensionless expression, Equation V-4, to describe the pitting geometry characteristics with respect to the generalized corrosion level was obtained from the model data. It was defined by the coefficient p/r_c (pitting depth (p) and the resulting corroded radius (r_c), Figure

V-7) and the steel bar corrosion level (generalized corrosion, g). Figure V-10 shows the aforementioned obtained relationship.

Equation V-4 $p/r_c = 2.318*g$ or $p/\phi_c = 1.159*g$

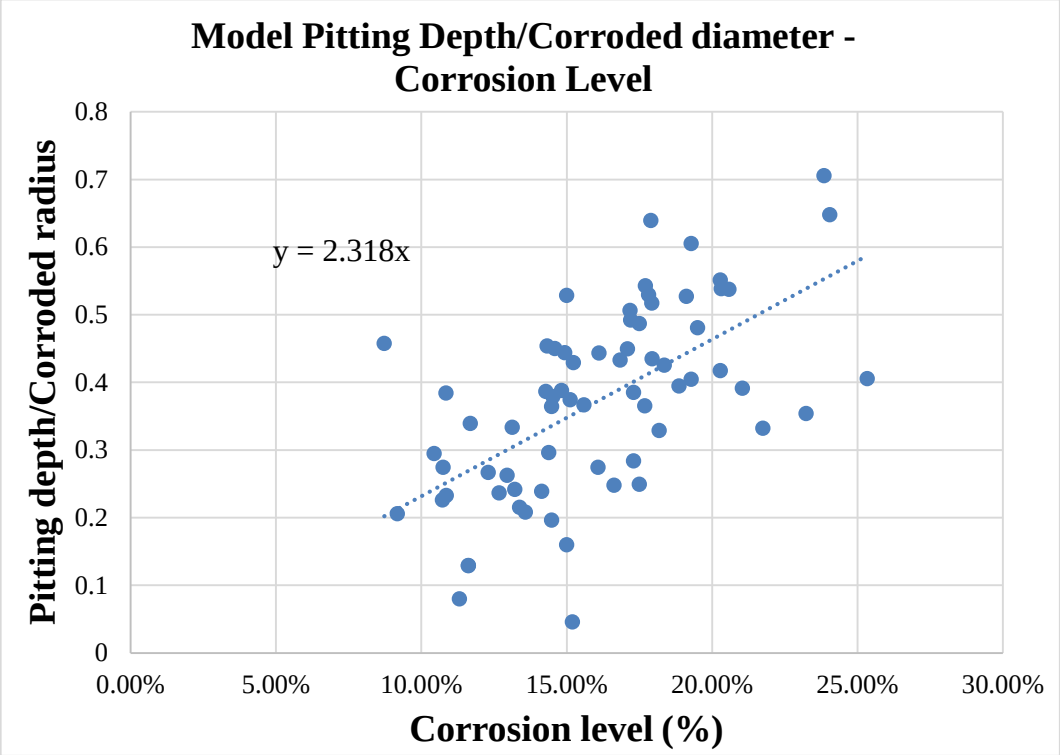

Figure V-10. Relationship between corrosion level and the quotient pitting- corroded bar diameter

V.2.4.2.1 Pitting depth statistical model adjustment

A log-Normal distribution adjusted very well to the obtained data, see Figure V-11, in which it is represented the probaiblity to obtain the same pitting depth by the model and the reality. The parameters of such distribution were mean=1.054, variance=0.092, mu=0.0134 and sigma=0.282.

The pitting depth values for 0.95 and 0.05 quantiles could be obtained multiplying the average depth value got from (4) by 1.62 and 0.61 respectively. So the upper and lower bounds were defined.

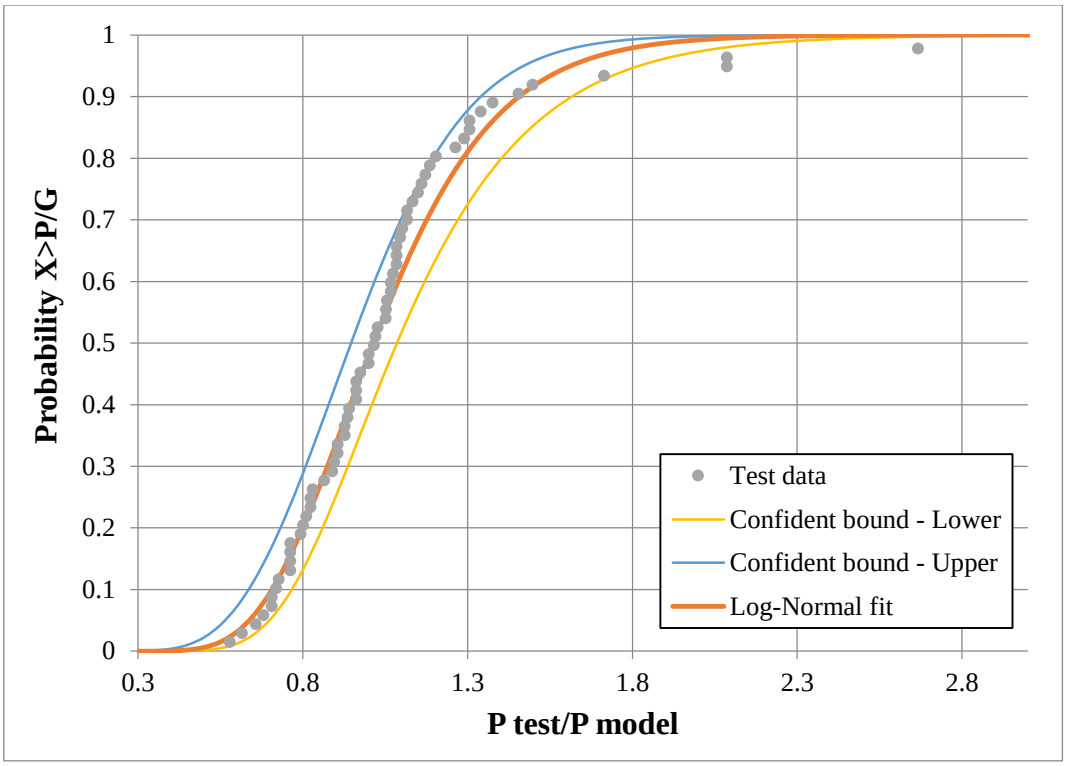

Figure V-11. Statistical distribution of the pitting depth and the log-Normal adjustment

V.2.4.3 Pitting characteristics sensitivity, depth, length and angle influence

A sensitivity study of the principal variables that defined the idealized pitting shape was performed.

V.2.4.3.1 Pitting angle and pitting depth

The pitting depth was indirectly defined by the pitting angle, so the pitting angle determined the pitting depth model sensibility. Different pitting angle apertures with respect to the corrosion level were defined to observe their influence in the corroded steel tensile properties. Fixed and variable angle apertures relationship were tested. In all the cases the same value for the pitting length was used.

Figure V-12a, Figure V-12b, Figure V-12c, and Figure V-12d, represent the evolution of the main tensile motonic parameters, yielding stress, ultimate stress, modulus of elasticity and maximum strain with respect to the corrosion level . Modulus of elasticity, yield stress and ultimate stress presented no significant variation with respect the different angle apertures used. However higher corrosion levels presented higher differences. Nevertheless, the differences between the different angle apertures used were less than 5%. Strains showed a slightly higher scatter behaviour.

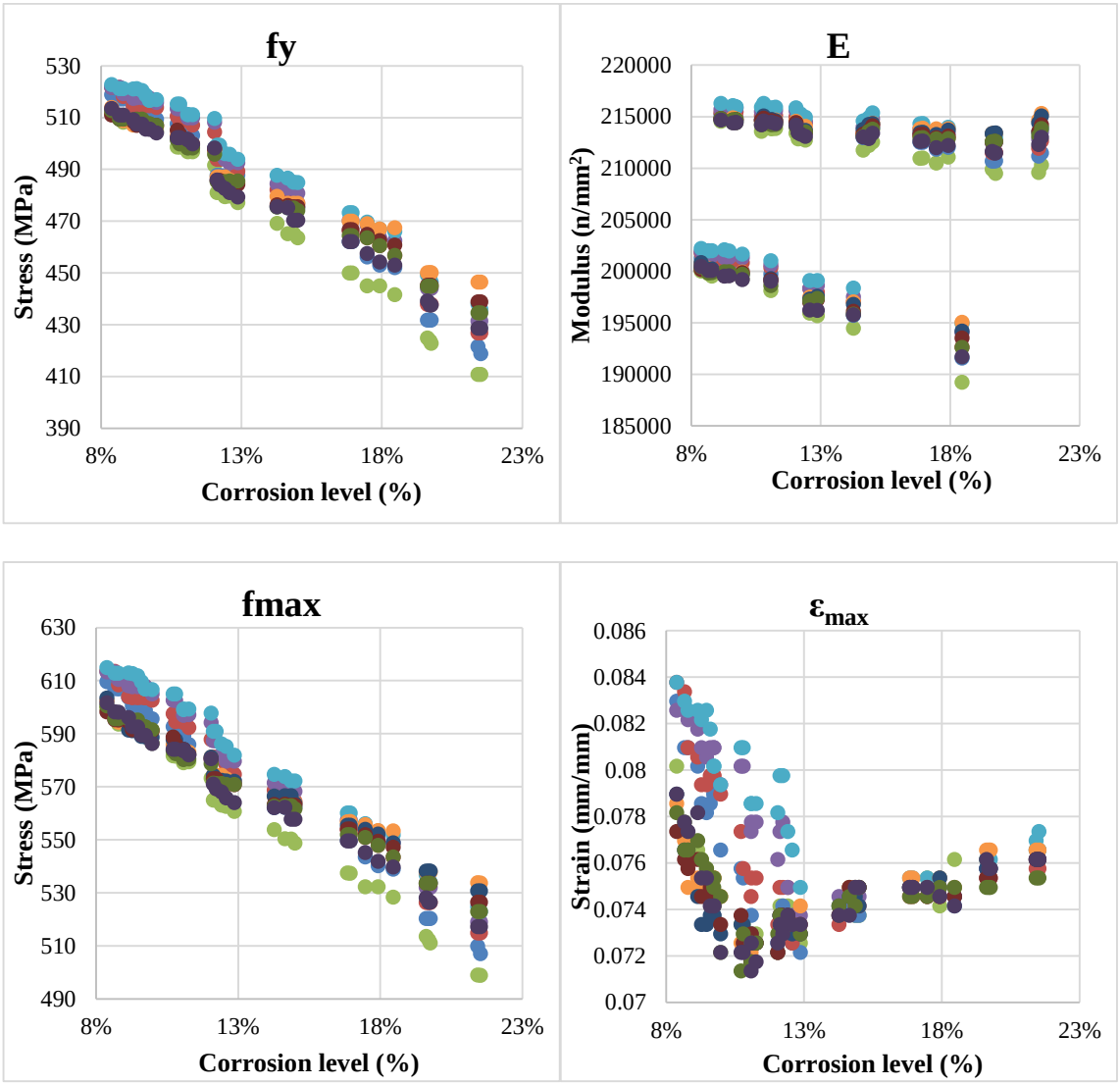

Figure V-12. Corroded steel tensile properties – Pitting angle variation

V.2.4.3.2 Pitting length

The same analysis was performed to study the pitting length sensitivity. Figure V-13a, Figure V-13b, Figure V-13c and Figure V-13d, shows the evolution of the same parameters depicted in Figure V-12, using different pitting length. The same pitting angle was used in all cases. Four different length hypotheses were made in order to test its influence on those parameters. The relationship between the pit length and the degree of corrosion almost did not affect to the obtained results.

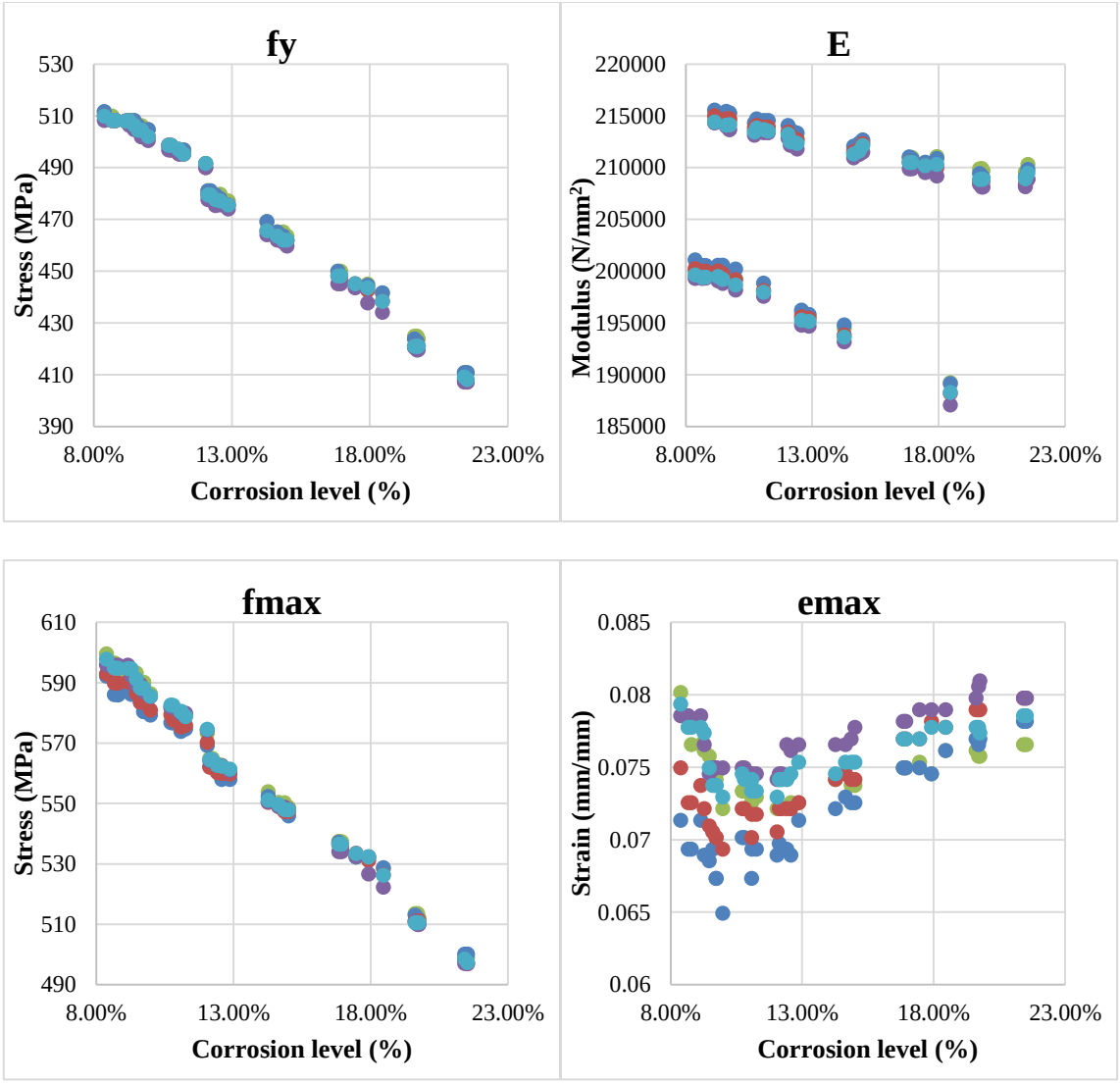

Figure V-13. Corroded steel tensile mechanical properties - Pitting length variation

V.2.4.3.3 Implemented pitting geometry relationships

Finally, the implemented pitting geometry characteristics regarding the corrosion level are shown in Figure V-14.

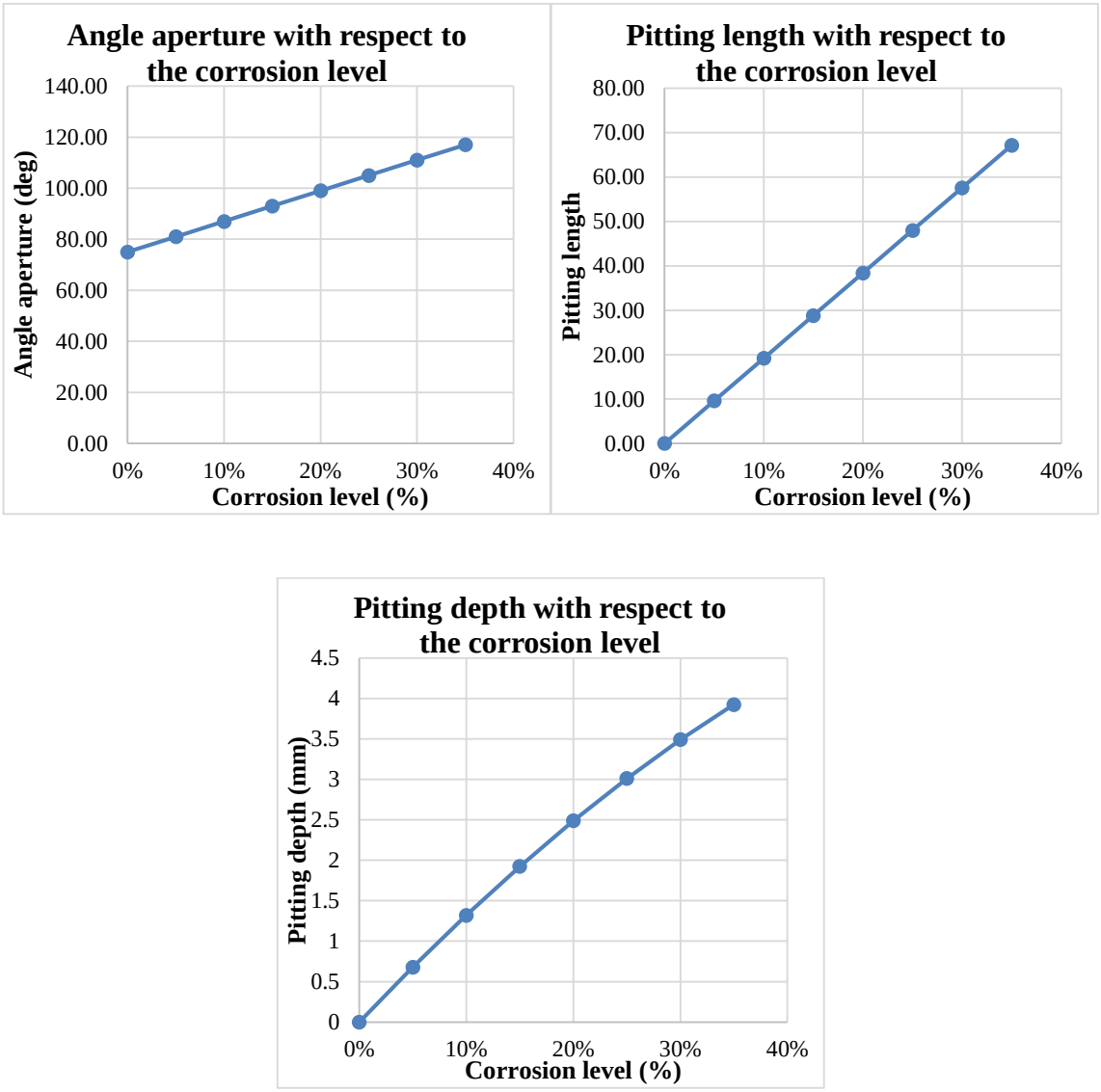

Figure V-14. Pitting geometry implementation

According to the relationships described in Figure V-14, the critical pited cross-section was defined and the notch performed. The different cross-section meshes that resulted after the application of the above criteria are reproduced in Figure V-15.

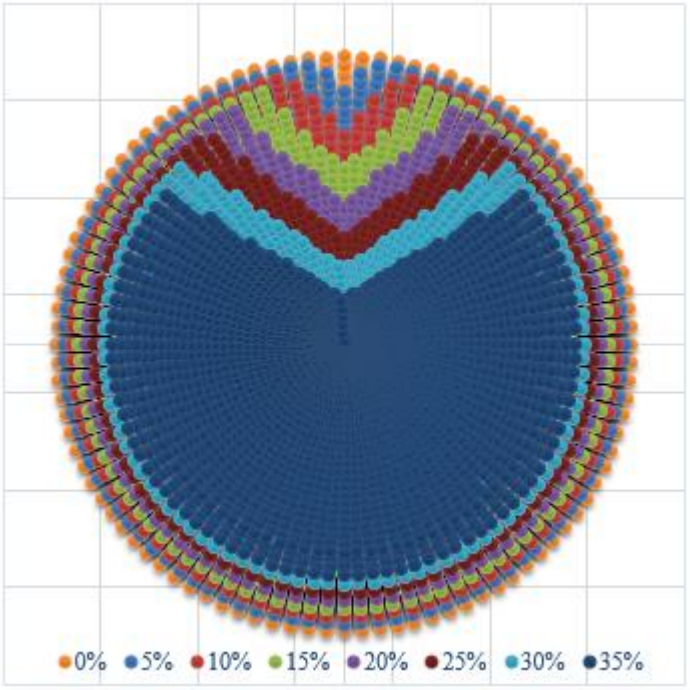

Figure V-15. Mechanical model meshes for different corrosion level (generalized corrosion)

V.2.5 S-N and σ-ε curves obtained from the calibrated mechanical model

The evolution of the corroded mechanical properties with respect to the corrosion level are presented in the next Figures. The values expressed in the figures were obtained using the 95% percentile of the statistical model presented before for the pitting depth. That percentile represented the most damage in the bar by means of deeper pits. Figure V-16 and Figure V-17 depicted the S-N and σ-ε curves for corrosion level between 5% up to 35%. The stress range represented in Figure V-16 were referred to the nominal area of the uncorroded bar, as it was done in the experimental work. However, depicted stresses in Figure V-17 were referred to the generalized corroded area, without take into account the pit. This allows describing the σ-ε behaviour considering the estimated corrosion level of the bar.

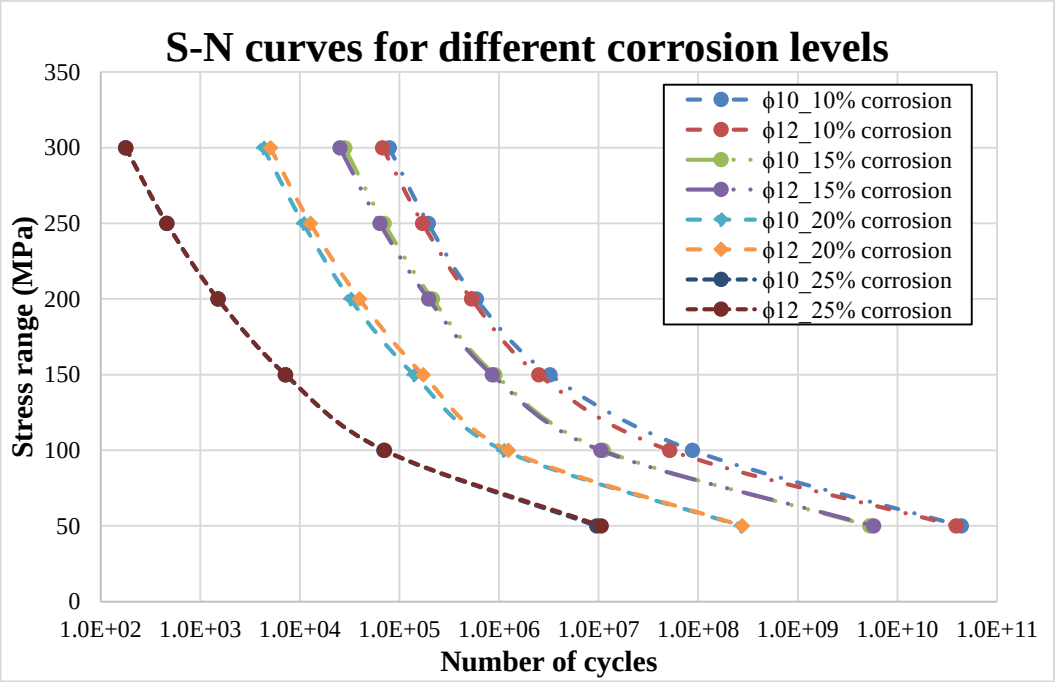

Figure V-16. Fatigue curves obtained with the presented model for different corrosion levels and two diameters according to 95% characteristic pitting – Stress range referred to nominal diameter

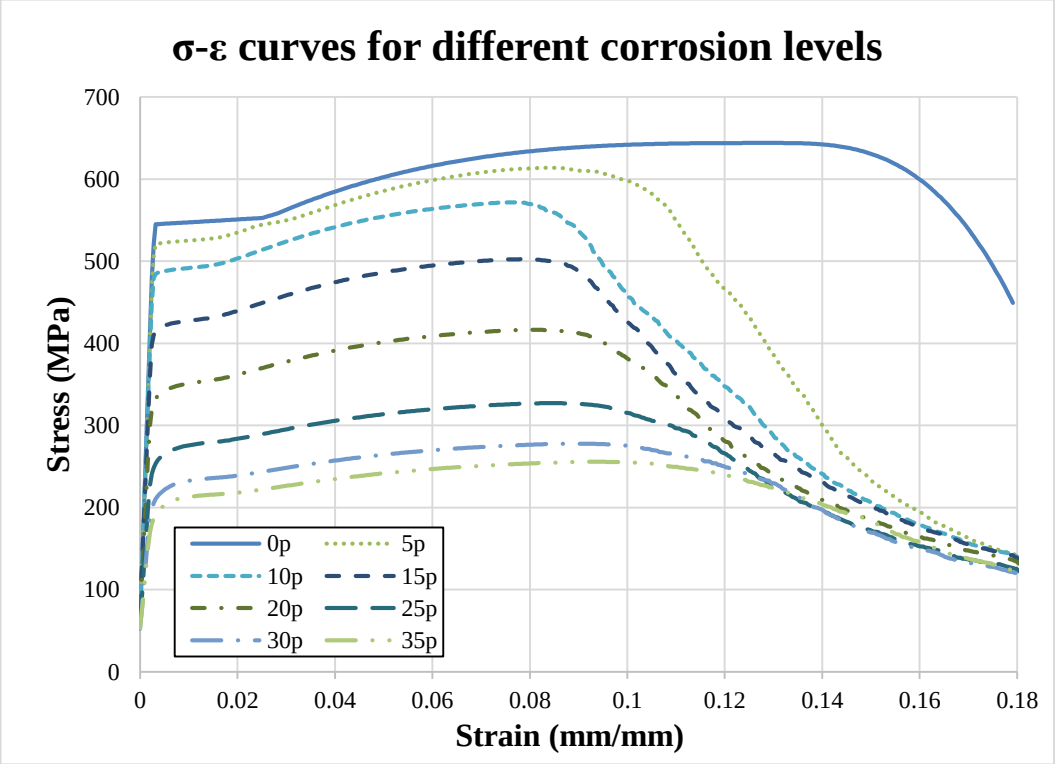

Figure V-17. σ-ε curves obtained with the model for different corrosion levels according to 95% characteristic pitting depth – Stresses referred to generalized corrosion level

Few conclusions are remarkable from the presented results. The diameter effect (10 mm and 12 mm diameter) is not as relevant as the degree of corrosion effect in the fatigue life reduction. Fatigue strength is gradually reduced with respect to the corrosion level. However, the fatigue limit was maintained constant at 30 MPa indistinctly the corrosion level was, at least up to 25% corrosion levels, which is a very high value.

An important reduction of the main parameters defining the σ-ε curves was presented. As it is possible to observe the parameters represented did not described a linear reduction with respect to the corrosion level, behaviour already reported by Fernandez et al. [16].

V.2.6 Model validation

V.2.6.1 Fatigue validation

Validation of the model for fatigue results was made using the other half specimens above described. A total of 66 specimens were used for validation purposes. The validation of the model consisted on the comparison of fatigue life value (number of resisted cycles) obtained from the test with respect to the achieved with the model, see Figure V-18. As it is possible to observe in the figure the data were well distributed along the line with slope 1, which means that the model thrown similar values to experimental data.

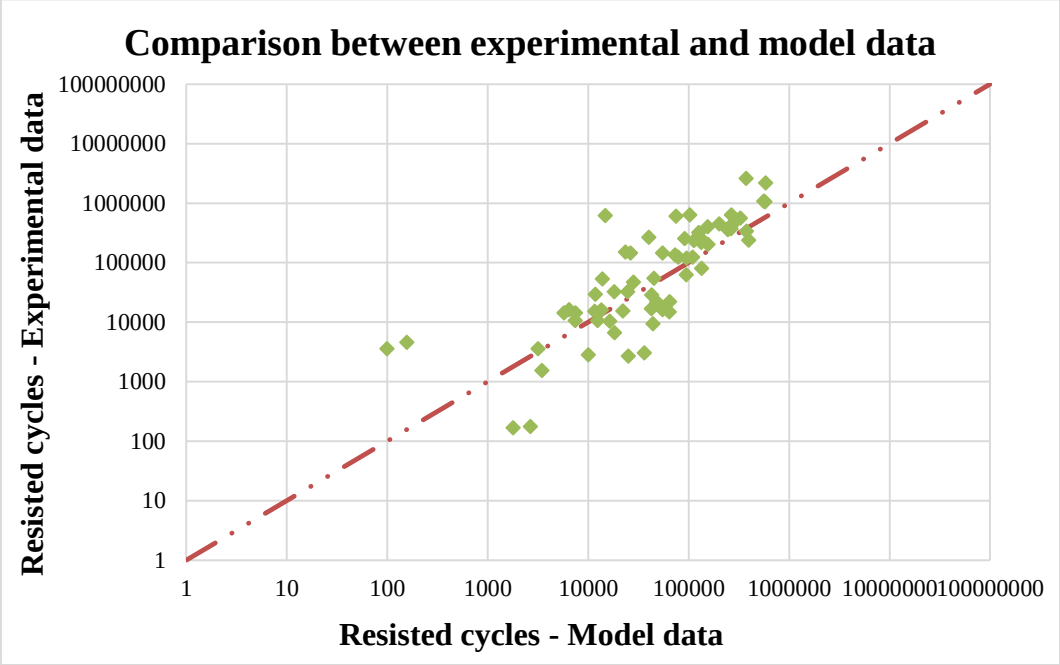

Figure V-18. Fatigue validation for corroded specimens

In Figure V-19 experimental and model data is compared. The pitting geometry characteristics upper and lower bound limits defined with the statistical model are also represented. All the tested stress range results were localized between the defined bounds. Very good agreement was observed for the corroded steel fatigue life value estimation.

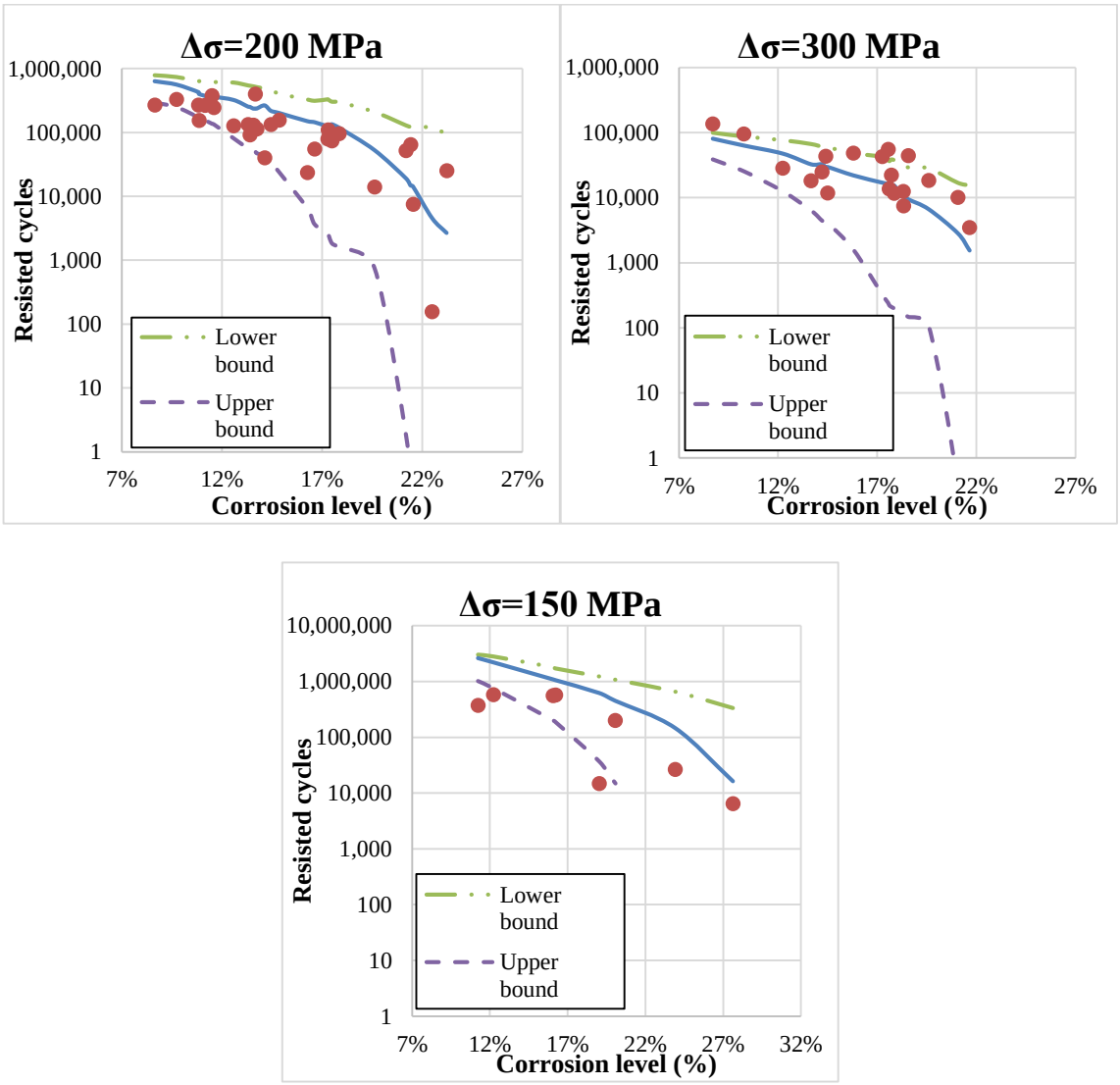

Figure V-19. Fatigue validation. Model curves and experimental for the testes stress range

V.2.6.2 Monotonic validation

Four different sets of experimental data were taken for the corroded steel tensile properties validation. Set one consisted of 25 specimens which include a wide range of corroded specimens from very little corrosion levels about 2% up to very high corrosion levels 60%. The second set of bars encompassed 23 specimens covering a closer range of corrosion levels

from 3% up to 16% [19]. The third set of specimens included 21 specimens also covering a full range of corrosion levels from 1% to 50% [18]. Finally the most extended database of specimens, which includes 54 specimens with two different bar diameter, ϕ10 mm and ϕ12 mm, and covering corrosions levels from 7% up to 25% [16]. The results of the model validations are presented in Figure V-20, Figure V-21, Figure V-22 and Figure V-23, in which are shown the experimental fy or fmax compared to the model results, which include the upper and lower bounds.

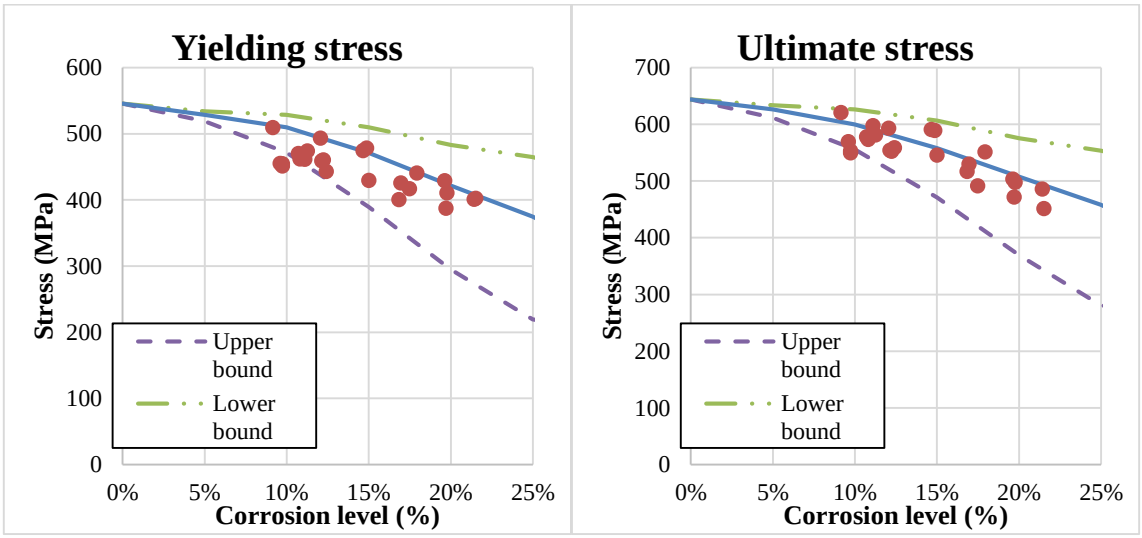

Figure V-20. Monotonic validation. Fernandez et al. test [16]

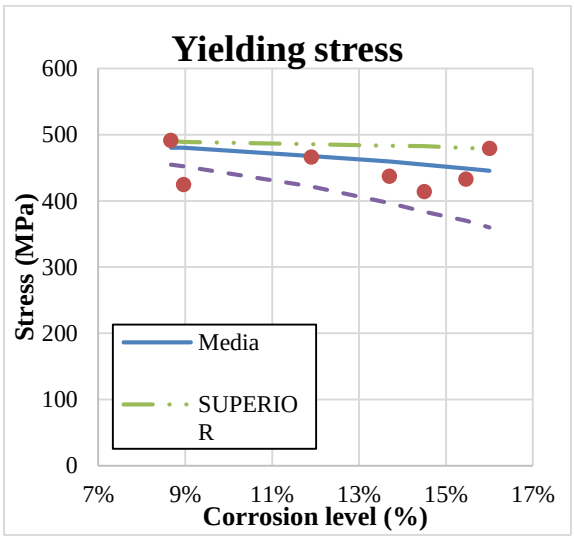

Figure V-21. Monotonic validation. Apostolopoulos et al. test [19]

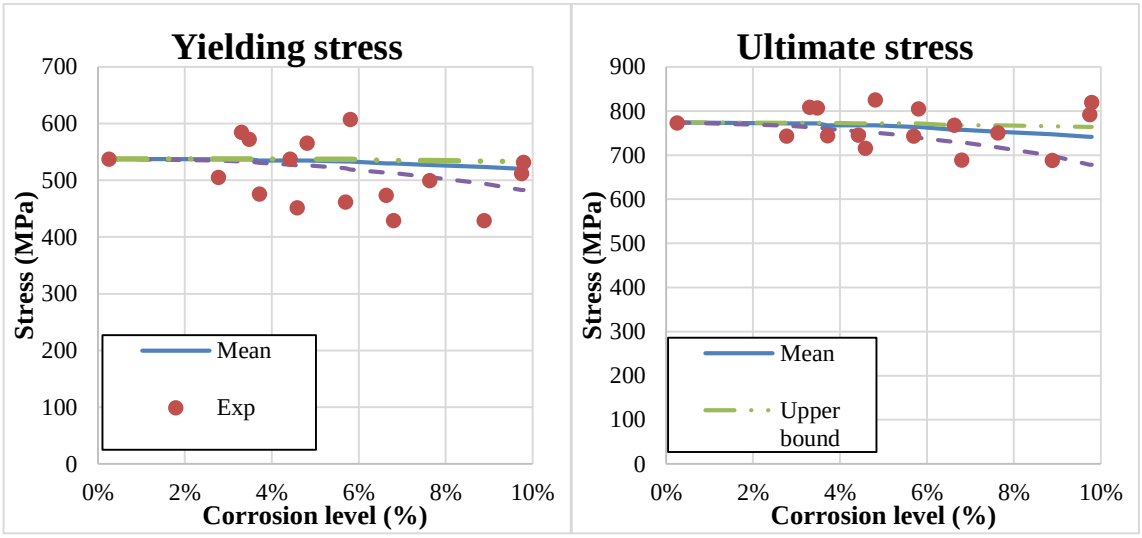

Figure V-22. Monotonic validation. Apostolopoulos et al. test [19]

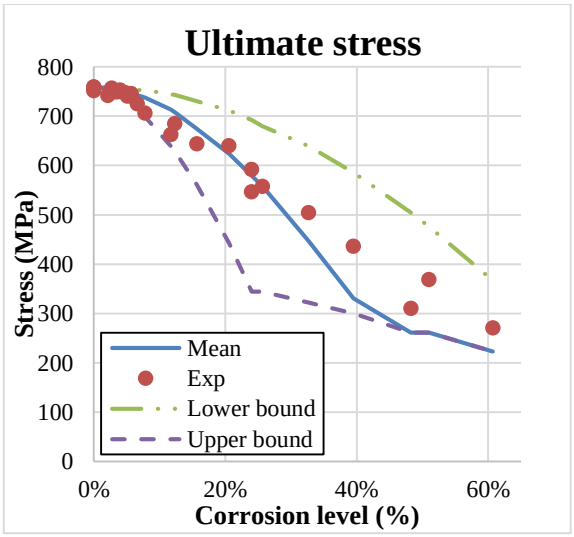

Figure V-23. Monotonic validation. Abdullah A. et al. test [18]

Very good agreement between experimental and numerical data was observed for yielding stress and ultimate stress. Almost all the experimental data were localized in between the confident bounds defined with the presented statistical model. However, modulus of elasticity and maximum strain estimations were not as accuracy as yielding stress and ultimate stress ones. It is necessary to underline that the elastic modulus was obtained directly from the monotonic test not using the code recommendations for this parameter; hence it could present some dispersion. Regarding maximum strain it is subjected to other phenomena such as fracture mechanics due to pits in the cross-section.

V.2.7 Conclusions

A mechanical model to evaluate the effect of steel reinforcement corrosion on σ-ε and fatigue behaviour has been extended and presented. Corrosion phenomena has been implemented by means of an idealized pitted cross-section.

The main conclusions of the presented work are described in the next points:

(1) The experimental study shows a non-uniform distribution of the material properties throughout the steel cross-section. An increasing strength of the outer layers is observed, where the outer martensitic layer achieved up to 806 MPa yielding stress. The inner ferrite core achieved up to 435 MPa yielding stress. The effect of material properties distribution is stated as relevant during a corrosion episode.

(2) The model calibration allows describing by means of the statistically model presented the pitting geometry characteristics regarding the corrosion level. The upper and lower bound limits of the pitting geoetry characteristics can be defined guarantying that the calculated properties will be inside those bounds with a 90% of confident.

(3) The mechanical model can describe the tensile steel reinforcement material properties with a range of 0% and 60% corrosion levels with an excellent agreement for yielding stress and ultimate stress. Elastic modulus and ductility showed more dispersion likely because of the dispersion of these parameters themselves. More detailed study is needed to better calibrate the model response for those values.

(4) The mechanical model can describe the fatigue behaviour under corrosion phenomenon with very good agreement with the experimental data. The characteristic fatigue curves with respect to the corrosion level can be defined.

In conclusion, the model leads to a good mechanical properties description for corroded and uncorroded bars, necessary properties to carry out with enough accuracy analysis and assessment of safety, serviceability and durability of deteriorated reinforced concrete structures.

Acknowledgments

The presented research was partially funded by the Ministry of Science and Innovation of the Government of Spain (MINECO) providing funds for the project BIA2009-11764. The authors also thank Infrastructures de Catalunya SAE by the economic support provided.

References

[1] L. Bertolini, B. Elsener, P. Pedeferri, R. Polder, Corrosion of Steel in Concrete. Prevention, Diagnosis, Repair., Wiley-VCH Verlag GmbH & Co. KGaA, Weinheim, Germany, 2004.

[2] K. Tutti, Corrosion of steel in concrete, (1997) 6–15. doi:10.4324/9780203414606_chapter_2.

[3] J. Broomfield, Corrosion of steel in concrete: understanding, investigation and repair, 2nd Ed., Taylor & Francis, Abingdon, United Kingdom, 2002.

[4] M. Raupach, B. Elsener, R. Polder, J. Mietz, Corrosion of reinforcement in concrete, Woodhead Publishing Limited, 2007. doi:10.1533/9781845692285.

[5] W. Zhang, X. Song, X. Gu, S. Li, Tensile and fatigue behavior of corroded rebars, Constr. Build. Mater. 34 (2012) 409–417. doi:10.1016/j.conbuildmat.2012.02.071.

[6] C.A. Apostolopoulos, Mechanical behavior of corroded reinforcing steel bars S500s tempcore under low cycle fatigue, Constr. Build. Mater. 21 (2007) 1447–1456. doi:10.1016/j.conbuildmat.2006.07.008.

[7] C.A. Apostolopoulos, M.P. Papadopoulos, S.G. Pantelakis, Tensile behavior of corroded reinforcing steel bars BSt 500s, Constr. Build. Mater. 20 (2006) 782–789. doi:10.1016/j.conbuildmat.2005.01.065.

[8] C. a. Apostolopoulos, V.G. Papadakis, Consequences of steel corrosion on the ductility properties of reinforcement bar, Constr. Build. Mater. 22 (2008) 2316–2324. doi:10.1016/j.conbuildmat.2007.10.006.

[9] H. Çetinel, M. Toparlı, L. Özsoyeller, A finite element based prediction of the microstructural evolution of steels subjected to the Tempcore process, Mech. Mater. 32 (2000) 339–347. doi:10.1016/S0167-6636(00)00009-0.

[10] I. Sankar, K. Rao, A. Gopalakrishna, Optimization of steel bars subjected to Tempcore process using regression analysis and harmony search algorithm, J Sci Ind Res. 69 (2010) 266–270. http://nopr.niscair.res.in/handle/123456789/7713 (accessed July 10, 2014).

[11] J. Nikolaou, G.. Papadimitriou, Microstructures and mechanical properties after heating of reinforcing 500 MPa class weldable steels produced by various processes (Tempcore, microalloyed with vanadium and work-hardened), Constr. Build. Mater. 18 (2004) 243–254. doi:10.1016/j.conbuildmat.2004.01.001.

[12] P. Simon, M. Economopoulos, P. Nilles, Tempcore: a new process for the production of high quality reinforcing bars, Iron Steel Eng. 61 (198AD) 55–67.

[13] J.M. Bairan, a. R. Marí, H. Ortega, J.C. Rosa, Efecto del enrollado y enderezado en las propiedades mecánicas de barras de acero de diámetro medio y grande fabricadas en rollo, Mater. Construcción. 61 (2011) 559–581. doi:10.3989/mc.2011.60110.

[14] A.G. Palmgren, Die Lebensdauer von Kugellagern (life length of roller bearings), VDI Z. 68 (1924) 339–341.

[15] M.A. Miner, Cumulative damage in fatigue, J. Appl. Mech. 12 (1945) A159–A164.

[16] I. Fernandez, J. Bairán M., A. Marí R., Corrosion effects on the mechanical properties of reinforcing steel bars. Fatigue and σ-ε behaviour, Constr. Build. Mater. (2015).

[17] S.L.W.Z.X.G.C. Zhu, Fatigue of Reinforcing Steel Bars Subjected to Natural Corrosion, Open Civ. Eng. J. (2011) Vol.5, p69. http://connection.ebscohost.com/c/articles/70458995/fatigue-reinforcing-steel-bars-subjected-natural-corrosion (accessed February 14, 2015).

[18] A. a. Almusallam, Effect of degree of corrosion on the properties of reinforcing steel bars, Constr. Build. Mater. 15 (2001) 361–368. doi:10.1016/S0950-0618(01)00009-5.

[19] C.A. Apostolopoulos, V.G. Papadakis, Consequences of steel corrosion on the ductility properties of reinforcement bar, Constr. Build. Mater. 22 (2008) 2316–2324. doi:10.1016/j.conbuildmat.2007.10.006.

[20] UNE-EN-ISO-15630-01, Acero para el armado y pretensado del hormigón - Métodos de ensayo. Parte 1: Barras, Alambre y Alambrón para el hormigón armado, (n.d.).

[21] A. Borruto, Meccanica della frattura, Milan, 2002.

[22] TNO Diana. Finite Element Analysis User's Manual - release 9.6.6: TNO, 2015.

[23] C.I.C. for N.M. in Engineering, GID. The personal pre and post processor, (2014).

[24] I. Fernandez, J. M. Birán, A. R. Marí, Mechanical model to evaluate steel reinforcement corrosion effects on σ-ε and fatigue curves. Experimental calibration and validation, (n.d.).

V.3 3D scan technique applied to corroded steel bars tested under cycling or monotonic loads. 3D solid model and crittical cross-section verification

Ignasi Fernandez*[1], Jesús Miguel Bairán[1], Antonio R. Marí[1]

[1] Department of Construction Engineering, Polytechnic University of Catalonia, Jordi Girona, 1-3, Barcelona 08034, Spain.

*corresponding author: ignasi.fernandez-perez@upc.edu

Highlights:

- 3D scan technique applied to corroded steel reinforcement bars.
- Study of corroded steel mechanical properties. Fatigue and σ-ε behaviour
- Pitting characterization in the critical cross-section.
- 3D model development from 3D scan surface bar

Keywords: Corrosion, Tensile properties, Mechanical properties, Fatigue, Durability

V.3.1 Introduction

Deteriorated structures can describe unexpected response under design loads. The steel susceptibility to being corroded beneath numerous conditions and the structural corrosion effects in local or global perspectives have been widely studied by many researchers [1–8]. Corrosion of steel reinforcement could be described by a large number of pits distributed along the steel bar. Either generalised or pitting corrosion could be understood in this way [9–11]. Pitting on the steel surface produce different local effects, which take into no uniform stress distribution throughout the cross-section, due to stress localization at the pit tip and centre of gravity displacement, for instance. Hence, what in first instance may be a uniaxial load, may turn into a multiaxial stress states in the surrounding of the pits. The study of corrosion in such a local ways could be interesting to go in depth in the corrosion phenomenon and its effects on the steel bar. Exploration of new techniques, which allow opening new possibilities to study the corrosion effects and its consequences on the bar from a local perspective are necessary. Hence, techniques such as a 3D scan of corroded steel bars are presented as powerful tools to study the aforementioned phenomena. With the application of this method, it is possible to analyse the local effects of steel corrosion produced by the bar. 3D scan, which is widely used in other fields such as industrial engineering, has not been commonly used in civil engineering. Since 3D scan is a relative new technique and even more when it is applied to deteriorated structures and the different structural elements, a scarce number of studies involving 3D scan and its applications are found in the literature [9]. These studies are mainly focused on the pit characterization of corroded steel members using the cross-section definition and the pit distribution along the corroded member. The use of this technique open a broad range of possibilities, a statistical analysis of the pitting distribution, a 3D solid model of the whole bar studying effects such as stress concentration, multiaxial stress behaviour or non-homogeneous material distribution, or the analysis of the critical cross-section and the pitting geometry, for instance.

In this study, a 3D scanning technique applied to corroded steel bars is presented. A complete high-resolution description of the outer surface from different corroded specimens was obtained. The study encompassed 14 bars, which were scanned and afterwards subjected to cyclic or monotonic loads until failure. Two different works were done from the obtained 3D scan result.

The first part consisted in the 3D model development of the scanned specimens, with the underlying purpose to reproduce the test condition and thereafter perform a comparison with

the experimental data. To pursue this goal, DIANA [22]finite element software combined with the pre and post processor GiD [23]developed at CIMNE were used. The direct tensile and cyclic load test were both reproduced with DIANA. Additionally a fatigue model to identify the damage level of each element after every cycle was developed by means of an external subroutine, which made possible removing the elements from the model for the next steps whether they were broken.

In the second part of the work, the experimental results obtained and the results achieved with the model developed by Fernandez et al. [11] were compared aiming to validate some made hypothesis to obtain the mechanical properties of corroded steel bars. This work consisted in the critical cross-section extraction from the scanned bars, previously identified in the monotonic tests. The FE discretization of the extracted cross-section using the pre and post processor GiD was performed. The meshes were introduced into the aforementioned model to obtain the corroded σ-ε curves and afterwards compared the idealized pitted cross-section σ-ε curves.

V.3.2 3D scan

V.3.2.1 Members extraction, cleaning and preparation

The specimens presented next are part of a larger experimental campaign , conducted at the Universitat Politècnica de Catalunya – Barcelona Tech (UPC), which encompassed a large amount of tensile and fatigue test of corroded and uncorroded reinforcing steel specimens [10].

Figure V-24. Statically-undetermined beams. Cleaned specimens

Steel bars were extracted from beams exposed to different corrosion levels through induced corrosion procedure [12–14]. The beams were casted incorporating in the mixture 4% NaCl in cement weight, breaking the steel passive protective layer. A particular current density was applied to assure the desired corrosion level. This was done through a DC power supply with an ammeter to monitor and fix the current intensity. The current direction was defined fixing the reinforcing steel as anode and the stainless steel bar as the cathode. Each beam had two different bar diameters (10 mm and 12 mm). Monotonic load tests were carried out in the continuous beams. Finally, bars were carefully extracted from the non-critical section of the beams to perform the characterization of the corroded bars under monotonic and fatigue loads.

Using gravimetric methods, the loss in weight of the specimens was determined according the ASTM code. A pressure sand cleaning method was applied to remove both rust and bonded cement, Figure V-24. In total 14 specimens were used for scanning purposes covering corrosion rates from 9% to 22% for 12 mm diameter bars, see Table V-3.

Table V-3. Specimen description, name and corrosion level

Tensile specimens	Corrosion level (%)	Fatigue Specimens	Corrosion level (%)
BN-01	9	BN-02	10
V2-B12-03	11	BN-04	12
V2-B12-24	15	V2-B12-06	11
V3-B12-01	22	V3-B12-09	14
V7-B12-21	10	V3-B12-16	10
V7-B12-24	21	V3-B12-24	15
-	-	V3-B12-03	17
-	-	V3-B12-05	17

V.3.2.2 3D scan results

A very fine mesh of triangular surface elements connected by nodes was resulted from the 3D scan. The average size of the element was 0.005 mm2. The numbers of triangular elements in each scanning were between 700,000 and 1,100,000 elements, depending on the member length. The average specimen length was 320 mm. Figure V-25 shows some specimens representing different corrosion levels as well as an uncorroded specimen. The high resolution of the surface mesh permits to define with a very great detail the pitting dimension, i.e., pitting depth and pitting length, which are the crucial parameters to describe the behaviour of corroded steel bars.

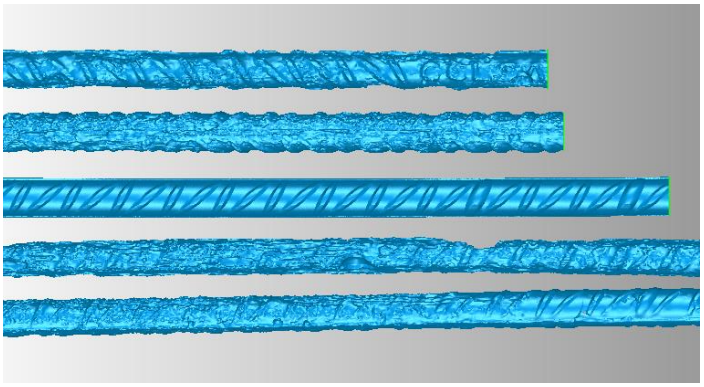

Figure V-25. Scanned specimens are representing different corrosion levels and uncorroded specimen (in the middle).

Figure V-26 depicted the critical pitting of one of the scanned bars. The characterization and assessment of the pitting geometry representing the pitting length, pitting depth, as well as the remaining cross-section were performed.

On the other hand, by substraction of the correded specimen from the reference uncorreded bars, it was possible to define the exact corrosion level, as reported in Table V-3.

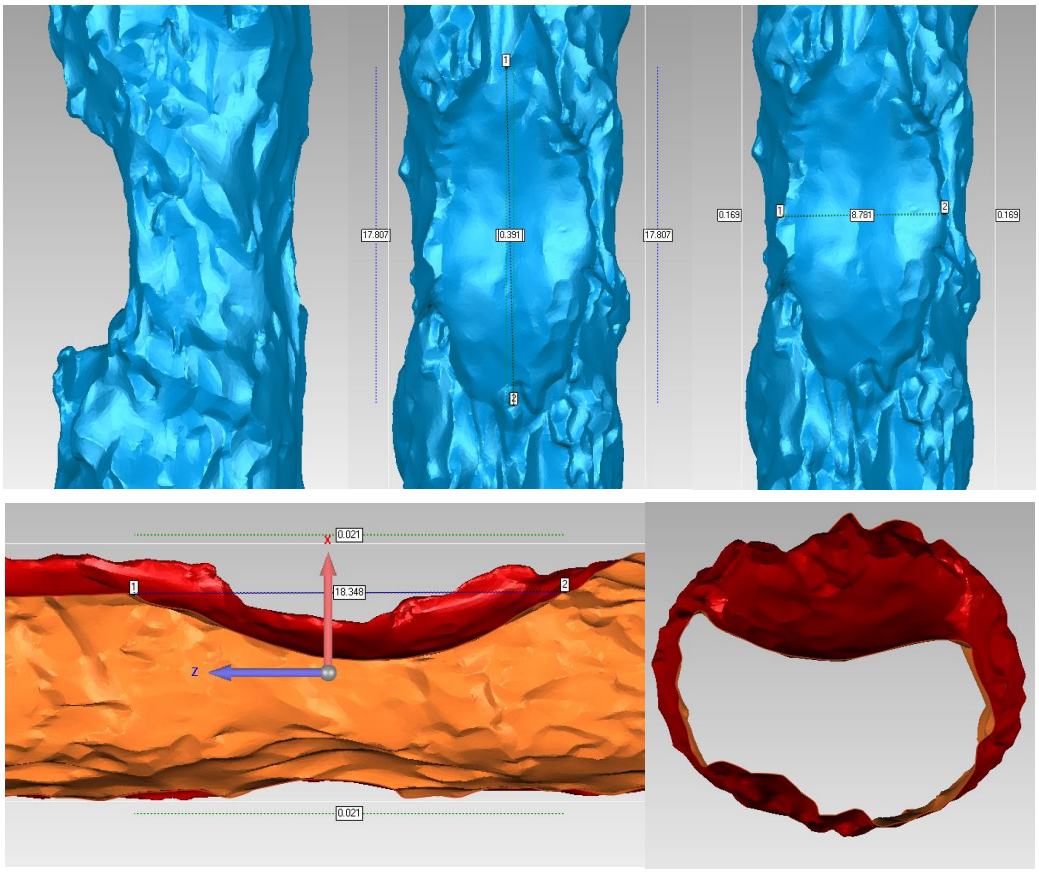

Figure V-26. Critical cross-section definition

V.3.3 Cyclic load and tensile tests

V.3.3.1 Test setup and execution

The presented test were part of a larger experimental study presented by Fernandez et al. [10] and focuses on direct monotonic and cyclic tests of the corroded reinforcement bars extracted from the above mentioned beams and previously scanned with the novel 3D scan technique, see Table V-1.

V.3.3.1.1 Monotonic test

The tests were carried out following the code recommendations [15] and an INSTRON 8803 Universal Testing machine.

The tested free length was for all the specimens 170 mm letting 70/75 mm length for each clamp. Monotonic tests were conducted using displacement control. Total displacement, as well as deformation, were registered too. The test was carried out until specimen failure. Fernandez et al. [10] describe further details.

V.3.3.1.2 Fatigue test

The tested free length was the same as tensile conducted tensile test. Fatigue test was conducted using load control instead displacement control.

Stress levels to apply in the fatigue tests were defined in terms of the uncorroded bar, in order to have an objective reference. One stress range was defined for fatigue tests, 200 MPa (ΔS=Smax – Smin). A non-zero minimum stress was used to avoid compression in the bar and its possible buckling effects. The maximum stress (Smax) was for uncorroded specimens lower than $0.6*f_{ym}$, which is the theoretical threshold for which there is no influence on the fatigue life due to the maximum stress. It should be pointed out that, as the maximum stress of $0.6*f_{ym}$ is referred to the uncorroded section, and because of local concentration of stresses, maximum stresses in some points of the corroded bars are likely to exceed $0.6*f_{ym}$.

The applied load range for corroded specimens was the same as for uncorroded samples, taking into account the uncorroded nominal diameter, see Equation V-5.

Equation V-5 $$\Delta S = S_{max} - S_{min} = \frac{F_{max}}{A_0} - \frac{F_{min}}{A_0}$$

The load was applied in same wave shape cycles of 15 Hz frequency. Eight specimens were tested with a range of corrosion levels between 8% and 24%. Fernandez et al. [10] describe further details.

V.3.3.2 Test results

V.3.3.2.1 Monotonic test

Figure V-27 described the σ-ε behaviour of the different tested corroded members. All the mechanical properties were affected by corrosion. A significant reduction of the yielding stress, as well as ultimate stress, was observed.

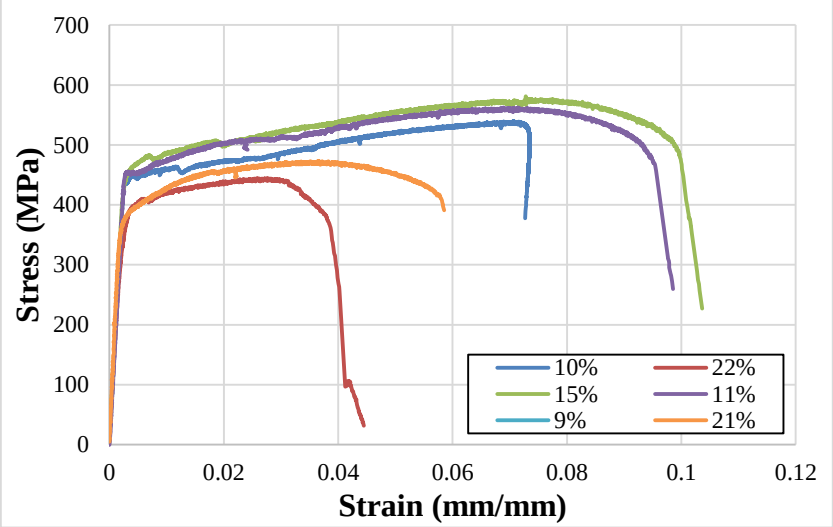

Figure V-27. σ-ε behaviour corroded specimens.

V.3.3.2.2 Fatigue test results

In Table V-4 are described the results of the performed fatigue tests. In the table are possible to see the fatigue life value and the corrosion level of the eight satisfactory tests carried out.

Table V-4. Fatigue results

Fatigue Specimens	Δσ (MPa)	Cycles resisted	Corrosion level (%)
BN-02	200	325922	10
BN-04	200	374083	12
V2-B12-06	200	267542	11
V3-B12-09	200	132905	14
V3-B12-16	200	325956	10
V3-B12-24	200	99365	15
V9-B12-03	200	887	17
V9-B12-05	200	156	17

V.3.4 3D model development from the 3D scan results

The 3D model development was based on the transformation of the triangular outer surface mesh into a solid tetrahedral element mesh. To proceed with the conversion, a data post-processing of the initial mesh was performed. First, the number of surface elements was reduced. Hence, to avoid spikes in the pits and badly shaped elements a surface smoothing was performed, by using nurb surfaces. A remeshing was done to satisfy the requirements aforementioned with the most rigour and respect to the initial geometrical bar description.

After the remeshing procedure, a suitable surface element mesh (acceptable number and shape of elements) to be transformed to a solid tetrahedral mesh could be obtained.

V.3.4.1 FE model development

A 3D nonlinear FE model of the presented bars was developed. The model aims to identify and assess the local effects produced by steel corrosion of reinforcing with the help of a local and detailed analysis. The 3D study of the bar permitted to understand and identify the corrosion local phenomena produced into the bar. In addition, the non-uniform material distribution throughout the cross-section was implemented using a previous work presented by Fernandez et al. [11]. Hence, the effect non-uniform mechanical properties due to TEMPCORE® production systems was included. The model validation was done using the experimental results of the same specimens.

V.3.4.2 Load and boundary conditions

The boundary conditions were defined to reproduce exactly the aforementioned test. One side of the bar was modelled using a fixed constrain. The other bar side was left unfixed, and the load was directly applied onto this face by means of displacement control or load control, depending the simulation type. Load steps were used for fatigue simulations whereas displacement control was defined for tensile tests. Figure V-28 describes the model scheme with the above mentioned constrains and the applied load/displacement point.

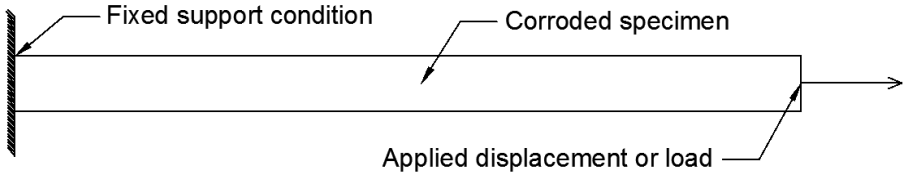

Figure V-28. 3D model scheme

V.3.4.3 Element types and material definition

3D tetrahedral elements (TE12L) were used for the steel bar definition. The bar was discretized with a significant number of 4 node tetrahedral elements. The models had an average of 800,000 elements. Two details of the latter meshes are shown in Figure V-31 and Figure V-32.

The material properties of the steel elements were defined according the experimental study presented by Fernandez et al. [11]. An experimental study was performed to identify and characterization the material properties of 12 mm diameter TEMPOCRE® produced bars. This work defined the material data in concentric martensitic layers and an inner ferrite core according to the Figure V-29.

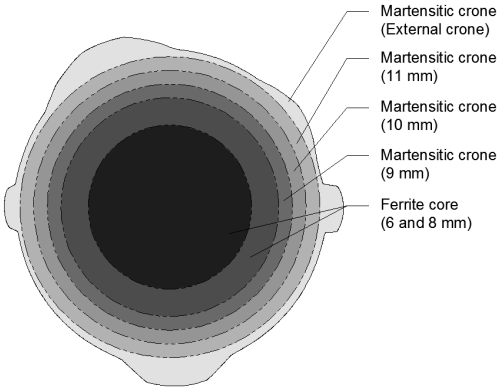

Figure V-29. Ferrite inner core and martensitic crown up to whole bar (typical TEMPCORE® production system non-uniform material distribution)

The final yielding and ultimate stresses values for the different layers are shown in Table V-5.

Table V-5. Real elastic limits and ultimate strength (MPa) obtained after post-processing test data

Specimens (ϕ12)	External radius (mm)	fy (MPa)	fu (MPa)
Ferrite core	4	435	575
Crone 1	4.25	522	601
Crone 2	4.5	583	642
Crone 3	4.75	655	682
Crone 4	5	705	718
Crone 5	5.25	749	757
Crone 6	5.5	783	789
Crone 7	5.75	806	824
Outer crone	6	806	824

The final material distribution throughout the cross-section is defined in Figure V-30, where are represented the σ-ε curves for each crown and the inner ferrite core. Fernandez et al. [11] describe further details of the material distribution and the test performed to obtain them.

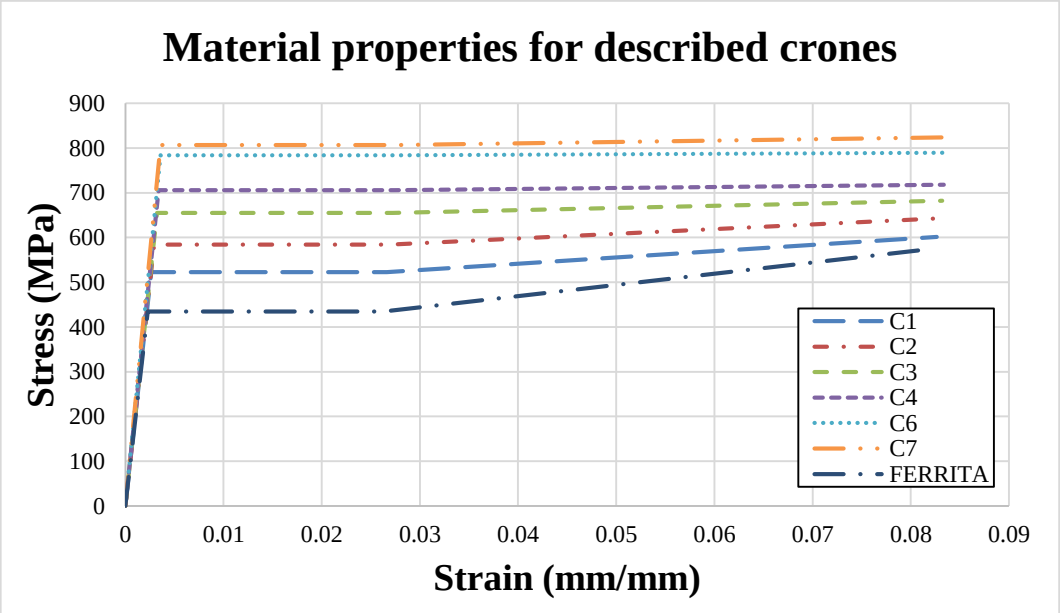

Figure V-30. Obtained stress profile from the tested bars

An independent subroutine to assign the 3D model element material properties was developed, which took the different element nodes coordinates and calculated the 3D tetrahedral element centre. According to the element centre distance with respect to the neutral axis of the bar, the material data, following Figure V-29 distribution, was assigned. A typical material data distribution are shown in Figure V-31, for a corroded specimen, and Figure V-32, for an uncorroded specimen.

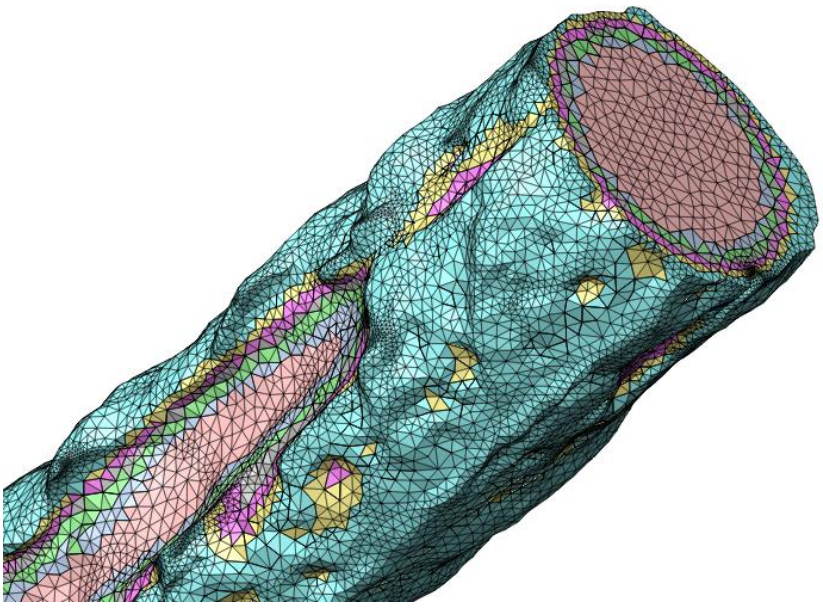

Figure V-31. Material data distribution corroded specimen

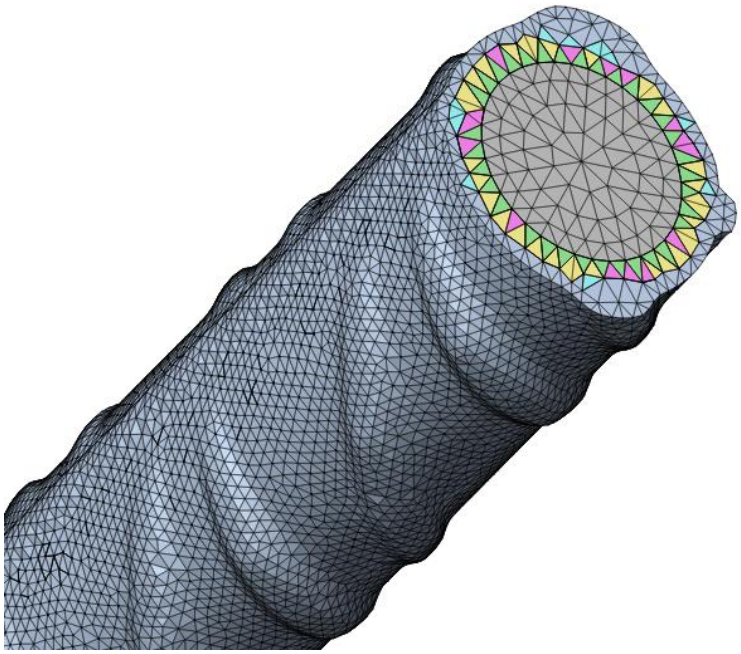

Figure V-32. Material data distribution uncorroded specimen

The incorporation of the non-homogeneous material distribution data described the TEMPCORE® material distribution effects in the developed 3D model.

V.3.4.4 Result comparison

A comparison between the model and the experimental data for both fatigue and tensile tests was done.

V.3.4.4.1 Fatigue test results

Fatigue model development

DIANA software package allows for fatigue analysis only on linear elastic regime. However, since the corrosion procedure reduced the steel cross-section using pitting distribution, non-uniform stress distribution throughout the cross-section, including possible local yielding, was expected. Hence, non-linear analysis to correctly assess the fatigue life of corroded members was necessary. That motivated an external fatigue life model development by which the corroded and uncorroded fatigue life analysis using the described non-linear 3D FE model with DIANA was possible. The model was capable to assess the fatigue life of every single element taking into account different considerations. According to the applied load, the stress range of the element by the maximum and the minimum stresses identification, obtained using non-linear DIANA analysis, was considered. From those values, the mean stress value was determined. In addition, an average stress modifying

factor was also calculated to examine the maximum stress and stress range effects [16,17]. That factor allowed to use the same reference fatigue curves indistinctly the mean stress and stress range values were, including element yielding, by modifying the S_{ref} value. The reference fatigue curve are represented in Figure V-33. The main material characteristic values used are described in Table V-6.

Table V-6. Fatigue curve definition

Material properties	
Reference stress	S_{ref}^{*}
Reference cycles number	2000000
Slope p1	5
Slope p2	9
Threshold 1	$0.6*f_u$ MPa
Threshold 2	f_u MPa
Exponent	2

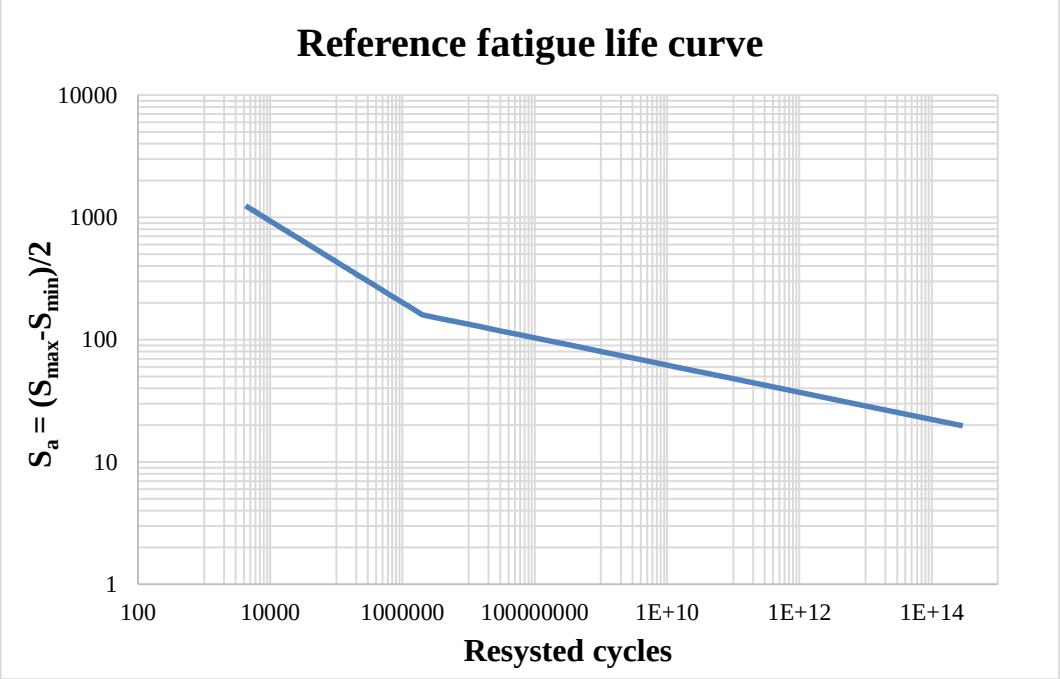

Figure V-33. Reference fatigue curve

In Figure V-34 it is possible to see the flowchart of the developed fatigue model, including all the phases and assessments performed to each element until the fatigue life value is reached.

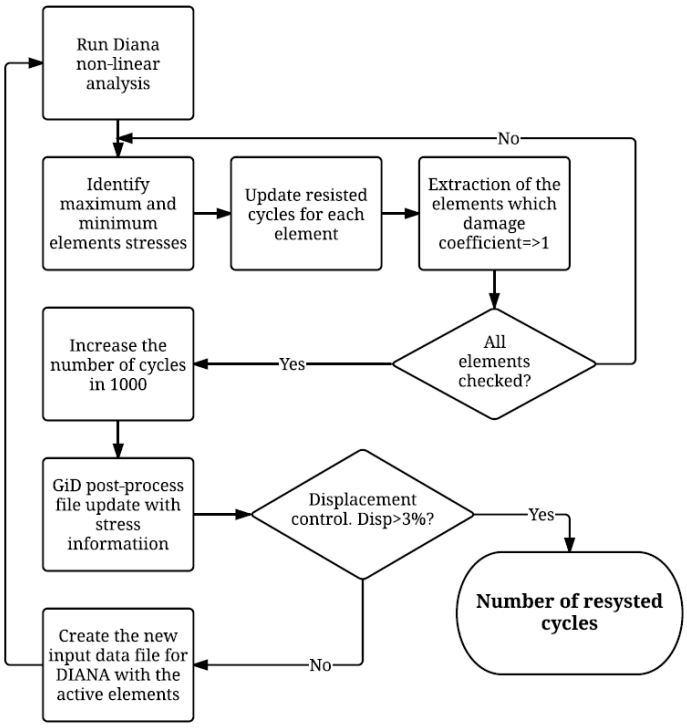

Figure V-34. Flowchart fatigue developed model

Results

Specimen V2-B12-6 is presented as an example of the capabilities of the developed 3D model from the 3D scan bar. This specimen achieved 12% of corrosion level and resisted 245160 cycles.

The numerical results predicted 287322 cycles before failure. Therefore, it is possible to observe that the agreement between experimental results and model results was good. Figure V-35 shows different output data from the 3D model. Surface increment stresses, total deformation, and the number of broken elements are depicted.

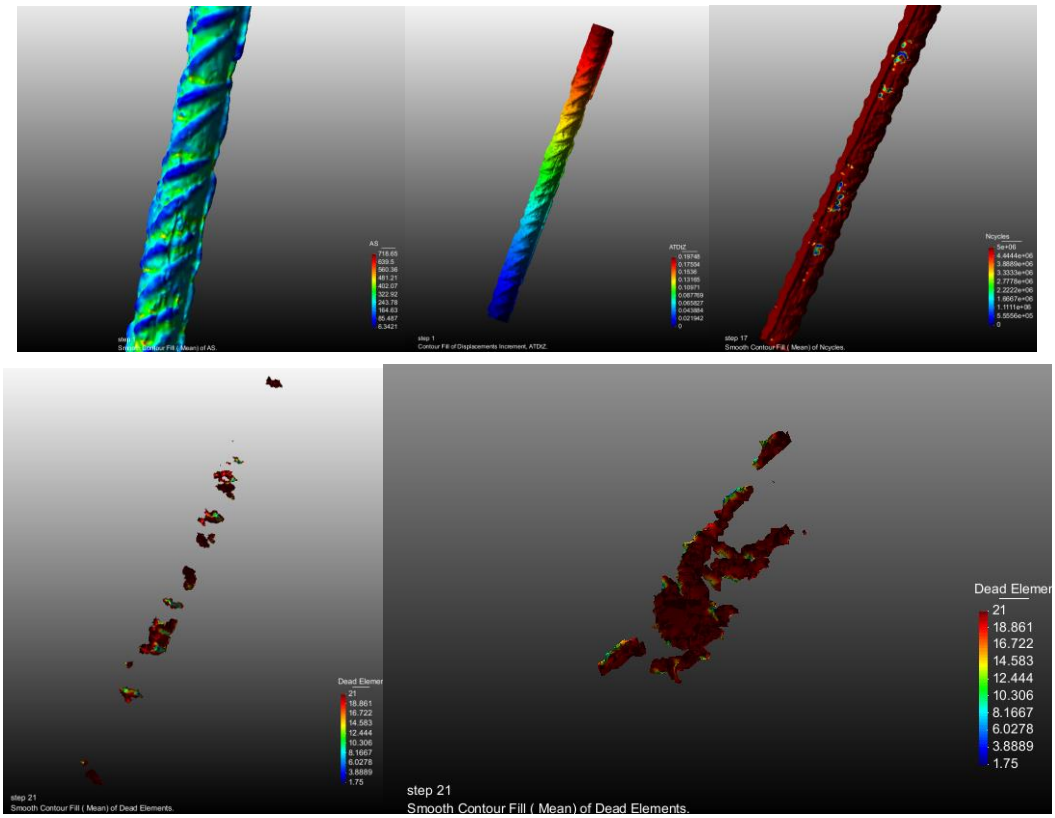

Figure V-35. Top pictures from left to right, stress distribution, total displacement, number of cycles resisted. Bottom figures dead elements whole bar (left), dead element critical cross-section zone (right figure)

The developed model did not present a clear failure cross-section such as the experimental test, but the zone where more elements failed because its fatigue life was reached concentrated in the region coinciding with the failure section in the experimental test. The fatigue failure is produced at microscopic level, hence the reproduction of such phenomenon considering a 3D solid mesh leads to bigger failure zones involving higher number of elements.

V.3.4.4.2 Tensile test results

A comparison between model and experimental results is presented in Figure V-36 and Figure V-37. Figure V-36 shows an uncorroded specimen. Excellent agreement between the uncorroded experimental and presented model data was observed. Both the yielding stress and the ultimate stress were well obtained. The implemented material model described well the hardening behaviour too, up to ultimate stress.

Figure V-37 shows a corroded specimen with 11% corrosion level. The agreement between the experimental and numerical data was also excellent. An overestimation less than 3% for the yielding stress was observed. However, the trend after yielding up to the ultimate load

was practically equal for both, the experimental and the model data. As described before a bilinear with a hardening material model was implemented for the different steel layers, so the softening branch after the ultimate stress level was not considered nor reproduced by the model.

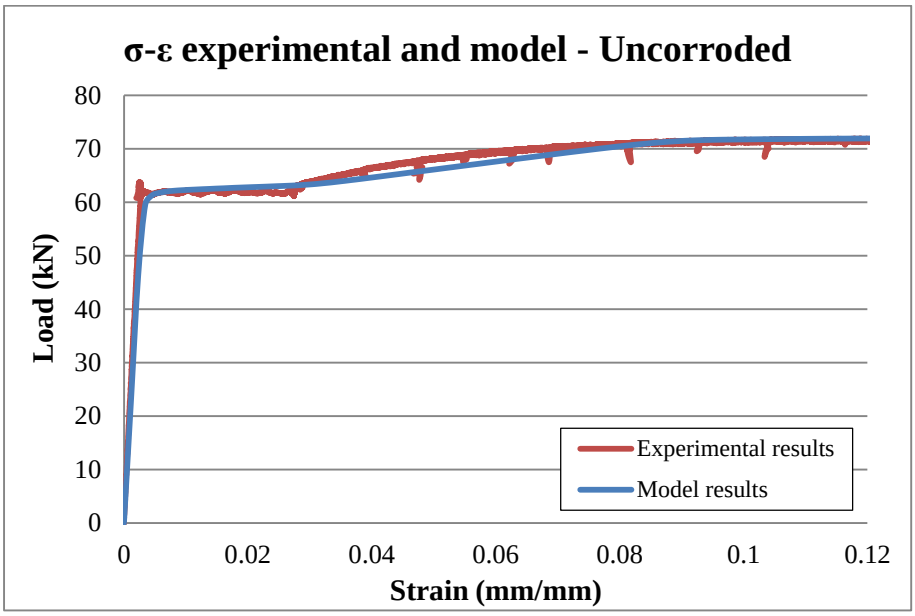

Figure V-36. σ – ε experimental and model results. Uncorroded specimen

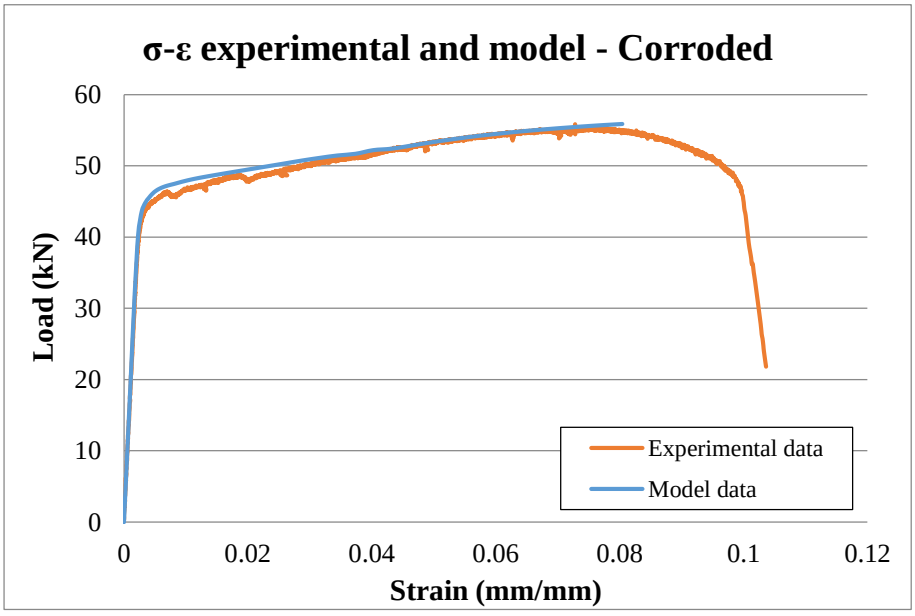

Figure V-37. σ – ε experimental and model results. Corroded specimen

V.3.5 Critical cross-section definition

A validation of the model developed by Fernandez et al. [11] using the 3D scan results was done. This model allowed obtaining the corroded or uncorroded steel mechanical properties. An extensive experimental study, which consisted in the fatigue life and tensile evaluation of corroded steel bars, was used for calibration and validation purposes. A critical cross-section using the pit definition was defined. The pitting depth was directly related to the corrosion level and the corroded diameter. Further a statistical model to describe the pitting depth variation was presented, by which the upper (95%) and lower (5%) bounds were defined. Fernandez et al. [11] describe a detailed explanation of the model.

A comparison between those above idealized critical cross-section and the real critical cross-section obtained from the 3D scan was performed. In addition, the model results were compared with the experimental data using two hypothesis, the idealized cross-section defined by the model, and the real cross-section defined by means of the 3D scan.

V.3.5.1 Real cross-section definition

Using the scanned data was possible to obtain the contour of the critical cross-section before failure. Some of the obtained cross-sections are described in Figure V-38.

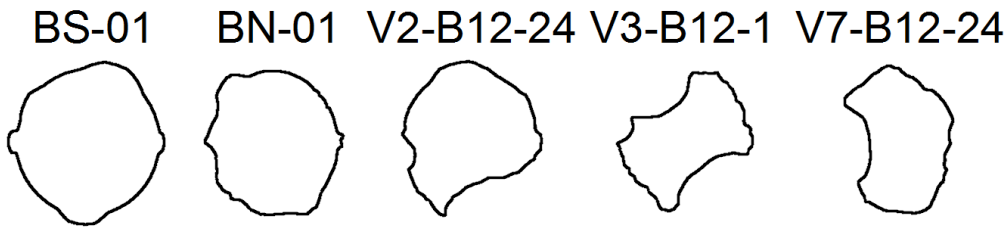

Figure V-38. Cross-section before failure from the scanned data

V.3.5.2 Mesh generation and material definition

The above-mentioned model used an FE mesh to discretise the specific cross-section. The mesh generation was performed using the pre and post processor GiD. Triangular elements were used to define the cross-section. The average number of elements use for its definition was around 5000 elements. The average element size was 0.15 mm. Figure V-39 shows the generated mesh for some of the specimens described in Figure V-38.

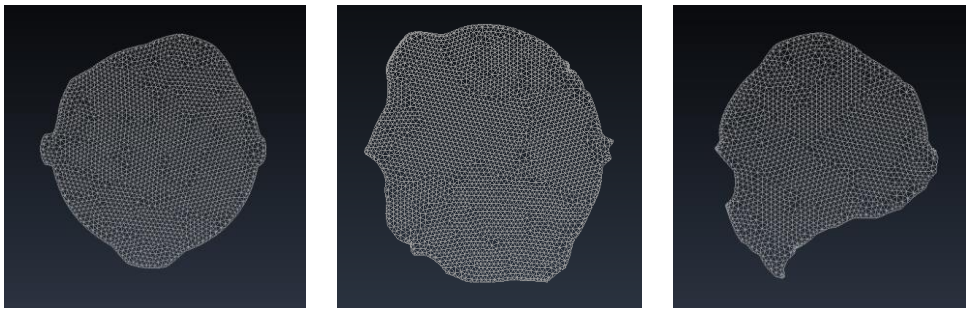

Figure V-39. Mesh generation from the above extracted cross-section

A variation of the material assignation subroutine developed for the presented 3D model was done to define the material data of the described cross-sections. As it was detailed by Fernandez et al. [11] only a bilayer material data were considered; the ferrite inner core and the martensitic external crown, which was defined using an average material properties defined by all the outer crones. Fernandez et al. [11] describe a detailed explanation of the used material model. Figure V-40 depicted different steel cross-sections with the material discretization performed.

V.3.5.3 Pitted cross-section validation

As it is observed in Figure V-40, as more corroded the cross-section was more differences between both hypotheses there was. In all the cases, the real cross-section presented higher steel cross-section reduction than the idealized cross-section. In addition, the analysed model presented all the pitting effect as one pit in the cross-section. Meanwhile, some scanned specimens presented pitting at different points.

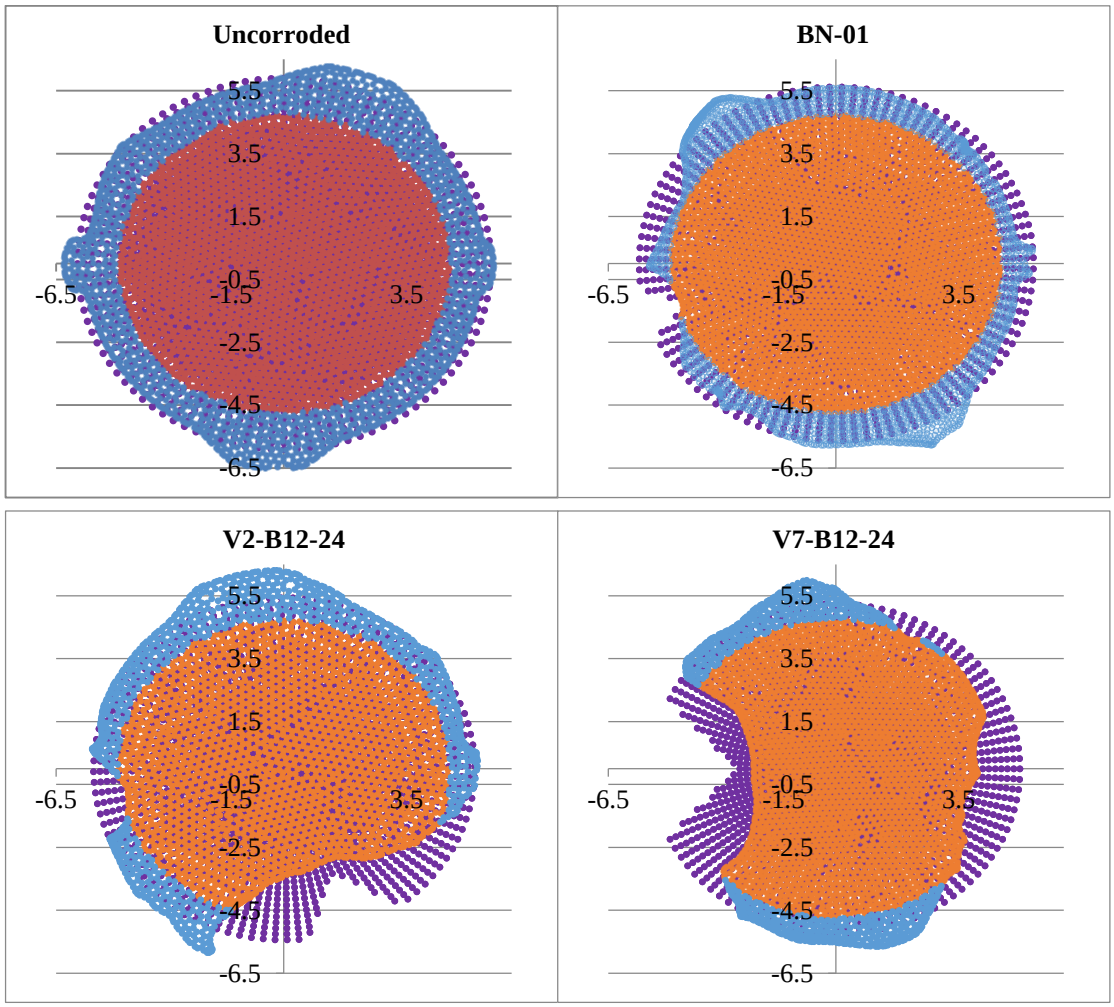

Figure V-40. Real cross-section from 3D scan and cross-section defined by model [24]

V.3.5.4 Results comparison

In the Figure V-41, are described the results for the different cross-section analysed.

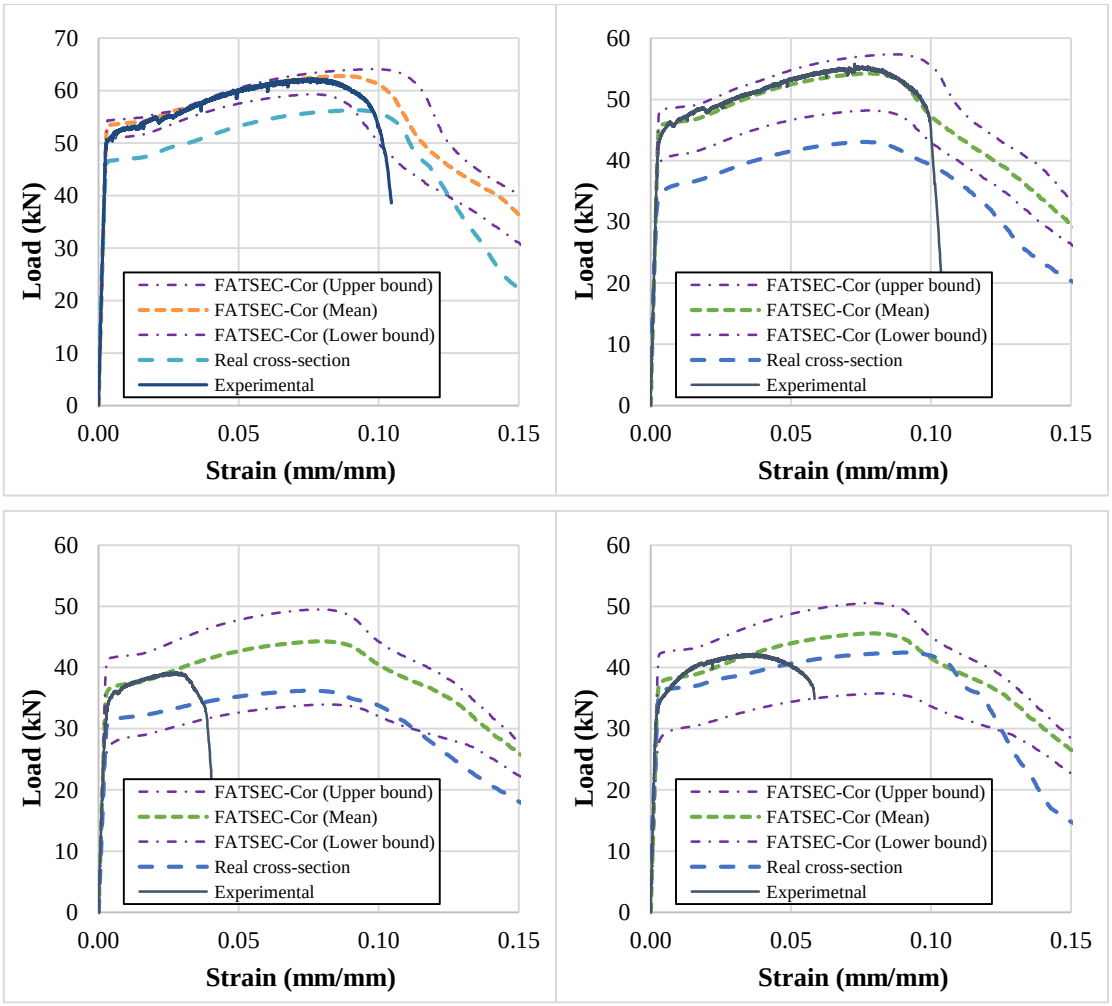

Figure V-41. Result comparison. Fernandez et al. [24] **(Upper, Lower and Mean pitting depth and real cross-section). Experimental results. In order BN-01 specimen, V2-B12-24 specimen, V3-B12-01 and V7-B12-24**

Fernandez et al. [11] model and experimental data adjusted very well. However, the same model applied to the real cross-section from the 3D scan scatter values for both yielding and ultimate stress were shown. As it is described in Figure V-40 the idealized pitted cross-sections always presented a significant increment of the area with respect to the 3D scan cross-sections. The model considered a uniaxial stress-strain state for the cross-section analysis, so other effects such as shear, torsion and multi-axial stress state of the bar are not included. For instance, is possible to obtain stresses in the σ_1 direction higher to the yielding stress provided that stresses in σ_2 and σ_3 direction are different to 0, using Von-Misses yielding criterion Figure V-42. Such phenomena produced that the overall response of the bar was higher than for the real critical cross-section itself analysed by uniaxial σ-ε state.

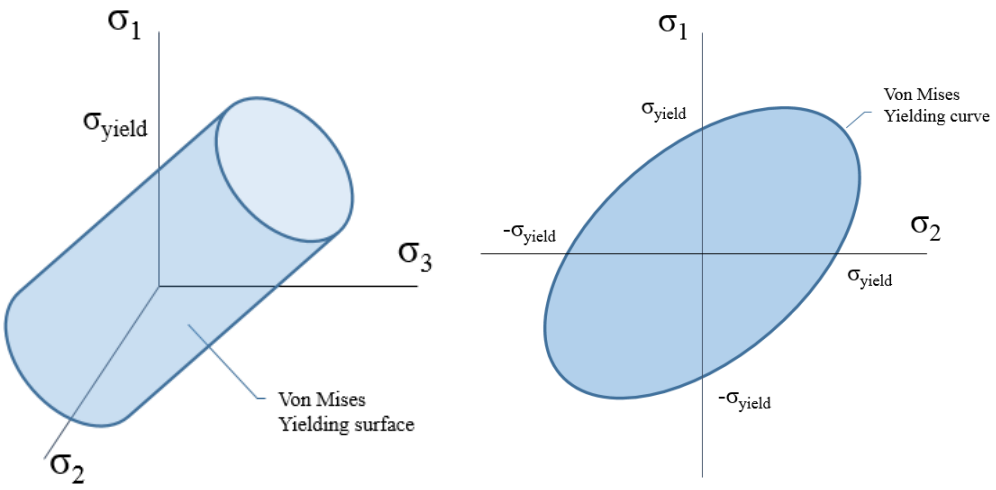

Figure V-42. Von Mises yielding criterion

On the other hand, the average behaviour could be studied using the average cross-section definition in one-half diameter up and down of the critical cross-section, see Figure V-43. Those cross-sections defined 60 mm up and down with respect to the critical one were obtained by means of the 3D scan too.

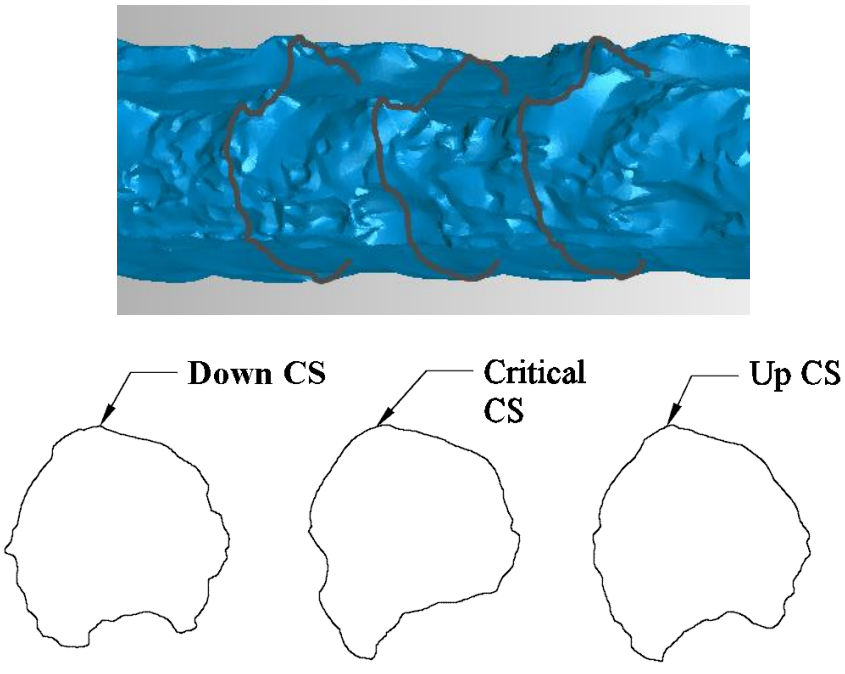

Figure V-43. Real critical cross-section in the middle and cross-section defined into 65 mm up and down from the critical CS

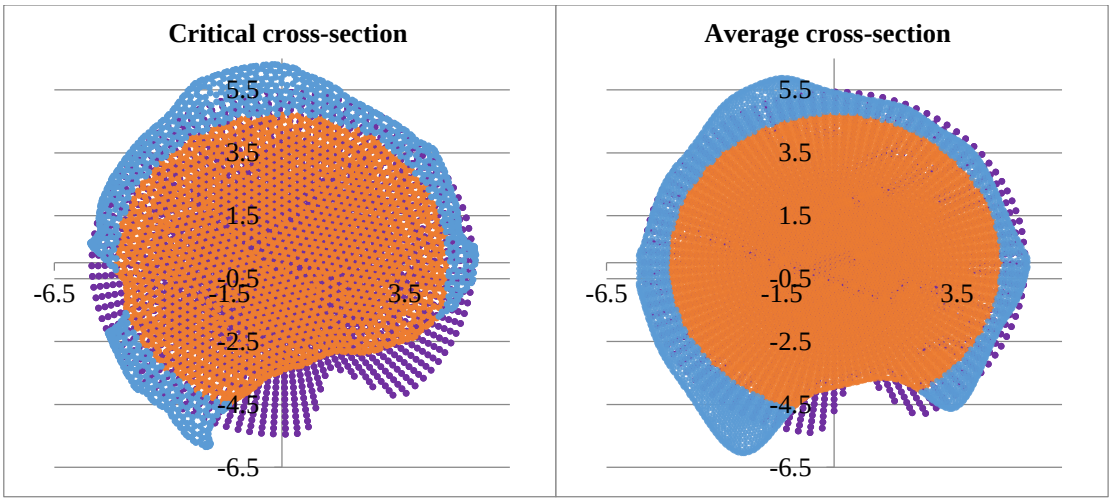

Figure V-44. Real critical cross-section compared to idealized pitted cross-section - Left. Average critical cross-section compared to idealized pitted cross-section – Right

As it described in Figure V-44 the average critical cross-section adjusted much better to the idealized hypothesis, showing similar areas and pitting depth. The numerical result of the average critical cross-section is depicted in Figure V-45. It is observed a very good agreement between the experimental and the developed 3D model presented before. That confirmed the hypothesis, which stated that the corroded steel behaviour describes an average response of the whole bar and it is not possible to study considering only the critical cross-section by means of a uniaxial model.

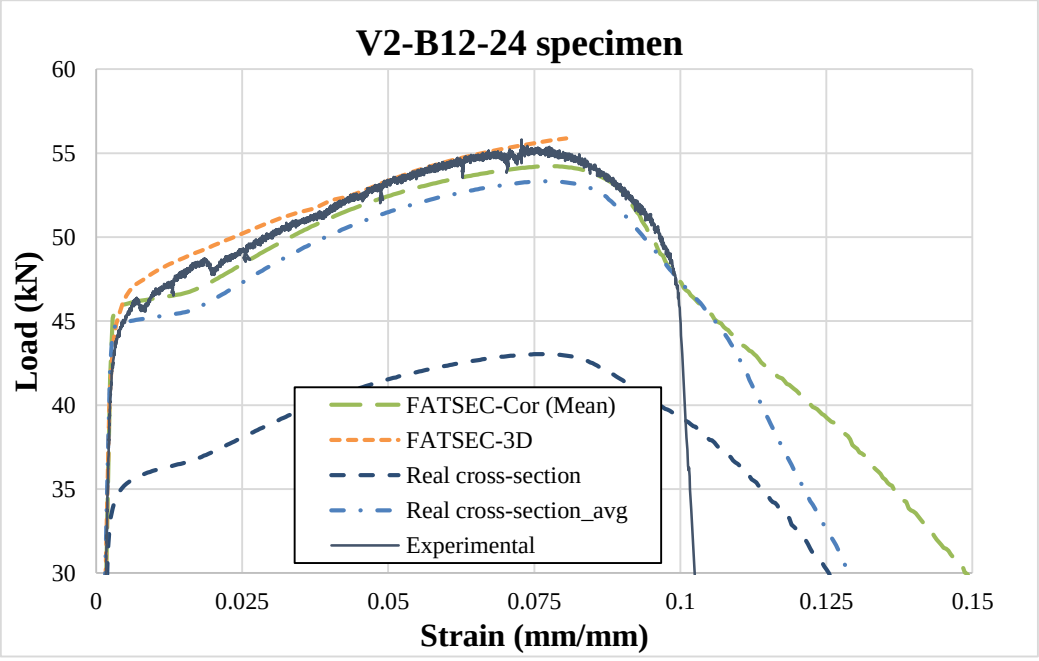

Figure V-45. Real critical cross-section, average critical cross-section and idealized pitted cross-section results comparison

V.3.5.4.1 FATSEC-3D results comparison

To confirm the multi-axial stress-strain state aforementioned different graphical outputs of the stress level in the critical cross-section are shown in Figure V-46. In the top pictures, the yielding point of the bar is depicted. In the left, the stresses using the aforementioned Von Mises criterion are represented. On the other hand, the uniaxial stresses in the longitudinal direction of the bar at the same load level in the right picture. As it possible to see, the uniaxial stresses were much higher than Von Misses ones and higher than the yielding stress. That confirmed the multi-axial effect induced by pitting in the cross-section. The bottom figures represented the same stresses at ultimate stress level. The same aforementioned effects are described.

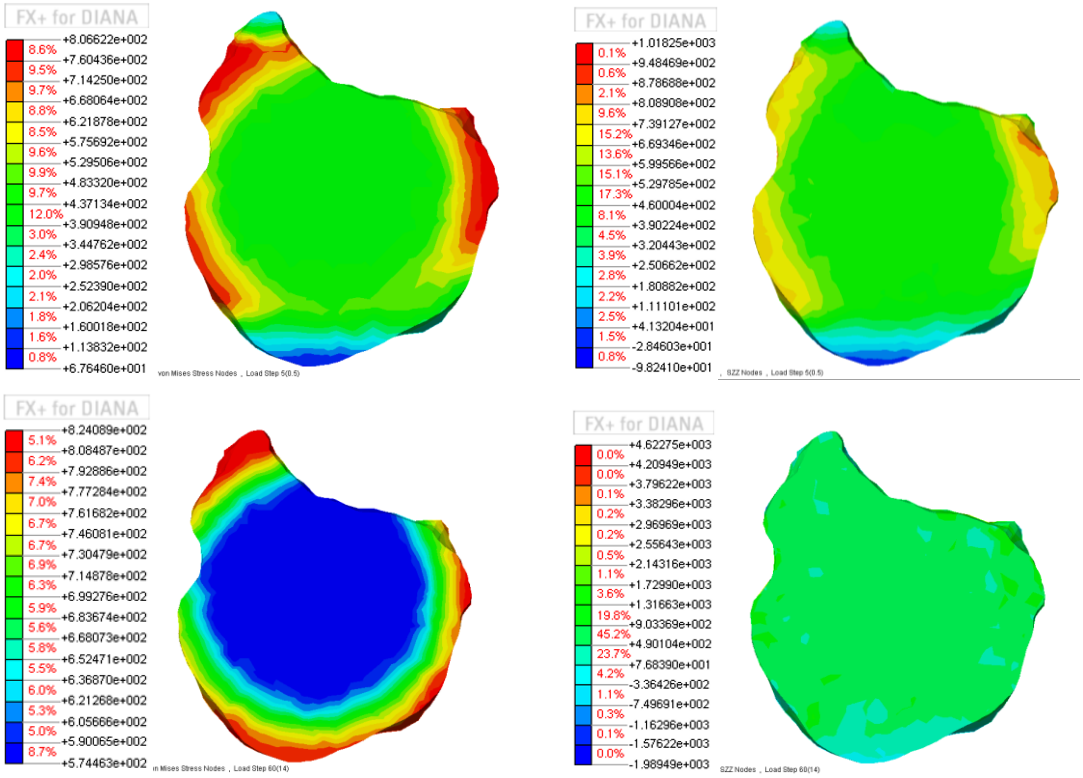

Figure V-46. Multi-axial stress behaviour of corroded specimens. Von-Misses multi-axial yielding criterion left, uniaxial stress right. Overall yielding stresses instant step with respect Von-Misses criterion top, ultimate stress step with respect to Von-Misses criterion bottom

V.3.6 Conclusions

The following conclusion can be drawn from the presented work.

(1) 3D scan technique is presented as useful tool with many different utilities. The description of the pitting distribution and the definition of the critical cross-section is possible with this kind of methods. In addition, the evaluation of the corrosion level using volume differences is possible, which might be more precise than gravimetric methods.

(2) 3D scan post-process remesh to transform the triangular surface mesh into a solid tetrahedral mesh is not easy and presented some technical issues. The definition of the pits has to be enough accurately to describe the local effect produced into the bar due to the 3D multi-axial state.

(3) The presented model allows reproducing the fatigue life and tensile behaviour with a very good agreement with respect to the experimental data. Fatigue life estimation require a high computational cost since in each load step the non-linear stress state has to be obtained. On the other hand, tensile test is low computational cost despite are needed many intermediate steps to describe the σ-ε behaviour until ultimate stress.

(4) The material model presented by Fernandez et al. [11] for TEMPCORE® bars adjusts very well for the uncorroded steel bars.

(5) As it is showed, a multi-axial behaviour is described in the critical pitted cross-section. Simplest uniaxial models require an overestimation of the steel critical cross-section area to include these effects and get a good estimation of the yielding and ultimate stresses. The higher corrosion was the larger difference between the 3D model and the uniaxial model was observed. As it was expected, since the multi-axial state in high-corroded cross-section is amplified.

Acknowledgments

The authors wish to acknowledge the financial support of The Ministry of Economy and Competitiveness of the Government of Spain (MINECO) for providing funds for projects

BIA2009-11764, as well as BIA2012-36848. The financial support of Infrastructures de Catalunya (ICAT) is also highly appreciated. Also acknowledge CIMNE to provide a free license for the software GiD [23] to develop the present work.

References

[1] L. Bertolini, B. Elsener, P. Pedeferri, R. Polder, Corrosion of Steel in Concrete. Prevention, Diagnosis, Repair., Wiley-VCH Verlag GmbH & Co. KGaA, Weinheim, Germany, 2004.

[2] K. Tutti, Corrosion of steel in concrete, (1997) 6–15. doi:10.4324/9780203414606_chapter_2.

[3] J. Broomfield, Corrosion of steel in concrete: understanding, investigation and repair, 2nd Ed., Taylor & Francis, Abingdon, United Kingdom, 2002.

[4] M. Raupach, B. Elsener, R. Polder, J. Mietz, Corrosion of reinforcement in concrete, Woodhead Publishing Limited, 2007. doi:10.1533/9781845692285.

[5] W. Zhang, X. Song, X. Gu, S. Li, Tensile and fatigue behavior of corroded rebars, Constr. Build. Mater. 34 (2012) 409–417. doi:10.1016/j.conbuildmat.2012.02.071.

[6] C.A. Apostolopoulos, Mechanical behavior of corroded reinforcing steel bars S500s tempcore under low cycle fatigue, Constr. Build. Mater. 21 (2007) 1447–1456. doi:10.1016/j.conbuildmat.2006.07.008.

[7] C.A. Apostolopoulos, M.P. Papadopoulos, S.G. Pantelakis, Tensile behavior of corroded reinforcing steel bars BSt 500s, Constr. Build. Mater. 20 (2006) 782–789. doi:10.1016/j.conbuildmat.2005.01.065.

[8] C. a. Apostolopoulos, V.G. Papadakis, Consequences of steel corrosion on the ductility properties of reinforcement bar, Constr. Build. Mater. 22 (2008) 2316–2324. doi:10.1016/j.conbuildmat.2007.10.006.

[9] H. Çetinel, M. Toparlı, L. Özsoyeller, A finite element based prediction of the microstructural evolution of steels subjected to the Tempcore process, Mech. Mater. 32 (2000) 339–347. doi:10.1016/S0167-6636(00)00009-0.

[10] I. Sankar, K. Rao, A. Gopalakrishna, Optimization of steel bars subjected to Tempcore process using regression analysis and harmony search algorithm, J Sci Ind Res. 69 (2010) 266–270. http://nopr.niscair.res.in/handle/123456789/7713 (accessed July 10, 2014).

[11] J. Nikolaou, G.. Papadimitriou, Microstructures and mechanical properties after heating of reinforcing 500 MPa class weldable steels produced by various processes (Tempcore, microalloyed with vanadium and work-hardened), Constr. Build. Mater. 18 (2004) 243–254. doi:10.1016/j.conbuildmat.2004.01.001.

[12] P. Simon, M. Economopoulos, P. Nilles, Tempcore: a new process for the production of high quality reinforcing bars, Iron Steel Eng. 61 (198AD) 55–67.

[13] J.M. Bairan, a. R. Marí, H. Ortega, J.C. Rosa, Efecto del enrollado y enderezado en las propiedades mecánicas de barras de acero de diámetro medio y grande fabricadas en rollo, Mater. Construcción. 61 (2011) 559–581. doi:10.3989/mc.2011.60110.

[14] A.G. Palmgren, Die Lebensdauer von Kugellagern (life length of roller bearings), VDI Z. 68 (1924) 339–341.

[15] M.A. Miner, Cumulative damage in fatigue, J. Appl. Mech. 12 (1945) A159–A164.

[16] I. Fernandez, J. Bairán M., A. Marí R., Corrosion effects on the mechanical properties of reinforcing steel bars. Fatigue and σ-ε behaviour, Constr. Build. Mater. (2015).

[17] S.L.W.Z.X.G.C. Zhu, Fatigue of Reinforcing Steel Bars Subjected to Natural Corrosion, Open Civ. Eng. J. (2011) Vol.5, p69. http://connection.ebscohost.com/c/articles/70458995/fatigue-reinforcing-steel-bars-subjected-natural-corrosion (accessed February 14, 2015).

[18] A. a. Almusallam, Effect of degree of corrosion on the properties of reinforcing steel bars, Constr. Build. Mater. 15 (2001) 361–368. doi:10.1016/S0950-0618(01)00009-5.

[19] C.A. Apostolopoulos, V.G. Papadakis, Consequences of steel corrosion on the ductility properties of reinforcement bar, Constr. Build. Mater. 22 (2008) 2316–2324. doi:10.1016/j.conbuildmat.2007.10.006.

[20] UNE-EN-ISO-15630-01, Acero para el armado y pretensado del hormigón - Métodos de ensayo. Parte 1: Barras, Alambre y Alambrón para el hormigón armado, (n.d.).

[21] A. Borruto, Meccanica della frattura, Milan, 2002.

[22] TNO Diana. Finite Element Analysis User's Manual - release 9.6.6: TNO, 2015.

[23] C.I.C. for N.M. in Engineering, GID. The personal pre and post processor, (2014).

[24] I. Fernandez, J. M. Birán, A. R. Marí, Mechanical model to evaluate steel reinforcement corrosion effects on σ-ε and fatigue curves. Experimental calibration and validation, (n.d.).

V.4 1D and 3D analysis of anchorage in naturally corroded specimens

Ignasi Fernandez Perez

Universitat Politècnica de Catalunya-BarcelonaTech
Department of Construction Engineering, Division of Structure Technology, Concrete Structures
Jordi Girona 31, Barcelona (08034), Spain
Supervisors: Antonio R. Marí, Jesús Bairán
Guest researcher at Chalmers University of Technology

Mohammad Tahershamsi

Chalmers University of Technology,
Department of Civil and Environmental Engineering, Division of Structural Engineering, Concrete Structures,
Sven Hultins gata 8, Gothenburg (412 96), Sweden
Supervisors: Karin Lundgren, Kamyab Zandi, Mario Plos

Abstract

Corrosion of reinforcement causes cracking and spalling of concrete cover which affects the bond; this is a crucial factor in deterioration of concrete structures. Earlier, tests have been carried out on specimens with naturally corroded reinforcements; in this study, the focus is given to the modelling of these specimens. The aim was to evaluate the scope of simpler and more complex bond models to assess the structural behaviour.

A comparison of two approaches to model the anchorage behaviour was done: (a) a one-dimensional analysis, where the bond-slip differential equation with a non-linear bond-slip constitutive model is numerically solved, and the mean bond strength as well as the required anchorage length to anchor the yield force are computed. (b) Finite element (FE) analyses were performed using 3D solid elements for concrete, and beam elements for reinforcement, where the interaction was explicitly described using the same bond-slip constitutive model as in approach (a).

The results show differences between the two approaches. Each of the modelling alternatives had both drawbacks and advantages; while the more complicated model accounting for more variables led to more realistic results in comparison with observations, the simpler 1D analysis was very fast and efficient.

V.4.1 Introduction

Corrosion of steel reinforcement is one of the main problems in reinforced concrete structures. Study of corrosion effects is crucial for a better understanding of the structural behaviour of existing impaired concrete structures. The most severe effect of reinforcement corrosion is the change in bond properties between the steel and concrete. Volumetric expansion of corrosion products causes splitting stresses along corroded reinforcement which might be harmful to the surrounding material. Generally, the splitting stresses are not tolerated by concrete, and that leads to cracking and eventually spalling of the cover. As the reinforcement becomes more exposed, the corrosion rate may increase and facilitate the deterioration process.

The effect of corrosion process on bond deterioration has been studied extensively by many researchers. Several studies have investigated parameters which may influence bond and anchorage capacity of corroded structures, see [1-4]. Even though tests of artificially corroded specimens with low corrosion rates indicated a closer relation to the natural corrosion conditions, literature shows that accelerated corrosion methods may still result in spurious bond deterioration and change the anchorage behaviour, [5], [6]. Thus, there was a strong need for experiments on naturally corroded specimens in order to facilitate the evaluation of the methods and models which were mostly developed based on accelerated-corrosion tests.

In the present paper, different approaches of modelling the anchorage capacity of naturally corroded specimens were used. A one-dimensional analytical model was used to calculate the local and global bond-slip behaviour along the naturally corroded reinforcements of the tested beams. Furthermore, three-dimensional non-linear finite element analyses were performed to describe the anchorage behaviour of the specimens. The results of the analytical and numerical models with different corrosion levels were compared with the experimental data.

V.4.2 Experiments

The tests have been carried out as a part of an experimental campaign at Chalmers University of Technology. The test setup and the test results are described in detail in [7] and [8]. The specimens were extracted from the edge beams of an existing girder bridge with a concrete slab; the edge beams showed different levels of corrosion-induced damage. Based on the damage patterns, the specimens were categorized in three different groups: Reference (R)

beams with minor or no-visible damage, Medium (M) damaged specimens with only spalling cracks, and Highly (H) damaged specimens with spalling of the cover. A total of 21 beams were tested in two test series. This work is focused on the second test series consisting of 13 tests described in [8], three of them are presented in this paper. The designed test set-up and specimens geometrical specifications are shown in Figure V-47(a) and Figure V-47(b), respectively. The edge beams were tested upside down compared to their placement on the bridge.

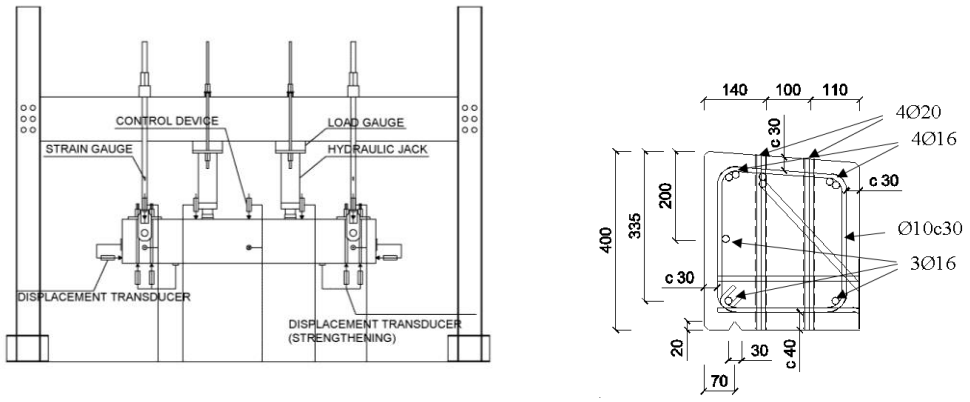

a) b)

Figure V-47. (a) Test-setup, and (b) cross-section of tested beams

An indirectly supported four point bending test configuration was used for the experiments. The load was applied by means of two hydraulic jacks defining a central constant moment zone and two shear spans. The beams were suspended by means of a frame which at the same time was used to fix the jacks. The support settlements as well as the mid-span deflection were measured by means of displacement transducers. The end-slip behaviour of the reinforcement bundles was recorded at both ends. The support zones were strengthened to avoid undesirable failure at these locations.

V.4.3 1D Bond-Slip Model

V.4.3.1 Bond model

An analytical 1D bond-slip model, developed in [9], was used to analyse the bond-slip behaviour of corroded and uncorroded ribbed steel reinforcement. Accordingly, the differential equation expressing equilibrium conditions along the reinforcement in tension can be defined as in Equation V-6:

Equation V-6 $$\frac{\pi \cdot d^2}{4} \cdot \frac{d\sigma}{dx} - \pi \cdot d \cdot \tau = 0$$

where d is the reinforcement diameter, σ is the stress in the reinforcement and τ is the bond stress.

The local bond-slip behaviour is computed based on the CEB-FIB Model Code 10. Corrosion effect of the reinforcement is taken into account by shifting the uncorroded local bond-slip relationship along the slip axis, as suggested in [9]. The model includes a modification of the first branch of the bond-slip curves compared to Model Code 10. To provide enough stiffness in the beginning, the parameter a was in this case modified to a value of 18, which is significantly higher than the original value of 2. For further information on how the bond-slip is obtained and the description of the equations used refer to [9]. The equivalent perimeter of the reinforcement bundles was taken following [10], considering the average value between the values given in Figure V-48b

The model was developed to analyse the bond-slip behaviour of steel reinforcement within the anchorage length, and the stress in the reinforcement is assumed to be in the elastic range. The deformation of the surrounded concrete is neglected, thus all the slip is assumed to be caused due to the reinforcement deformation. By solving the differential equation, the load versus end-slip curves for a given embedded length as well as the distribution of slip, bond and steel stresses along the bar are obtained.

V.4.3.2 Structural model

The tensile load, F_t, at the end of the remaining available anchorage length is obtained by integrating the local bond-slip along the bar according to Equation V-6. To obtain the equivalent load, P, applied on the tested beam, the same structural model presented in [7] was used, see Figure V-48a.

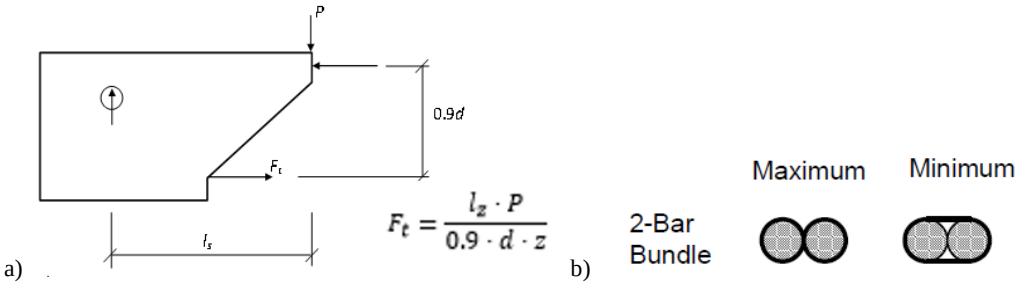

Figure V-48. (a) Structural scheme to obtain the applied load from the tensile load reinforcement, and (b) Equivalent perimeter for bundled reinforcement bars proposed by [10]

V.4.3.3 Results

A comparison between the analytical model and the test data for some of the specimens is shown in Figure V-49. The corrosion level of the damaged specimens was estimated to be around 2-3% [7]. As can be seen in Figure V-49, the agreement between the experimental and 1D analysis results is reasonably good; this is true for all specimens. Thus, a reasonable good estimation for the remaining anchorage capacity of corroded specimens can be obtained using the model provided the available anchorage length is known. It should be noted that "all other bond conditions" according to Model Code 10 was assumed to get the local bond-slip curves, taking into account that the specimens were damaged and taken from a real bridge; the assumption of "good bond conditions" would have overestimated the capacity. There is not experimental data for the local bond-slip behaviour from the tests.

The 1D model generally reproduces the pre-peak behaviour and the capacity accurately. The post peak behaviour however does not show the same agreement, whereas the remaining capacity in most of the specimens is estimated reasonably well.

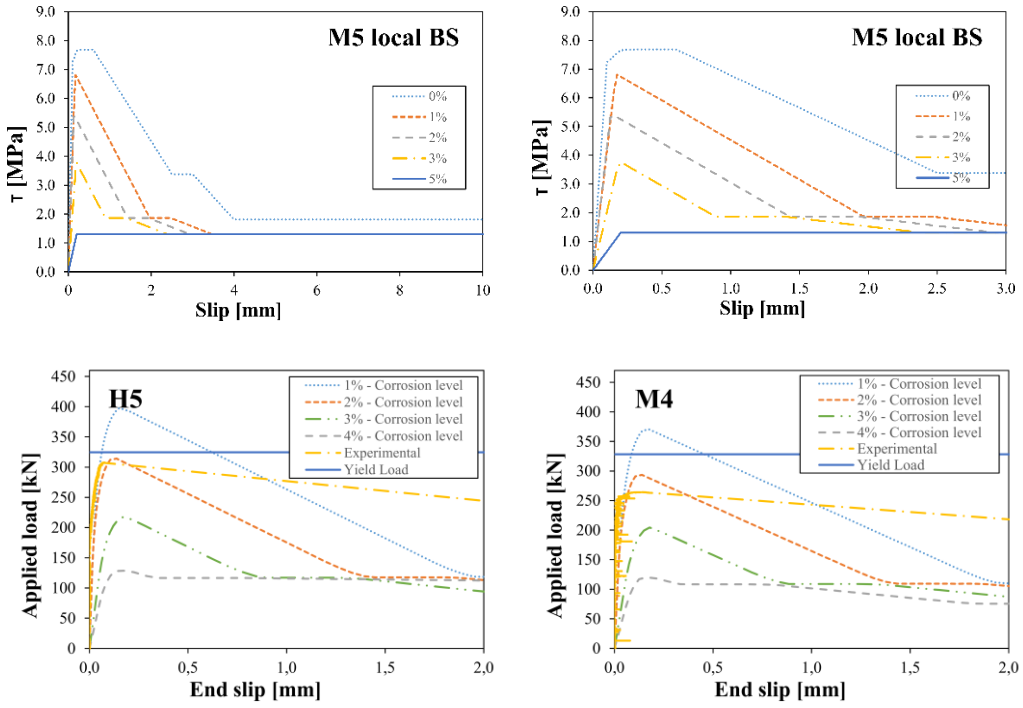

Figure V-49. Top, Bond-slip curves accounting for four different corrosion levels, obtained by means of the 1D bond-slip model for beam M5 (Right figure is enlargement of left). Bottom, Applied load end-slip curves for H5 and M4 specimens accounting for 1 to 4 % co

V.4.4 3D model with 1D bond-slip relationship

V.4.4.1 FE model

3D non-linear finite element analyses were performed to describe the behaviour and capacity of the anchorage zone. The commercial software DIANA with pre- and post-processor FX+ was used for the numerical simulations.

The beams that were modelled had the same dimensions as the tested specimens accounting for the different geometrical specifications of each specimen. The exact positions of the reinforcements as well as the stirrups were taken into account in the development of each model. The symmetry of the test-setup allows for half of the span and loading being considered in the model as shown in Figure V-50. Boundary conditions were applied on the top node of the suspension drill, supporting the displacements in the vertical axis and out of plane one. The load was applied by means of displacement control.

3D tetrahedral elements (TE12L) were used for the concrete and the reinforcement bars were embedded into concrete element; this allowed describing the concrete-rebar interaction using a bond-slip relation. An analytical local bond-slip relationship for each specimen was defined according to the outputs of the 1D bond-slip; i.e. the same local bond-slip as used in the 1D analyses, Figure V-49. Five different bond-slip relations were used for each specimen taking 5 different corrosion levels into account. The loading zone was modelled by means of a wood board and a steel plate using triangular-prism elements (TP18L). An overview of the model and the boundary conditions are shown in Figure V-50. Tying elements with eccent properties were disposed in fixed nodes of the support to avoid undesairble local failure. This tying fixed the upper node with two slave nodes imposing the same rotation respect the master node.

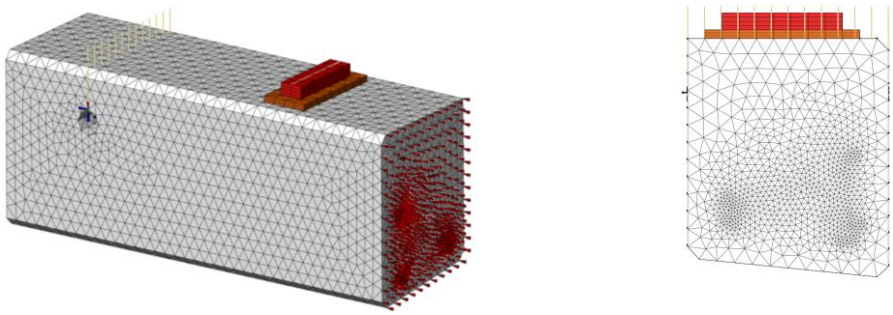

Figure V-50. Overview of the FE model

The concrete was modelled with a constitutive model based on non-linear fracture mechanics using a total strain based smeared-crack model with rotating crack approach. Thorenfeldt

compression curve was used in order to more realistically describe the behaviour of concrete in compression. The softening behaviour of this curve was adapted to the element size as described in [11]. The tensile behaviour was modelled using a stress-strain relation proposed by Hordijk for tension softening. The reinforcing steel was modelled with an isotropic plasticity model with Von Mises yielding criterion including hardening. The material properties for steel and concrete used in the analysis can be found in [7] and [8]. Compressive concrete strength, $f_{c,}$ was obtained in the laboratory from every specimen by means of cylindrical specimens. The E modulus tensile concrete strength was the average from 3 of the first round specimens. The energy fracture was calculated by means of the expression proposed in the fib MC 10.

V.4.4.2 Results

The results from 3D FE analysis, see Figure V-51, show a pull-out failure in most of the cases for a corrosion level of 2% and above. For values below 2%, the reinforcement yields. In general, the maximum load capacity is reasonably well described by these analyses. However, the overall stiffness is overestimated in several cases, most likely because of the pre-existing internal damage of the specimens was not reproduced in the described models. For some of the tests, the initial stiffness of the local bond-slip curve used as input in the model was not enough, yielding high slip values at the first load steps in the applied load versus end slip curves; however, in general the local bond-slip curves yields in a good overall behaviour as it is shown in Figure V-51Figure V-51.

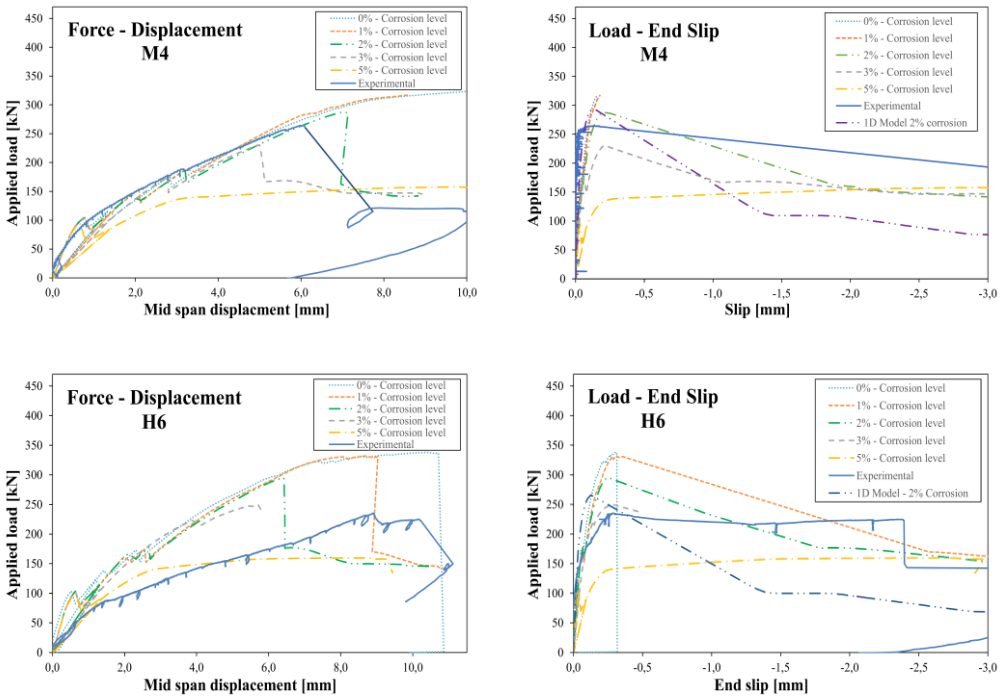

Figure V-51. Results of 3D FE analysis in comparison with experiments and 1D Bond-slip Model

Figure V-52Figure V-52 shows the crack pattern and the remaining anchorage length for specimen M4. As can be seen, there were two shear cracks between the loading plate and the support in the experiment (marked with 2 and 3 in the figure), while there was only one shear crack in the corresponding region in the analysis. Thus, in the 3D model, all the damage tends to concentrate to the first shear crack. This results in larger remaining anchorage lengths in the analyses than in the experiments for several specimens. Accordingly, the remaining load capacity was slightly higher in comparison to the tested beams as it is directly related with the anchorage length. A probable reason for this discrepancy is that the modelling does not describe the splitting stresses and cracks in a correct way; in the tested beams the splitting cracks connected with the second shear crack. To describe this interaction, simple bond-slip input is too simplified; more sophisticated modelling including the splitting stresses of both the corrosion and the slip would be needed.

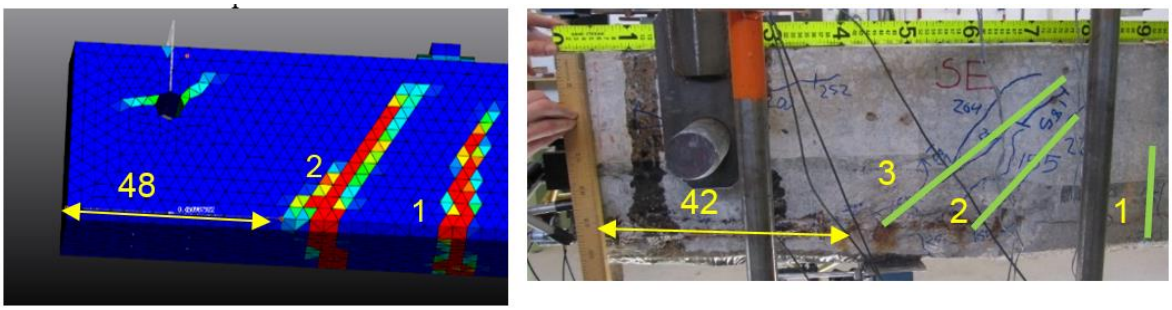

Figure V-52. Crack pattern comparison of M4 specimen; the anchorage length is given in mm

V.4.5 Conclusions and Outlook

It was shown that simplified 1D model can be used to obtain rough estimations of the ultimate anchorage capacity. From that point of view these models are very useful, but they are strongly dependent of the available data such as the available anchorage length; data that is not always easy to obtain. More complex models are necessary to describe the overall structural behaviour. Using simple bond-slip relationships between concrete and steel in complex models is useful and relatively fast to obtain a good approximation to the real behaviour. However, it was shown that also this modelling technique has shortcomings, mainly because the splitting action is not included. In future work, a frictional model where the effect of corrosion is taken into account by introducing the swelling action and the flow of rust through cracks will be used, to account for both the internal concrete damage due to steel corrosion and splitting stresses generated by the slip .

References

[1] Regan PE and Kennedy Reid IL (2010) Assessment of Concrete Structures Affected by Delamination – 2, Graduate School in Concrete Structures – Fratelli Pesenti, Politecnico di Milano, Italy

[2] Zandi Hanjari K, Coronelli D and Lundgren K (2011) Bond capacity of severely corroded bars with corroded stirrups. Magazine of concrete Research 63(12): p532-541

[3] Sæther I (2011) Bond deterioration of corroded steel bars in concrete. Structure and Infrestructure Engineering 7(6): p 415-429.

[4] Coronelli D, Hanjari KZ and Lundgren K (2013) Severely Corroded RC with Cover Cracking. Journal of Structural Engineering 139(2): p 221-232

[5] Austin SA, Lyons R and Ing MJ (2004) Electrochemical behaviour of steel-reinforced concrete during accelerated corrosion testing. *Corossion* 60(2): p 203-212

[6] Saifullah M and Clark LA (1994) Effect of Corrosion Rate on the Bond Strength of Corroded Reinforcement. In R. N. Swamy, ed *Corrosion and Corrosion protection of Steel in Concrete*. University of Shefield, South Yorkshire, Great Britain, p 591- 602

[7] Lundgren K, Tahershamsi M, Zandi Hanjari K and Plos M (2013) Tests on Anchorage of Naturally Corroded Reinforcement in Concrete. Accepted in "Journal of Materials and Structures."

[8] Tahershamsi M, Zandi K, Lundgren K and Plos M (2013) Anchorage of Naturally Corroded Bars in RC Structures. Submitted to "Magazine of Concrete Research"

[9] Lundgren, K., et al., Analytical model for the bond-slip behaviour of corroded ribbed reinforcement. Structure and Infrastructure Engineering, 2012. 8(2): p. 157-169.

[10] Jirsa JO, Chen W, Grant DB, Elizondo R (1995) Development of bundled reinforcing steel. Center for transportation research, University of Texas at Austin, Texas, USA.

[11] Zandi Hanjari, K.: Load-carryng capacity of damaged concrete structures. Lic, in Civil and Enviromental Engineering. Chalmers University of Technology: Gothenburg, SE.

V.5 Pull-out of Textile Reinforcement in Concrete

Natalie Williams Portal, M.Sc.[1], Ignasi Fernandez Perez, M.Sc.[2]

Lars Nyholm Thrane, Ph.D.[3], Karin Lundgren, Professor[4]

[1]Dept. of Civil and Environmental Engineering, Chalmers University of Technology, Gothenburg 412 96, Sweden, E-mail: Natalie.williams@chalmers.se

[2]Dept. of Construction Engineering, Universitat Politècnica de Catalunya – Barcelona Tech, Barcelona, 08034, Spain, E-mail: Ignasi.fernandez-perez@upc.edu

[3]Dept. of Building Technology - Concrete, Danish Technological Institute, Taastrup 2630, Denmark, E-mail: lnth@dti.dk

[4]Dept. of Civil and Environmental Engineering, Chalmers University of Technology, Gothenburg 412 96, Sweden, E-mail: Karin.lundgren@chalmers.se

Highlights:

- Pull-out tests of TRC to gain better knowledge of the complex bond behaviour.
- Local-bond slip relationship evaluated from experimental data.
- 1D and 3D numerical models to simulate complex global bond behaviour.
- 3D models validated the simplified assumptions applied in the 1D model.

Abstract:

Textile Reinforced Concrete (TRC) has emerged as a promising novel alternative offering corrosion resistance and both thinner and light-weight structures. Although TRC has been extensively researched, the formalization of experimental methods and design standards is still in progress. The aim of this work was to extract local-bond behaviour from pull-out tests of basalt and carbon TRC and utilize these in both simple (1D) and advanced models (3D) to yield the global structural behaviour. The simulation results from the 1D and 3D models are able to simulate the complex behaviour of TRC with a reasonable level of correlation.

Keywords: Textile reinforced concrete (TRC); Bond-slip; Pull-out tests; Experimental tests, Finite-element modelling

V.5.1 Introduction

A recent innovative attempt to improve the sustainability of reinforced concrete is the development of Textile Reinforced Concrete (TRC) encompassing a fine-grained concrete matrix reinforced by a multi-axial non-corrosive textile mesh. This relatively new composite material has been extensively researched at collaborative research centres 532 and 528 at RWTH Aachen University and Dresden University of Technology [1] over the past decade. Collaborative efforts spreading across USA, Germany, Brazil and Israel have also played a major role in this field [2]. It was discovered that TRC can be utilized to build slender, lightweight, modular and freeform structures and eliminate the risk of corrosion. The completion of a pedestrian bridge fabricated solely of TRC [3] and the development of thin self-supporting TRC sandwich elements [4] are examples of the possible realizations. It was also proven to be an adequate strengthening material for existing reinforced concrete structures in a variety of applications [5, 6]. To sum up, a report entitled RILEM TC 232-TDT encompassing test methods and design of Textile Reinforced Concrete, in progress since 2009, has been compiled, however is not yet available for public use [7]. The purpose of this particular report is to provide guidelines for testing methods, a design manual and an update of the TRC state-of-the-art report [8].

In fibre composite materials, such as TRC, bond behaviour between the yarn or roving and the cementitious matrix is a principal factor influencing the global structural behaviour [9]. Yarns or rovings consist of multitudes of filaments which creates a complex heterogeneous structure. For that reason, the characterization of the bond behaviour is critical in terms of input for numerical models analysing the structural behaviour of TRC. Pull-out testing is a typical method utilized to gain understanding of bond phenomenon related to reinforced concrete. Since the lack of standards in this field, testing methods and numerical methods to evaluate the pull-out behaviour of yarns or rovings in TRC used in similar research need to be explored and considered. Bond properties of TRC have been investigated using various textile pull-out test configurations while focusing on differing textile meshes and influential parameters by Krüger [10], Xu and Li [11], Sueki, Soranakom et al [12], Ortlepp, Curbach et al [13], Lorenz and Ortlepp [14] and Zhang, Aljewifi et al [15]. For instance, in [12], a parametric study of varying embedment lengths, textile meshes and cement mix types as well as processing methods were incorporated. Specimens reinforced by alkali-resistant (AR) glass, polypropylene and polyvinyl acetate meshes were prepared using casting, pultrusion or vacuum techniques. Successively, the use of analytical methods followed the experiments of the abovementioned works such that the experimental pull-out behaviour of a single continuous yarn from a matrix was described analytically using closed form

equations [9, 12, 14-16]. Various damage models such as a triple linear shear-stress slip model have been assumed to characterize the yarn pull-out behaviour incorporating both adhesion and frictional load transfer [9, 16]. In brief, experimental results from pull-out tests appear to successfully verify the developed analytical and numerical models [9, 12, 14-16].

Direct pull-out tests are included in this research to characterize the complex pull-out behaviour of a textile mesh-structure embedded in a concrete matrix with a particular focus on basalt and carbon TRC. More specifically, the pull-out of a single roving from the textile mesh was carried out which resulted in a representative smeared pull-out behaviour of the embedded mesh structure. Varying embedment lengths were used to quantify bond capacity and textile rupture failure modes. Based on the experimental results, a local bond stress-slip curve was obtained. Thereafter, the calibrated local behaviour was used as material input data in two numerical models to simulate the global behaviour experienced by the pull-out specimens. An analytical 1D bond model originally developed by Lundgren, Kettil et al [17] to analyse the bond stress-slip behaviour of corroded ribbed steel reinforcement was modified for textile reinforcement. Also, in the 1D model, a stepwise calculation and superposition is needed to obtain the bond stress-slip behaviour for the entire pull-out specimen. Moreover, a 3D non-linear finite element model of the conducted pull-out tests was developed and used to validate the assumptions related to the simplest 1D bond model. Using simplified models to study bond capacity of TRC concrete is necessary to better understand complex structural behaviour.

V.5.2 Experimental study

The presented work is a part of a larger experimental scope, primarily conducted at the Danish Technological Institute (DTI) and evaluated at Chalmers, which encompassed flexural and pull-out tests of TRC. The experimental work presented here focuses on direct pull-out tests of TRC specimens reinforced by basalt and carbon meshes having the underlying purpose to characterize the corresponding bond phenomenon. The mechanical properties of the cementitious matrix were also obtained through compressive and tensile splitting tests.

V.5.2.1 Pull-out testing

At present, no standard test setup to investigate the pull-out behaviour of TRC is available; as such, relevant experimental work from literature was revealed to help establish an

experimental setup. The main types of test configurations known from literature include one-sided and double-sided pull-out tests. For example, one-sided tests were conducted by Banholzer [18], wherein single yarns were embedded in a concrete matrix at one end and in an epoxy resin block at the other. This type of test is, however, said to yield a behaviour that is incomparable of that of a textile mesh [14]. As for two-sided tests, either symmetrical [19] or unsymmetrical anchoring lengths [10] can be implemented. The benefit of using unsymmetrical anchoring lengths is that a longer length guaranteeing adequate anchoring of the yarn/roving can be incorporated into the setup [14].

The pull-out test setup and specimen configuration employed in this work was designed based on the double-sided unsymmetrical test by Krüger [10] and Lorenz and Ortlepp [14]. The pull-out test specimens used in the presented experimental work measured 400 x 100 x 15 mm and reinforced by one layer of reinforcement mesh. Unsymmetrical anchorage lengths, denoted A and B in Figure V-53, were defined for each specimen. A singular roving from the textile mesh was exclusively tested from the TRC specimen in order to yield representative smeared pull-out behaviour. The embedment length chosen was generally based on the distance of the cross-threads, specified as *Short* (35 mm), *Medium* (70 mm) and *Long* (87.5 mm) for basalt and *Short* (25 mm), *Medium* (50 mm) and *Long* (75 mm) for carbon. The prescribed embedded length was limited to the upper end of the specimen by means of a single saw cut crossing the roving to be tested and a breaking point marked by two saw cuts isolating the examined roving. The breaking point does not designate the definitive breaking point of the roving in itself, but rather the location of crack initiation.

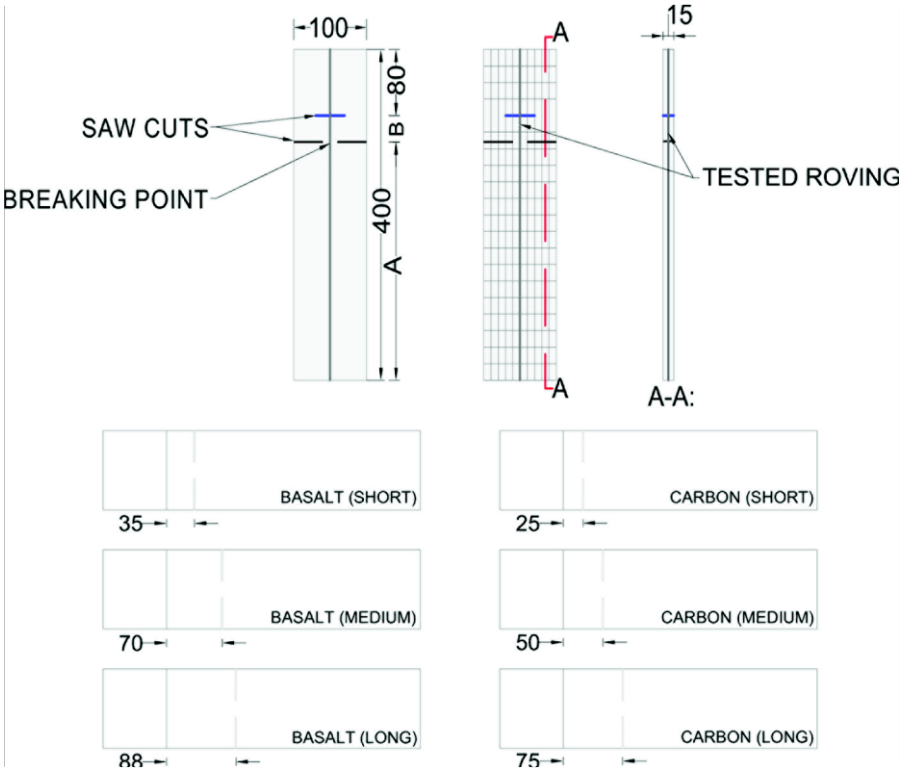

Figure V-53. Test specimen configuration and embedment length (mm)

The pull-out tests encompassed the evaluation of varying embedment lengths in order to characterize both pull-out and rupture of the textile roving as failure modes. Up to three specimens were produced for each selected embedment length in order to obtain a representative trend of the pull-out behaviour. The pull-out test specimens were configured such that the rovings along the pull-out direction later shown in Figure V-55 were positioned in the direction of the machine pull-out force (see Figure V-54). The layer of textile mesh was fastened by the framework used to cast the specimens causing the mesh to become slightly taut yet not pre-stressed which could have slightly reduced the initial waviness of the mesh. As per [1], pre-stressed TRC members exhibit higher peak loads at the expense of lower slip and a more brittle behaviour.

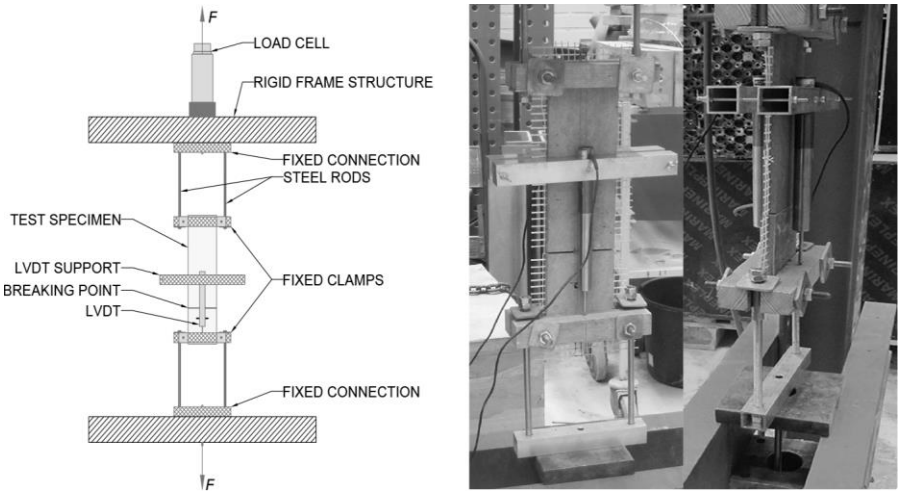

Figure V-54. Sketch (left) and photo (right) of experimental test setup

The experimental setup developed to conduct the pull-out tests is illustrated in Figure V-54. The load was applied by a hydraulic jack on top of the rigid frame structure. On top of the hydraulic jack, a 25 kN load cell was placed in order to measure the load. The ends of the test specimen were affixed by two wood clamps which were used to transfer the load to the specimen. The load was transferred symmetrically to the wood clamps by means of steel rods on both sides of the specimen which were further linked to connections fixed to the rigid frame structure. The total specimen deformation, i.e. crack-opening relationship at the breaking point, of the test specimen was measured using two linear variable displacement transducers (LVDT) positioned on either side of the centre of the specimen. Load and deformations were measured and stored every second by means of a data logger.

V.5.2.2 Material description

The pull-out test specimens were fabricated of a fine-grained concrete matrix according to the mix composition stated in Table V-7. Composition of the fine-grained concrete, mass in kg per m3 of concrete**¡Error! No se encuentra el origen de la referencia.**.The mean concrete cylinder compressive strength corresponding to 28 days, f_{cm}, was derived from material test results to be 53.6 MPa. Based on f_{cm}, the mean modulus of elasticity, E_{cm}, was estimated to be 36.4 GPa using CEN [20]. Lastly, the mean value of the tensile splitting strength tests was found to be 4.7 MPa.

Table V-7. Composition of the fine-grained concrete, mass in kg per m3 of concrete

Matrix composition	Density [kg/m^3]	Quantity [kg/m^3]
Low alkali cement (Z 52.5)	3200	406.0
Fly ash	2300	121.0
Microsilica	2200	22.0
Glenium SKY 532 – SU	1100	7.6
Amex SB22 (air entrainer)	1010	3.0
0/4 Sand	2640	1400.0
Water	1000	170.6

Two different types of textile meshes fabricated of carbon and basalt were included in this study. The carbon mesh used was produced by SGL group (Germany) is SIGRATEX grid 300 with a mesh spacing of 30 x 30 mm with roving fineness of 1600 tex. Lastly, Geo-grid mesh (Zhejiang GBF, China) fabricated of basalt with silane sizing. It has a configuration of 25 x 25 mm with a roving fineness of 2000 tex. The geometry, configuration of the cross-threads and pull-out direction pertaining to these textile meshes are depicted in Figure V-55. As well, corresponding nominal material properties from the manufacturers are listed in Table V-8.

Table V-8. Material properties for textile reinforcement alternatives.

Material	Roving cross-sectional area [m^2]	Specific surface weight [g/m^2]	Tensile strength [MPa]	Young's Modulus [GPa]
Basalt	0.755×10^{-6}	303	1898	100
Carbon	0.889×10^{-6}	300	3800	230

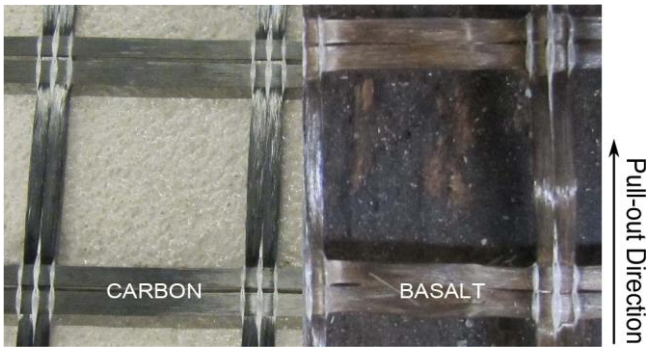

Figure V-55. Overview of the textile meshes

V.5.2.3 Result summary

V.5.2.3.1 Basalt

The force versus total deformation trend corresponding to the basalt specimens for all embedment lengths are described in Figure V-56. The total displacement corresponds to the mean displacement recorded by the two LVDTs for the entire specimen. In Figure V-56, it is observed that as the embedment length increases, the maximum force increases and occurs at a larger deformation. A pull-out failure mode was solely yielded for *Short* specimens, while rupture was the common failure mode for both *Medium* and *Long* specimens. In the case of pull-out failure, the pre-peak bond behaviour is governed by adhesive bond which is followed by the destruction of the adhesive bond occurring due to debonding of the roving from the matrix. Lastly, the remaining pull-out force is based on friction, as described in [16]. As can be seen in Figure V-56, there was, however, especially for the tests with embedment length 87.5 mm, a rather long plateau with roughly constant load, before a sudden loss of capacity at rupture of the textile roving.

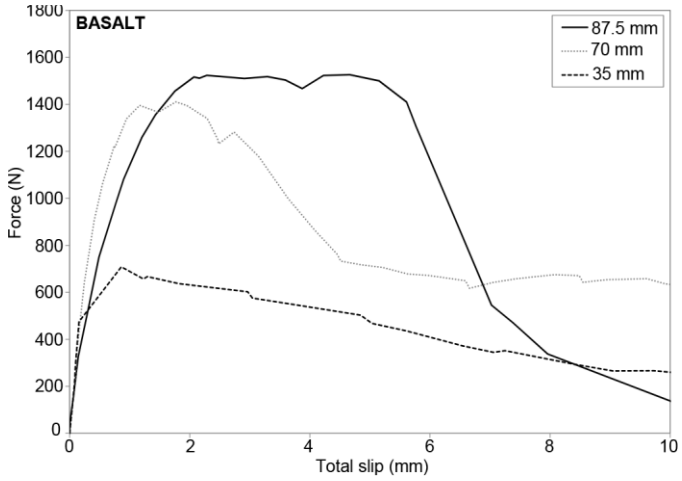

Figure V-56. Basalt average experimental results (all embedment lengths)

The average maximum force corresponding to *Short* specimens was 721 N (σ = 79), 1423 N (σ = 63) for *Medium* and 1662 N (σ = 139) for *Long*. Causes of variability in the results are presumed to be: uneven bond penetration through cross-section of roving, potential bond irregularities along embedment length (weak zones), human error in sample preparation as well as limited experimental sample size.

V.5.2.3.2 Carbon

Figure V-57 depicts the force versus total deformation trend for the carbon specimens for all embedment lengths. Similarly to basalt, the maximum force increases and the related

deformation also slightly increases as the embedment length gets larger. The maximum force corresponding to *Short* specimens was 629 N (σ = 32), 1050 N (σ = 154) for *Medium* specimens and 1333 N (σ = 298) for *Long* specimens. Moreover, variability in the presented results is likely due to the similar aforementioned reasons related to the basalt specimens.

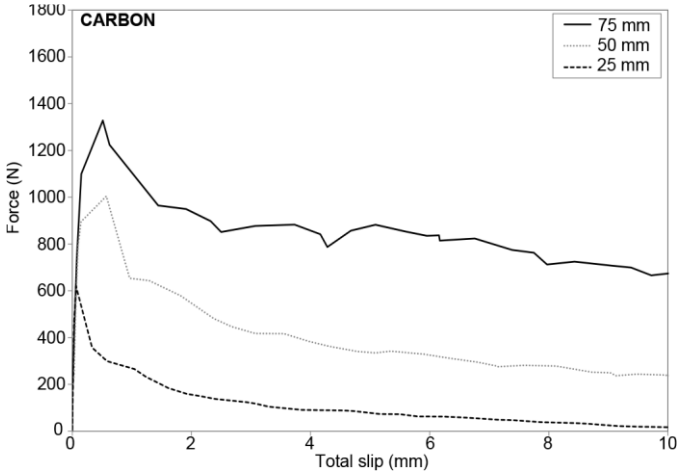

Figure V-57. Carbon average experimental results (all embedment lengths).

The common failure mode for the carbon textile roving was marked by pull-out of the roving in this study. It should be noted that an uneven pull-out of the roving was observed, presumably due to the heterogeneous bond existing between the roving structure and matrix. The mechanical description of the pull-out phenomenon is thought to be similar to that previously explained for basalt. Furthermore, it is believed that rupture failure was inhibited by the surface smoothness of the uncoated fibres as well as insufficient embedment length. Likewise, Lorenz and Ortlepp [21] demonstrated that to yield rupture of the roving, uncoated carbon textile rovings requires an embedment length of 80 mm which is 50 % greater than needed for the same textile roving with epoxy coating.

V.5.3 Local Bond Stress-Slip Curve

The shape of the local bond stress-slip function depends on concrete material properties (i.e. compressive strength), textile roving geometry (i.e. perimeter) as well as the configuration of the mesh cross-threads. The local bond stress-slip function can typically be estimated using various numerical [22] or analytical methods [9, 12, 14]. In this study, the first estimate of a local bond stress-slip function was obtained from the experimental results (force versus total deformation) from the *Short* specimens (refer to Figure V-53). The typical assumption for short pull-out tests with ribbed steel reinforcement bars, defined by embedment length

of less than five times the bar diameter, is that the distribution of bond stresses is uniform along the reinforcement [23, 24]. Concerning textile reinforcement it is difficult to foresee that this simplified condition could apply due to the heterogeneous behaviour of the roving, nevertheless it was tested and evaluated in this study. Accordingly, the uniform bond stresses hypothesis was assumed for the Short embedded length specimens, such that the general bond stress could be estimated as:

Equation V-7 $\tau = P / \pi \Phi L$

where, P is the load, Φ is the nominal diameter of the roving; and L is the embedded length. Initially, for the *Short* specimen, it was assumed that the slip was entirely taken by the Short zone before and after the peak. Since this hypothesis underestimates first bond stress values for the Short zone, the initial estimation of the local bond-slip was modified, particularly in the pre-peak region, until a reasonable fit for all embedment lengths was obtained, as further described in Section V.5.4. Due to the performed pull-out test and type of method used to record the slip, the non-linearity of the post-peak region was not adequately characterized. However, within this region, the slip distribution can be assumed to be entirely taken by the Short zone (refer to Section V.5.4). The calibration of the bond stress-slip curve was accomplished by a power function in the pre-peak region, i.e. from zero to the slip at ultimate bond stress, $s(\tau_{ult})$, and by a linear functions in the post-peak region, i.e. from the slip at ultimate bond stress, $s(\tau_{ult})$, to the ultimate slip, s_{ult} , as per Equation V-8. This calibration method is similar to that proposed in the *fib Bulletin 55: Model Code 2010* for bonded FRP rebars [22].

Equation V-8

$$\tau(s) = \tau_{ult} \cdot (s/s_{ult})^{B} \quad \epsilon\, 0 \le s \le s(\tau_{ult}),\ \textit{Power function - Basalt}$$

$$\tau(s) = -\tau_{ult} \cdot (1-s/s_{ult})^{B} + \tau_{ult} \quad \epsilon\, 0 \le s \le s(\tau_{ult}),\ \textit{Power function - Carbon}$$

$$\tau(s) = m \cdot s + b \quad \epsilon\, s(\tau_{ult}) \le s \le s_{ult},\ \textit{Linear function - All}$$

where, s is a given slip value, *B* is the weighting factor; and *m* and b are the corresponding slope and y-intercept of the linear function. The calibrated local bond-slip curves for basalt and carbon TRC are shown in Figure V-58 together with the first estimate obtained as described above. The calibrated bond-slip curves described in Table V-9 were subsequently used as input in non-linear finite element modelling to simulate the global behaviour of the pull-out specimens.

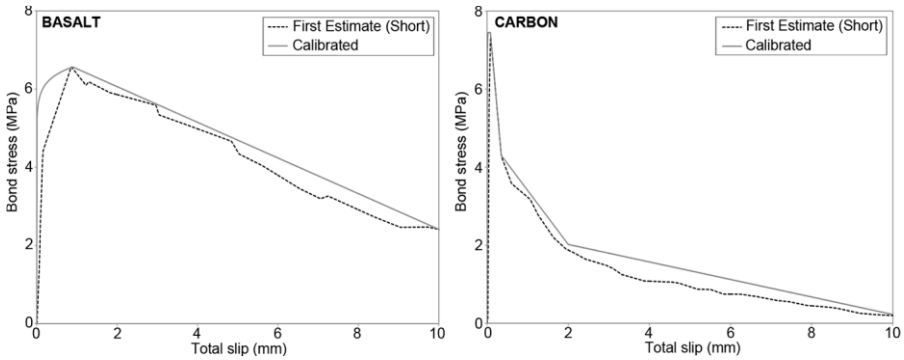

Figure V-58. Calibrated local bond-slip for basalt (left) and carbon (right).

Table V-9. Input for the calibration of local bond-slip curves

Material	Power function B, weighting factor (-)	Linear function m, slope (N/mm^3)	Linear function b, y-intercept (N/mm^2)
Basalt	0.05	-0.46	6.98
Carbon	100	-11.67	8.38
		-1.38	4.78
		-0.22	2.47

V.5.4 Numerical Modelling

A 1D model was used in this work to simulate the bond behaviour observed in the experimental study. The assumptions and limitations of this presented model were validated using a 3D non-linear model developed in the finite element analysis commercial software DIANA (DIsplacement ANAlyser) with pre- and post-processor Midas FX+.

V.5.4.1 1D Bond model

An analytical 1D bond-slip model developed by [17], principally used to analyse the bond stress-slip behaviour of corroded and uncorroded ribbed steel reinforcement, was modified for textile reinforcement in this study. To commence, the steel reinforcement is replaced by a singular continuous textile roving assumed to be homogeneous with a circular cross-section wherein the transverse rovings of the mesh are excluded. The stress and strain distribution for the conducted pull-out test can be described using Figure V-59. Accordingly, the differential equation expressing equilibrium conditions along the reinforcement in tension can be defined as Equation V-9:

Equation V-9 $\pi\Phi^2 / 4 \cdot d\sigma_t / dx - \pi\Phi\tau = 0$

where, ϕ is the reinforcement diameter, σ_t is the stress in the textile reinforcement and τ is the bond stress. The model was developed to analyse the bond stress-slip behaviour of the equivalent textile roving within the so-called anchorage length, thus the stress in the reinforcement is assumed to be in the elastic range according to Equation V-10:

Equation V-10 $\sigma_t = E_t \varepsilon_t, \ \varepsilon_t = du / dx$

where, E is Young's modulus, ε is the strain and u is the displacement of the reinforcement. Also, in this model, the bond stress follows an elasto-plastic law implying that the deformation of the surrounding concrete is assumed to be negligible; thereby the displacement of the reinforcement is equal to the slip. Furthermore, to solve the equilibrium equation stated in Eq. 3, boundary conditions based on the pull-out of an equivalent textile roving having a length of L and a prescribed displacement u_L were defined as per Equation V-11:

Equation V-11 $\sigma_t (0) = 0, \ u (L) = u_L$

The response of the pull-out tests were computed using a differential equation solver in MATLAB [25]. For further details regarding the development and implementation of the 1D bond-slip model refer to Lundgren, Kettil [17]. Moreover, to determine the total slip from the 1D bond-slip model, the slip contributions from the Short and Long zones were added to result in the total slip distribution which could thereafter be compared to the experimental results. The slip from the Long zone includes an assumed linear-elastic recovery curve to zero slip after the peak force. The corresponding results are presented and evaluated in Section V.5.5.

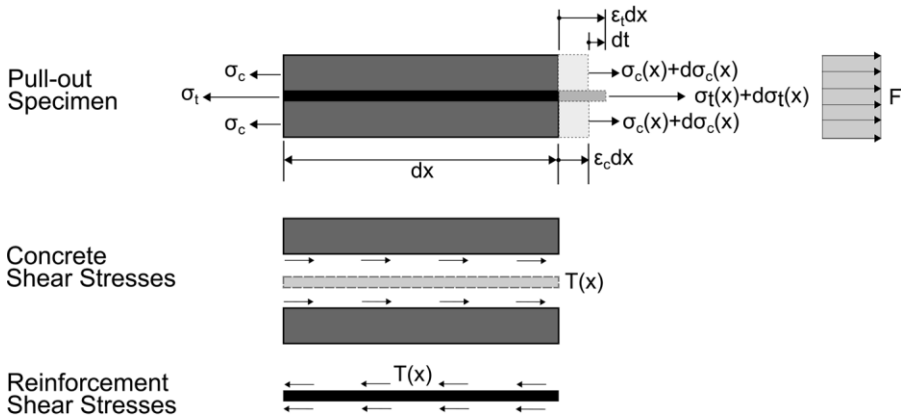

Figure V-59. Distribution of stresses and strains of the pull-out test; where subscript c and t denotes concrete and textile roving stresses or strains, respectively

V.5.4.2 Non-linear FE analysis

3D non-linear finite element analyses were performed to describe the non-linear behaviour of the bond-slip relationship between concrete and the textile reinforcement mesh. The verification of the model was accomplished by means of the experimental results obtained from the pull-out tests carried out in the laboratory. The results were also used to validate the assumptions included in the above-mentioned analytical 1D bond-slip model presented in Section V.5.4.1. DIANA with pre- and post-processor Midas FX+ was used for the numerical simulations [26]. The pull-out specimens that were modelled had the same dimensions as the tested specimens, incorporated the different embedded lengths prescribed based on the material and included exclusively a singular roving.

V.5.4.2.1 Load and boundary conditions

The idealized pull-out specimen, shown in Figure V-60 was loaded until bond failure similarly as in the laboratory conditions. Concerning the Long zone of the specimen, fixed supports were considered in three principal directions at the end side. The load was applied onto the Short zone by means of displacement, such that an imposed displacement was uniformly applied over the entire end surface. Additional supports were defined in some points along the specimen as a mesh stabilizer to avoid displacements in other directions as well as torsion. The analysis was carried out using a stepwise non-linear analysis with controlled displacement of the Short zone.

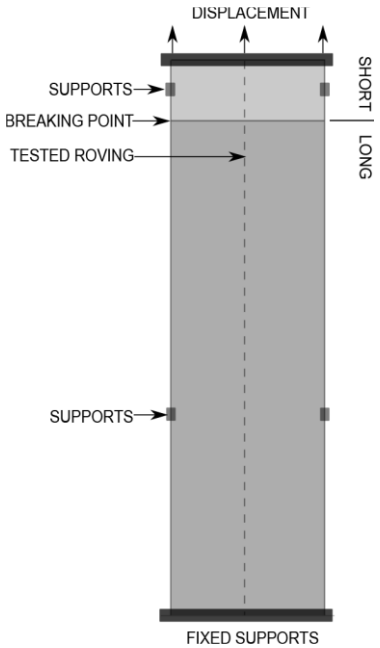

Figure V-60. Idealized 3D model of pull-out test

V.5.4.2.2 Element types & materials

The model, illustrated in Figure V-61, included four-node 3D isoparametric solid pyramid linear elements for concrete entitled TE12L in DIANA, embedded reinforcement for the textile and interface elements between the specimen's contact planes in a 3D configuration. Interface elements were used to make the connection of the two bodies of the specimens (Short and Long) possible and to be able to use embedded reinforcement for the textile roving with an assigned calibrated bond-slip relationship. The interface layer was defined as a discrete crack layer without tensile strength. Furthermore, tyings were defined at the prescribed pull location which ensures an even displacement along the surface where the clamps were acting. Essentially, all the nodes of this surface were tied to the centre node which was loaded by the prescribed displacement.

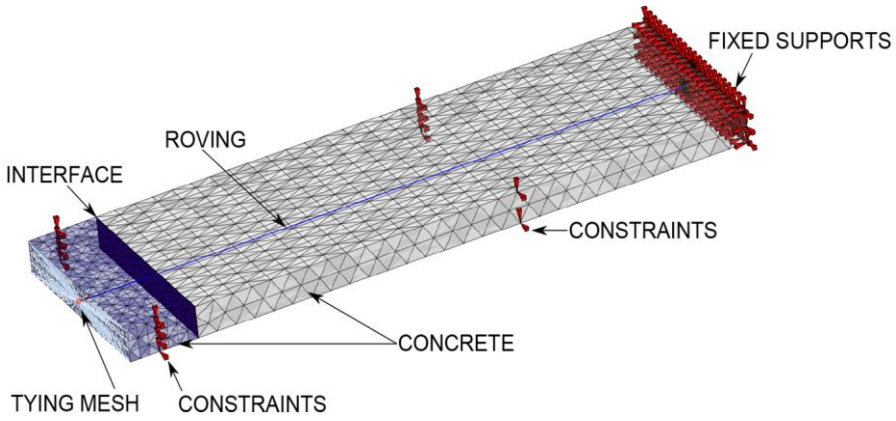

Figure V-61. Overview of 3D model in DIANA

The element size was chosen ranging from 5 to 10 mm, regarded as a fine mesh, in order to obtain sufficient intersection points between the embedded textile reinforcement and the mesh, as well as to properly characterize the bond stresses along the textile roving. Material properties for both concrete and textile were chosen as linear-elastic, which corresponds to the outcome of the experiment. The tensile stress range for concrete was found to be under the corresponding tensile strength and the textile being a brittle material, has a linear- elastic behaviour until failure. However, the designed bond-slip relationship between both materials was chosen as non-linear to reproduce the behaviour of the tested specimens and to be able to compare with the 1D analysis results. The calibrated bond-slip relationship used in the model was identical to that used in the 1D model as previously described. The mechanical properties of both the concrete and textile reinforcement were obtained either based on experimental results or derived from manufacturer data, as aforementioned in Section V.5.2.2.

V.5.5 Comparison and discussion

The slip distributions of Short and Long zones versus total slip are shown in Figure V-62 (left) for basalt and Figure V-63 (left) for carbon. The experimental and numerical results for all embedment lengths compared in Figure V-62 (right) for basalt and Figure V-63 (right) for carbon depict a reasonably good correlation. The 1D model generally simulates the stiffness prior to the peak and the maximum force with reasonable good agreement. As for post-peak behaviour, the rupture of the roving causing a sudden drop in stiffness is not captured using the 1D model for the *Medium* and *Long* specimens because of the linear elastic material assumption.

The 3D models were used to evaluate the scope of the 1D model related to basalt as well as to validate the different assumptions. The concrete stress/strain distribution in the 3D analysis results confirm that the contribution of the deformation of the concrete to the slip is negligible (see Figure V-64), thus validating the main assumption of the 1D model. Furthermore, the 3D model was able to capture the variation of bond stresses occurring during post-peak loading along the Short and Long zones because it reproduces the interaction between both parts and includes unloading. Figure V-65 depicts that the bond stress distribution for the short embedment length was non-uniform for the initial slip values (i.e. 0.01-0.3 mm). Therefore, the local-bond values in the first estimate from the experimental data were initially underestimated and adjustment was necessary particularly in the pre-peak region to take into account the non-uniform bond stress distribution.

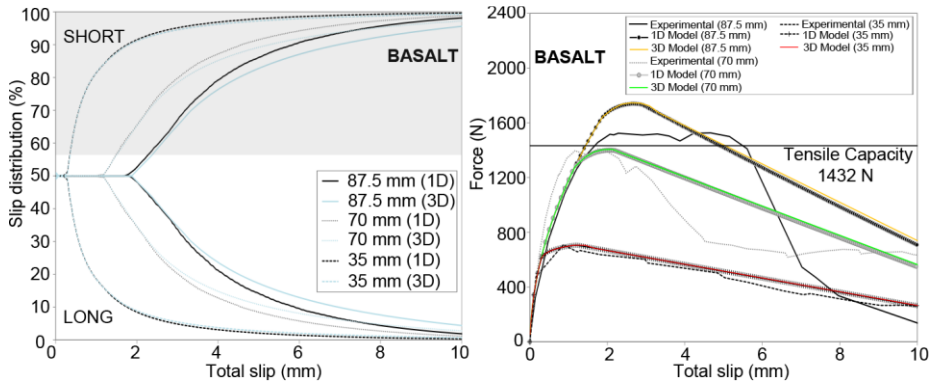

Figure V-62. Slip distributions of Short and Long zones versus total slip (left) and experimental results versus 1D and 3D model for basalt (right)

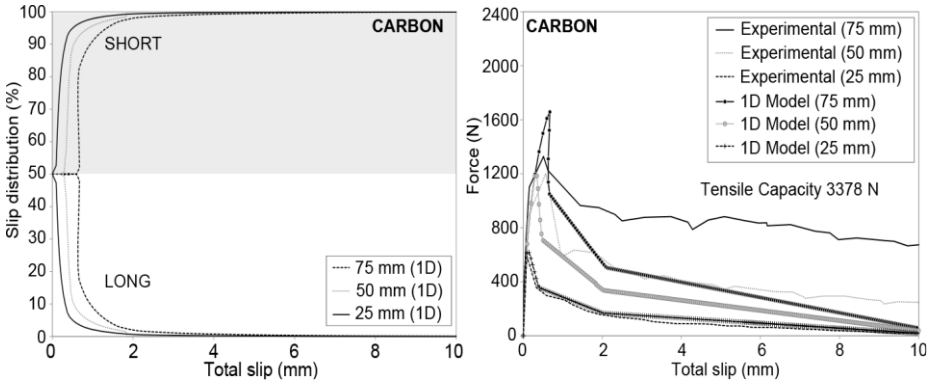

Figure V-63. Slip distributions of Short and Long zones versus total slip (left) and experimental results versus 1D model for carbon (right)

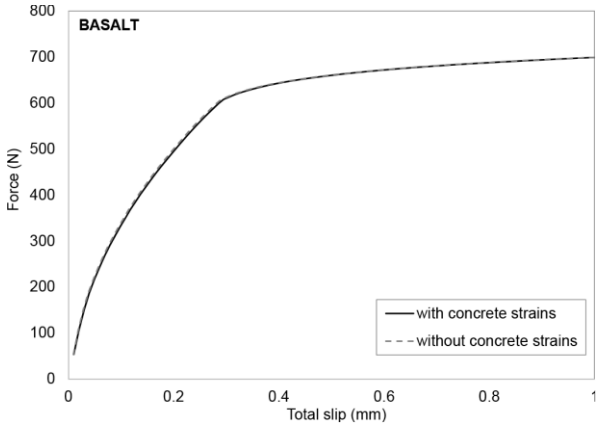

Figure V-64. Total deformation with and without concrete strains simulated by 3D model for basalt Short specimens

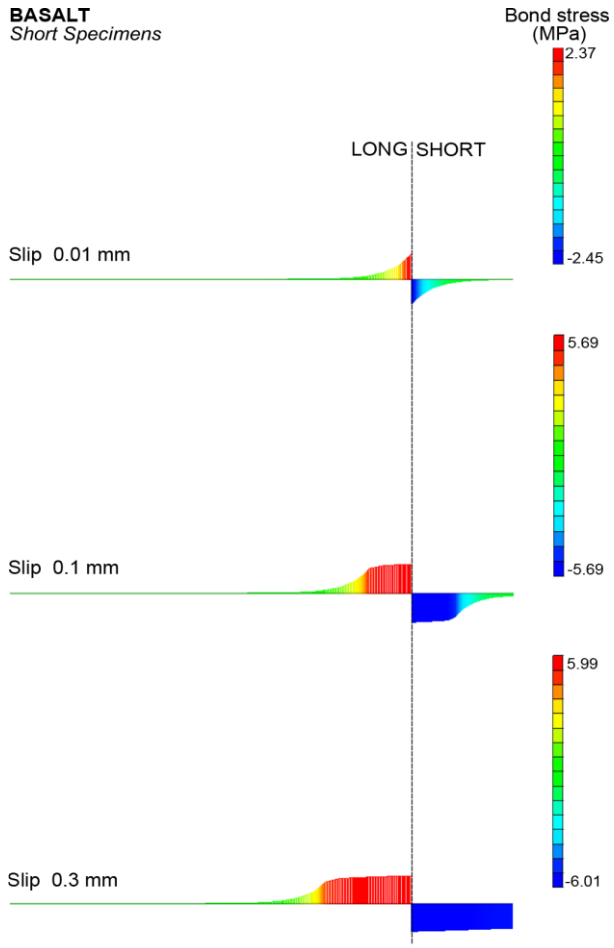

Figure V-65. Bond stress evolution simulated by 3D model for basalt Short specimens at different load steps corresponding to various slips (0.01 mm, 0.1 mm and 0.3 mm)

V.5.6 Conclusions

The bond behaviour of basalt textile reinforced concrete was characterized in this work by means of direct pull-out tests. Pull-out failure was observed for *Short* specimens, while rupture failure was noted for *Medium* and *Long* in the experimental pull-out tests for basalt textile reinforced concrete specimens. As for carbon, pull-out failure was the common failure mode experienced by all specimens. Thereafter, a local bond stress-slip curve was calibrated for the basalt and carbon specimens based on the experimental results related to the *Short* specimens. Moreover, applying this local bond stress-slip curve in a simple 1D bond model demonstrated a reasonable force versus total displacement correlation with the experimental results for the longer embedment lengths as well. The pull-out test setup presented in this work is suitable to obtain and characterize local bond behaviour for different TRC materials, particularly in the case of short embedment lengths. Non-linear 3D models proved that the

assumptions made to obtain the adjusted local bond-slip behaviour are acceptable and capture a sufficient amount of accuracy. Also, these models were valuable tools which validated the different hypothesis made in the simpler 1D model used to describe the bond behaviour of textile reinforcements. In view of that, it can be concluded that the 1D model is a valid tool to describe pull-out failure of textile reinforcement concrete specimens. In contrast to the 1D model, 3D models are especially useful to model the presented complex pull-out test with non-symmetrical embedment lengths such that full interaction (i.e. total slip and unloading) between both Short and Long parts of the pull-out specimen can be included simultaneously.

Acknowledgments

The presented research was funded by the European Community's Seventh Framework Programme under grant agreement NMP2-LA-2009-228663 (TailorCrete) and FORMAS (Homes for Tomorrow). More information about the research projects, TailorCrete and Homes for Tomorrow, can be found at www.tailorcrete.com and www.homesfortomorrow.se, respectively. Special thanks are also extended to the Ministry of Science and Innovation of the Government of Spain (MINECO) for funding Ignasi Fernandez Perez to carry out a research and knowledge exchange at Chalmers University of Technology.

References

[1] Orlowsky J, Raupach M. Textile reinforced concrete-from research to application. Cement Wapno Beton. 2011;16(6):323-31.

[2] Mobasher B. Mechanics of fiber and textile reinforced cement composites: CRC Press; 2012.

[3] Hegger J, Goralski C, Kulas C. A pedestrian bridge made of textile reinforced concrete. Schlanke Fußgängerbrücke aus Textilbeton. 2011;106(2):64-71.

[4] Insu-Shell-Projekt LIFE. Life insu-Shell-Projekt • Institut Für Textiltechnik Der Rwth Aachen. 2009.

[5] Ortlepp R, Curbach M. Strengthening of Columns using Textile Reinforced Concrete (TRC). Beton- Und Stahlbetonbau. 2009;104(10):681-9.

[6] Ortlepp R, Schladitz F, Curbach M. Textilbetonverstärkte Stahlbetonstützen. Beton- Und Stahlbetonbau. 2011;106(9):640-8.

[7] Brameshuber W. Test methods and design of Textile Reinforced Concrete Report of RILEM TC 232-TDT: RILEM publications; Not yet available.

[8] Brameshuber W. Report 36: Textile Reinforced Concrete-State-of-the-Art Report of RILEM TC 201-TRC: RILEM publications; 2006.

[9] Zastrau B, Richter M, Lepenies I. On the Analytical Solution of Pullout Phenomena in Textile Reinforced Concrete. Journal of Engineering Materials and Technology. 2003;125(1):38-43.

[10] Krüger M. Vorgespannter textilbewehrter Beton: University of Stuttgart; 2004.

[11] Xu S, Li H. Bond properties and experimental methods of textile reinforced concrete. Journal of Wuhan University of Technology--Materials Science Edition. 2007;22(3):529-32.

[12] Sueki S, Soranakom C, Mobasher B, Peled A. Pullout-slip response of fabrics embedded in a cement paste matrix. Journal of Materials in Civil Engineering. 2007;19(9):718-27.

[13] Ortlepp R, Curbach M, Weiland S. Rehabilitation and strengthening of a hypar concrete shell by textile reinforced concrete. Excellence in Concrete Construction through Innovation: Taylor & Francis; 2009.

[14] Lorenz E, Ortlepp R. Bond Behavior of Textile Reinforcements-Development of a Pull-Out Test and Modeling of the Respective Bond versus Slip Relation. High Performance Fiber Reinforced Cement Composites 6: Springer; 2012. p. 479-86.

[15] Zhang XB, Aljewifi H, Li J. Failure behaviour investigation of continuous yarn reinforced cementitious composites. Construction and Building Materials. 2013;47(0):456-64.

[16] Richter M, Lepenies I, Zastrau BW. On the influence of the bond behaviour between fiber and matrix on the material properties of textile reinforced concrete. International Symposium of Anisotropic Behaviour of Damaged Materials2002. p. 1-24.

[17] Lundgren K, Kettil P, Hanjari KZ, Schlune H, Roman ASS. Analytical model for the bond-slip behaviour of corroded ribbed reinforcement. Structure and Infrastructure Engineering. 2012;8(2):157-69.

[18] Banholzer B. Bond of a strand in a cementitious matrix. Materials and structures. 2006;39(10):1015-28.

[19] Butler M, Mechtcherine V, Hempel S. Experimental investigations on the durability of fibre-matrix interfaces in textile-reinforced concrete. Cement and Concrete Composites. 2009;31(4):221-31.

[20] CEN. Eurocode 2: Design of Concrete Structures: Part 1-1: General Rules and Rules for Buildings: British Standards Institution; 2004.

[21] Lorenz E, Ortlepp R. Basic research on the anchorage of textile reinforcement in cementitious matrix. 9th international symposium on fiber-reinforced polymer reinforcement for concrete structures (FRPRCS-9), book of abstract2009. p. 136.

[22] International Federation for Structural Concrete (fib). fib Bulletin 55: Model Code 2010, First complete draft2010.

[23] Ruiz MF, Muttoni A, Gambarova P. Analytical modeling of the pre-and postyield behavior of bond in reinforced concrete. Journal of Structural Engineering. 2007;133(10):1364-72.

[24] Losberg A. Sprickbildning i kontinuerliga betongbeläggningar och andra betongkonstruktioner, låsta mot rörelser av temperatur och krympning (Cracks in continuous concrete road slabs and other concrete structures locked against movements from temperature and shrinkage). Chalmers University of Technology, Institution of Building Technology 1962;No 607:45.

[25] MATLAB. The MathWorks, Inc; 1994-2013.

[26] TNO Diana. Finite Element Analysis User's Manual - release 9.4.4: TNO; 2011.

Chapter VI

CONCLUSIONS AND FUTURE WORK

VI.1 Conclusions

The present research work has allowed to contribute to the knowledge of the structural response of continuous structures under deterioration due to corrosion of steel reinforcement. Particular conclusions have been described in detail at the end of each chapter of the thesis. The general conclusions are outlined below.

Corrosion of steel reinforcement has showed as an important deterioration cause of reinforced steel concrete members, which produced the next structural effects:

- The performance of reinforced concrete members was considerably reduced due to steel corrosion. Higher deflections were observed during the corrosion phase than in the case of un-corroded beams. If corrosion is produced under high load situations, this increasing deflections effect is amplified

- Redistributions of internal forces in the tested continuous beams were observed during the corrosion phase, as a consequence of the changes in the stiffness of the corroded zones. However, the internal forces redistribution was mitigated with the applied load: the higher the applied load, the less redistribution and vice-versa.
- Due to internal forces redistribution, steel stress described important variations during corrosion phase.
- The structural redundancy and redistribution capacity enlarge the exposition period of statically undetermined beams, which can achieve higher corrosion levels than simpler structures without compromise structural safety.
- It has been observed that the reduction of the mechanical properties of corroded steel bars is relevant in the structural behaviour, since they are modified by corrosion.
- Load carrying capacity was also highly reduced. The observed reduction was higher than expected only taking into account the reinforcement steel cross-section reduction, which means that other local phenomena affect the structural response.
- Bond behaviour between concrete and steel was the main parameter that affected the structural response. Very high corrosion levels produced a severe drop of bond strength, which in all the cases mainly governed the specimens' failure mode and load carrying capacity.

The study of change of mechanical properties of corroded steel bars and bond behaviour in different concretes submitted to steel corrosion resulted crucial to a better understanding of the statically undetermined deteriorated members' structural behaviour:

- A substantial reduction of all the mechanical steel properties was observed. Yield and ultimate stresses measured in the monotonic test were found strongly dependent on the corrosion level. Modulus of elasticity and ultimate strains also were affected by steel corrosion. Furthermore, mechanical properties reduction defined a non-linear relationship with respect to the corrosion level, mainly due to bar local corrosion effects amplification.
- Fatigue life of corroded steel bars was also affected, as the observed reduction of cycles to failure in corroded bars was relevant.
- The loss of bond due to corrosion increased with the corrosion level; however, concretes such as recycled aggregates concretes, which presented higher porosity, described better bond performance for very low corrosion levels. That behaviour was consequence of the higher dispersion capacity throughout the concrete pours mesh that corrosion products have.

Modelling of concrete reinforced steel members is necessary to well understand their behaviour and to predict possible unexpected situations. Modelling deterioration phenomena is a difficult task, which should include many different elements. On the one hand penetration phase of the external aggressive agents, on the other hand models decribing local deterioration effects have to be implemented on global structural models to define a good structural response and make good numerical predictions under different situations.

- It has been demostrated that the corroded mechanical steel properties can be obtained using a simplified model by taking into account pitting along the steel bar, either generalized or pitting corrosion, as well as non-homogeneous material properties throughout the cross-section. The non-homogeneous material properties induced by the modern production systems like TEMPCORE®, widely used in Europe, is well described by sectional fibre models, in which the material properties can be assigned filament by filament.
- New novel techniques, such as 3D scan, are proved to be useful to the knowledge of the local corrosion effects over the steel bar. A very fine description of the outer surface leads to a good understanding of the pitting distribution along the steel bar. Also the characterization of the critical pitted cross-section, where the bar most probably would fail, coul be identified. A whole bar 3D models can successfully carry out from that detailed surfaces. Numerical simulations proved that a multi-axial stress behaviour takes place in the critical pitted cross-section zone. Thus 3D stress state inferred by corrosion in steel cannont be be represented by uniaxial sectional fibre models, which are intended to reproduce the overall corroded bar behaviour, not the critical cross-section only.
- Modelling anchorage failure using 3D global models or 1D simplified models is possible considering different degrees of complexity in the bond interaction between concrete and steel. 1D simplified models showed good results to estimate the ultimate load, but the overall structural behaviour required complex models, which take into account complex bond behaviour. However, the complexity of the last demand more computational cost and a more detailed definition of the problem.

VI.2 Recomendations for future research lines

The present research has covered significant aspects of the local effects that corrosion produces to the structure. However, many interesting topics aroused due to the work performed. Therefore, some research works are suggested below.

- Mechanical model for corroded steel bars properties

  An experimental study to accurately define the evolution of modulus of elasticity and ultimate strain properties due to steel corrosion should be performed. The presented model showed less accuracy in the prediction of those parameters than for yielding and ultimate stresses. However, the observed characteristics of the failure suggested a concentration of the strains in the critical section. Therefore, it is recommended the problem to be addressed from fracture mechanics perspective. The definition of the necking length as a material parameter, which depends on the corrosion level, can be useful to estimate the ultimate strain of corroded bars with more accuracy. A specific work to determine the modulus of elasticity evolution with respect to the corrosion level should be performed.

- Bond between steel and different concrete types

  An experimental study extending the presented study on bond wold be useful. Two variables should be modified: the corrosion rate and the type of concrete. Even lower corrosion rates should be applied to get closer to naturally corrosion procedures. The dispersion of the corrosion products throughout the pours mesh is expected to improve as low corrosion rates are used. Concretes with different recycled aggregates origin should be employed to define the impact of the aggregate employed in the bond.

  Also a model to estimate the bond strength for recycled aggregate concrete as well as recycled aggregates concretes with steel corrosion should be developed. There is a lack of models to predict the bond behaviour, which include the concrete type effect, in the existing literature.

- Integrate deterioration model

  The main proposal is to develop an integrate deterioration model which should include all the corrosion phases as well as the local induced effects aforementioned.

The model should consider the initiation phase where the external agents penetrate inside the concrete and reach the reinforcement steel. Different considerations must take into account in the penetration phase:

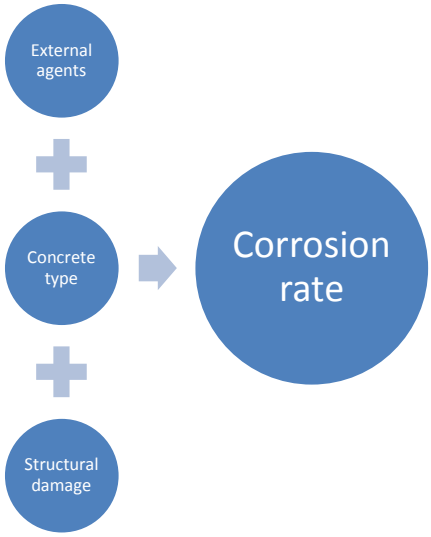

Figure VI-1. Parameters which define the corrosion rate

The obtained corrosion rate should interact with the structure and should be enough to define the different local properties which define the structural behaviour under a corrosion procedure.

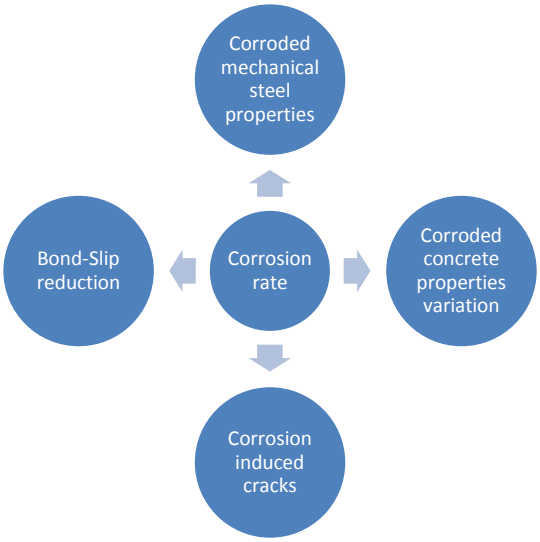

Figure VI-2. Local effects of steel corrosion on the structures

A feedback subroutine should be implemented to interact with the different parts of the model and asses the structural state under the new conditions.

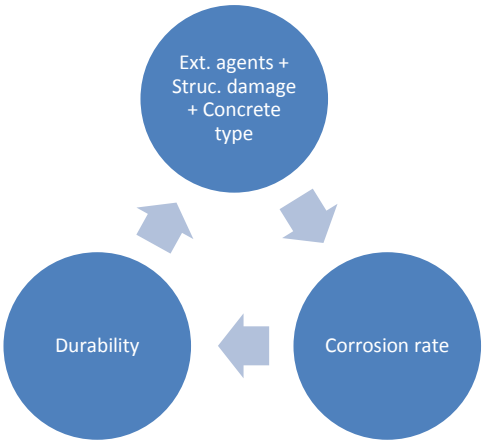

Figure VI-3. Retrofitting of the different parameters in the model

- Bond-slip implementation

  The implementation of bond slip between concrete and steel in sectional fibre structural models has sowed to be strongly mesh size dependent. Furthermore, the addition of new degrees of freedom to consider the relative displacement between steel and concrete increase the computational cost of those models, which are characterized by its simplicity and usability as well as reliability.

  One possible approach to consider bond-slip effect in such models could be modifying the tension-stiffening law, including a time depending and corrosion linked law. This might be affordable to develop due to those models usually have implemented tension stiffening in different ways either for concrete or steel constitutive models.